https://ntrs.nasa.gov/search.jsp?R=19850009690 2020-03-20T20:13:04+00:00Z

NASA Technical Memorandum 86299

NASA-TM-86299 19850009690

Effect of Jet Exit Vanes on Flow Pulsations in an Open-Jet Wind Tunnel

William L. Sellers III, Zachary T. Applin,
John K. Molloy, and Garl L. Gentry, Jr.

MARCH 1985

NASA

NASA Technical Memorandum 86299

Effect of Jet Exit Vanes on Flow Pulsations in an Open-Jet Wind Tunnel

William L. Sellers III, Zachary T. Applin,
John K. Molloy, and Garl L. Gentry, Jr.
Langley Research Center
Hampton, Virginia

National Aeronautics
and Space Administration

**Scientific and Technical
Information Branch**

1985

Summary

An investigation was conducted of various jet exit vane configurations in the open test section of the Langley 4- by 7-Meter Tunnel to determine their effectiveness in reducing flow pulsations. The devices consisted of rectangular or triangular vanes mounted on the periphery of the jet exit and protruding into the flow. The streamwise and vertical velocity fluctuations were measured at the centerline of the tunnel, 39.5 ft (12.0 m) downstream of the jet exit, with hot-wire anemometers. This report describes the various vane configurations and their effect on the measured root-mean-square turbulence levels in the test section and presents time series analyses of the data for the baseline jet exit configuration (without vanes) and for the most effective vane configuration, which consisted of triangular vanes alternating into and out of the flow.

Introduction

Open-jet wind tunnels are particularly susceptible to a phenomenon known as flow pulsation, or surging. Flow pulsations are characterized by periodic oscillations in velocity and pressure and occur only within certain tunnel speed ranges. In some large open-jet wind tunnels, the flow pulsations may be so severe that they could threaten the structural integrity of the tunnel. In less severe cases, the flow pulsations degrade the flow quality and limit testing to the speed ranges at which they do not occur.

The flow pulsations are self-excited and are created by the unstable shear layer which is formed at the jet exit when the jet is dumped into an open test chamber. The airstream in the open test section is typically directed back into the tunnel circuit by a collector. Vortex rings form in the unstable shear layer surrounding the free jet. When the vortices strike the collector, they cause a pressure fluctuation which travels upstream at essentially sonic velocity and causes the shear layer at the jet exit to deform and shed another vortex. When the vortices strike the collector with a steady beat frequency, they can build up resonances in various air columns throughout the tunnel circuit.

References 1 through 4 describe devices, referred to as vanes, tabs, or teeth, that protrude into the airstream around the jet exit and effectively reduce the magnitude of the flow pulsations. The exact mechanism by which the flow pulsations are reduced is not precisely known. Seiferth suggests in reference 2 that the devices cause intense mixing in the jet shear layer. This mixing spreads out the vortex rings such that they no longer strike the collector at the same time and, therefore, disturb the critical phasing that is required for resonances to develop.

The jet exit vanes do present some problems. The vanes reduce the tunnel efficiency and disturb the velocity distribution of the potential core and the longitudinal static-pressure distribution in the test section. In addition, the thickness of the jet shear layer is increased by the mixing caused by the vanes and may adversely affect acoustic measurements. It has also been found that jet exit vanes are not always successful. Brodzki states in reference 4 that vanes of various sizes, shapes, and configurations were tried in a 16.4-ft (5.0-m) tunnel with no significant improvement in flow pulsation dampening, and that in another case involving a 1.6-ft (0.5-m) tunnel, jet exit vanes were successful in reducing the flow pulsations. In addition, he mentions experiments which also showed that in some instances, the jet exit vanes were only successful in dampening the flow pulsations when used along with other dampening techniques such as holes or slots in the tunnel circuit.

When jet exit vanes are successful by themselves, they represent an inexpensive and quick way to dampen the flow pulsations. For general aerodynamic force and pressure measurements, the adverse effect of the vanes may be tolerated, especially if the vanes can provide greater speed range due to flow pulsation dampening.

The 4- by 7-Meter Tunnel develops flow pulsations in the open test-section configuration. These pulsations have degraded the capability of the tunnel to support research in areas where nonperiodic, low-turbulence flow is crucial. An investigation was conducted to document the flow pulsation problem in the 4- by 7-Meter Tunnel and to evaluate the effectiveness of jet exit vanes in reducing the flow pulsations. This paper presents experimental results of various configurations of jet exit vanes and their effect on the flow pulsations. The data represent the most extensive data base available relating to flow pulsations and consist of the instantaneous velocity fluctuations measured with hot-wire anemometers located 39.5 ft (12.0 m) downstream of the jet exit. The report includes data describing the vertical component of velocity fluctuations and, therefore, provides valuable information on flow angularity, which has a major influence on angle-of-attack variations in wind-tunnel testing.

Symbols and Abbreviations

Values are given in U.S. Customary Units, often with equivalent values in the International System of Units (SI) given in parentheses for the convenience of readers. Measurements and calculations were made in U.S. Customary Units.

E	mean hot-wire voltage
e	fluctuating hot-wire voltage

G_{uu}, G_{ww}	autopower spectral density function of streamwise velocity fluctuations and vertical velocity fluctuations, respectively, Hz^{-1}
PSD	autopower spectral density
q	test-section dynamic pressure, lb/ft^2 (Pa)
R_{uu}, R_{ww}	normalized autocorrelation function, $\frac{\lim_{T\to\infty} 1/T \int_0^T x(t)\ x(t+\tau)\ dt}{\lim_{T\to\infty} 1/T \int_0^T x(t)\ x(t)\ dt}$, where $x = u$ for R_{uu} and $x = w$ for R_{ww}
RMS	root-mean-square
S_u	hot-wire sensitivity to velocity
S_α	hot-wire sensitivity to α
STA.	station
T	observation time or period of data, sec
t	time, sec
u	axial or streamwise velocity component, ft/sec (m/sec)
w	vertical velocity component, ft/sec (m/sec)
α	angle of attack of hot-wire probe, rad
σ	$\sqrt{\lim_{T\to\infty} 1/T \int_0^T x(t)\ x(t)\ dt}$, where $x = u$ or w
τ	time delay, msec
ψ	inclination angle of hot wire from free-stream velocity, rad
Subscripts:	
b	baseline configuration
1,2	wire 1 or 2 of x-wire probe
∞	free stream
Superscripts:	
~	root-mean-square value of fluctuating component
′	instantaneous fluctuating or perturbation component

Tunnel Description

The Langley 4- by 7-Meter Tunnel (see fig. 1) is a closed-circuit, single-return, atmospheric wind tunnel. Figure 2 is a sketch showing the general arrangement of the tunnel. The test section is 14.5 ft (4.42 m) high, 21.75 ft (6.63 m) wide and 50.0 ft (15.2 m) long. The tunnel provides maximum test-section velocities ranging from 225 ft/sec (68.6 m/sec) in the open test section to 325 ft/sec (99.1 m/sec) in the closed test section.

The open test-section configuration used for these tests is open on only three sides. The walls and ceiling are raised to the top of the test chamber, but the floor remains in place. Figure 3 is a photograph of the open test-section configuration. The view is looking downstream from the jet exit toward the collector, which directs the free jet back into the first diffuser. The collector is constructed of 0.25-in-thick (0.64-cm) steel plate rolled to form a circular arc with a radius of 10 ft (3.0 m).

Instrumentation and Data Reduction

Constant-temperature hot-wire anemometers were used to measure the fluctuating velocity components in the streamwise (u') and vertical (w') directions. The data were obtained by using a commercially available x-wire probe and a single normal-wire probe located on the horizontal and vertical tunnel centerline 39.5 ft (12.0 m) downstream of the jet exit. The probe used 0.00015-in-diameter (4-μm) platinum-coated tungsten wire with a typical sensor length of 0.050 in. (1.27 mm). The data from the normal-wire probe were used during the test to provide an on-line evaluation of the RMS of the u-component velocity fluctuations ($\tilde{u}/u_\infty$). The data from the x-wire probe were used during posttest data reduction to compute u'/u_∞ and w'/u_∞ and their respective RMS levels and autopower spectral density and autocorrelation functions.

An x-wire probe consists of two wires inclined ±45° to the probe axis. The mean voltage from an inclined wire is a function of the flow velocity and the inclination angle ψ of the wire. This relationship may be written as

$$dE = \frac{\partial E}{\partial u} du + \frac{\partial E}{\partial \psi}\, d\psi \tag{1}$$

After some algebraic manipulation, equation (1) may be rewritten as

$$\frac{dE}{E} = \frac{\partial \ln E}{\partial \ln u}\frac{du}{u} + \frac{\partial \ln E}{\partial \psi}\, d\psi \tag{2}$$

The differentials dE and du may be replaced by the perturbations e and u', respectively, to yield

$$\frac{e}{E} = \frac{\partial \ln E}{\partial \ln u}\frac{u'}{u} + \frac{\partial \ln E}{\partial \psi}\, d\psi \tag{3}$$

If you make the assumption of small perturbations, for example, $u \gg u'$ and $u \gg w'$, then

$$d\psi = \tan^{-1}\left(\frac{w'}{u+u'}\right) \approx \frac{w'}{u+u'} \approx \frac{w'}{u}$$

Equation (3) may then be rewritten as

$$\frac{e}{E} = \frac{\partial \ln E}{\partial \ln u}\frac{u'}{u} + \frac{\partial \ln E}{\partial \psi}\frac{w'}{u} \tag{4}$$

Let

$$S_u = \frac{\partial \ln E}{\partial \ln u}$$

and

$$S_\alpha = \frac{\partial \ln E}{\partial \psi}$$

then the output of the inclined wire may be written as

$$\frac{e}{E} = S_u\frac{u'}{u} + S_\alpha\frac{w'}{u} \tag{5}$$

The S_u sensitivity constants were determined from linear least-squares curve fits of ln E versus ln u_∞ with the hot-wire probe set at 0° with respect to the free-stream velocity. The S_α sensitivity constants were determined from linear least-squares curve fits of ln E versus α over a range of ±8°.

The x-wire probe with its two wires therefore provided two linear equations for u'/u_∞ and w'/u_∞

$$\left.\begin{aligned}\left(\frac{e}{E}\right)_1 &= S_{u,1}\frac{u'}{u_\infty} + S_{\alpha,1}\frac{w'}{u_\infty}\\ \left(\frac{e}{E}\right)_2 &= S_{u,2}\frac{u'}{u_\infty} + S_{\alpha,2}\frac{w'}{u_\infty}\end{aligned}\right\} \tag{6}$$

The fluctuating output voltage of each wire was bandpass filtered between 1 Hz and 10 kHz and recorded on FM magnetic tape. The voltage data were digitized and the fluctuating velocity components computed by solving equations (6) simultaneously for each digitized point. The RMS velocity fluctuations were also computed for each velocity component. The autopower spectral density (PSD) and autocorrelation functions were computed for each fluctuating velocity component by using the Acoustic Analysis Program described in reference 5.

Jet Exit Configurations

Six different jet exit configurations were investigated. These configurations can be divided into two broad categories, depending on whether a rectangular or triangular vane geometry was used. Figures 4 and 5 show typical installations of the rectangular and triangular vanes, respectively, on the jet exit. Figures 6 and 7 are sketches of the vane geometries. The vanes were mounted on steel rails that stood 4.0 in. (10 cm) off the inside of the jet exit on sections of steel channels or I beams. The rectangular and triangular vanes were cut from 0.25-in-thick (0.64-cm) aluminum plate. The size of the rectangular vanes was determined by proportionally increasing the dimensions provided by Eckelmann in reference 6 for a similar vane that was tested in the 9.8-ft (3.0-m) wind tunnel of the Aerodynamics Research Institute in Göttingen. The rectangular vanes had a span of 12.0 in. (30.5 cm) and were bent to form a 25° or 40° flap, with chords of 3.20 and 4.20 in. (8.1 and 10.7 cm), respectively. The size of the triangular vanes was determined by proportionally increasing the dimensions of a set of triangular vanes that were successful in dampening the pulsations in a 1/24-scale model of the 4-by 7-Meter Tunnel. The triangular vanes had a span of 23.75 in. (60.32 cm) and were bent to form a 45° flap with a chord of 5.70 in. (14.5 cm).

The jet exit configuration was varied by reversing the position of the rectangular vanes (i.e., 40° vanes pointing into the flow and 25° vanes pointing out), by alternating the triangular vanes into and out of the flow, or by selectively removing certain vanes. Figure 8 shows sketches of the various jet exit vane configurations. Table I provides a short description of the vane type and arrangement for each configuration.

Presentation of Results

Dynamic-flow quality may be presented in a variety of ways, depending on the information that is of interest. For example, the overall RMS levels, spectral content, and peak-to-peak values of the velocity fluctuations are useful for determining the structural loading of the tunnel caused by the flow pulsations. In another example, the autopower spectral density (PSD) and autocorrelation functions are useful for investigating the physics of the pulsation phenomenon or modeling turbulence.

The data are presented in several formats to make it valuable to a wide variety of potential users. The formats include the overall RMS levels, time history plots, and PSD and autocorrelation functions. The RMS levels of the velocity fluctuations are approximately 1 percent. The time history plots of the velocity fluctuations provide insight into the periodic nature of the flow and aid in the determination of the peak-to-peak levels. Each time history plot represents a typical 5-sec time slice of the data.

The PSD function provides critical information relating to the frequency content of the velocity fluctuations. This information is needed for an analysis of the pulsation phenomenon, since it identifies the discrete or "resonant frequencies" in the flow pulsation. The PSD was computed by using standard fast Fourier transform (FFT) techniques. A Hanning window was applied to the data to compensate for the finite record lengths involved with the FFT. The data were digitized at a rate of 200 samples per second and transformed by using a 2048-sample block size, which provided a spectral resolution of approximately 0.09 Hz. Ten ensemble averages were typically obtained at each tunnel speed. Anti-aliasing filters were set at 50 Hz. A description of

the various time series analysis techniques and windowing functions is given in reference 5.

The autocorrelation is the Fourier transform of the PSD and is a function of the time delay (τ) between samples. It typically is used to describe the dependence of data values on data at a different time. The autocorrelation was normalized by the mean-square value of the data as determined by the value of the function at $\tau = 0$. The normalizing value is shown for each plot as σ, which is the root of the mean-square value. The autocorrelation function was computed by using the boxcar window function.

Discussion of Results

Baseline Tunnel Configuration

The flow pulsations in the open test section of the 4- by 7-Meter Tunnel cause the RMS levels of the velocity fluctuations to reach extremely high values in three distinct speed ranges as shown in figure 9. The three "resonant" regions are centered about q = 8, 18, and 48 lb/ft^2 (0.38, 0.87, and 2.28 kPa) will be referred to as modes 1, 2, and 3, respectively. The streamwise RMS velocity fluctuations reach values of about 8 percent at modes 1 and 2 and 4.5 percent at mode 3. The vertical RMS velocity fluctuations are roughly half the RMS levels of the streamwise fluctuations in each mode. At speeds outside of the modes, the RMS levels of the velocity fluctuations are approximately 1 percent.

The dynamic-flow quality is shown in figures 10 through 12 at the velocity corresponding to the peak RMS level for each mode. The flow is characterized at each of the modes by an almost purely sinusoidal variation in velocity. At mode 1, the flow pulsates at a frequency of 1.26 Hz and at the first harmonic (2.52 Hz), as shown in figure 10(c). The autocorrelation functions presented in figures 10(d) and 10(f) show that the periodic portion of the velocity fluctuations accounts for about 98 percent of the total mean-square value of the streamwise velocity fluctuations and 90 percent of the vertical velocity fluctuations. Figures 11(c) and 11(e) show that at mode 2, the flow pulsates at a frequency of 2.22 Hz and at the first harmonic (4.4 Hz). The periodic portion of the velocity fluctuations again represents more than 90 percent of the total mean-square value of the velocity fluctuations.

The PSD functions presented in figure 12 show that at tunnel velocities near mode 3, the spectra of the velocity fluctuations are more complex. The flow pulsations have dominant resonant frequencies at 3.83 Hz and the first harmonic (7.66 Hz). There are additional discrete frequencies at 1.26, 2.22, and 3.09 Hz in the streamwise velocity fluctuations, which are not significantly above the background level of the vertical velocity fluctuations. The periodic portion of the velocity fluctuations near mode 3 accounts for 90 and 80 percent of the total mean-square values for the streamwise and vertical fluctuations, respectively.

The flow still has periodic fluctuations at test-section velocities outside of the three modes. (See figs. 13 and 14.) The PSD functions presented in figures 14(c) and 14(e) show that there are discrete frequencies present, but no one frequency appears to dominate. The autocorrelation functions show that the influence of the periodic portion of the velocity fluctuations has dropped to about 15 percent of the total mean-square value of the velocity fluctuations. Appendix A shows the time histories and PSD and autocorrelation functions of the velocity fluctuations corresponding to the baseline RMS data points shown in figure 9.

Effect of Jet Exit Vanes

The effect of the various jet exit vane configurations in reducing the flow pulsations is shown in figures 15 to 20. The effectiveness of the vanes is shown by comparing the RMS velocity fluctuations of each configuration with those of the baseline configuration. (See fig. 9.) The RMS level of the streamwise velocity fluctuations in the baseline configuration is shown as a dashed line in figures 15 to 20 to aid in the comparison.

The RMS velocity fluctuations for configurations 1 and 2 are shown in figures 15 and 16, respectively. These vanes were only partially successful in reducing the flow pulsations. Both configurations were able to eliminate mode 3 at q = 48 lb/ft^2 (2.28 kPa). They also produced about a 20-percent reduction in the RMS levels in modes 1 and 2 and reduced the width of each mode. Both configurations produced a slight reduction in the RMS levels at q values outside of the modes.

Triangular vane configuration 3 had very little effect on the flow pulsations, as shown in figure 17. There are still three modes or regions with high levels of RMS velocity fluctuations, and the modes have been shifted to lower tunnel speeds. The RMS levels in mode 3 have been reduced about 50 percent, but the levels in modes 1 and 2 show a slight increase.

Triangular vane configuration 4 had essentially the same geometry as configuration 3 except that every other vane was removed. As shown in figure 18, configuration 4 provided almost the same pulsation dampening as the rectangular vane configurations 1 and 2. It is interesting to note that the results for vane configurations 3 and 4 contradict an observation made by Brodzki in reference 4, in which he states that the greater the number of vanes, the better the dampening of the pulsations. It may be that with too close a vane spacing and with all the vanes pointed into the flow (as in configuration 3), a cancellation of the vorticity shed by adjacent vanes may occur and thus reduce the effectiveness.

Configurations 5 and 6 provided the greatest dampening of the flow pulsations, as shown in figures 19 and 20. In each of these configurations, the triangular vanes were pointing alternately into and out of the flow. Both configurations completely eliminated modes 2 and 3. The remaining portion of mode 1 is now centered about $q = 5.0$ lb/ft^2 (0.24 kPa). Configurations 5 and 6 support Brodzki's observation, since removing half the vanes did cause a slight increase in the RMS levels in mode 1.

Of all the configurations that were investigated, vane configuration 6 was judged to be the best. Configurations 5 and 6 provided about the same reduction in the RMS velocity fluctuations. Vane configuration 6, however, generated about 2 dB less acoustic noise in the 6- to 16-kHz frequency range. The dynamic-flow quality has improved greatly with vane configuration 6 when compared with the baseline. Figures 21 and 22 show that the periodic portion of the velocity fluctuations has been dramatically reduced at tunnel speeds corresponding to modes 2 and 3 in the baseline configuration. (See figs. 11 and 12 for comparison.)

In that part of mode 1 that remains in figures 19 and 20, the flow pulsates at frequencies of 1.2 and 2.3 Hz, and the periodic portion of the velocity fluctuations still accounts for about 90 percent of the total mean-square value of the velocity fluctuations. The data indicate that the jet exit vanes do not completely eliminate the pulsations. Appendix B shows the time histories and PSD and autocorrelation functions corresponding to the RMS data for configuration 6 in figure 20.

Even though the flow quality has been improved with vane configuration 6, some periodicity in the velocity fluctuations still remains throughout the entire tunnel speed range. This may hamper certain tunnel tests, and the data provided in appendix B should be useful in determining whether the remaining turbulence is acceptable. A second form of pulsation dampening such as venting the tunnel circuit or redesigning the collector (refs. 1 and 4) may be required to eliminate the remaining high RMS velocity fluctuations in mode 1.

Concluding Remarks

The Langley 4- by 7-Meter Tunnel develops flow pulsations in the open test-section configuration. The root-mean-square levels of the velocity fluctuations reach extremely high values in three distinct tunnel speed ranges. These three speed ranges are centered about test-section dynamic pressures of 8, 18, and 48 lb/ft^2 (0.38, 0.87, and 2.28 kPa). The flow in the three resonant regions, or modes, is characterized by an almost purely sinusoidal variation in velocity. The pulsation frequencies range from 1.3 to 7.7 Hz. The periodic portion of the velocity fluctuations accounts for about 90 percent of the total mean-square value of the velocity fluctuations.

Six different configurations of jet exit vanes were tested to determine their effectiveness in reducing the flow pulsations. Rectangular and triangular vane planforms were investigated. A configuration consisting of triangular vanes alternating into and out of the flow was shown to be the most successful in reducing the flow pulsations, in that the two high-speed modes were eliminated, and the magnitude and speed range of the first mode were reduced. At the two high-speed modes, the periodic portion of the velocity fluctuations was dramatically reduced.

Langley Research Center
National Aeronautics and Space Administration
Hampton, VA 23665
October 29, 1984

TABLE I. JET EXIT CONFIGURATIONS

Configuration	Description
Baseline	Jet exit clear (no vanes)
1	Rectangular vanes, alternating 25° into the flow and 40° out of the flow
2	Rectangular vanes, alternating 40° into the flow and 25° out of the flow
3	Triangular vanes, 45° into the flow
4	Triangular vanes, 45° into the flow, every other vane removed
5	Triangular vanes, 45° alternating into and out of the flow
6	Triangular vanes, 45° alternating into and out of the flow, every other vane removed

L-81-5962

Figure 1. Exterior view of Langley 4- by 7-Meter Tunnel.

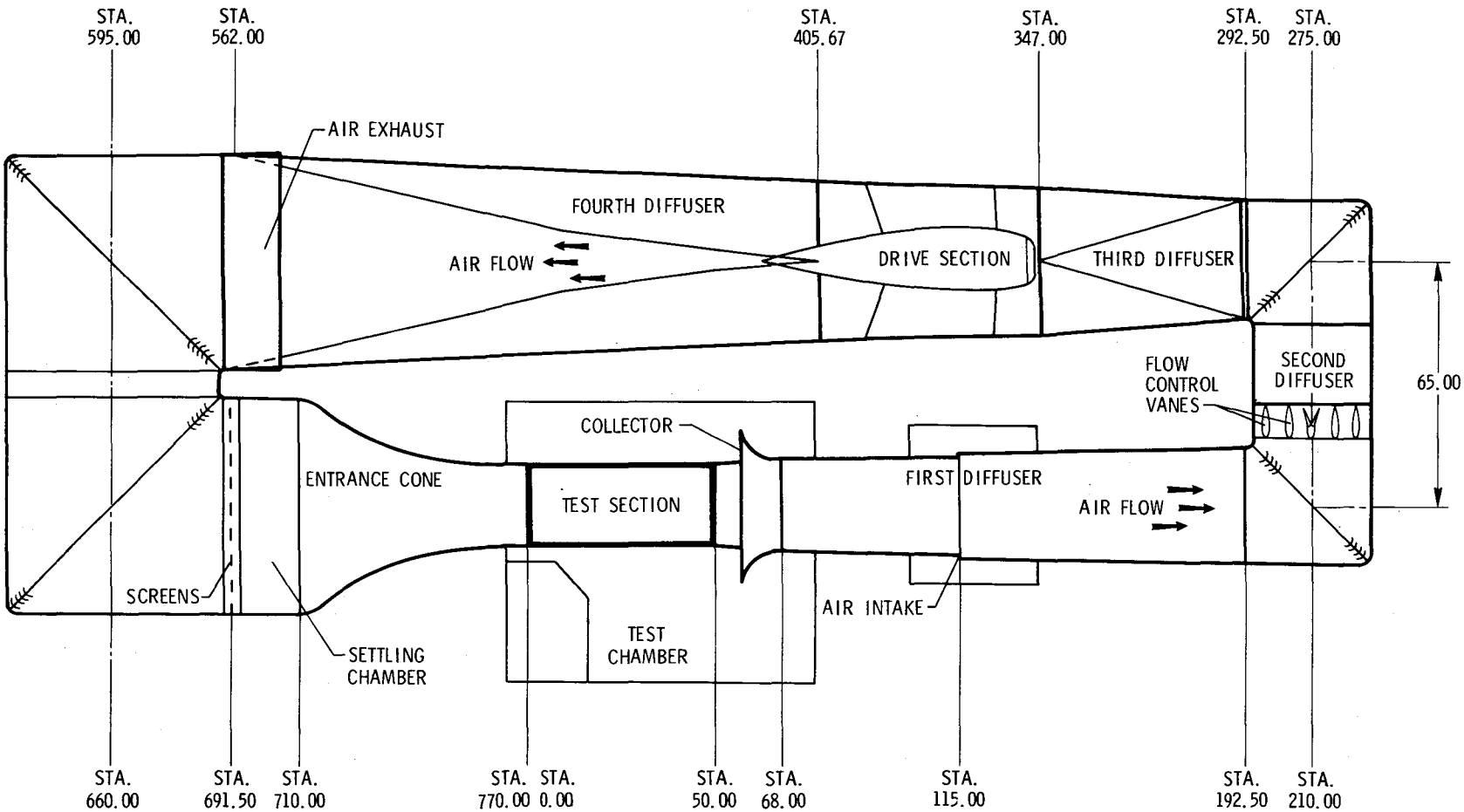

Figure 2. General arrangement of Langley 4- by 7-Meter Tunnel. All dimensions are in feet.

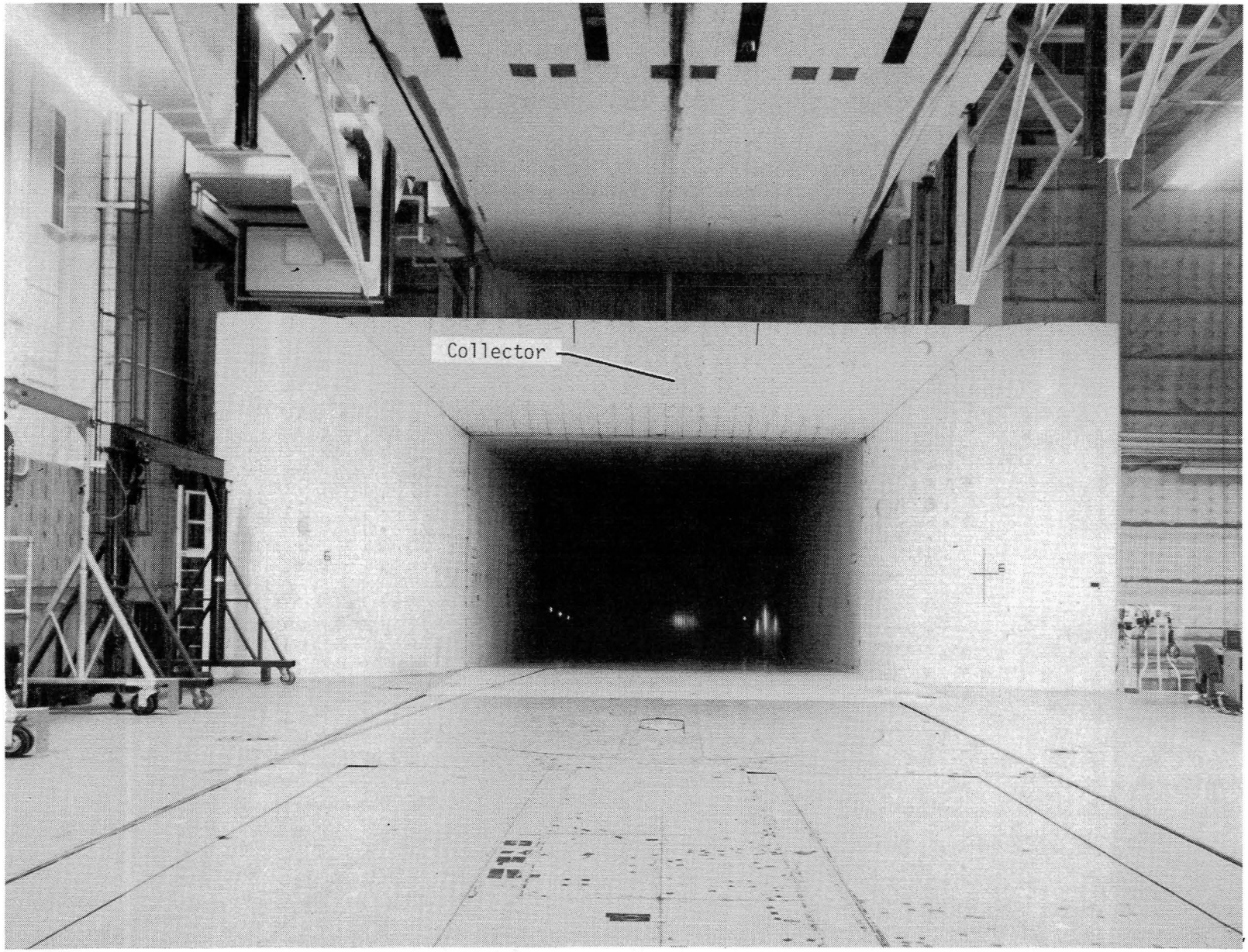

L-82-9483

Figure 3. View looking downstream at collector of open test section.

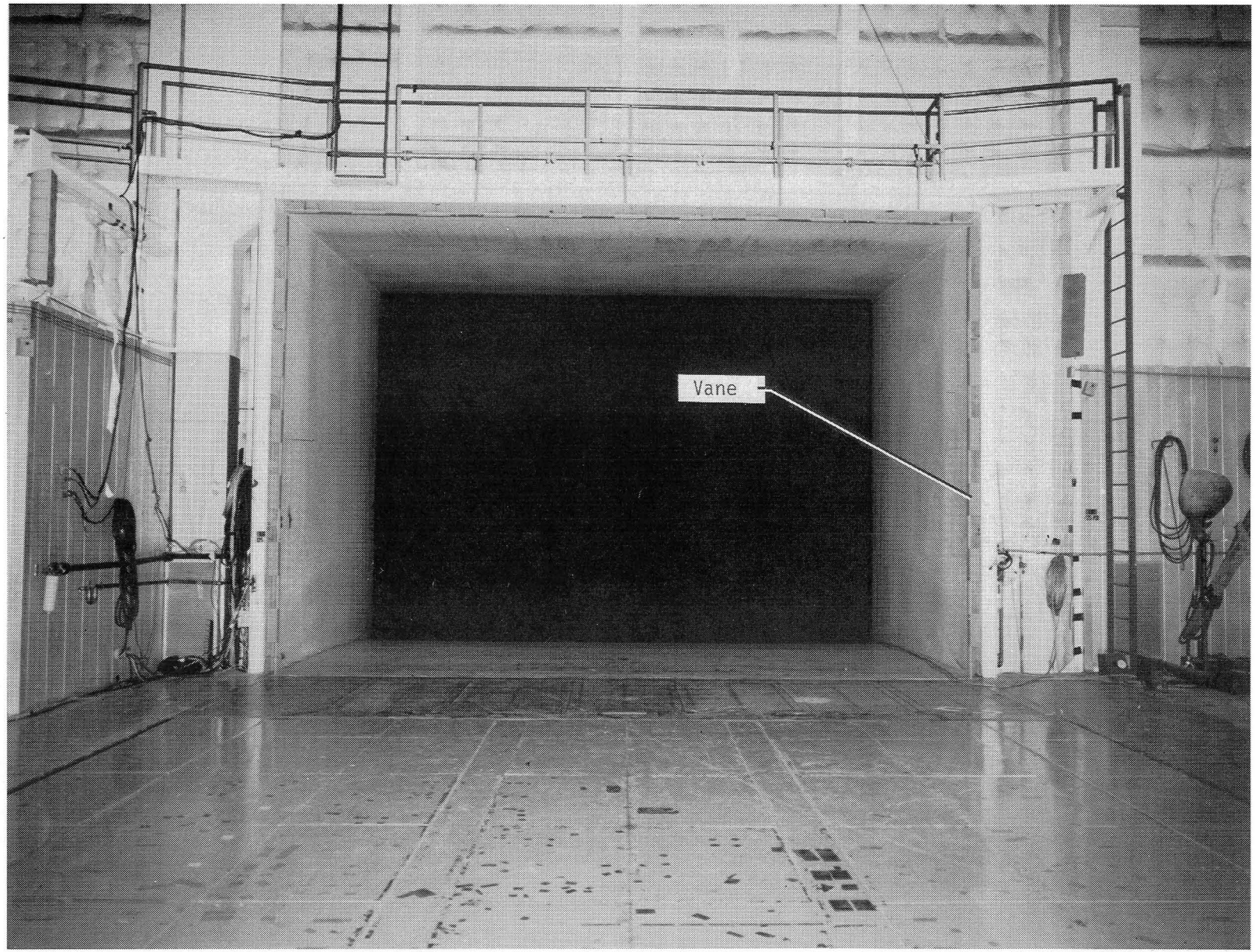

L-82-10,576

(a) Overall view.

Figure 4. View looking upstream at jet exit. Configuration 1.

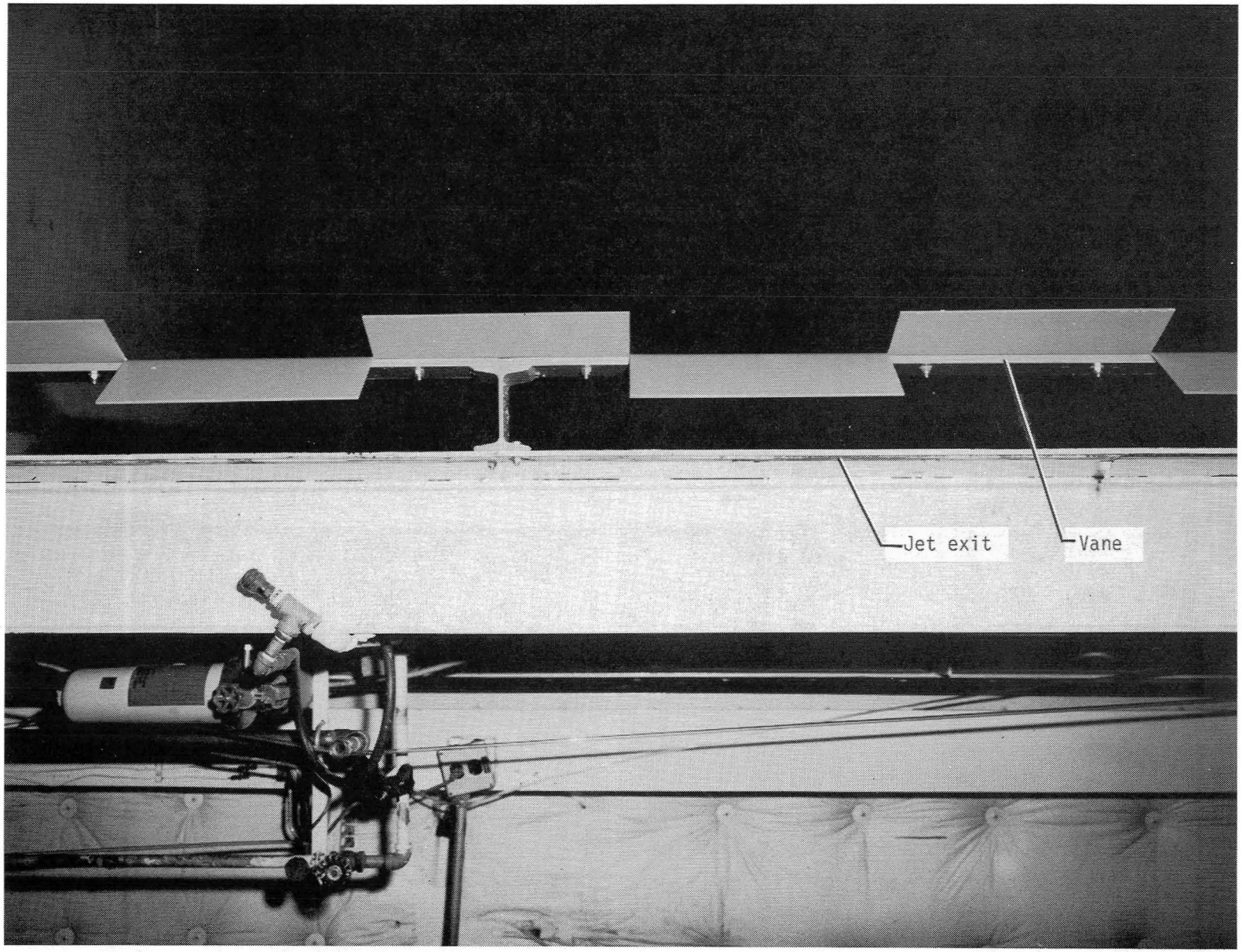

L-82-10,573

(b) Close-up view.

Figure 4. Concluded.

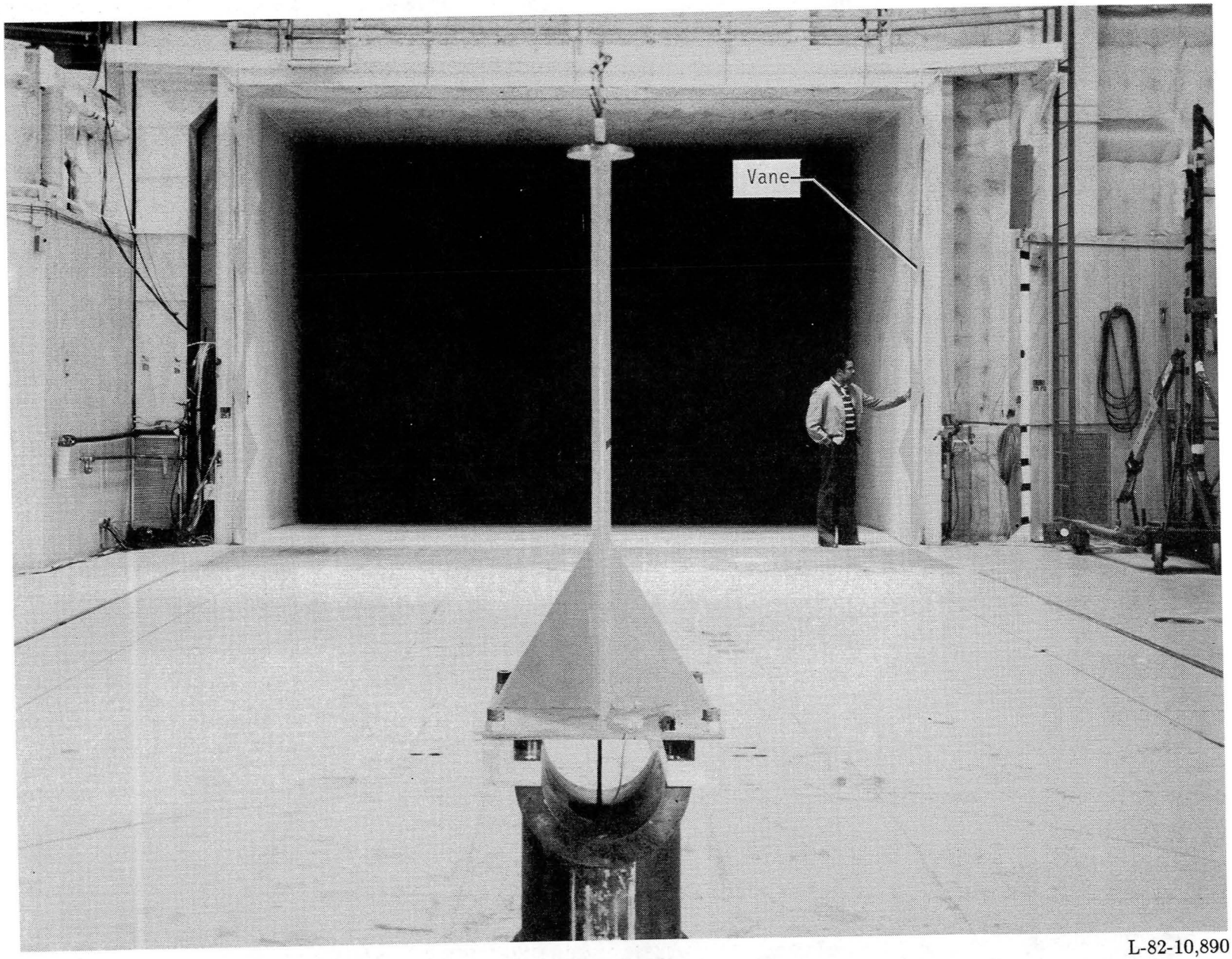

L-82-10,890

(a) Overall view.

Figure 5. View looking upstream at jet exit. Configuration 5.

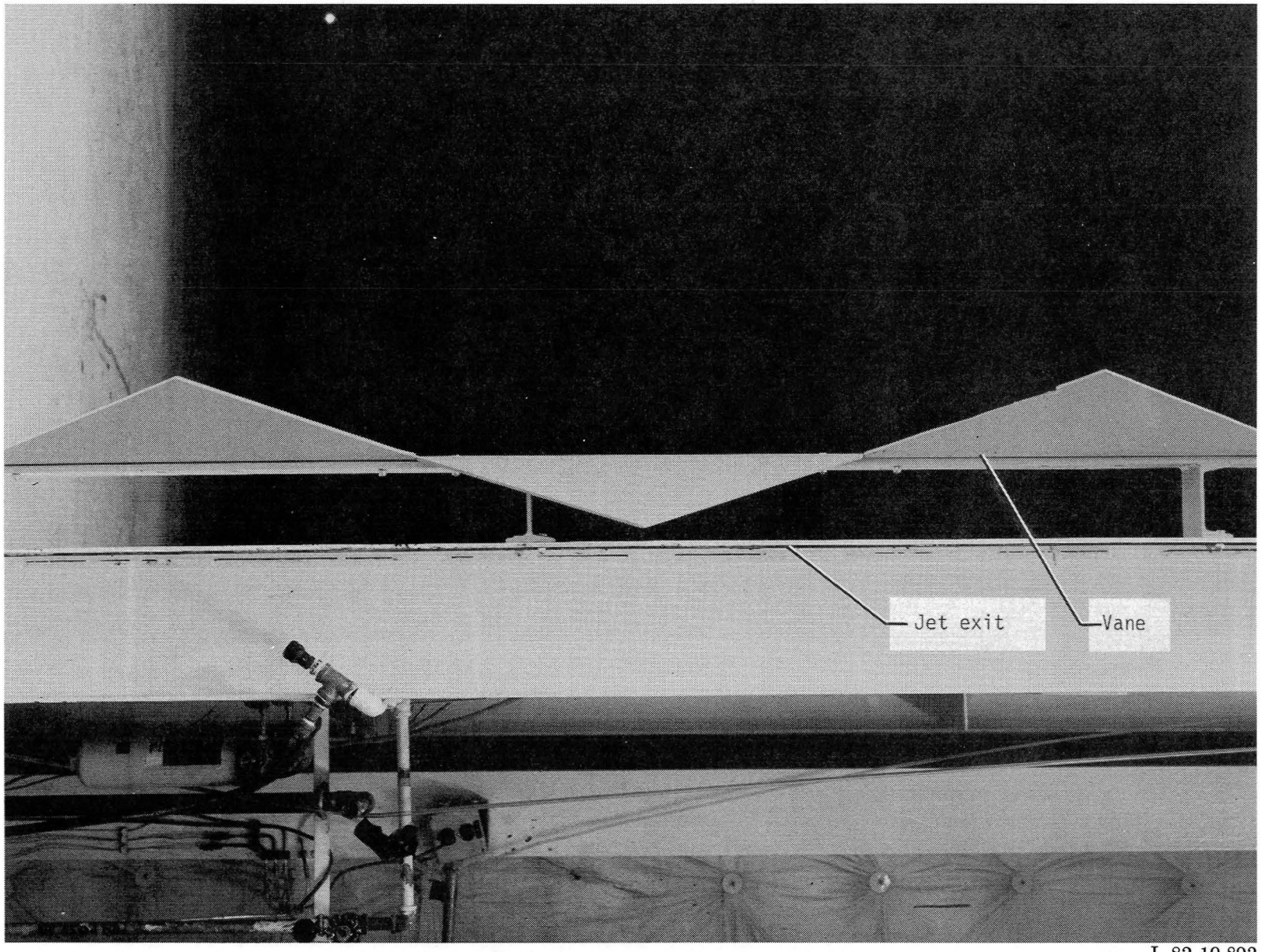

L-82-10,892

(b) Close-up view.

Figure 5. Concluded.

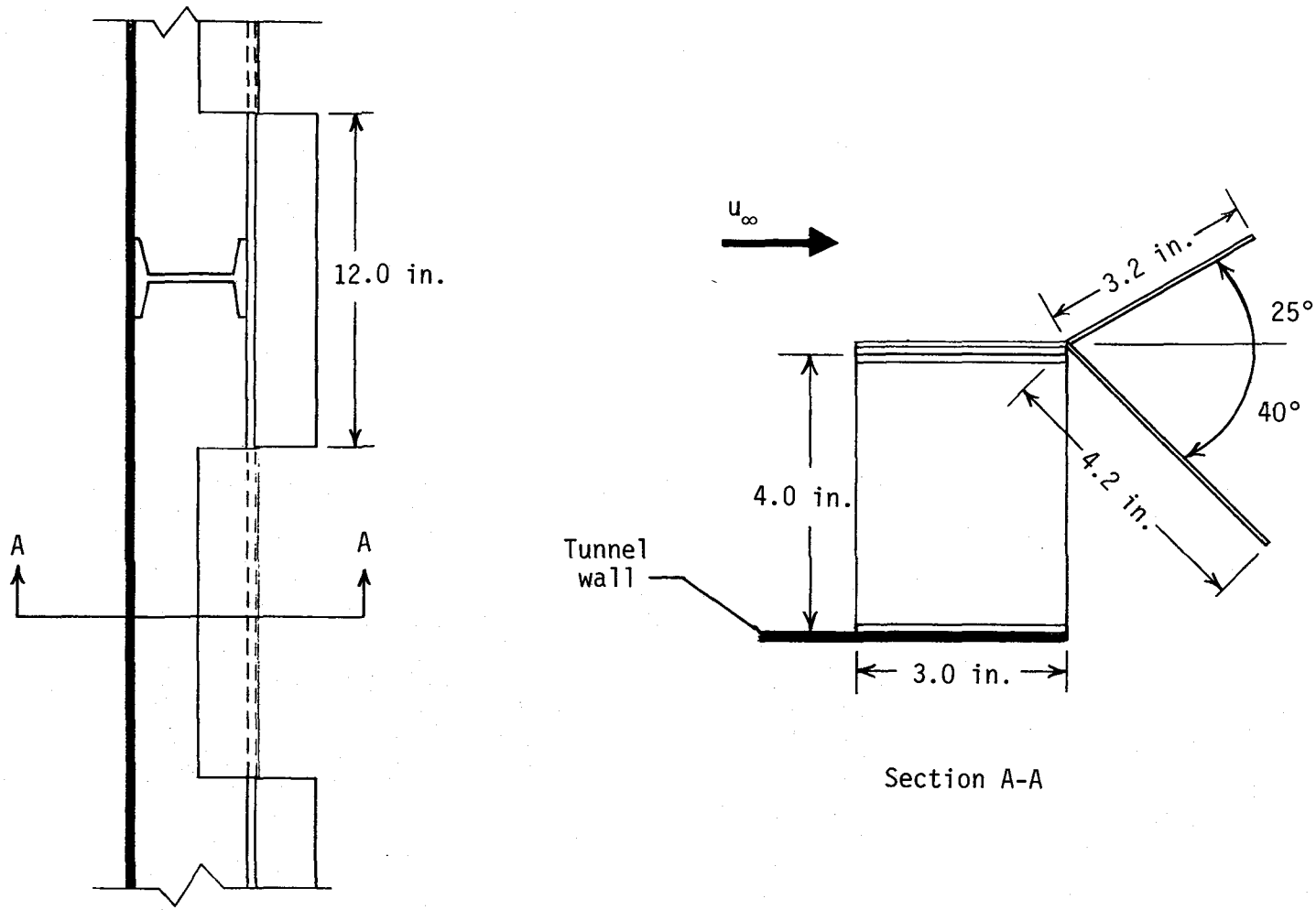

Figure 6. Sketch of rectangular vane geometry.

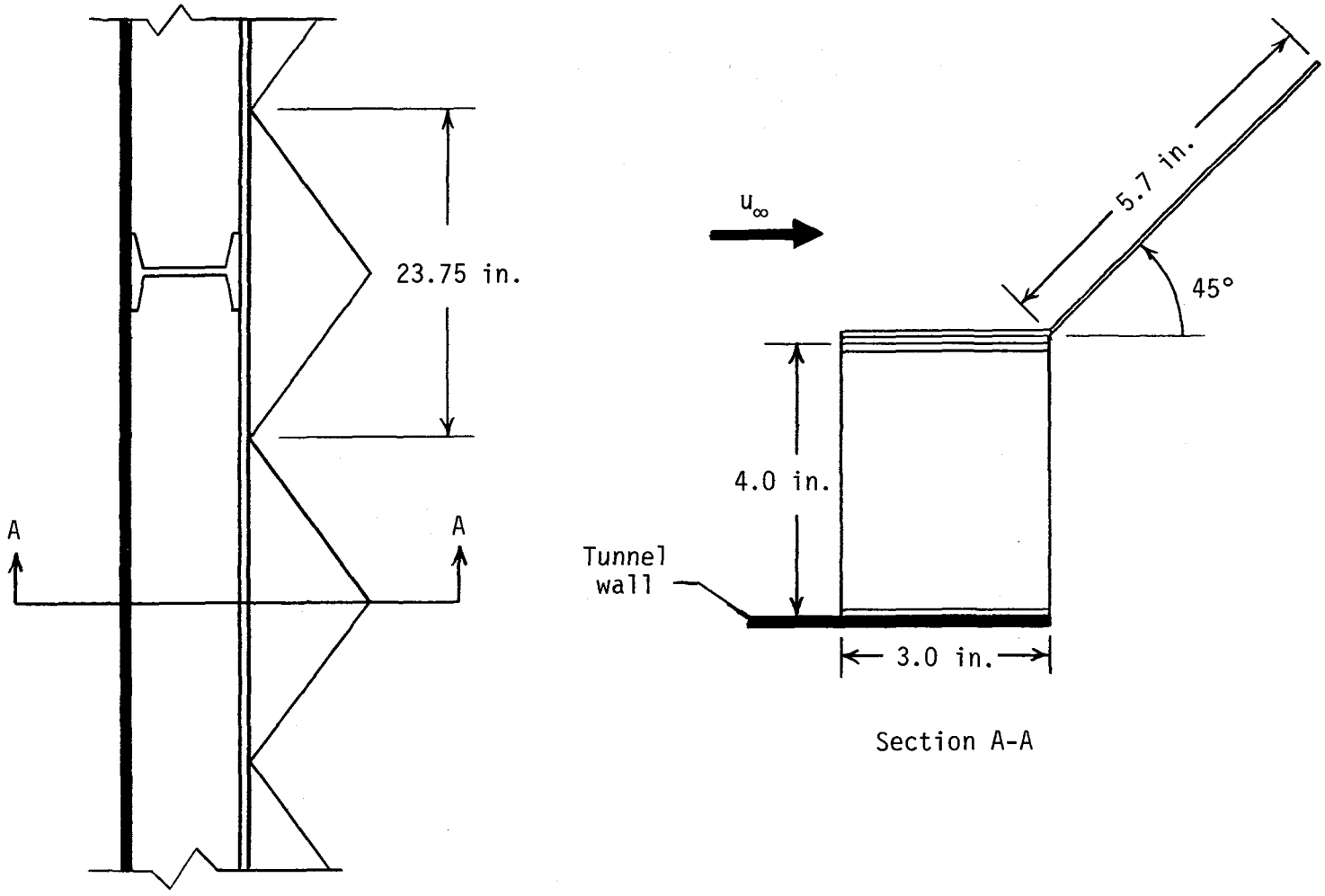

Figure 7. Sketch of triangular vane geometry.

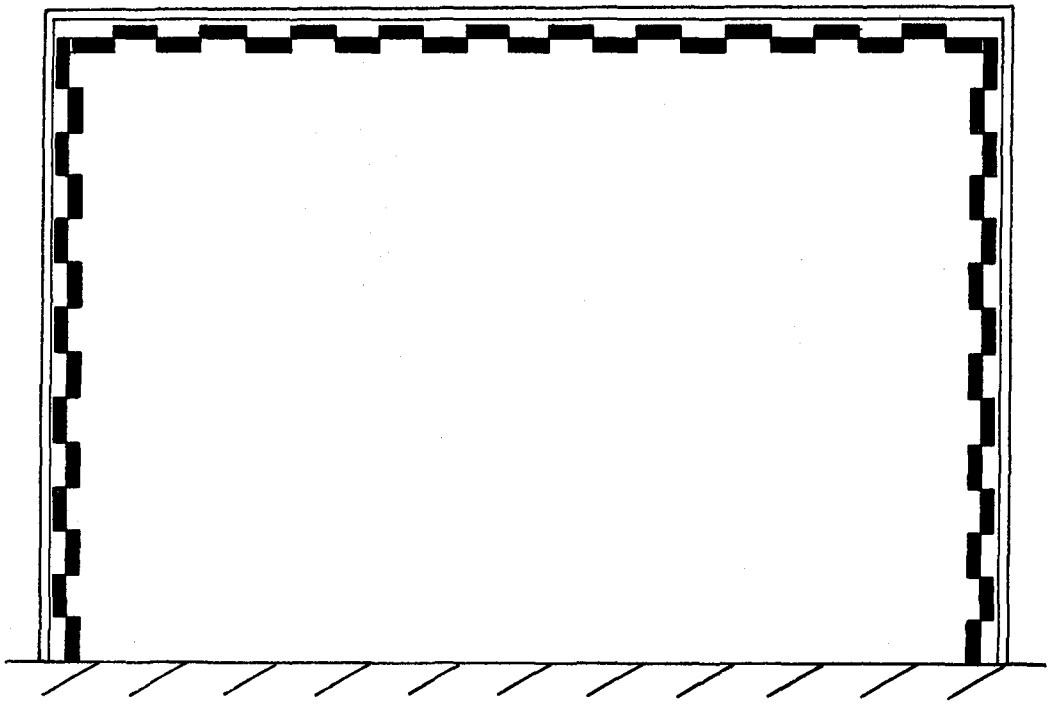

(a) Configurations 1 and 2.

Figure 8. View looking upstream at jet exit vane configurations.

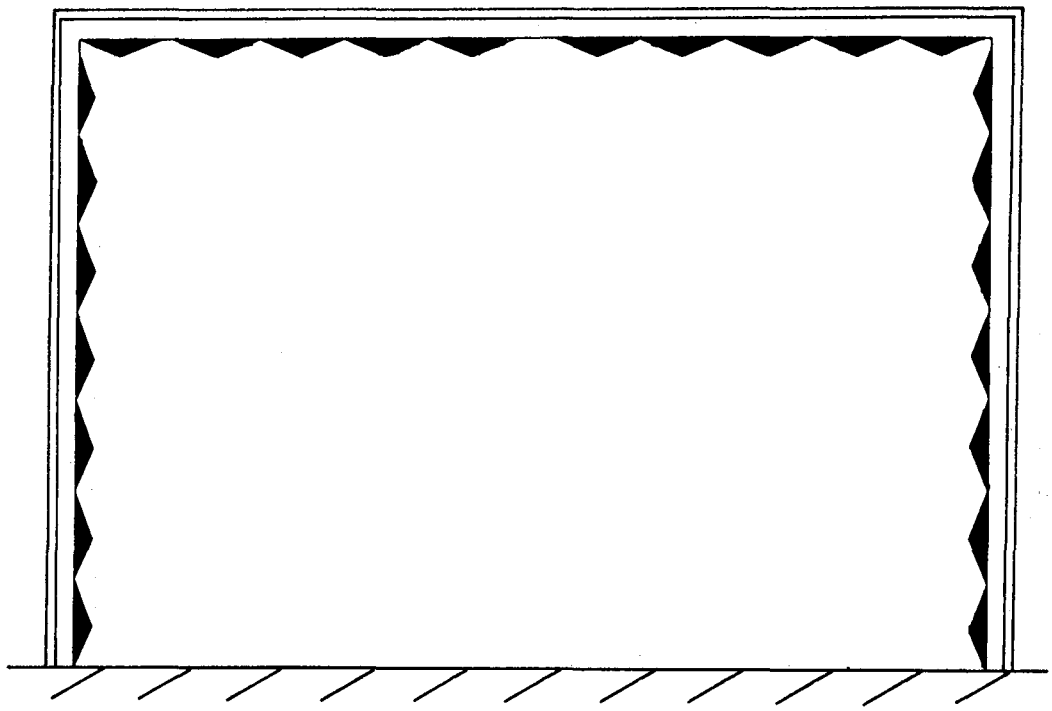

(b) Configuration 3.

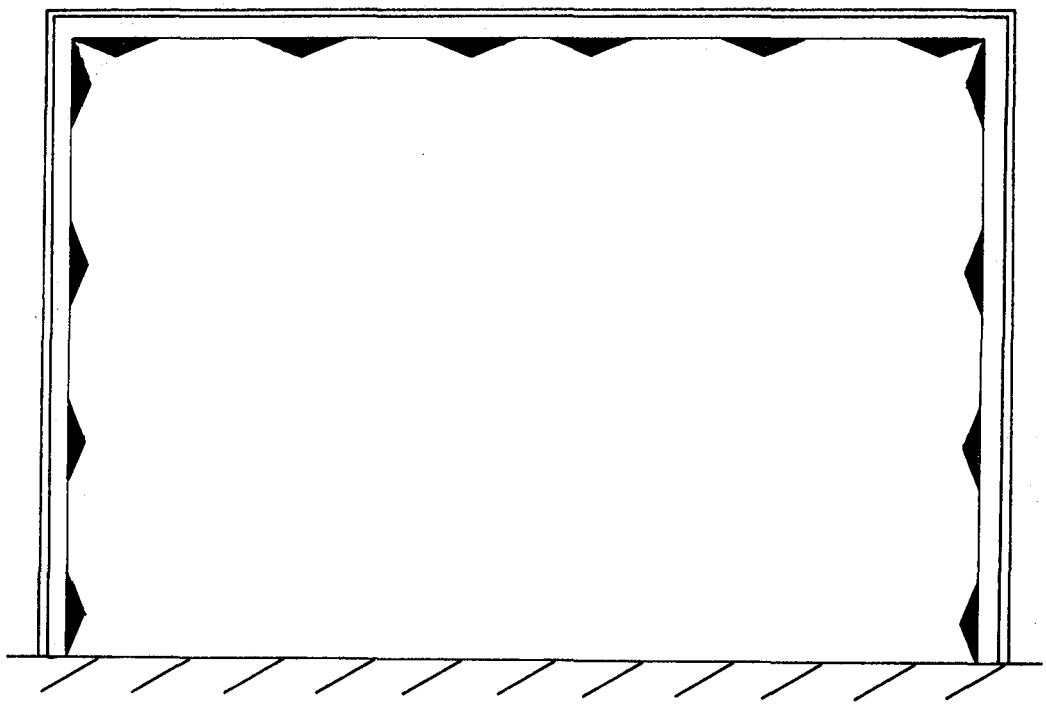

(c) Configuration 4.

Figure 8. Continued.

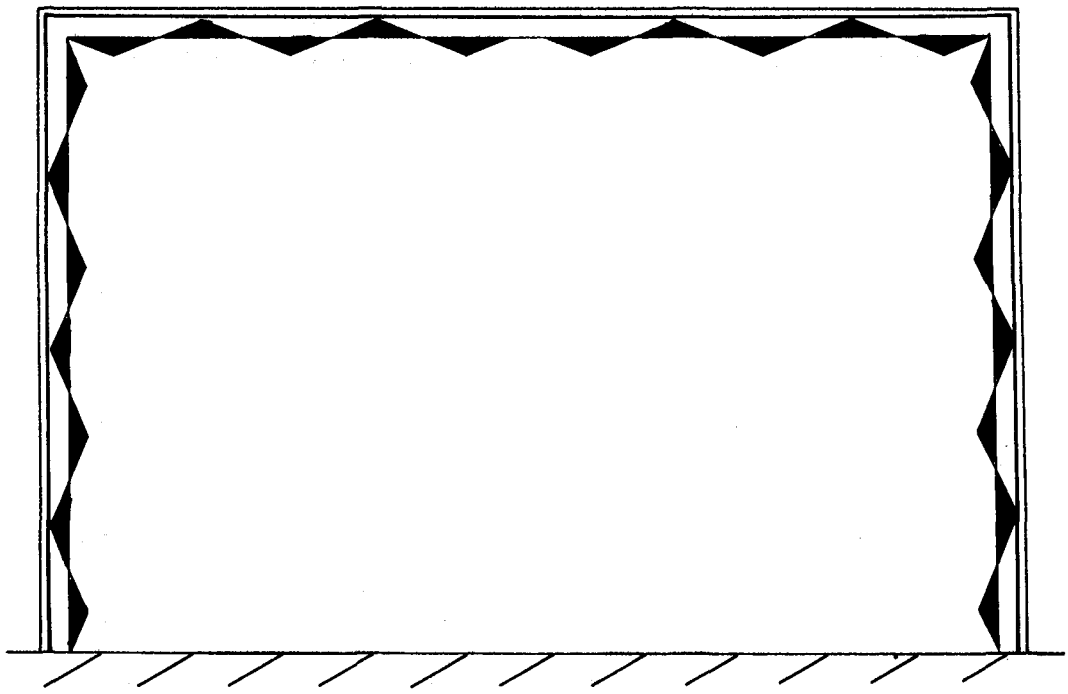

(d) Configuration 5.

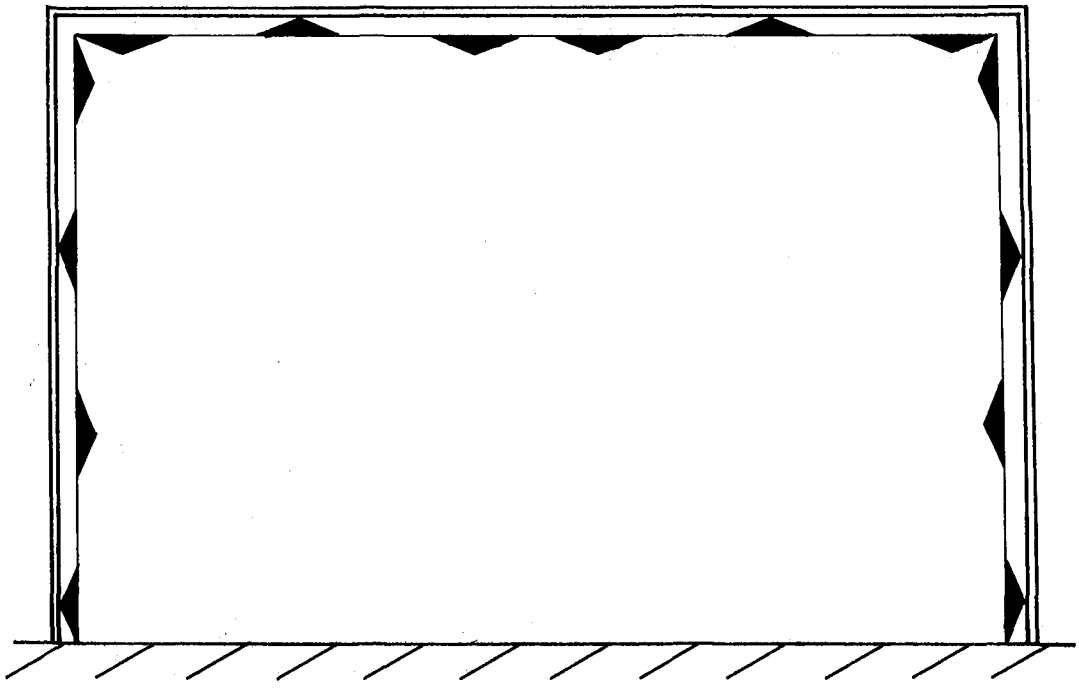

(e) Configuration 6.

Figure 8. Concluded.

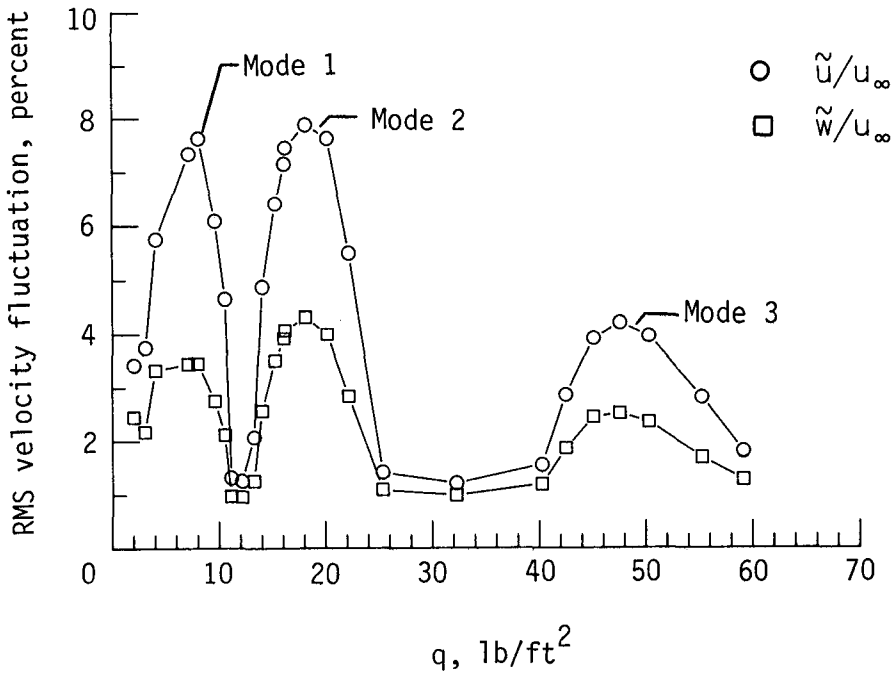

Figure 9. RMS velocity fluctuations for baseline configuration.

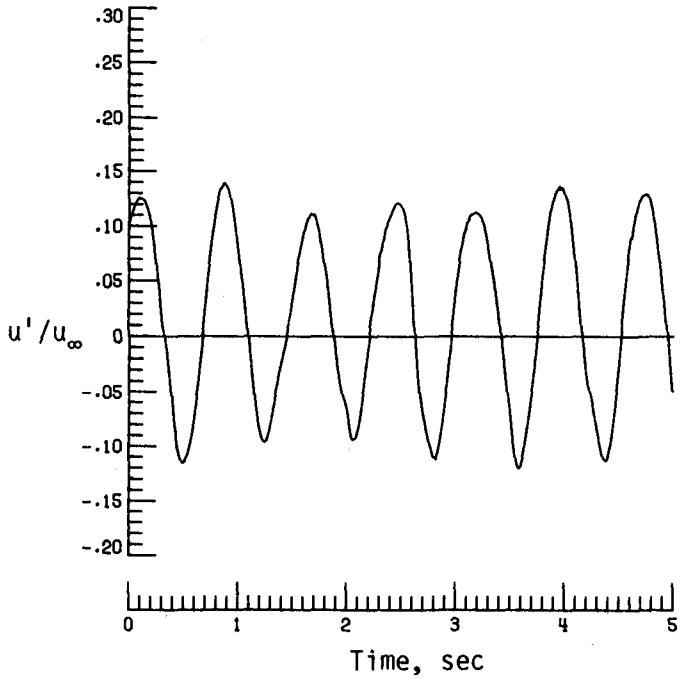

(a) Time history of streamwise velocity fluctuations.

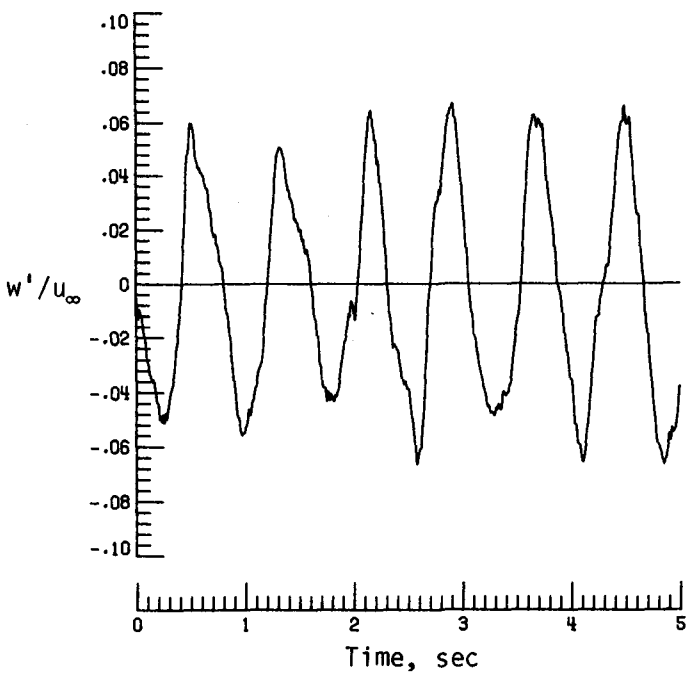

(b) Time history of vertical velocity fluctuations.

Figure 10. Dynamic-flow quality for baseline configuration at $q = 8.03$ lb/ft^2 (mode 1).

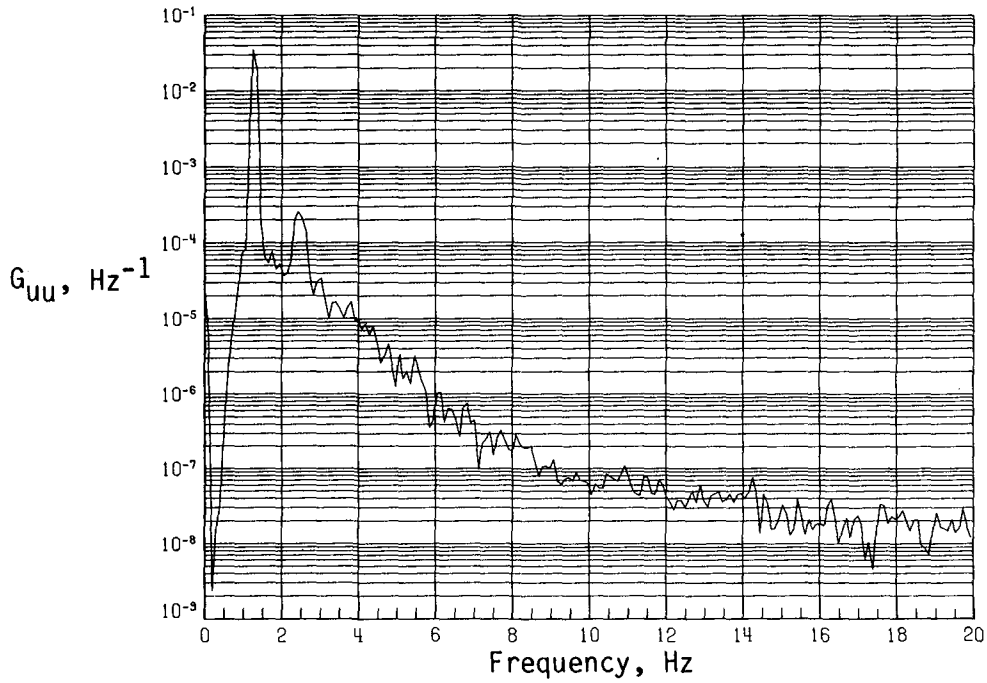

(c) PSD of streamwise velocity fluctuations.

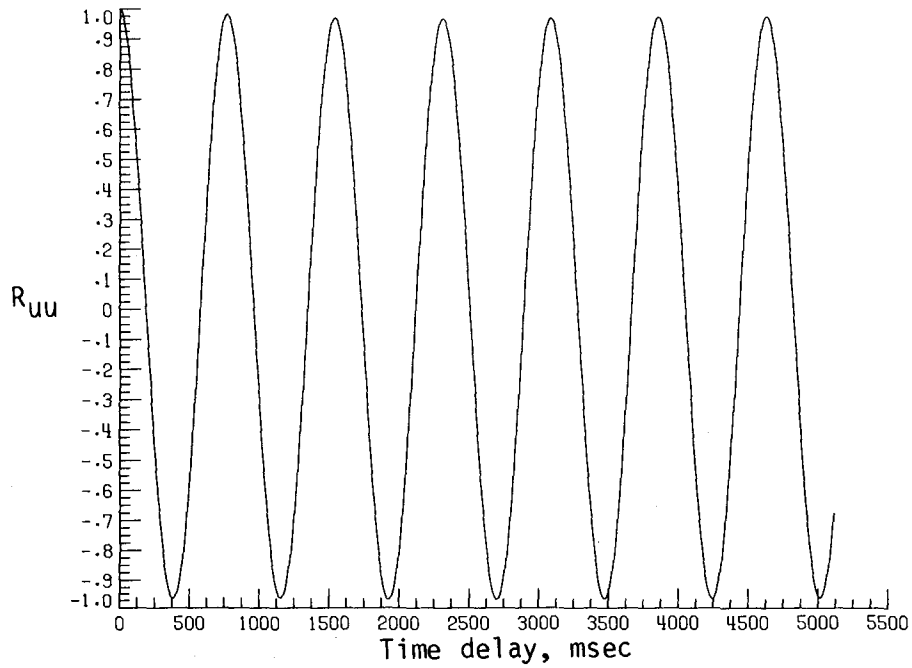

(d) Normalized autocorrelation of streamwise velocity fluctuations. $\sigma = 0.0763$.

Figure 10. Continued.

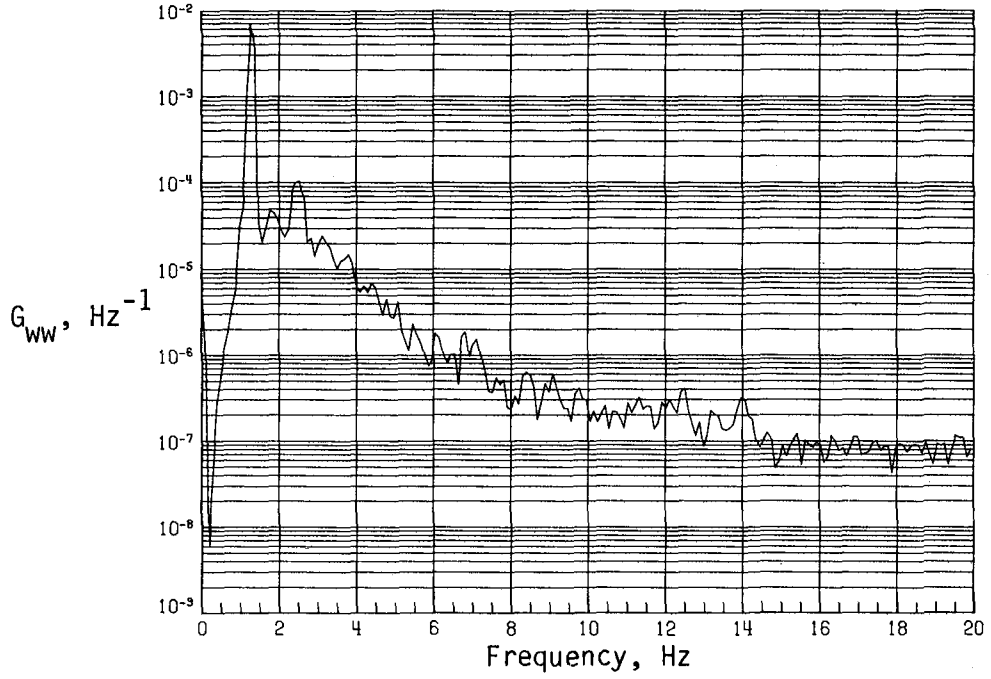

(e) PSD of vertical velocity fluctuations.

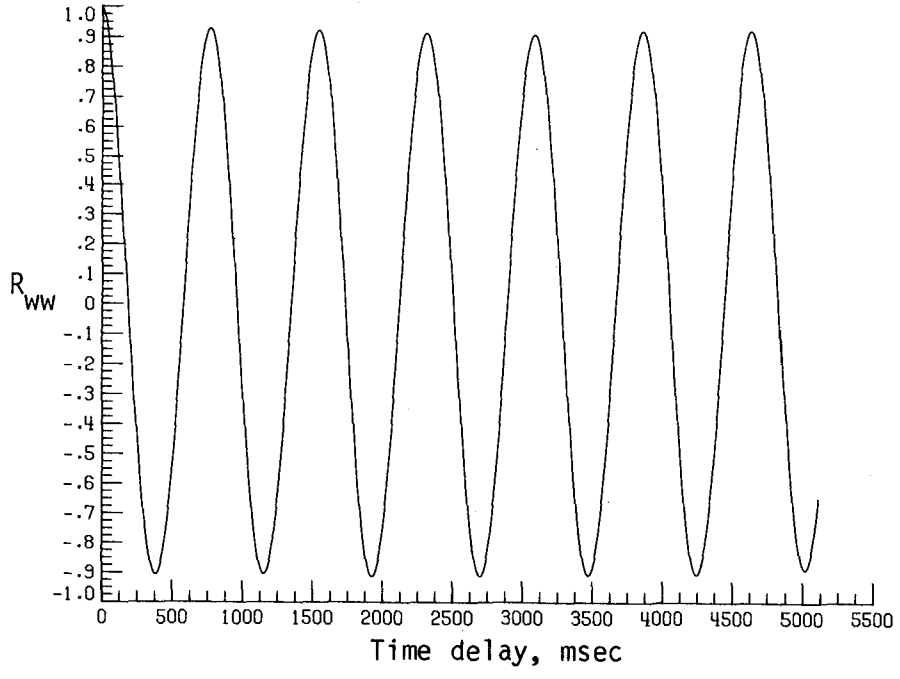

(f) Normalized autocorrelation of vertical velocity fluctuations. $\sigma = 0.0345$.

Figure 10. Concluded.

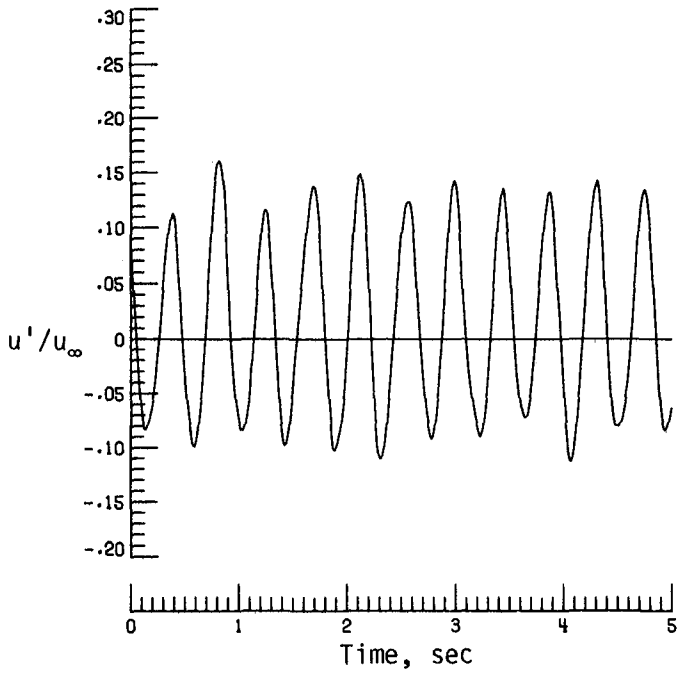

(a) Time history of streamwise velocity fluctuations.

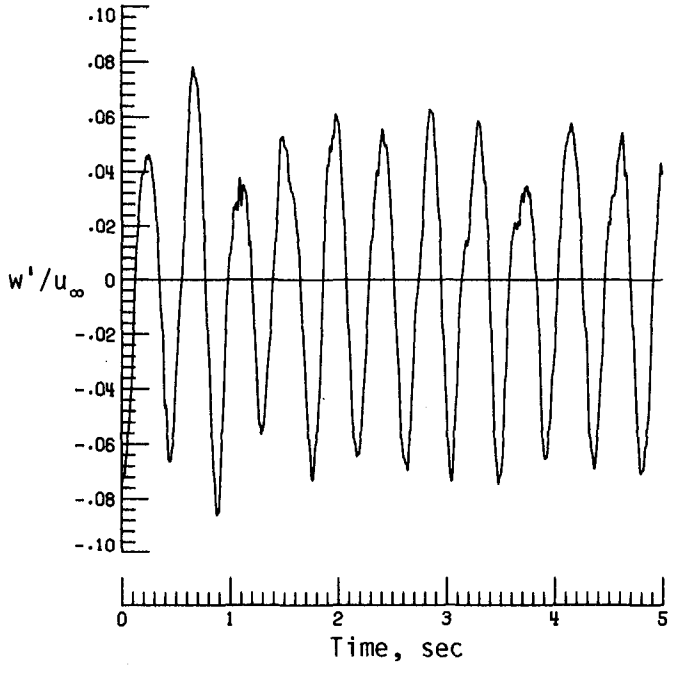

(b) Time history of vertical velocity fluctuations.

Figure 11. Dynamic-flow quality for baseline configuration at $q = 18.08$ lb/ft^2 (mode 2).

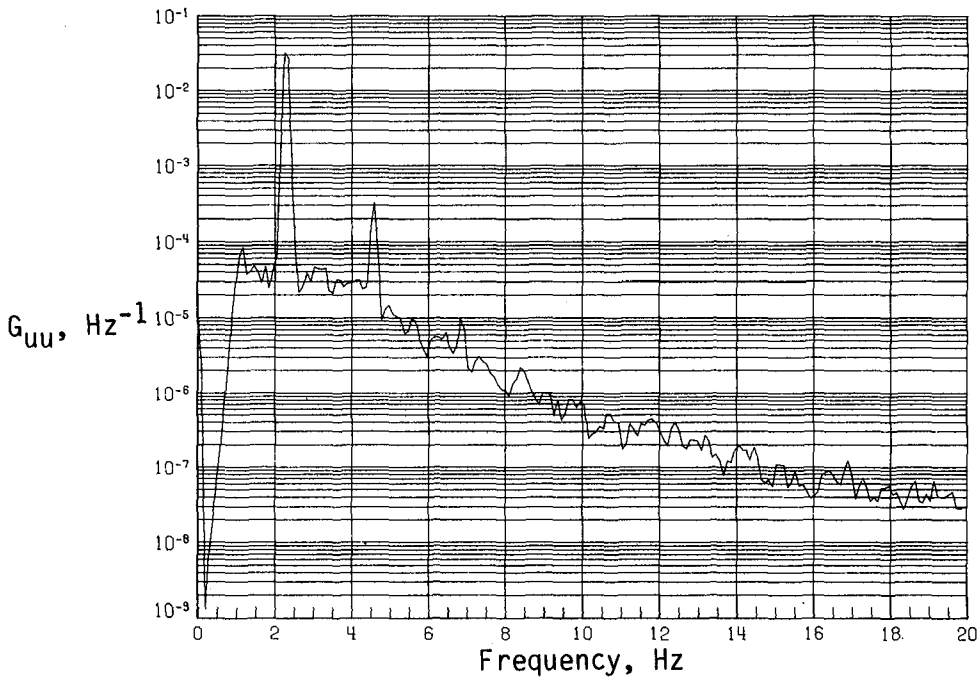

(c) PSD of streamwise velocity fluctuations.

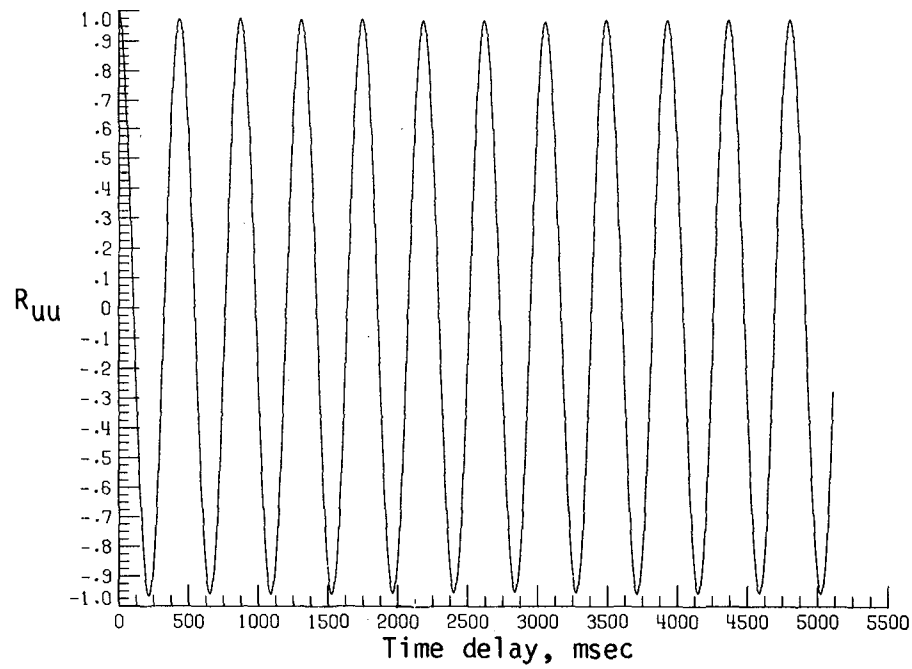

(d) Normalized autocorrelation of streamwise velocity fluctuations. $\sigma = 0.0789$.

Figure 11. Continued.

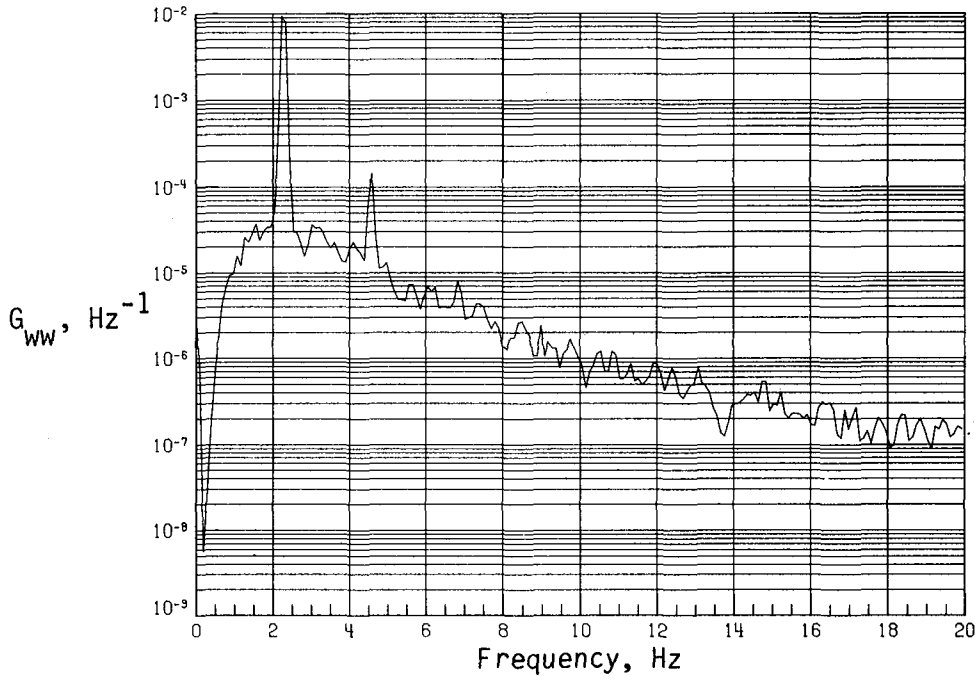

(e) PSD of vertical velocity fluctuations.

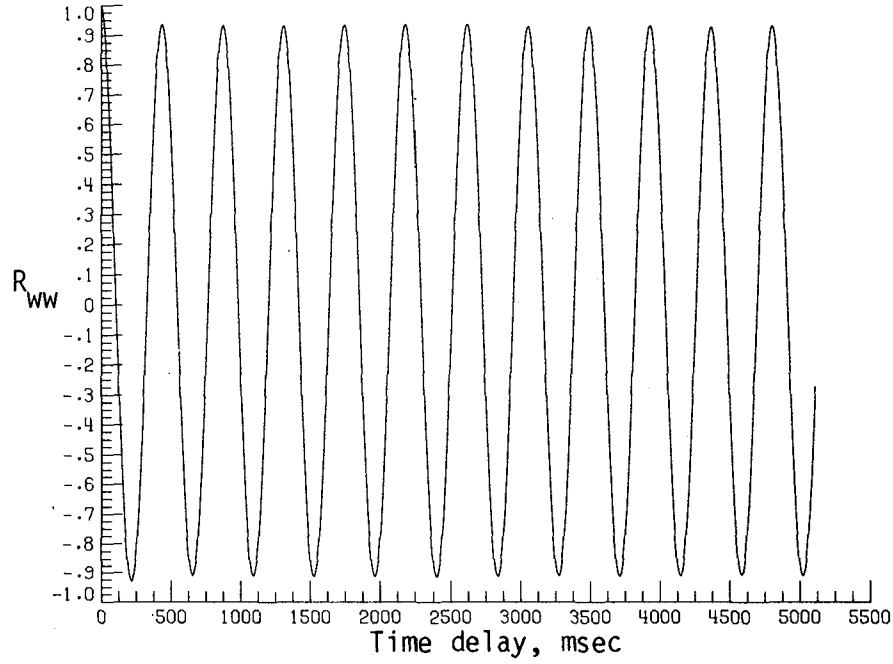

(f) Normalized autocorrelation of vertical velocity fluctuations. $\sigma = 0.0433$.

Figure 11. Concluded.

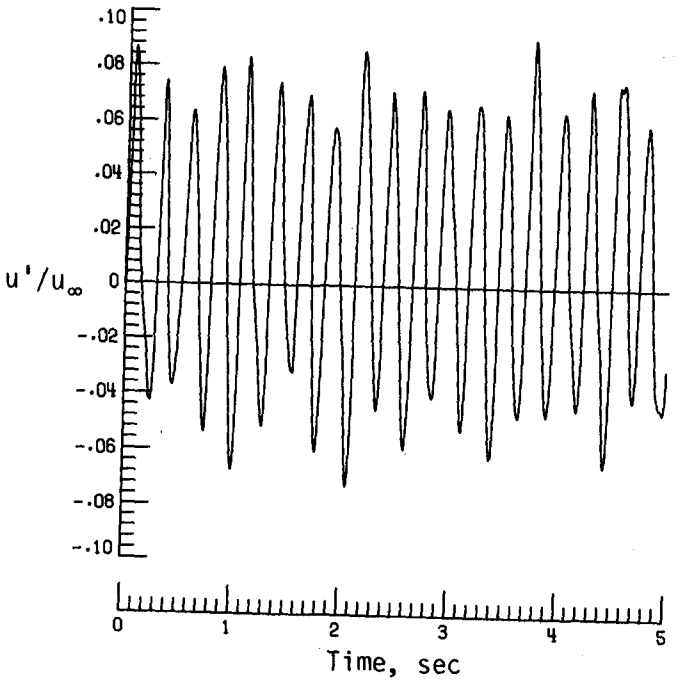

(a) Time history of streamwise velocity fluctuations.

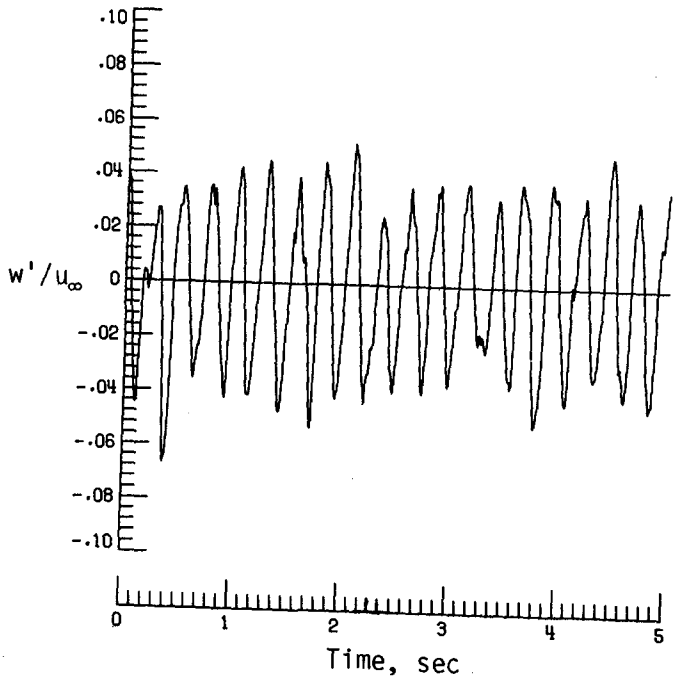

(b) Time history of vertical velocity fluctuations.

Figure 12. Dynamic-flow quality for baseline configuration at $q = 47.58$ lb/ft^2 (mode 3).

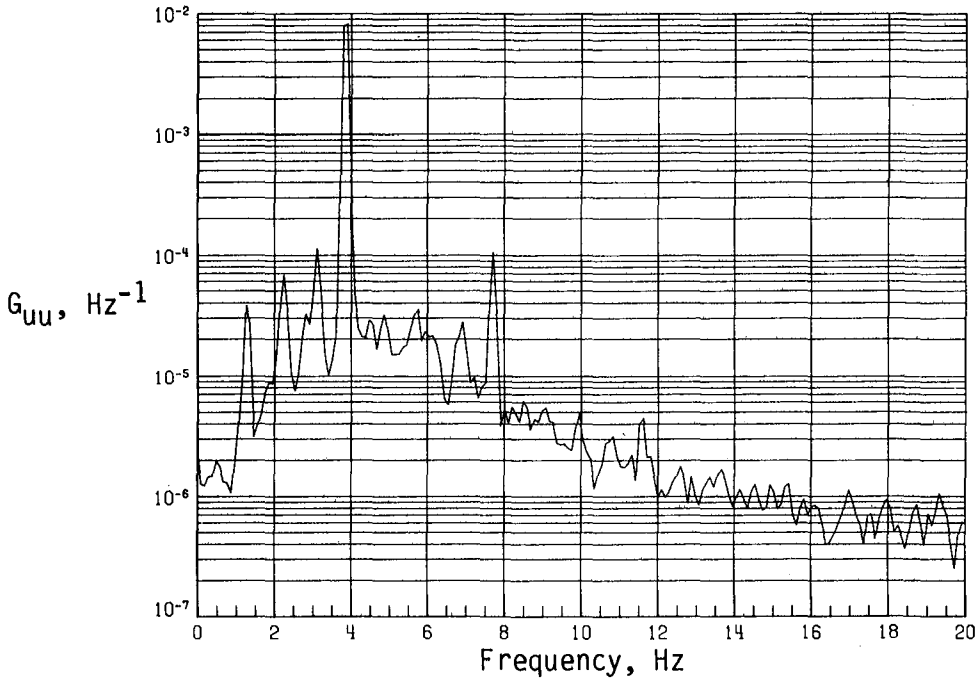

(c) PSD of streamwise velocity fluctuations.

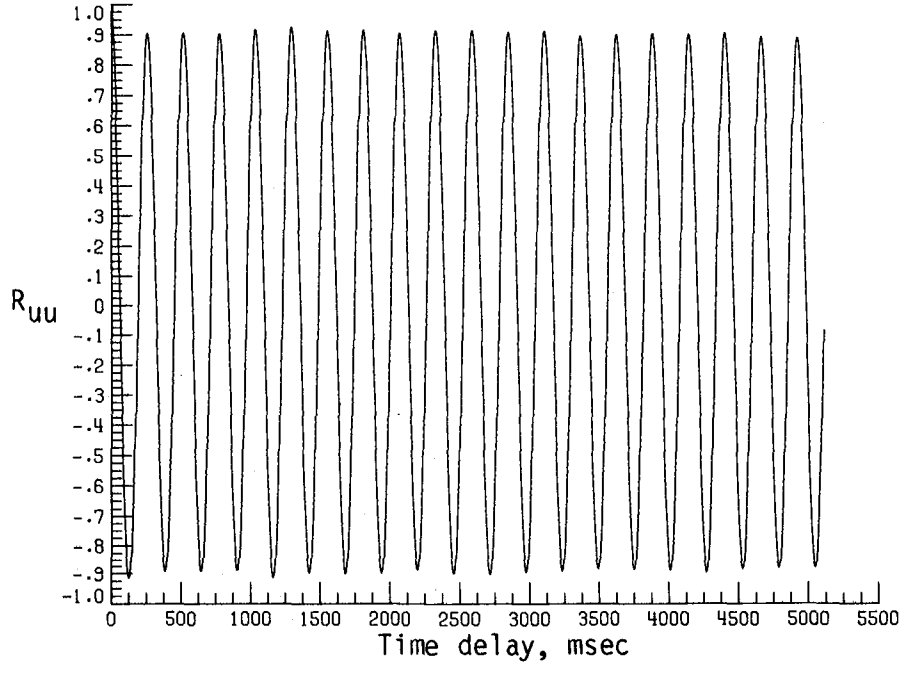

(d) Normalized autocorrelation of streamwise velocity fluctuations. $\sigma = 0.0421$.

Figure 12. Continued.

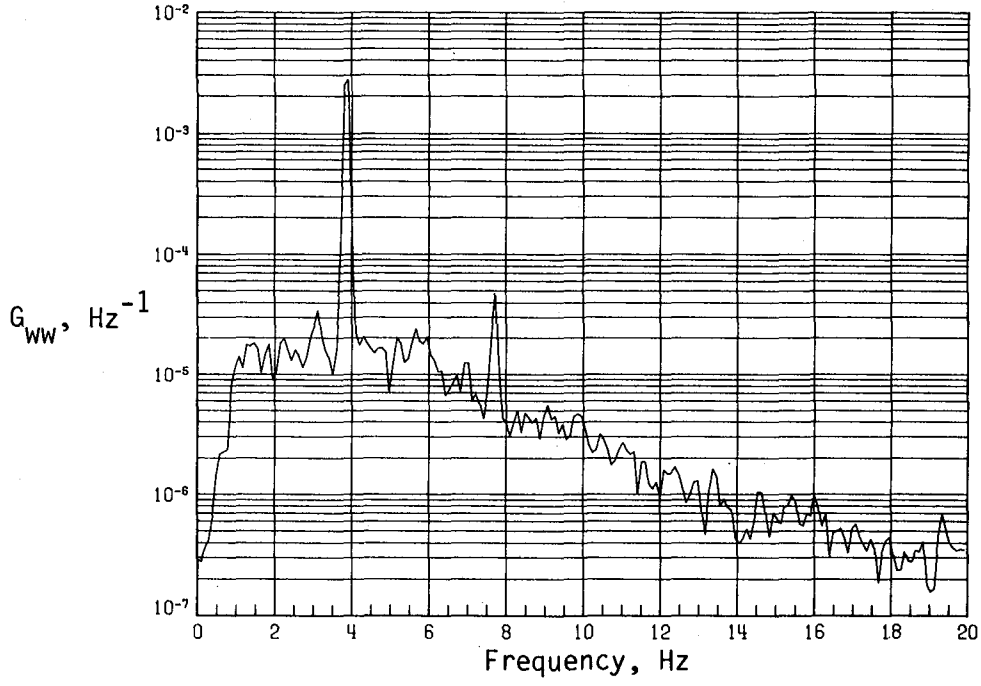

(e) PSD of vertical velocity fluctuations.

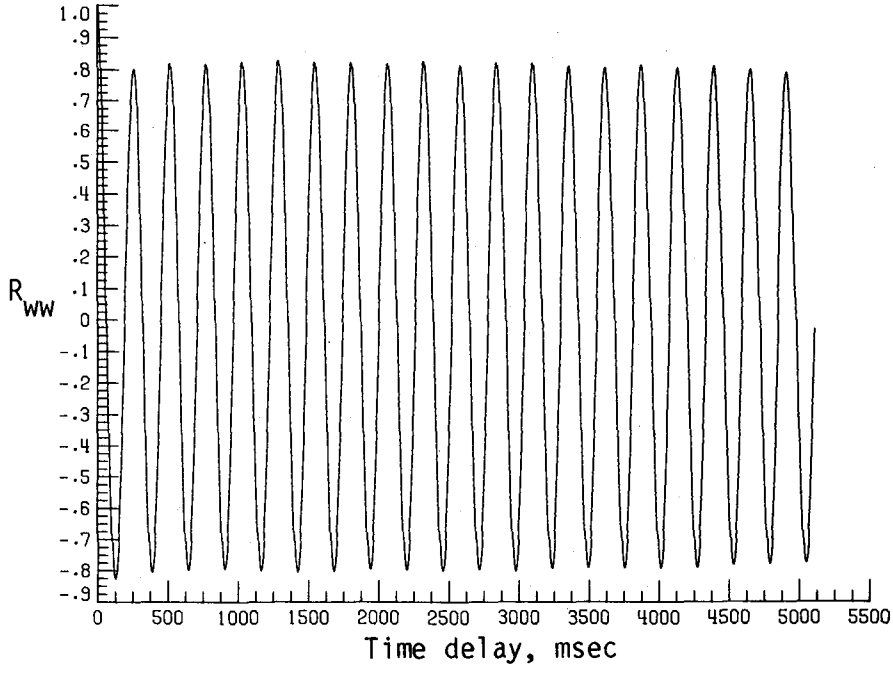

(f) Normalized autocorrelation of vertical velocity fluctuations. $\sigma = 0.0252$.

Figure 12. Concluded.

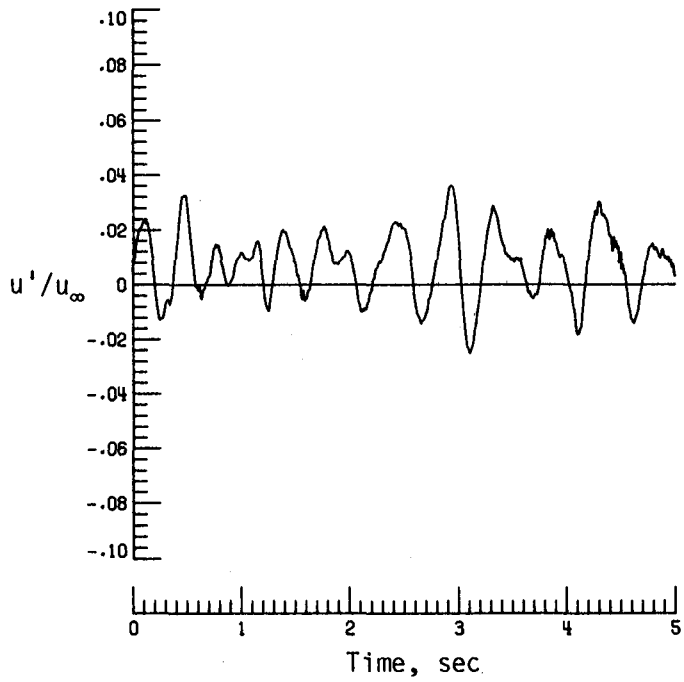

(a) Time history of streamwise velocity fluctuations.

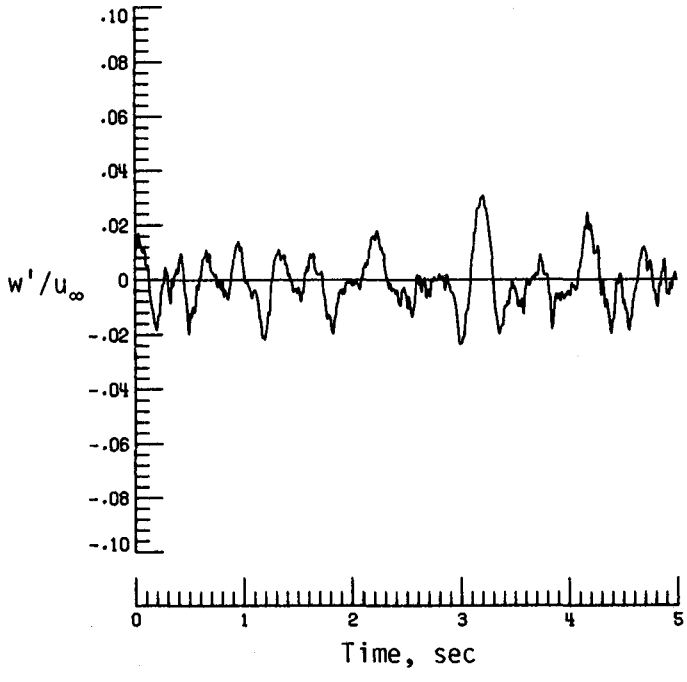

(b) Time history of vertical velocity fluctuations.

Figure 13. Dynamic-flow quality for baseline configuration at $q = 12.09$ lb/ft^2.

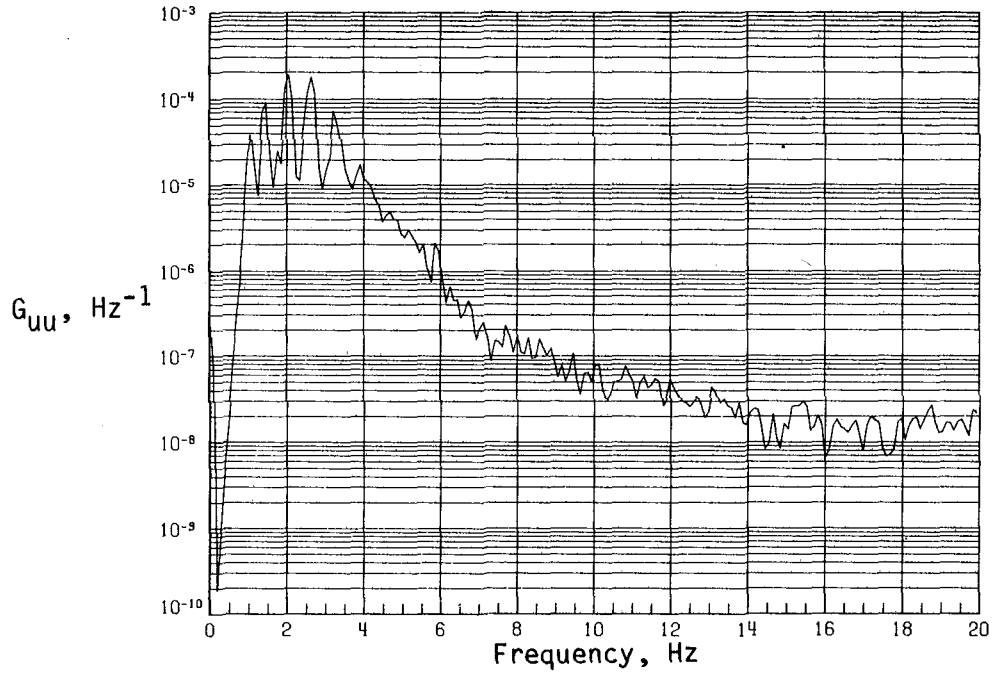

(c) PSD of streamwise velocity fluctuations.

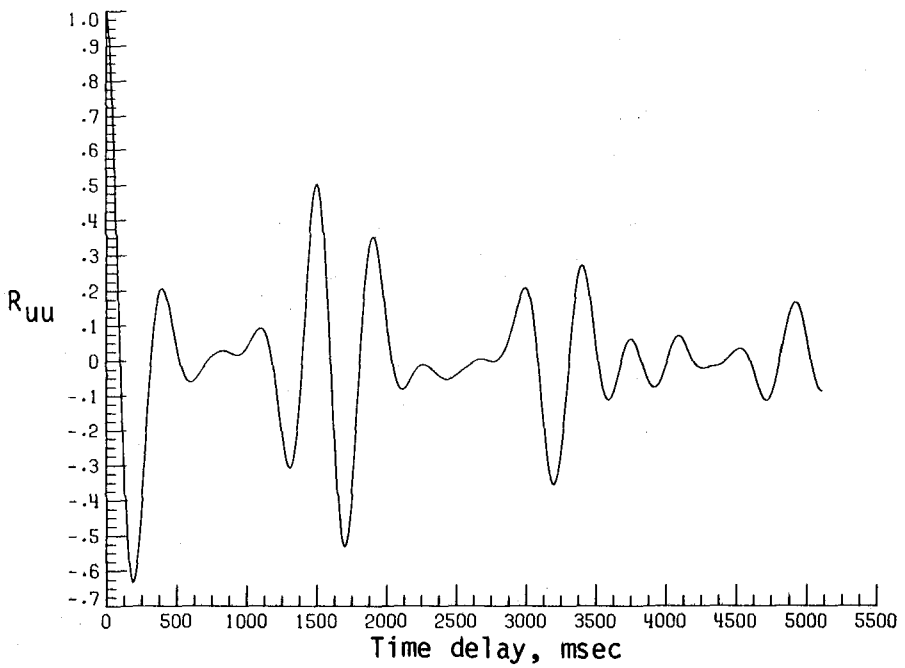

(d) Normalized autocorrelation of streamwise velocity fluctuations. $\sigma = 0.0127$.

Figure 13. Continued.

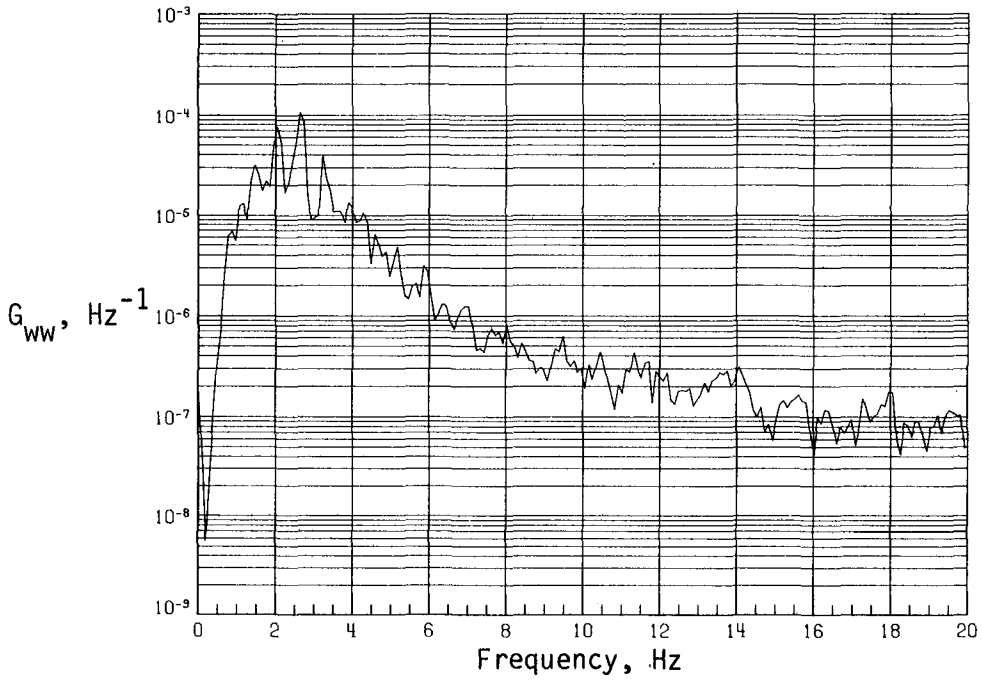

(e) PSD of vertical velocity fluctuations.

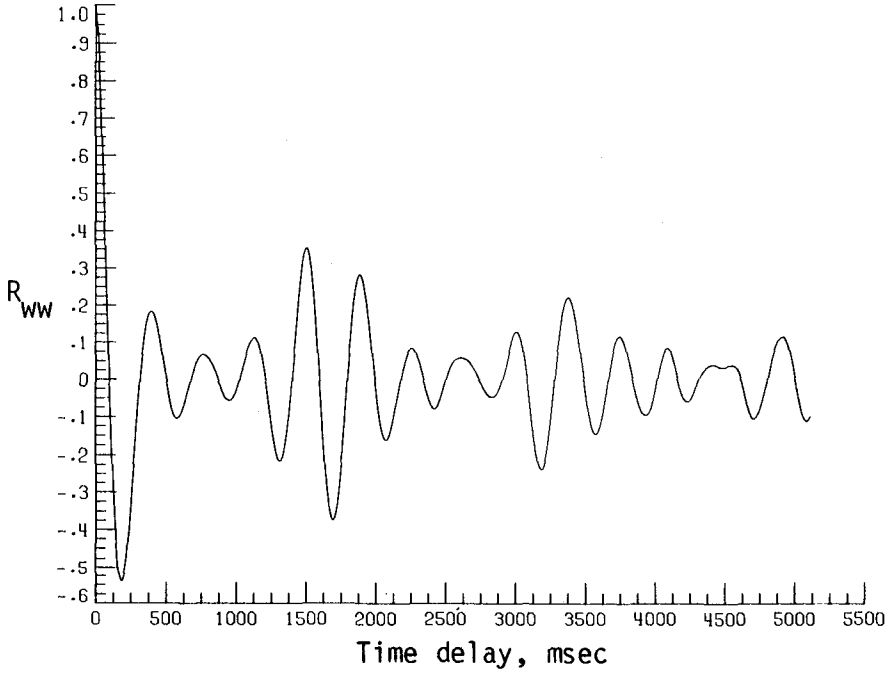

(f) Normalized autocorrelation of vertical velocity fluctuations. $\sigma = 0.0098$.

Figure 13. Concluded.

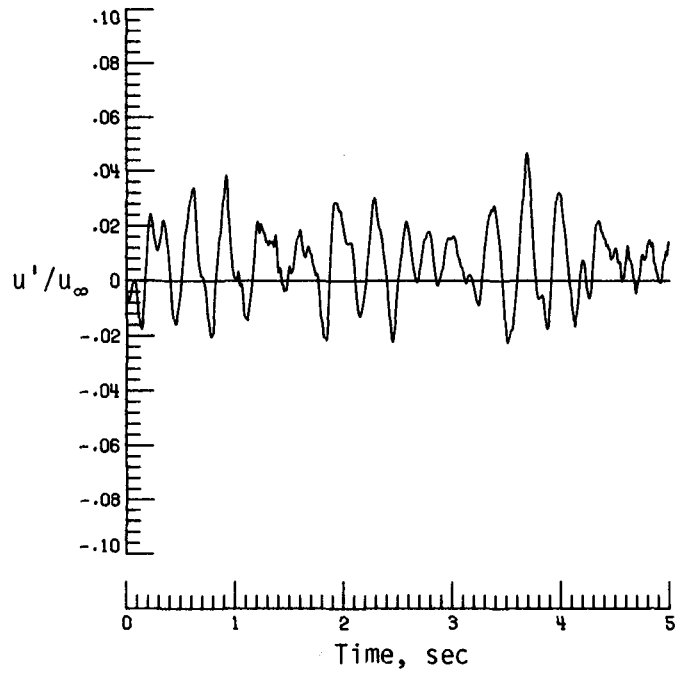

(a) Time history of streamwise velocity fluctuations.

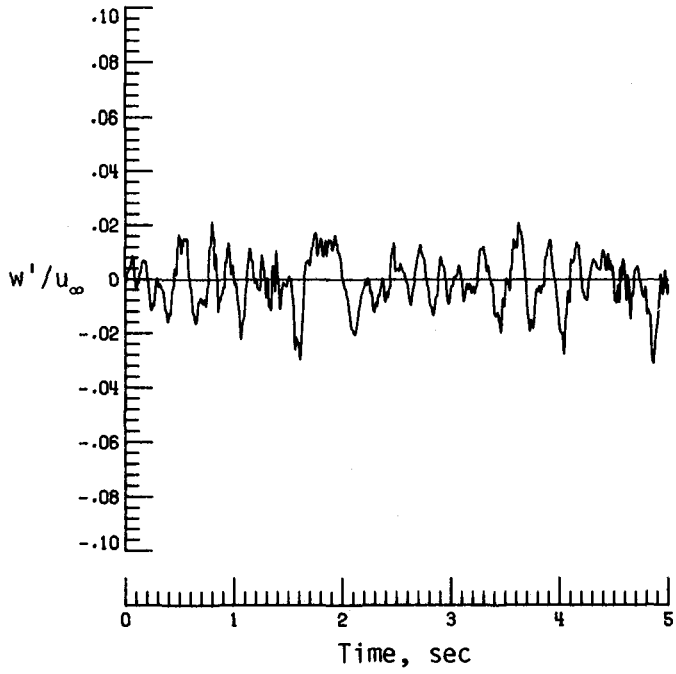

(b) Time history of vertical velocity fluctuations.

Figure 14. Dynamic-flow quality for baseline configuration at $q = 32.21$ lb/ft^2.

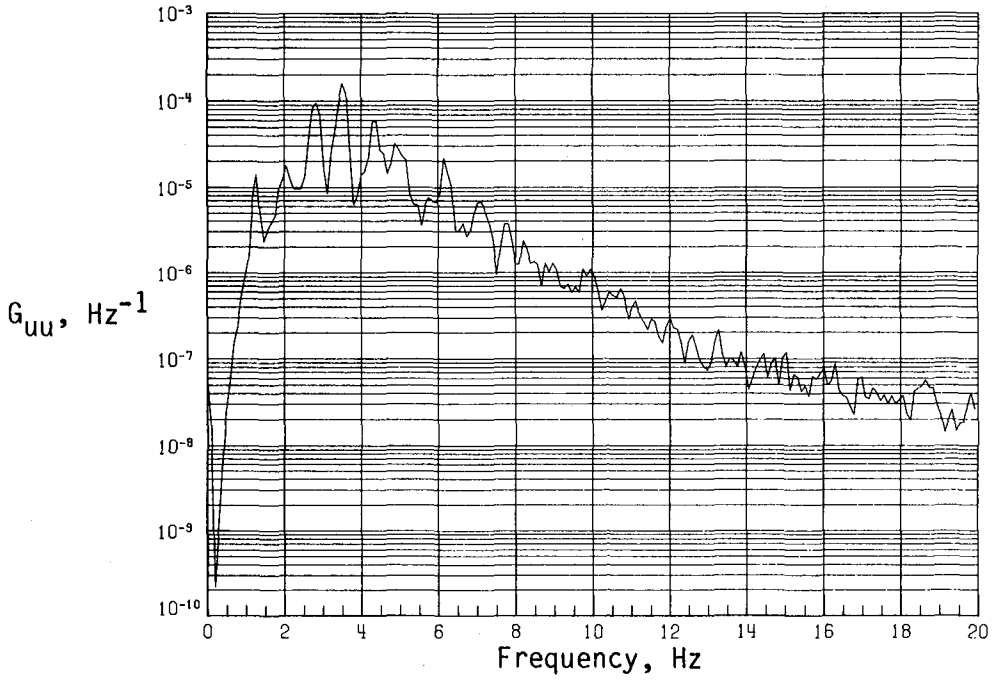

(c) PSD of streamwise velocity fluctuations.

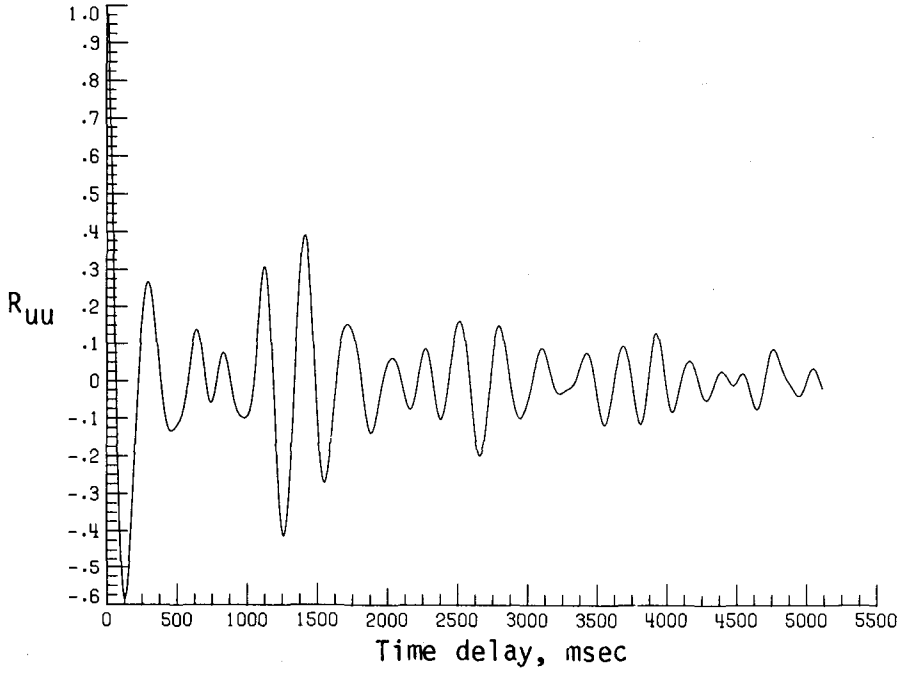

(d) Normalized autocorrelation of streamwise velocity fluctuations. $\sigma = 0.0122$.

Figure 14. Continued.

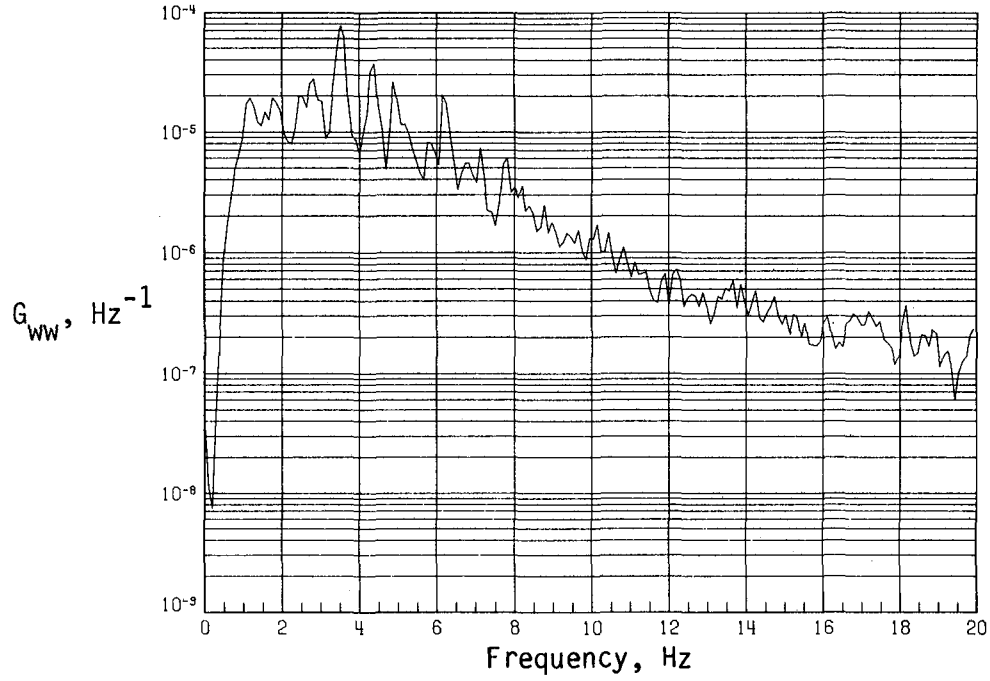

(e) PSD of vertical velocity fluctuations.

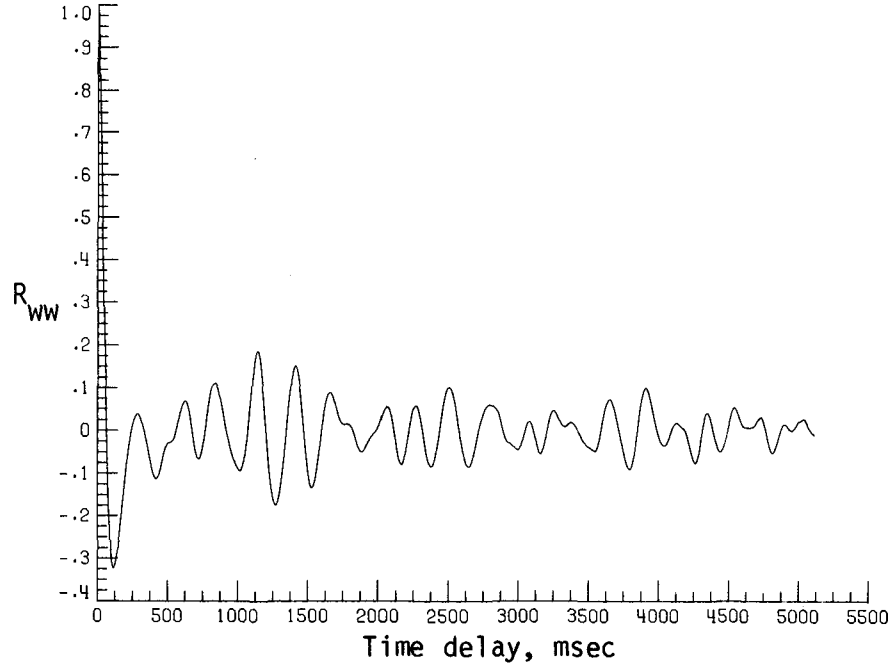

(f) Normalized autocorrelation of vertical velocity fluctuations. $\sigma = 0.0100$.

Figure 14. Concluded.

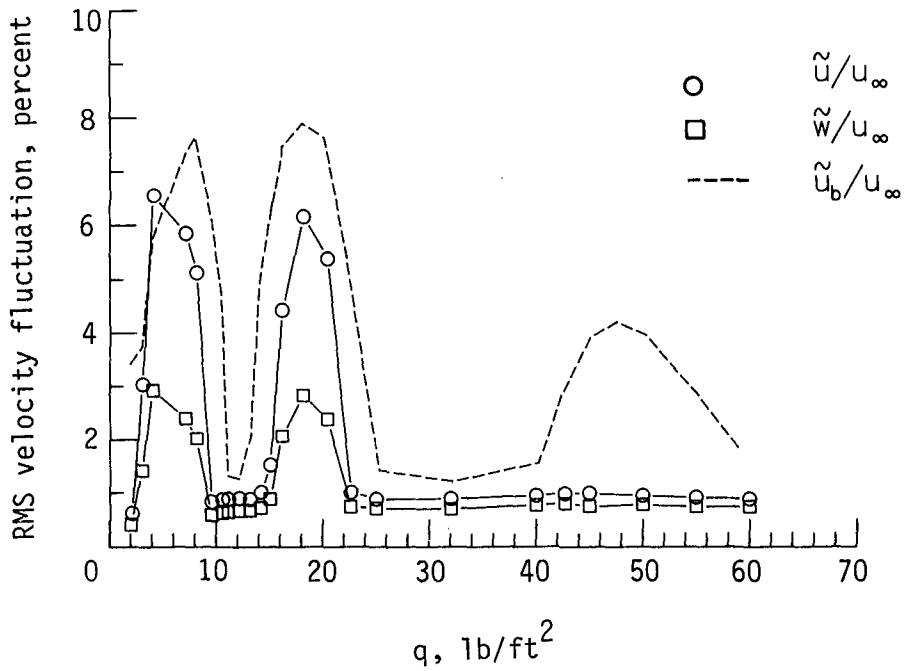

Figure 15. RMS velocity fluctuations for jet exit configuration 1.

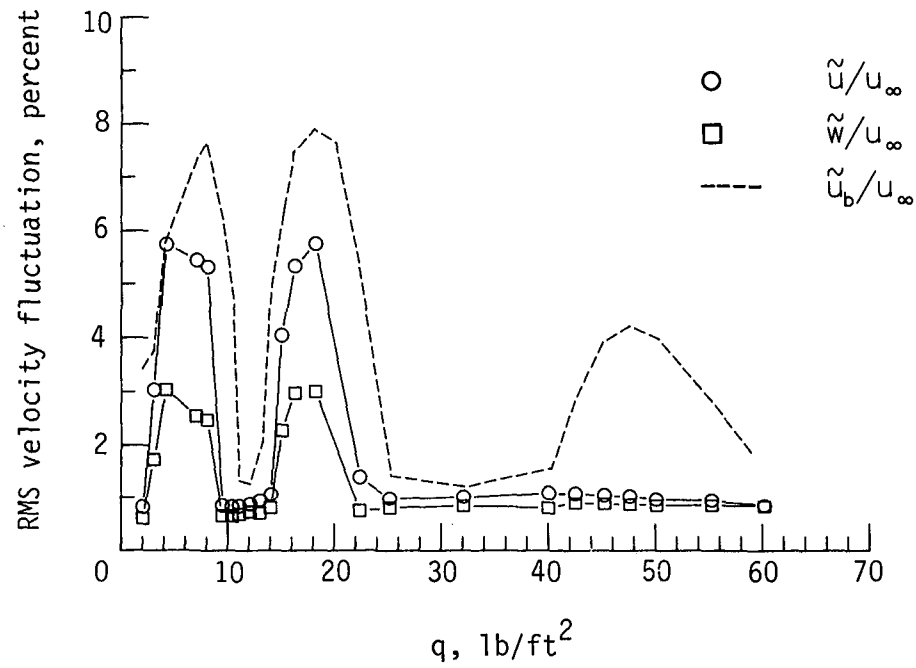

Figure 16. RMS velocity fluctuations for jet exit configuration 2.

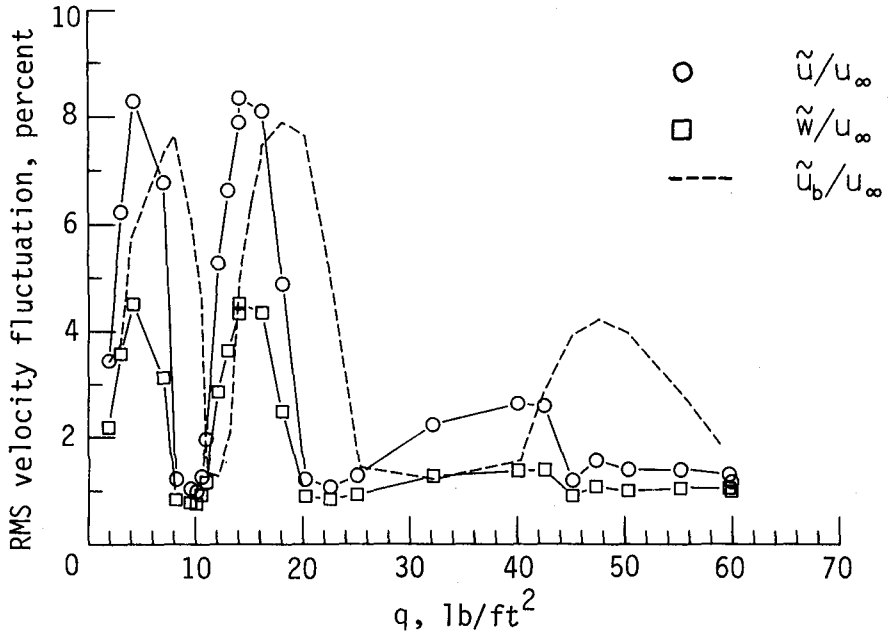

Figure 17. RMS velocity fluctuations for jet exit configuration 3.

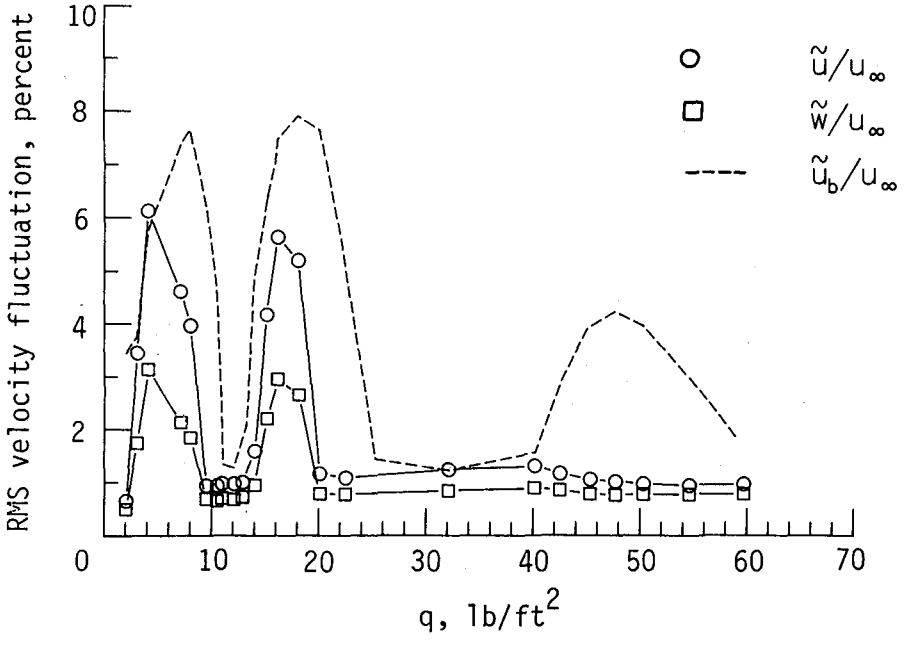

Figure 18. RMS velocity fluctuations for jet exit configuration 4.

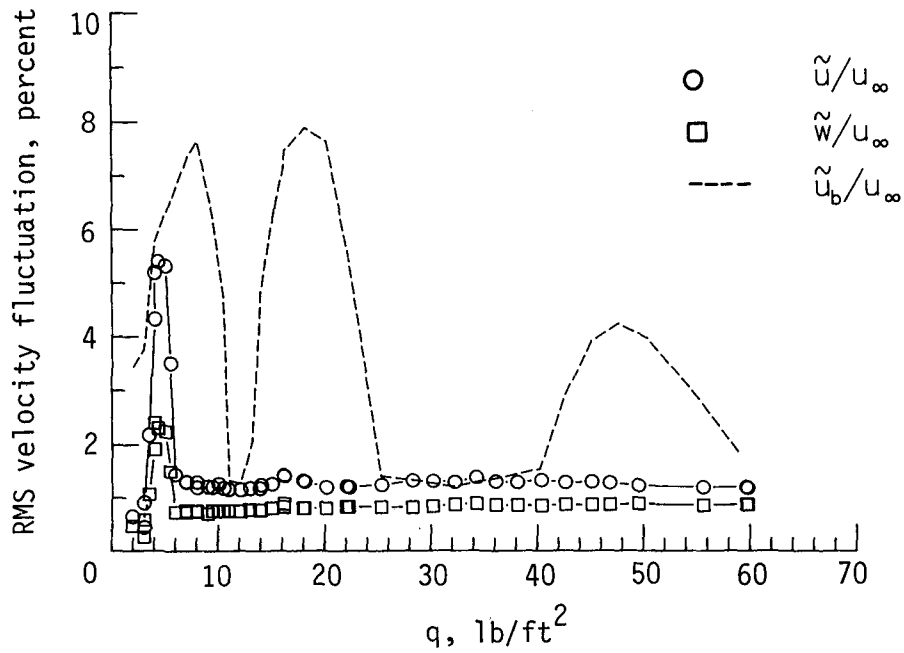

Figure 19. RMS velocity fluctuations for jet exit configuration 5.

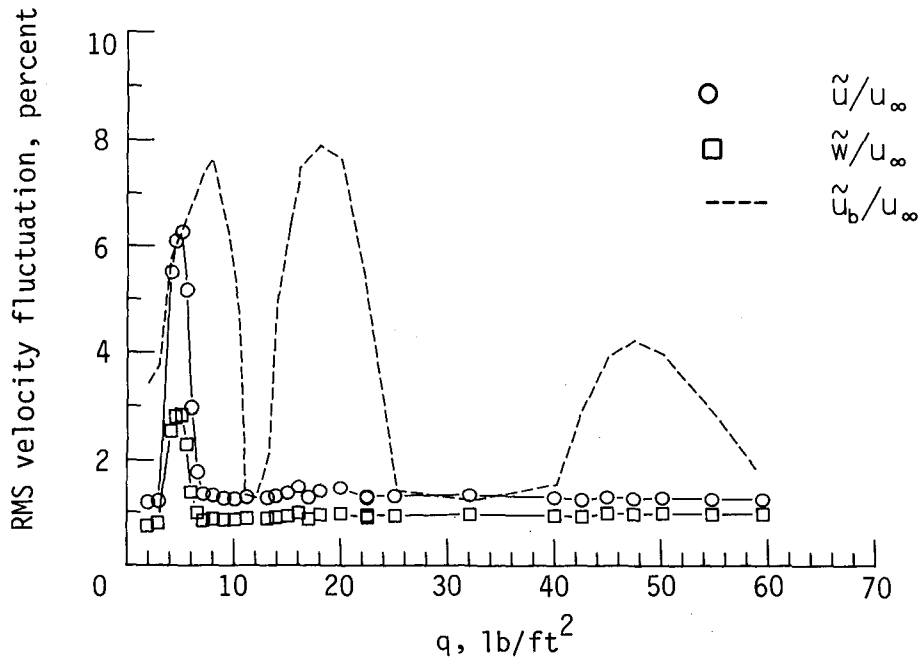

Figure 20. RMS velocity fluctuations for jet exit configuration 6.

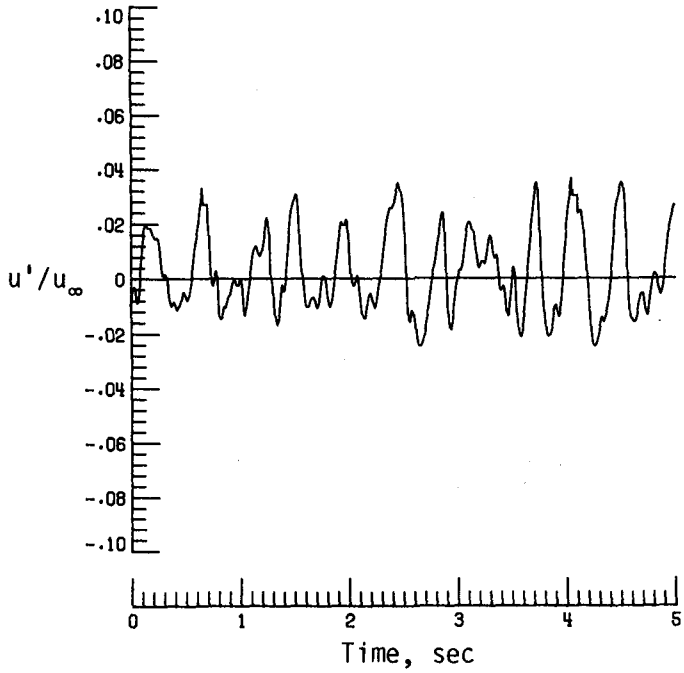

(a) Time history of streamwise velocity fluctuations.

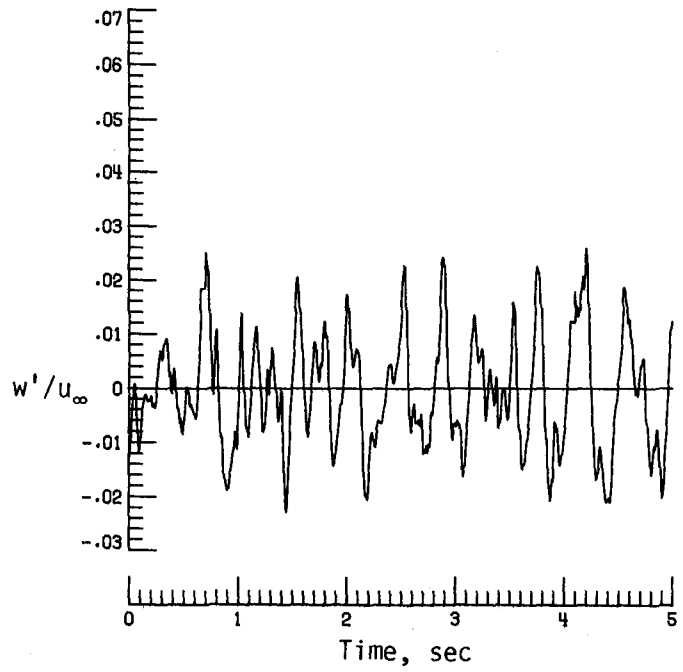

(b) Time history of vertical velocity fluctuations.

Figure 21. Dynamic flow quality for configuration 6 at $q = 18.08$ lb/ft^2 (mode 2).

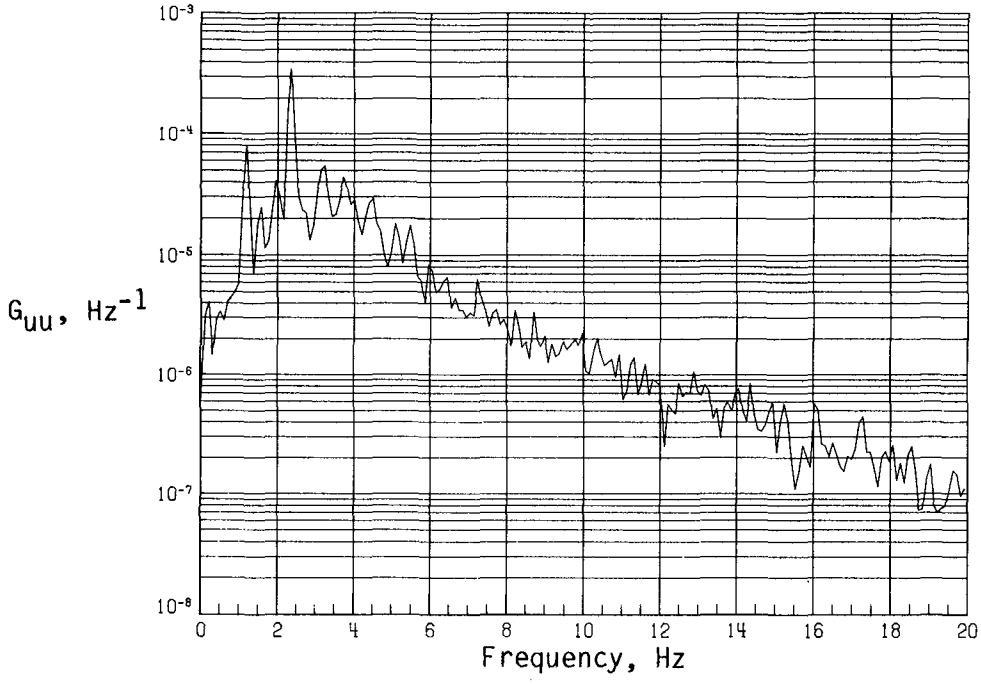

(c) PSD of streamwise velocity fluctuations.

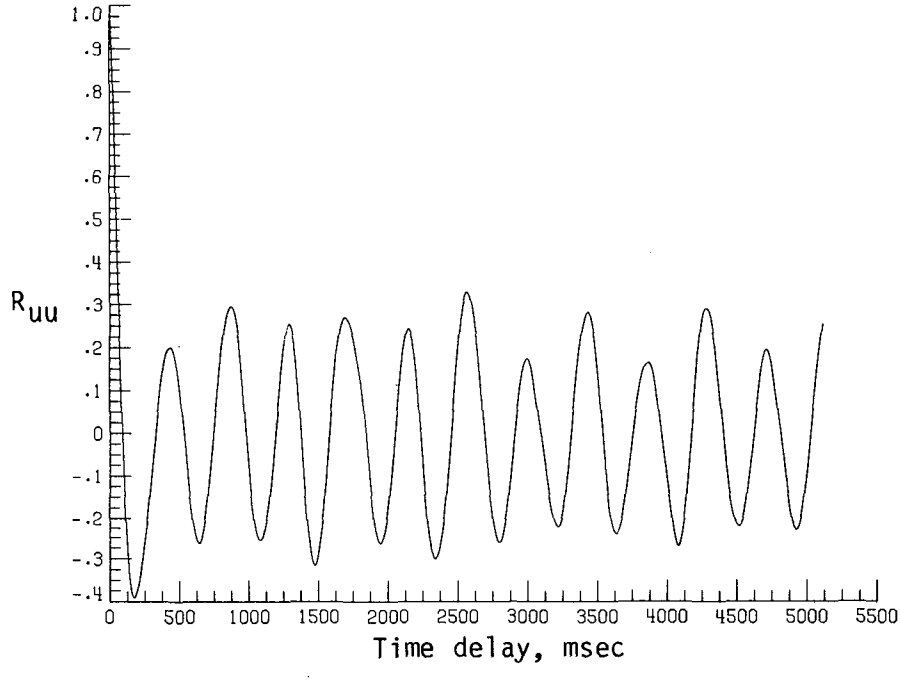

(d) Normalized autocorrelation of streamwise velocity fluctuations. $\sigma = 0.0140$.

Figure 21. Continued.

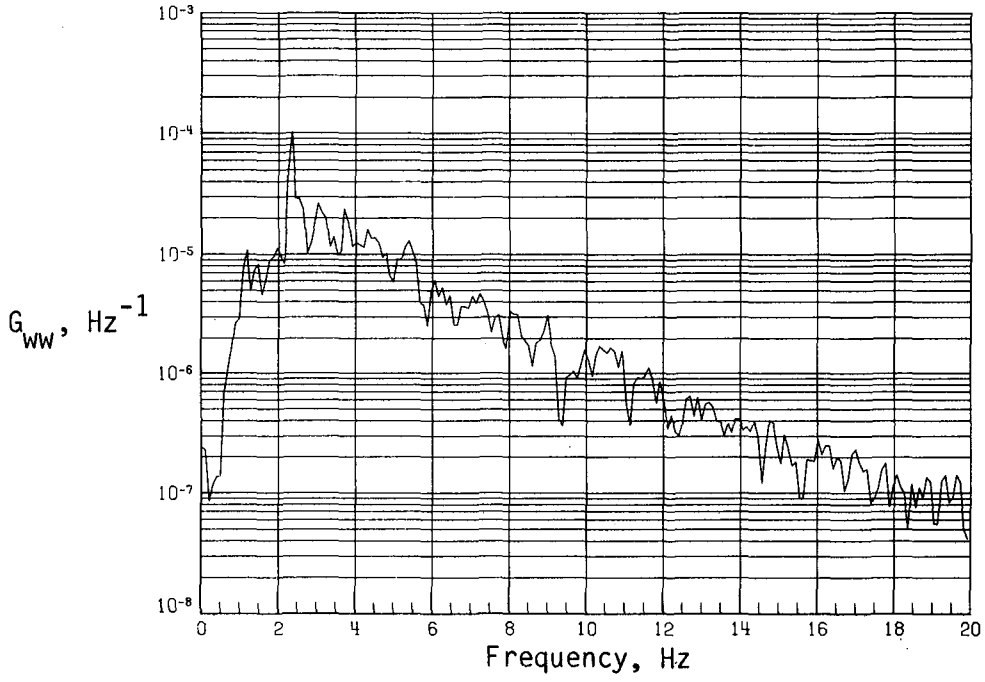

(e) PSD of vertical velocity fluctuations.

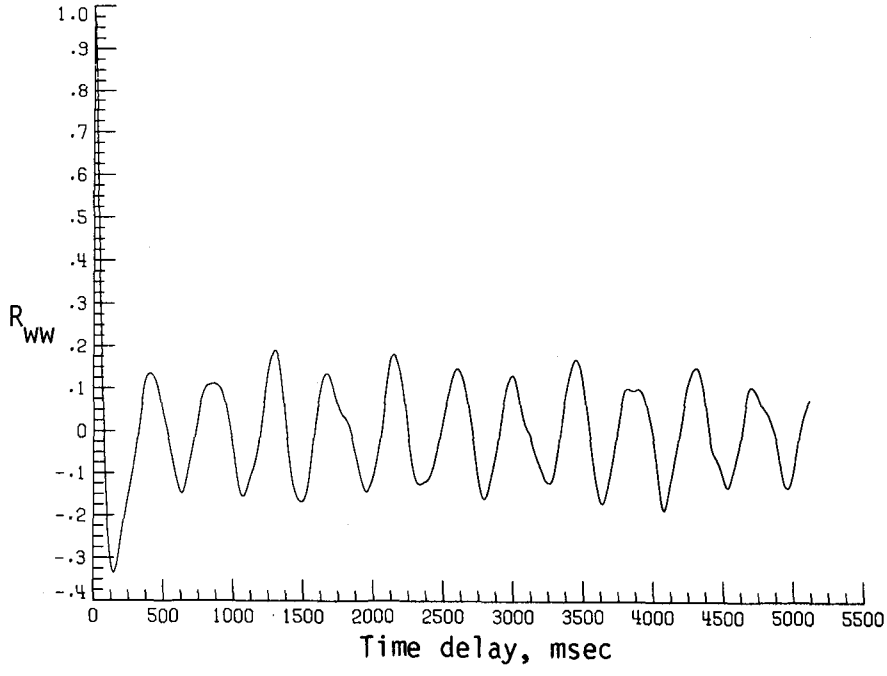

(f) Normalized autocorrelation of vertical velocity fluctuations. $\sigma = 0.0095$.

Figure 21. Concluded.

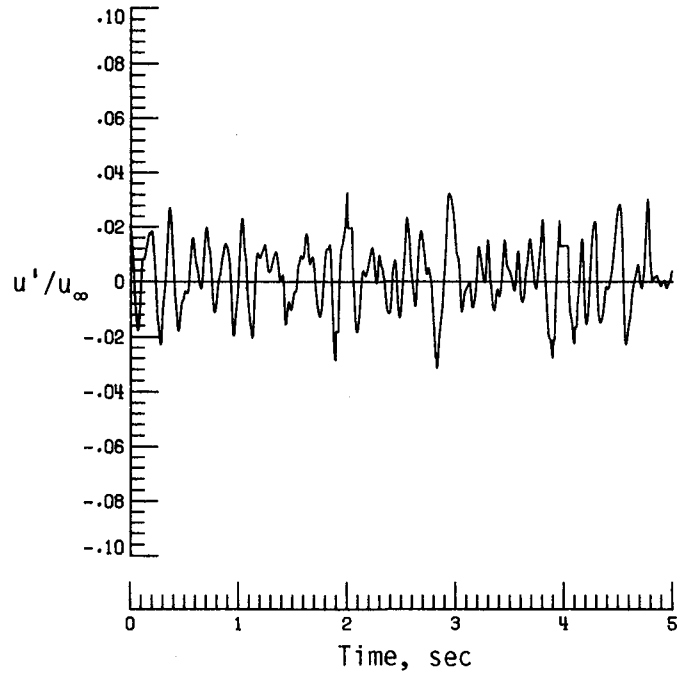

(a) Time history of streamwise velocity fluctuations.

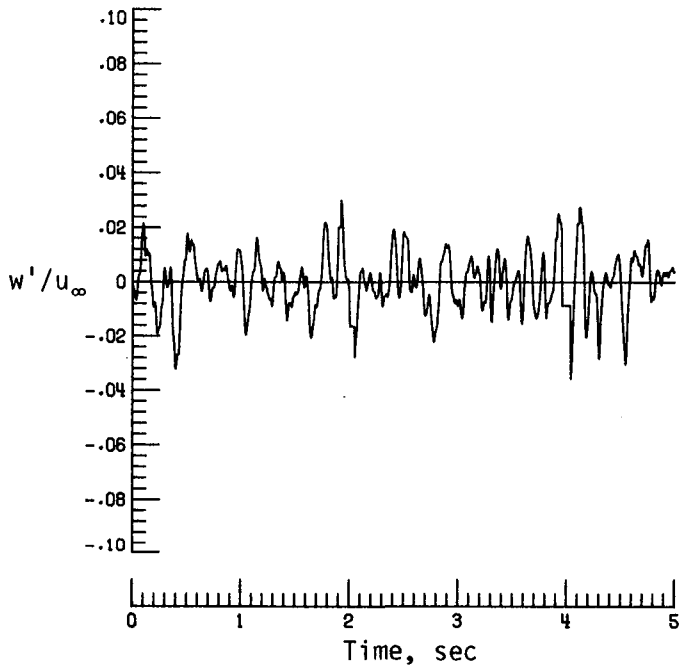

(b) Time history of vertical velocity fluctuations.

Figure 22. Dynamic flow quality for configuration 6 at $q = 47.46$ lb/ft^2 (mode 3).

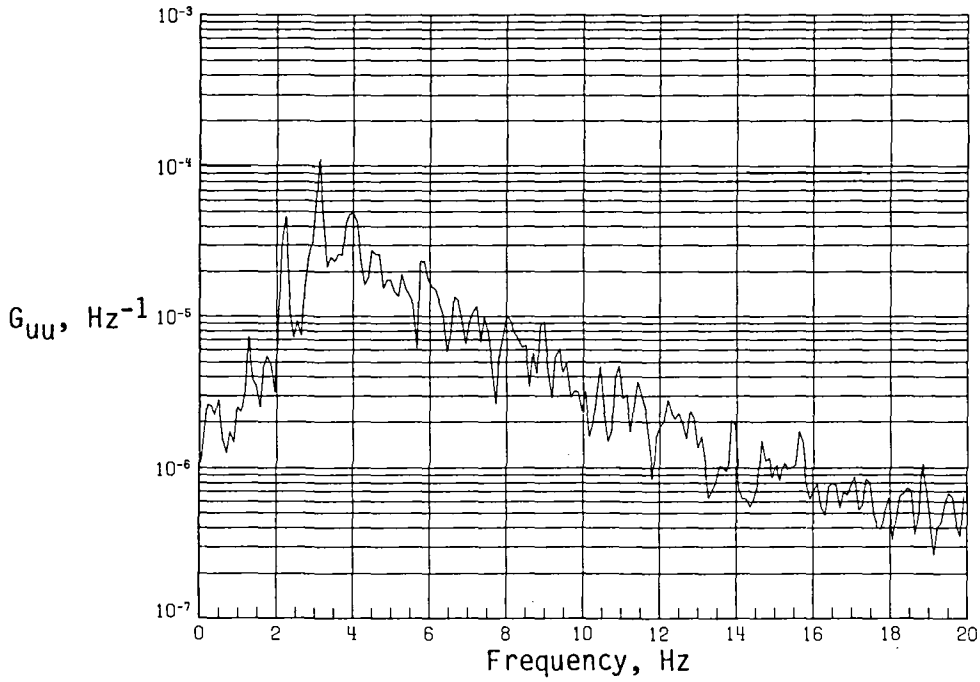

(c) PSD of streamwise velocity fluctuations.

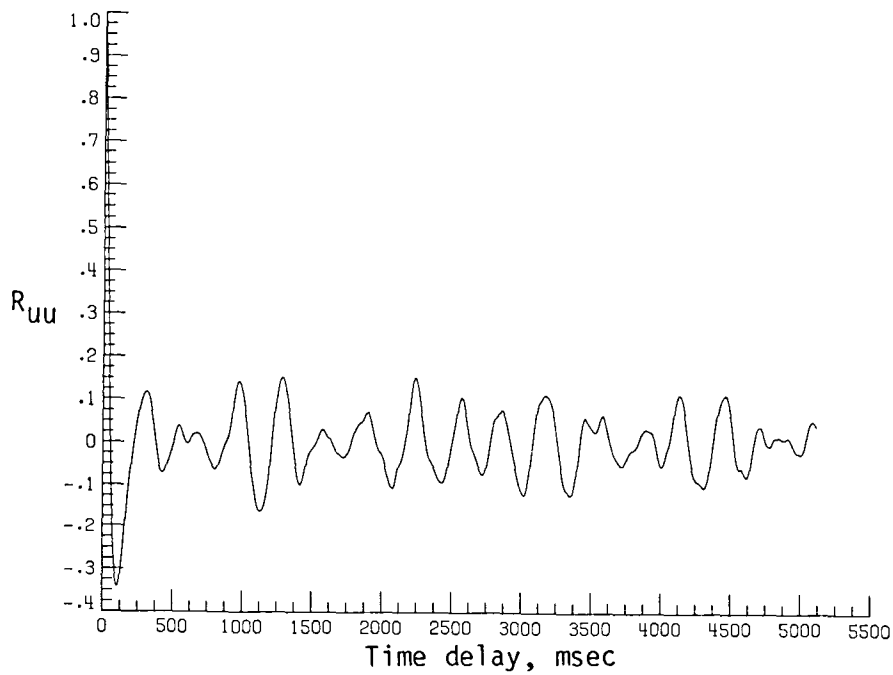

(d) Normalized autocorrelation of streamwise velocity fluctuations. $\sigma = 0.0125$.

Figure 22. Continued.

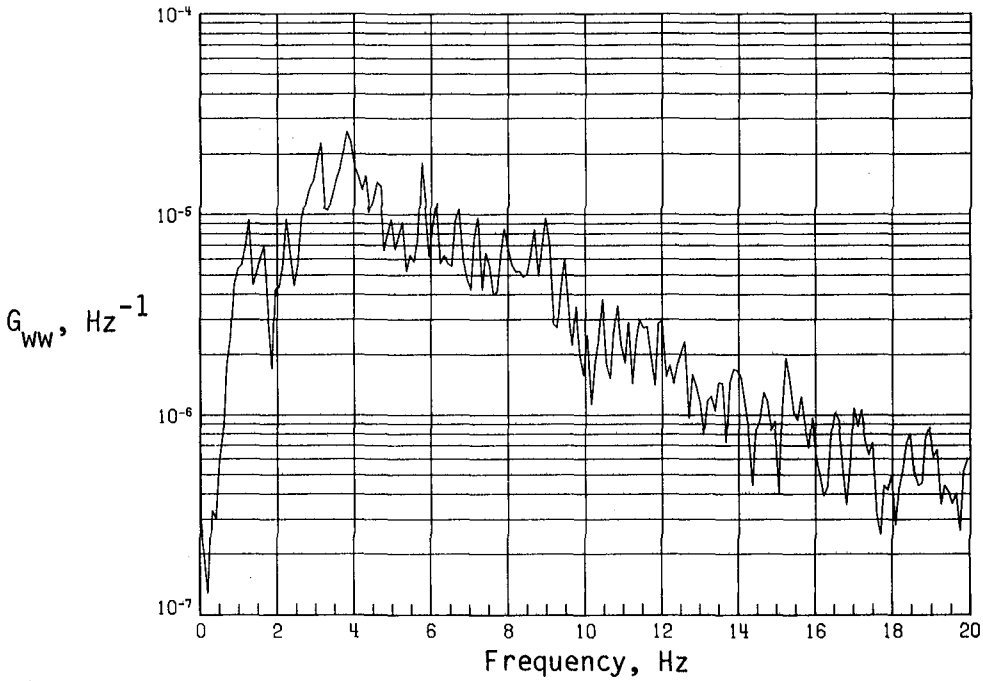

(e) PSD of vertical velocity fluctuations.

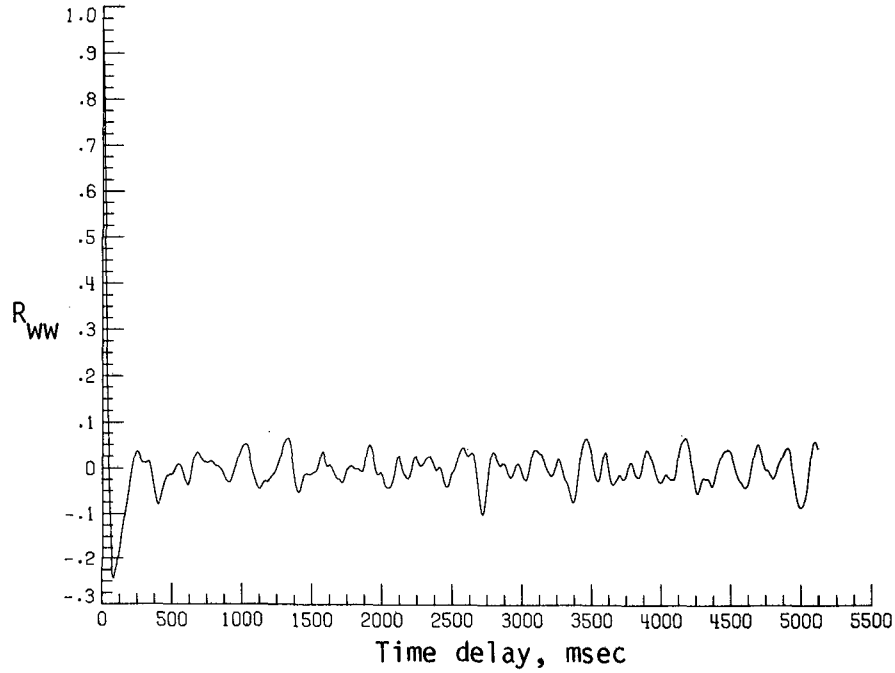

(f) Normalized autocorrelation of vertical velocity fluctuations. $\sigma = 0.0096$.

Figure 22. Concluded.

Appendix A

Dynamic-Flow Quality for Baseline Jet Exit Configuration

Appendix A presents the dynamic-flow-quality data for the baseline jet exit configuration. It includes the time histories and autopower spectral density (PSD) and autocorrelation functions of the velocity fluctuations corresponding to the RMS data points shown in figure 9. The time history plots show a typical 5-sec time slice for the streamwise (u') and vertical (w') velocity fluctuations. The data are presented in the following order:

Figure	q, lb/ft^2
A1	2.03
A2	3.05
A3	4.07
A4	7.12
A5	8.03
A6	9.60
A7	10.51
A8	11.07
A9	12.09
A10	13.23
A11	14.02
A12	15.26
A13	16.05
A14	16.16
A15	18.08
A16	20.12
A17	22.16
A18	25.31
A19	32.21
A20	40.23
A21	42.49
A22	45.09
A23	47.58
A24	50.29
A25	55.26
A26	59.10

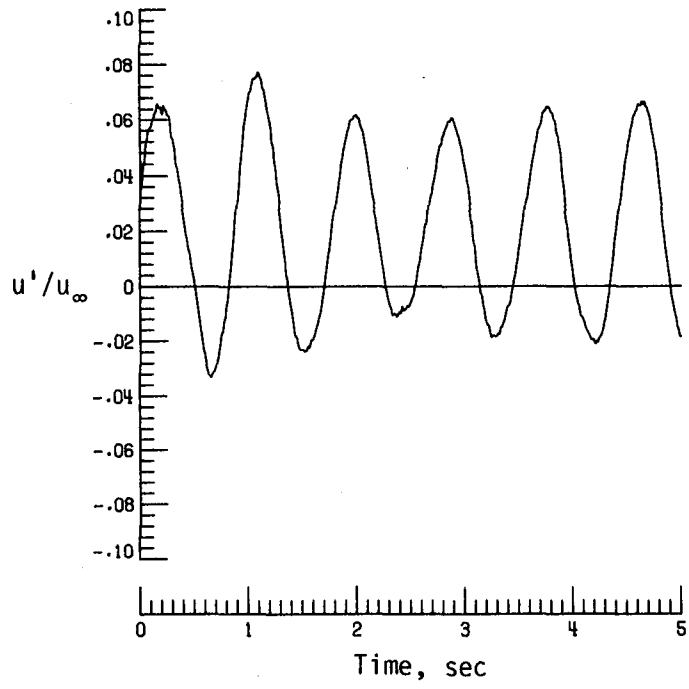

(a) Time history of streamwise velocity fluctuations.

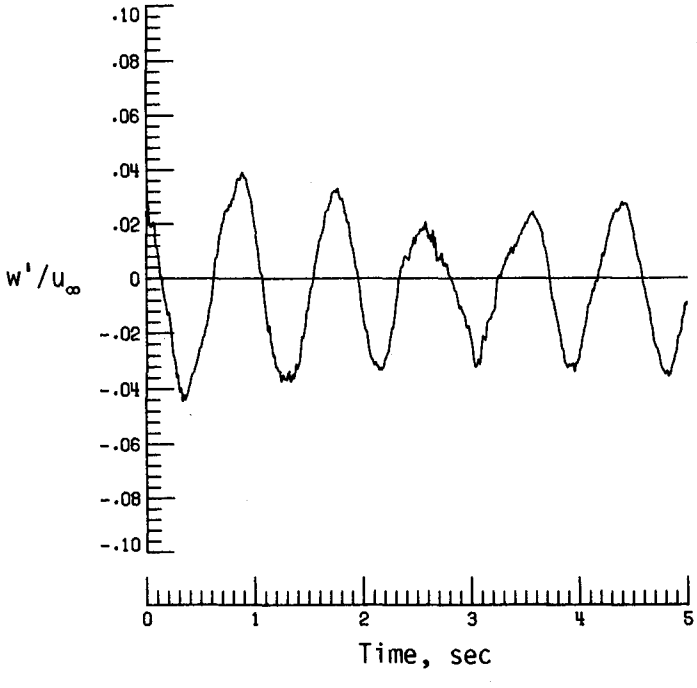

(b) Time history of vertical velocity fluctuations.

Figure A1. Dynamic-flow quality for baseline configuration at $q = 2.03$ lb/ft^2.

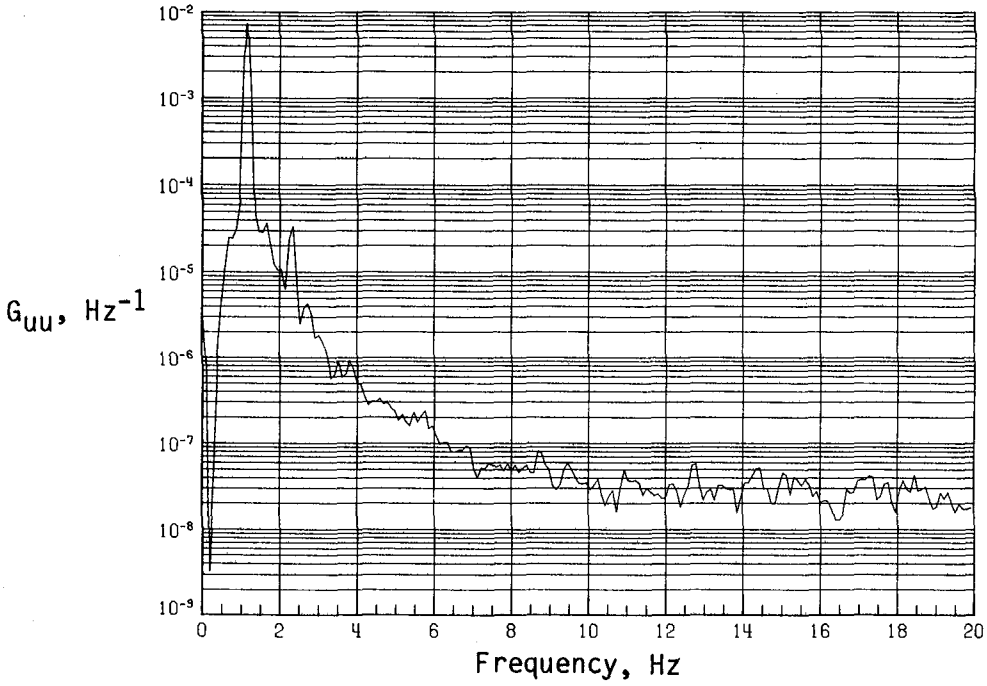

(c) PSD of streamwise velocity fluctuations.

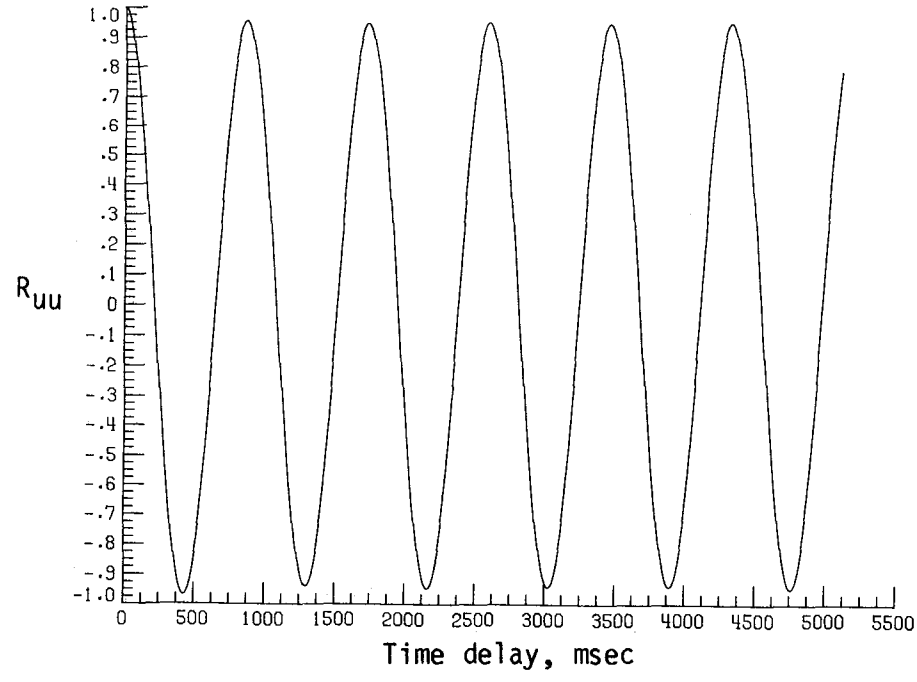

(d) Normalized autocorrelation of streamwise velocity fluctuations. $\sigma = 0.0343$.

Figure A1. Continued.

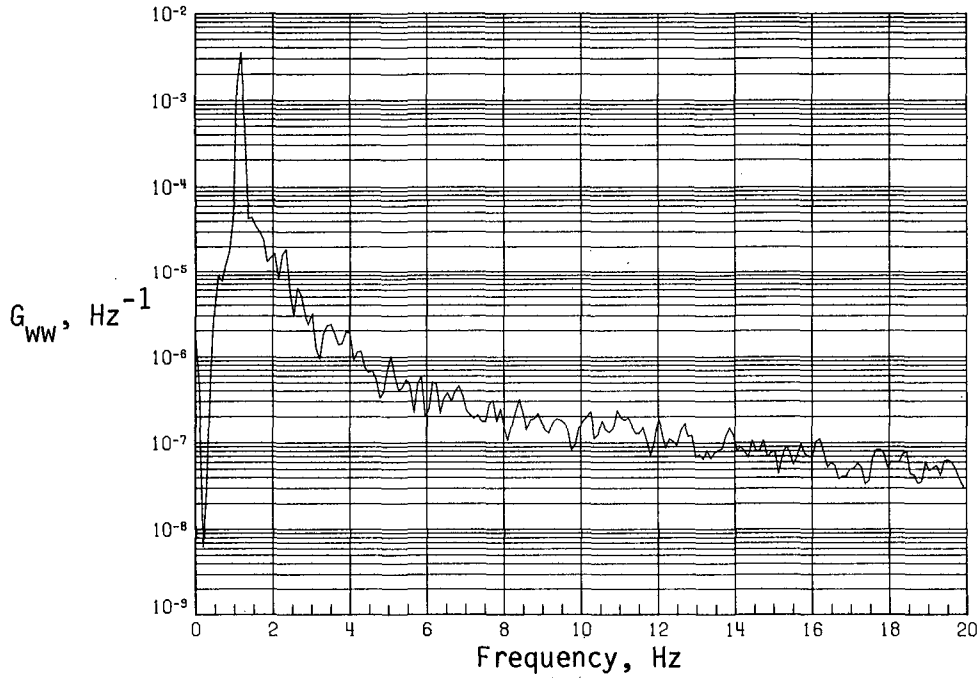

(e) PSD of vertical velocity fluctuations.

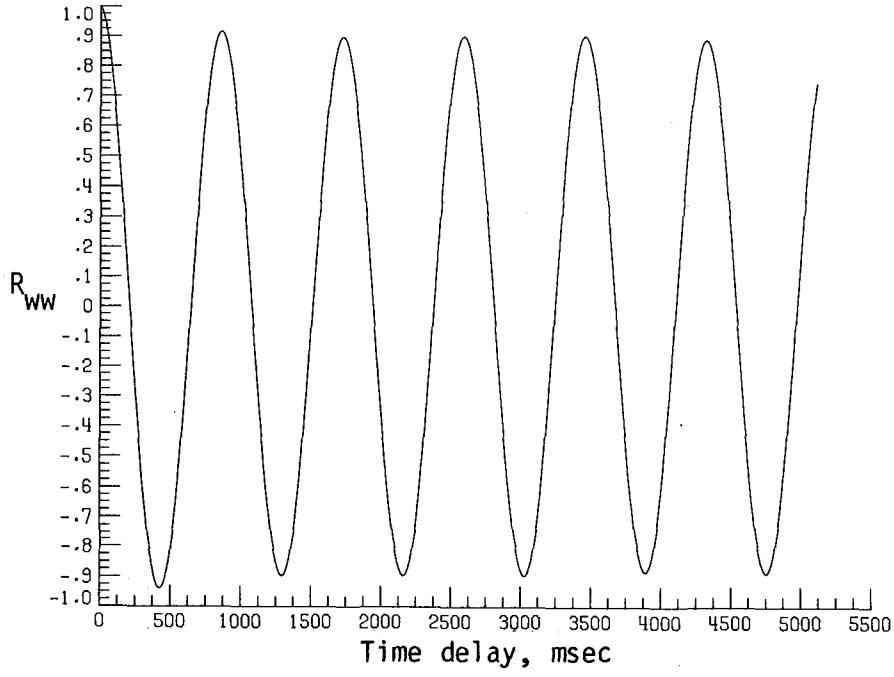

(f) Normalized autocorrelation of vertical velocity fluctuations. $\sigma = 0.0244$.

Figure A1. Concluded.

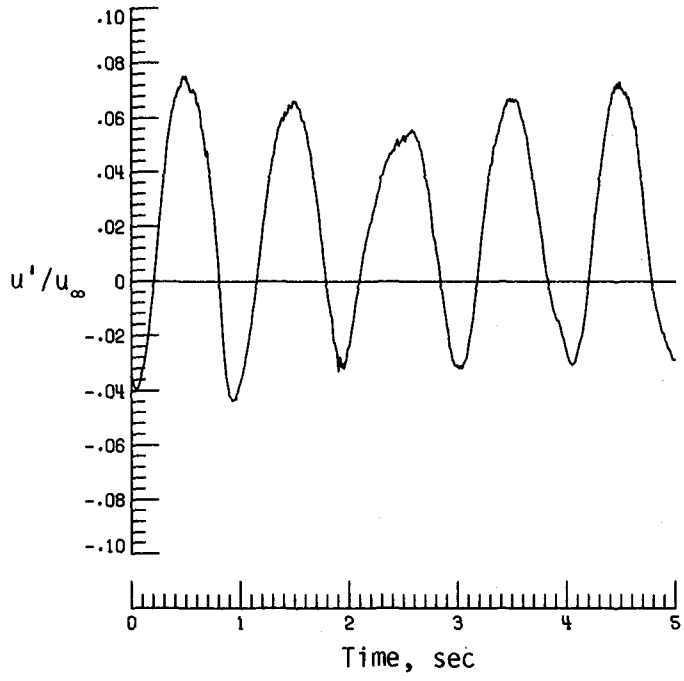

(a) Time history of streamwise velocity fluctuations.

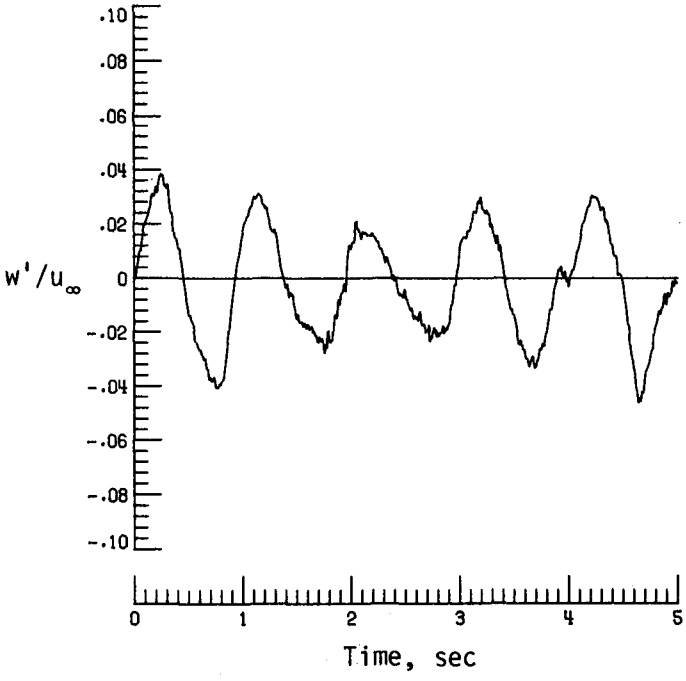

(b) Time history of vertical velocity fluctuations.

Figure A2. Dynamic-flow quality for baseline configuration at $q = 3.05$ lb/ft^2.

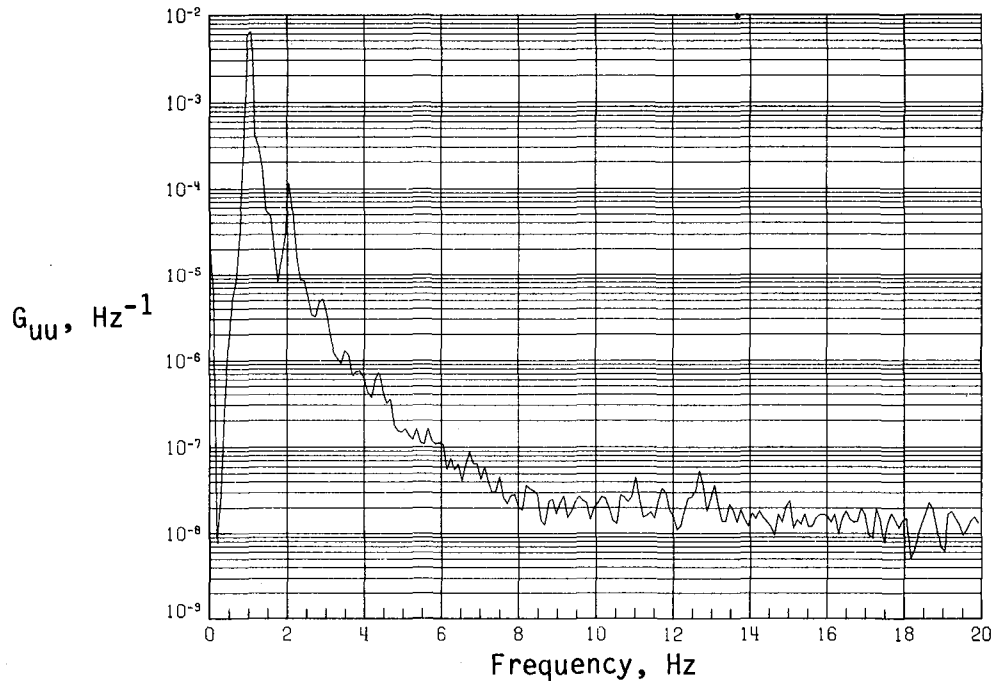

(c) PSD of streamwise velocity fluctuations.

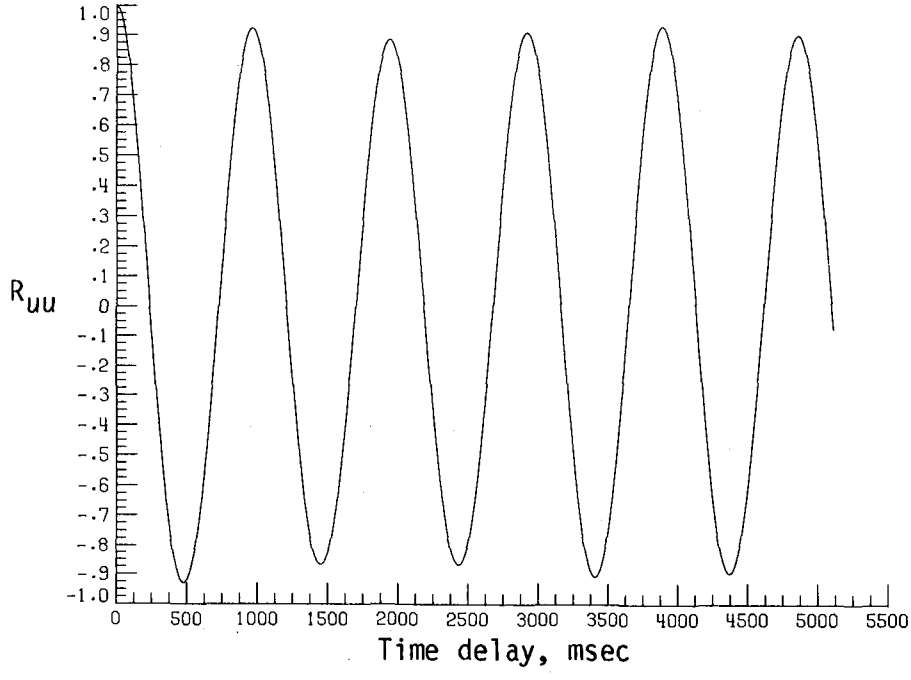

(d) Normalized autocorrelation of streamwise velocity fluctuations. $\sigma = 0.0377$.

Figure A2. Continued.

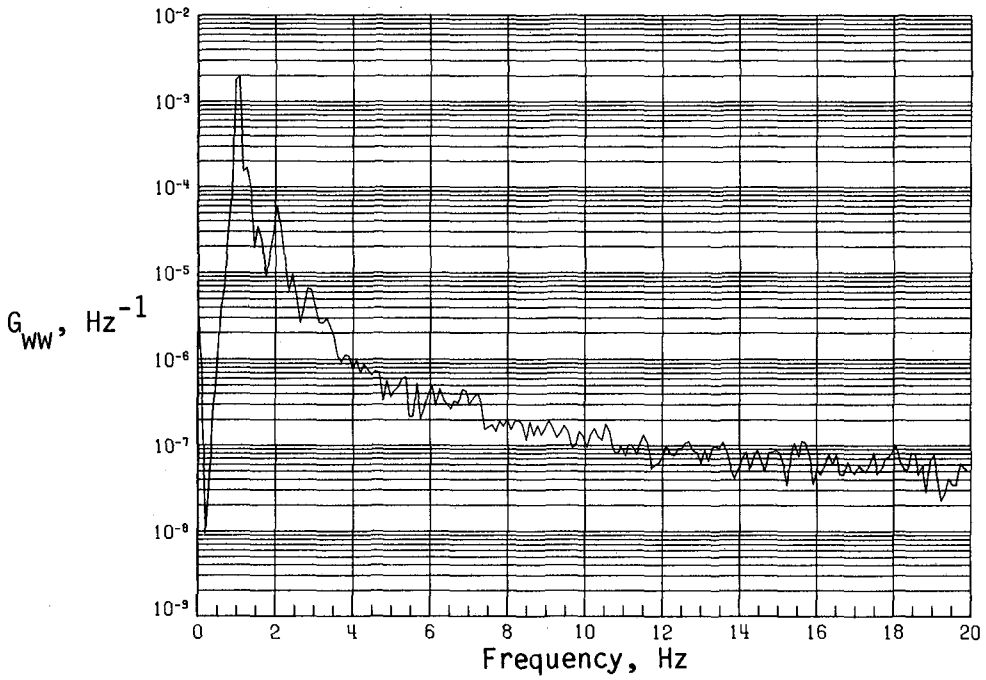

(e) PSD of vertical velocity fluctuations.

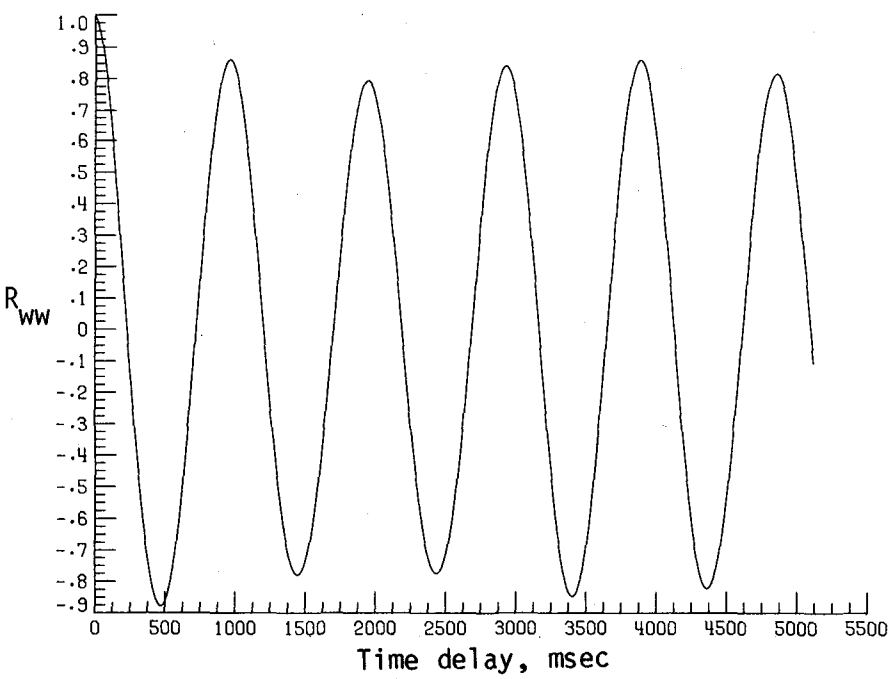

(f) Normalized autocorrelation of vertical velocity fluctuations. $\sigma = 0.0218$.

Figure A2. Concluded.

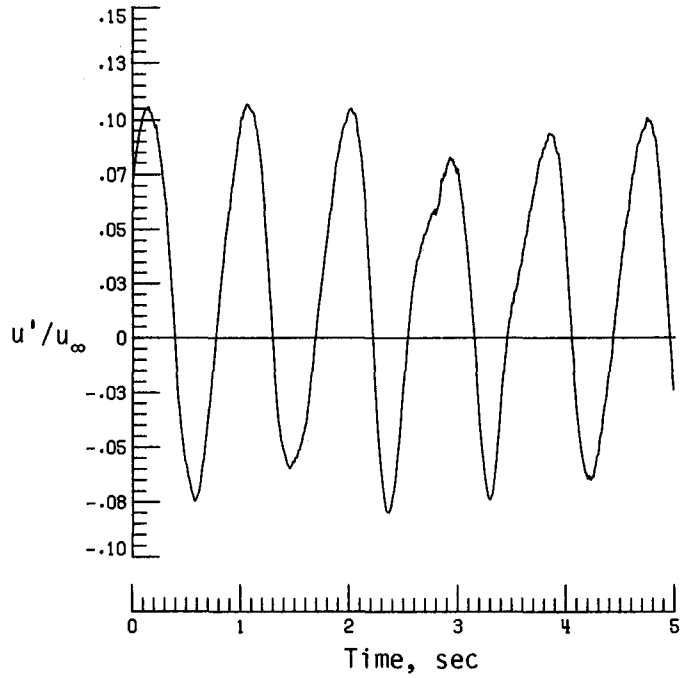

(a) Time history of streamwise velocity fluctuations.

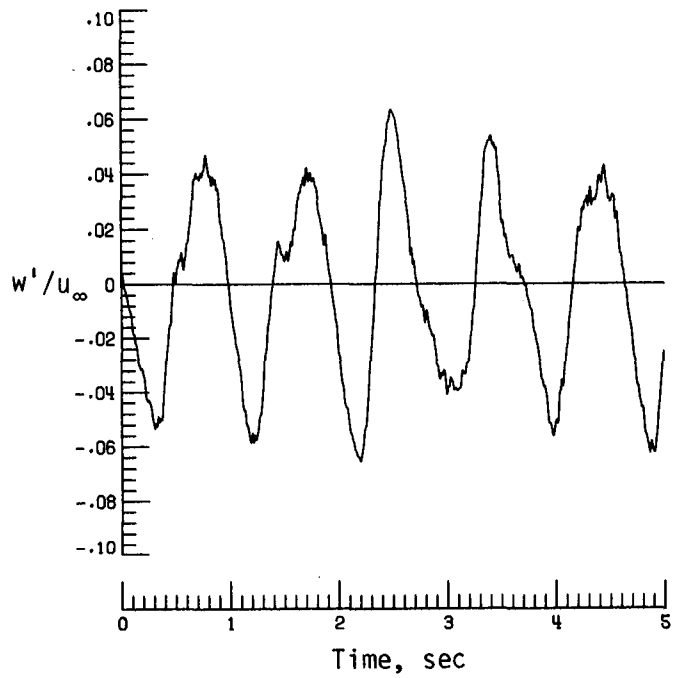

(b) Time history of vertical velocity fluctuations.

Figure A3. Dynamic-flow quality for baseline configuration at $q = 4.07$ lb/ft^2.

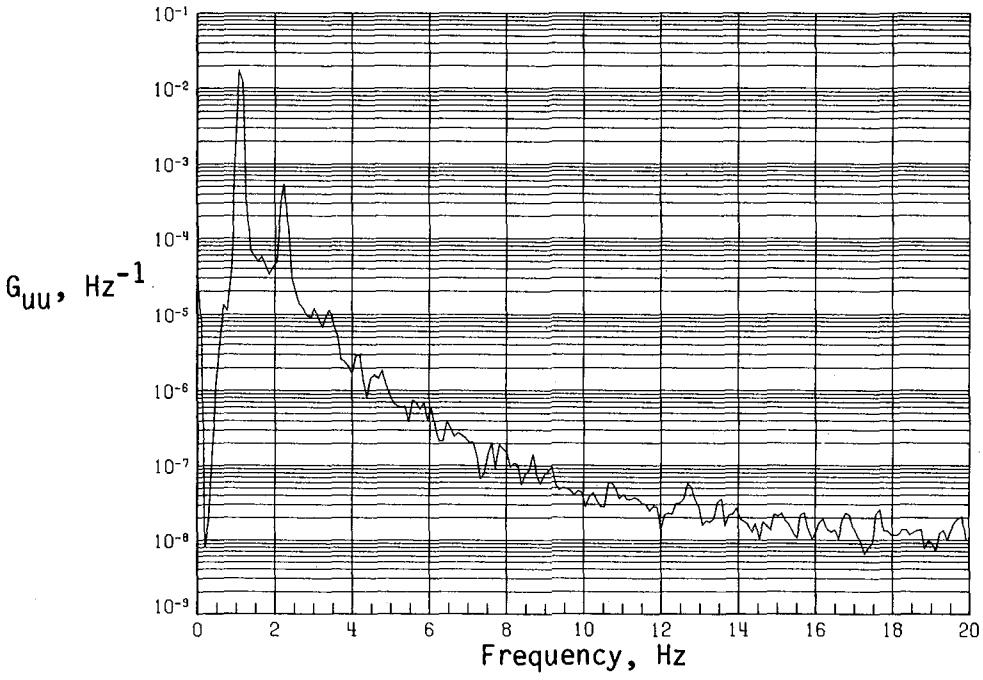

(c) PSD of streamwise velocity fluctuations.

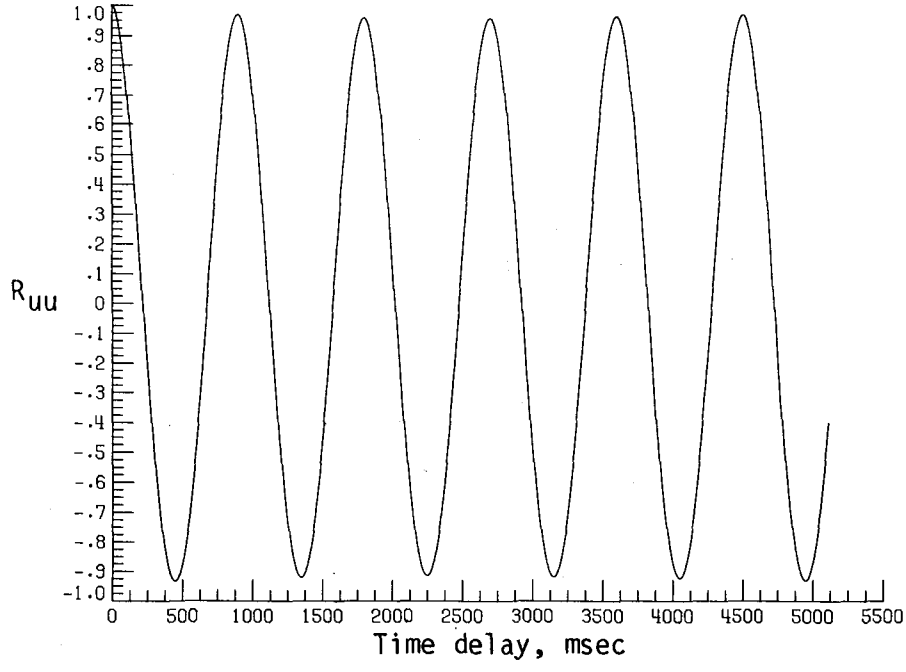

(d) Normalized autocorrelation of streamwise velocity fluctuations. $\sigma = 0.0576$.

Figure A3. Continued.

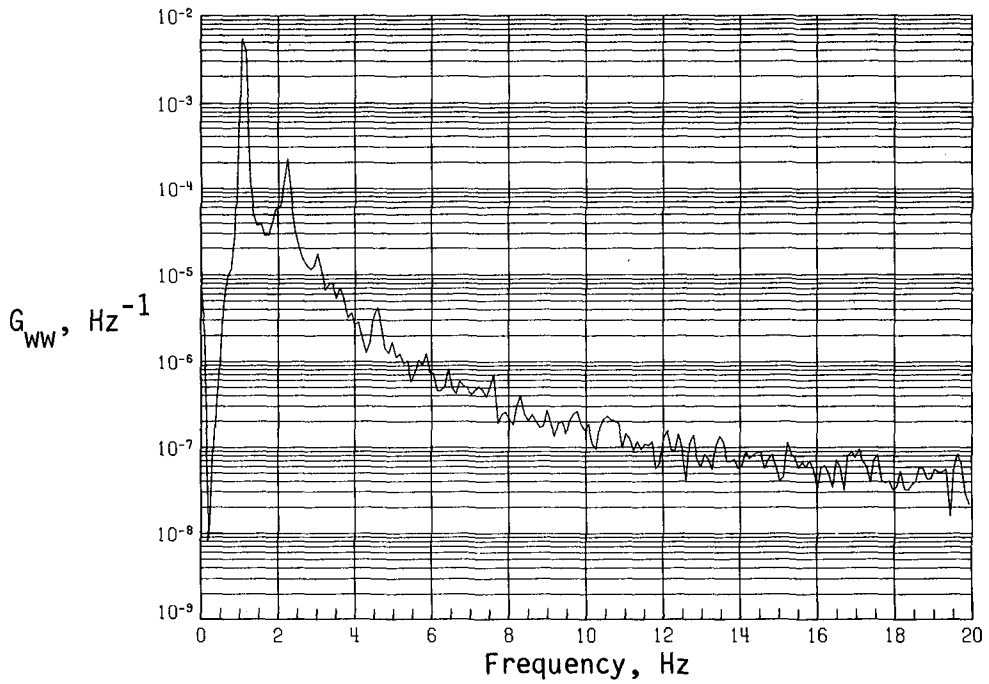

(e) PSD of vertical velocity fluctuations.

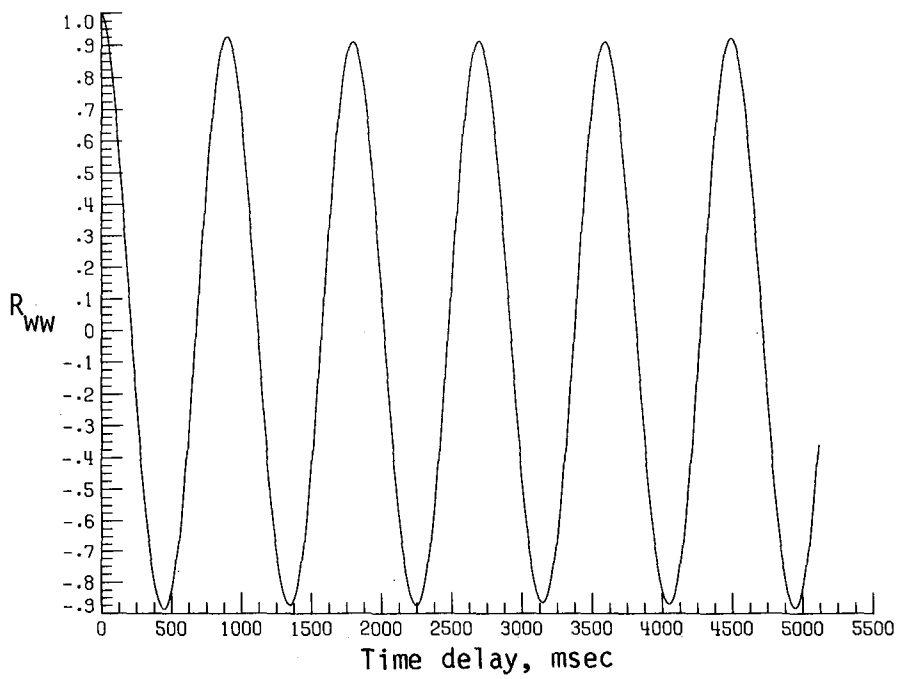

(f) Normalized autocorrelation of vertical velocity fluctuations. $\sigma = 0.0333$.

Figure A3. Concluded.

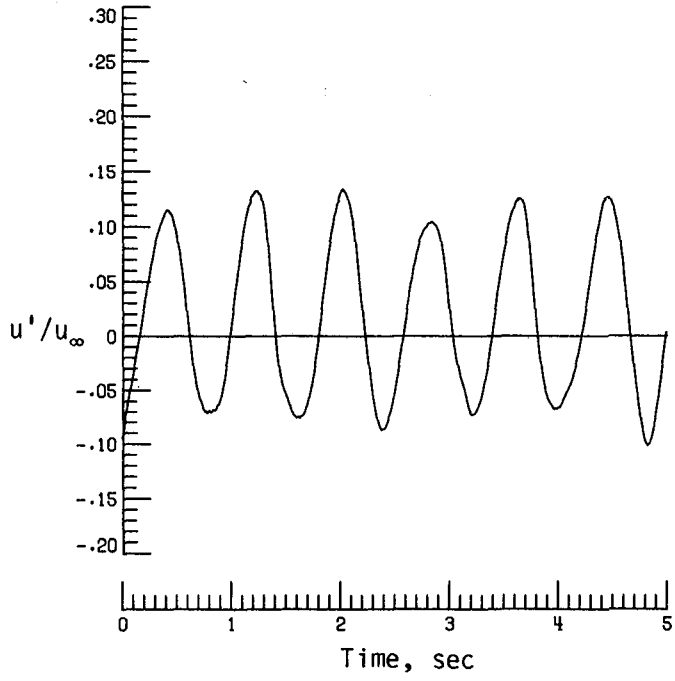

(a) Time history of streamwise velocity fluctuations.

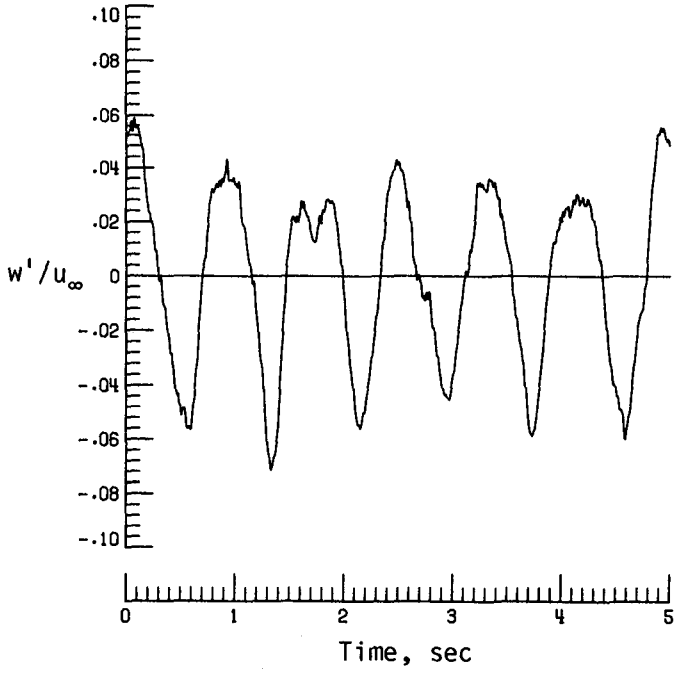

(b) Time history of vertical velocity fluctuations.

Figure A4. Dynamic-flow quality for baseline configuration at $q = 7.12$ lb/ft^2.

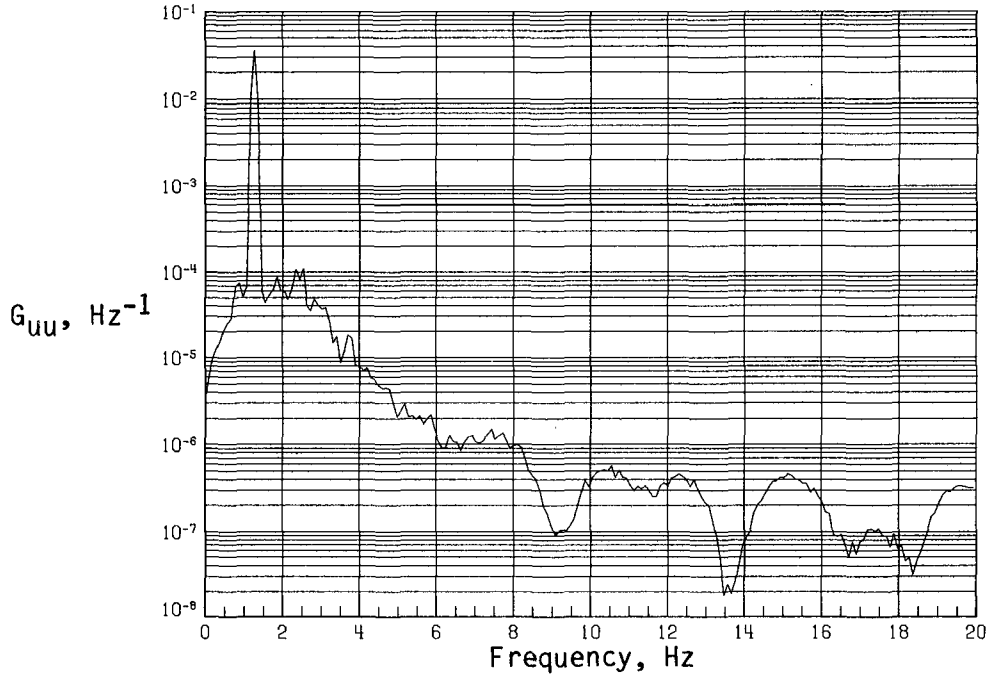

(c) PSD of streamwise velocity fluctuations.

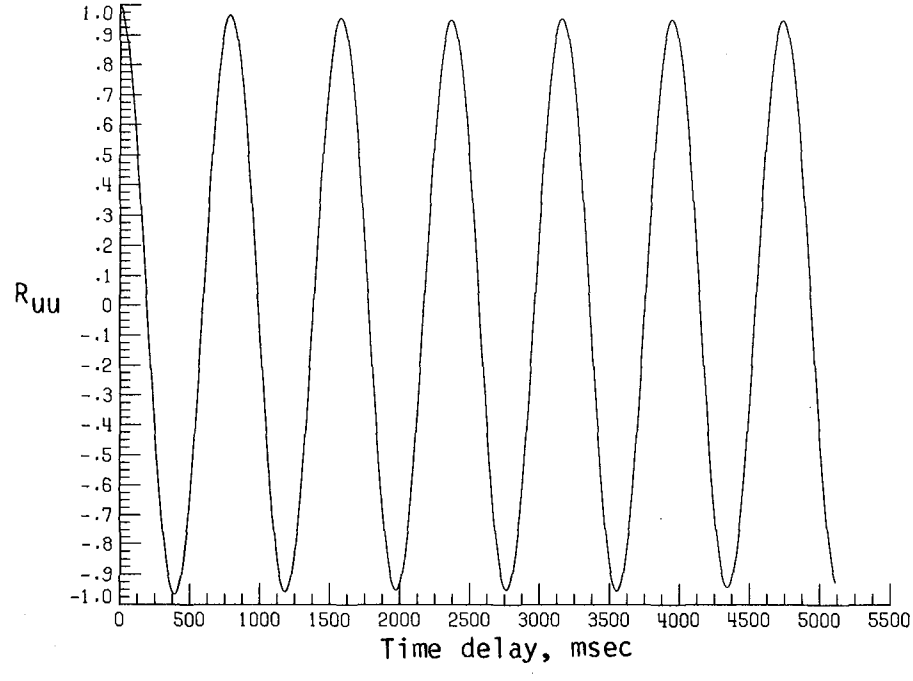

(d) Normalized autocorrelation of streamwise velocity fluctuations. $\sigma = 0.0737$.

Figure A4. Continued.

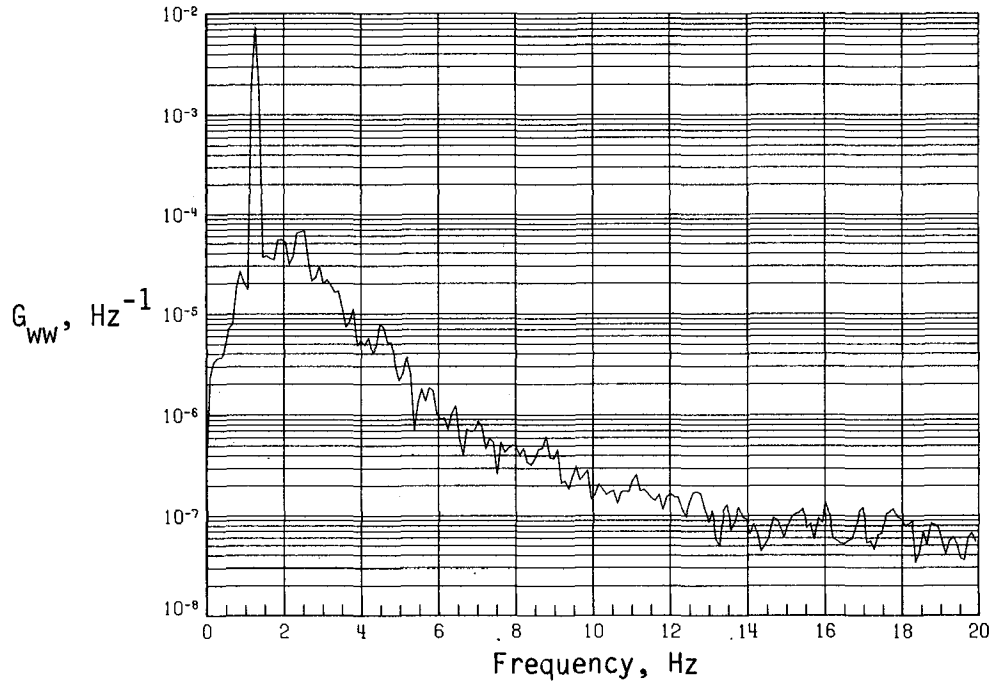

(e) PSD of vertical velocity fluctuations.

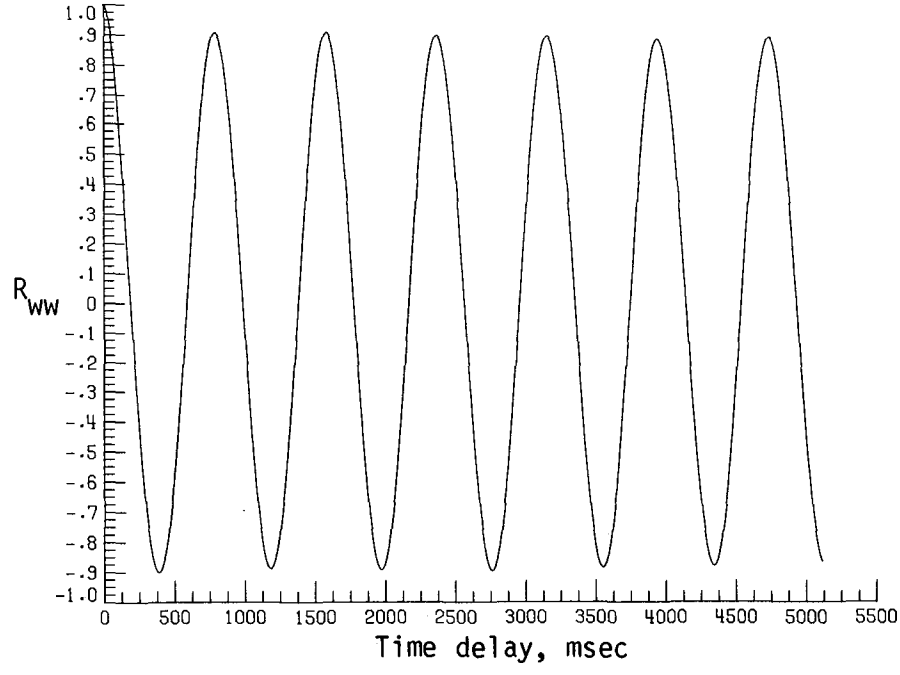

(f) Normalized autocorrelation of vertical velocity fluctuations. $\sigma = 0.0344$.

Figure A4. Concluded.

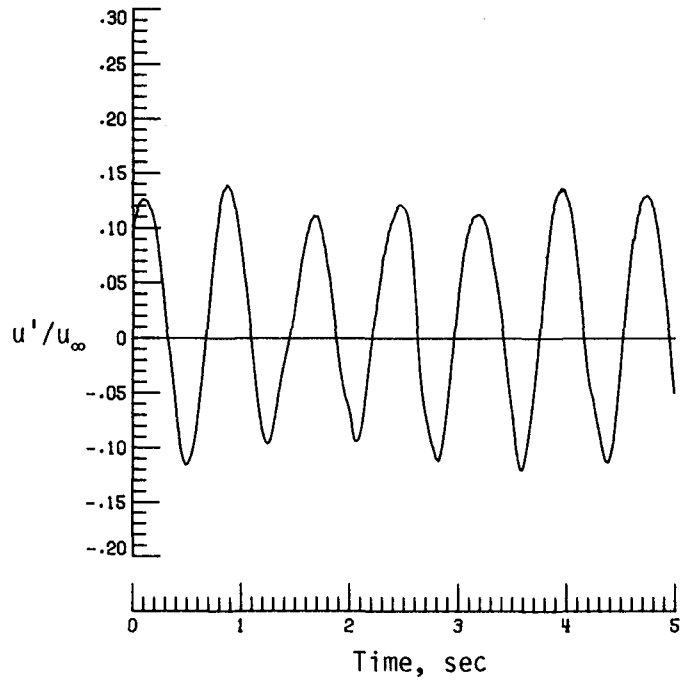

(a) Time history of streamwise velocity fluctuations.

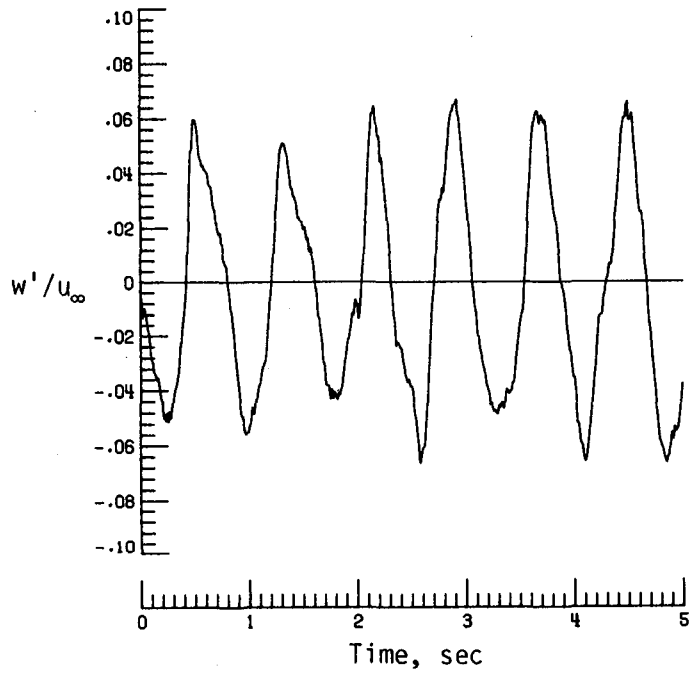

(b) Time history of vertical velocity fluctuations.

Figure A5. Dynamic-flow quality for baseline configuration at $q = 8.03$ lb/ft^2.

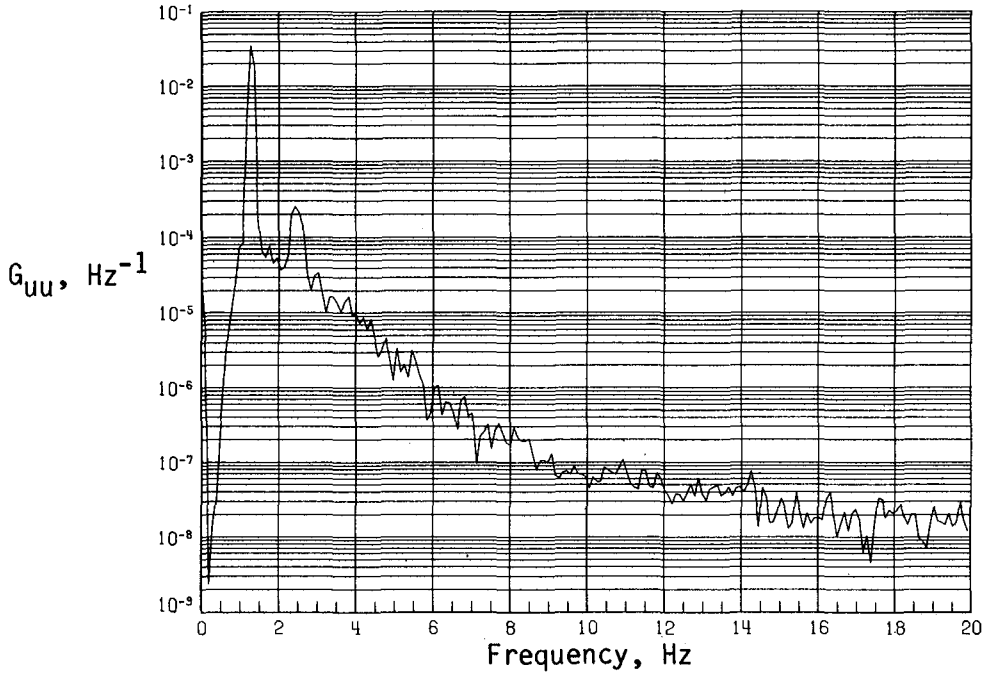

(c) PSD of streamwise velocity fluctuations.

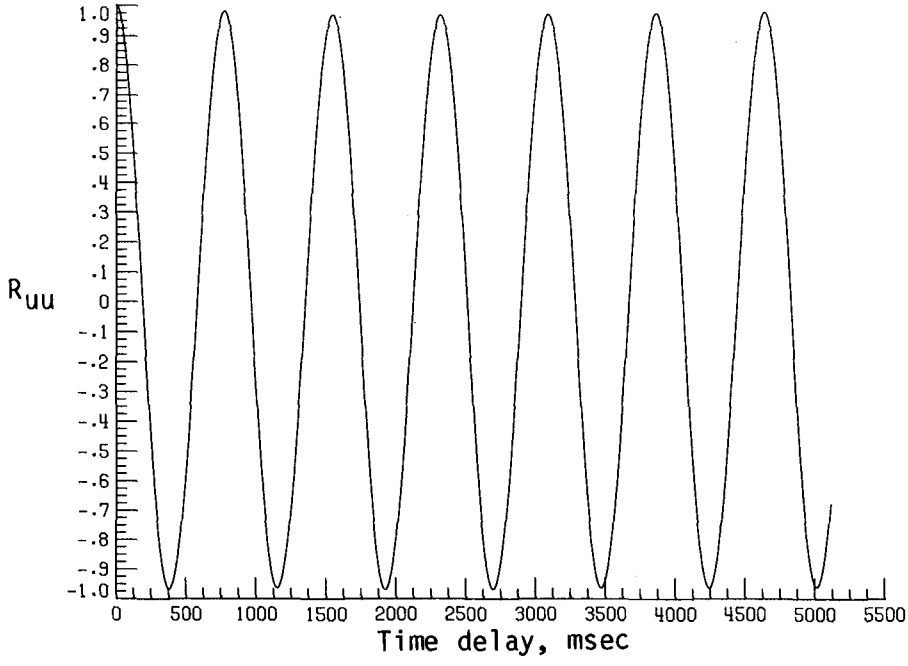

(d) Normalized autocorrelation of streamwise velocity fluctuations. $\sigma = 0.0763$.

Figure A5. Continued.

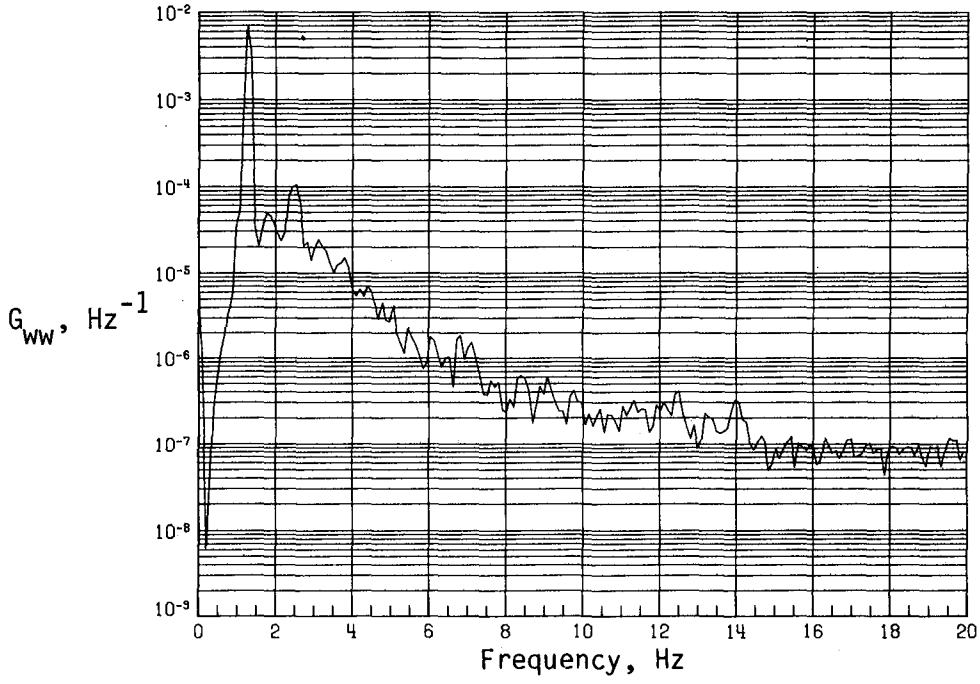

(e) PSD of vertical velocity fluctuations.

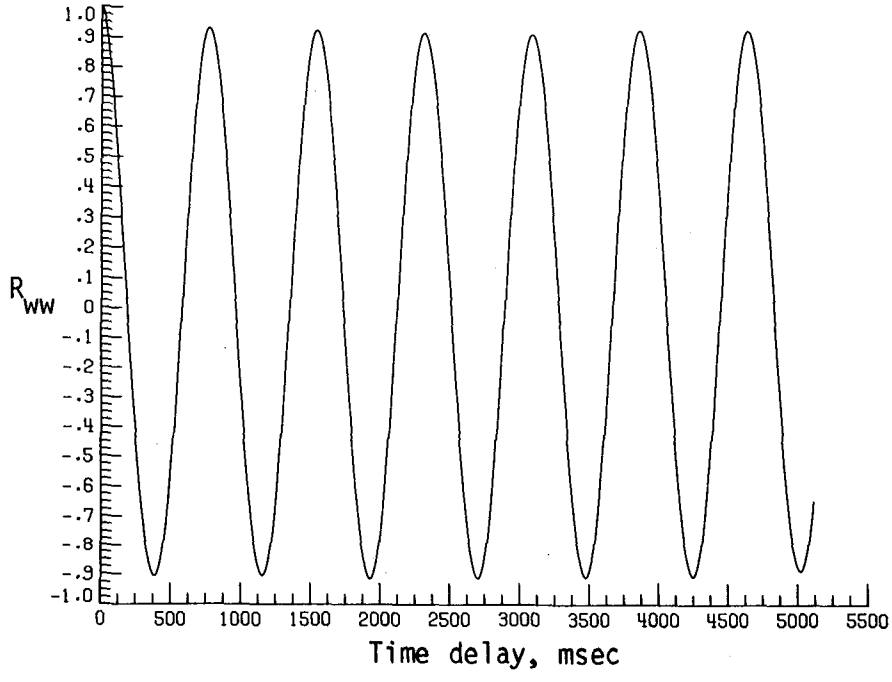

(f) Normalized autocorrelation of vertical velocity fluctuations. $\sigma = 0.0345$.

Figure A5. Concluded.

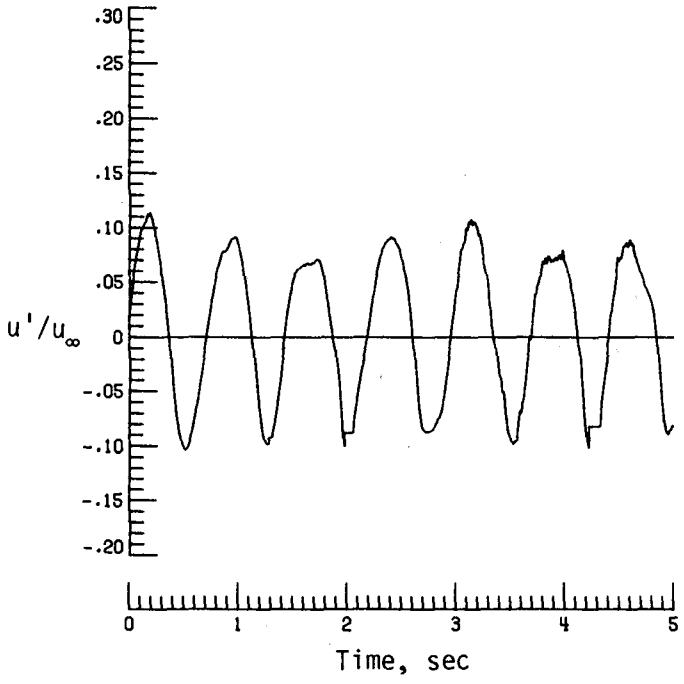

(a) Time history of streamwise velocity fluctuations.

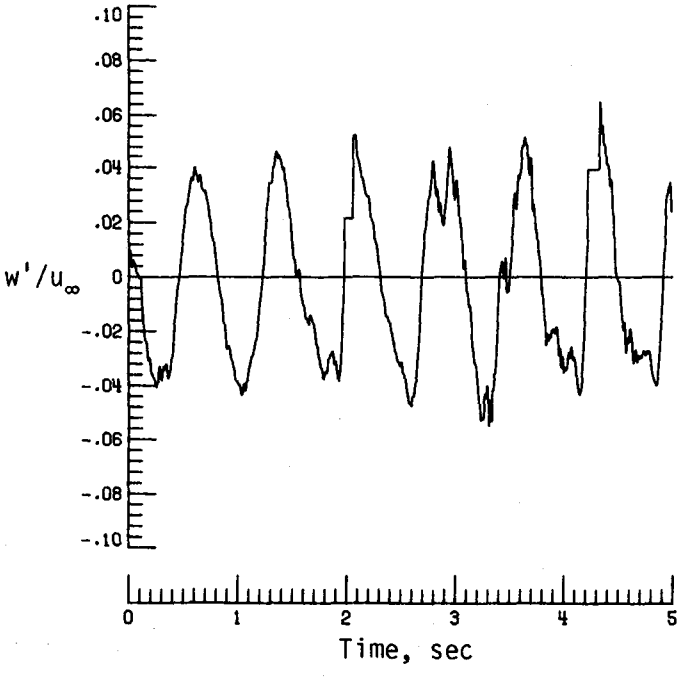

(b) Time history of vertical velocity fluctuations.

Figure A6. Dynamic-flow quality for baseline configuration at $q = 9.60$ lb/ft^2

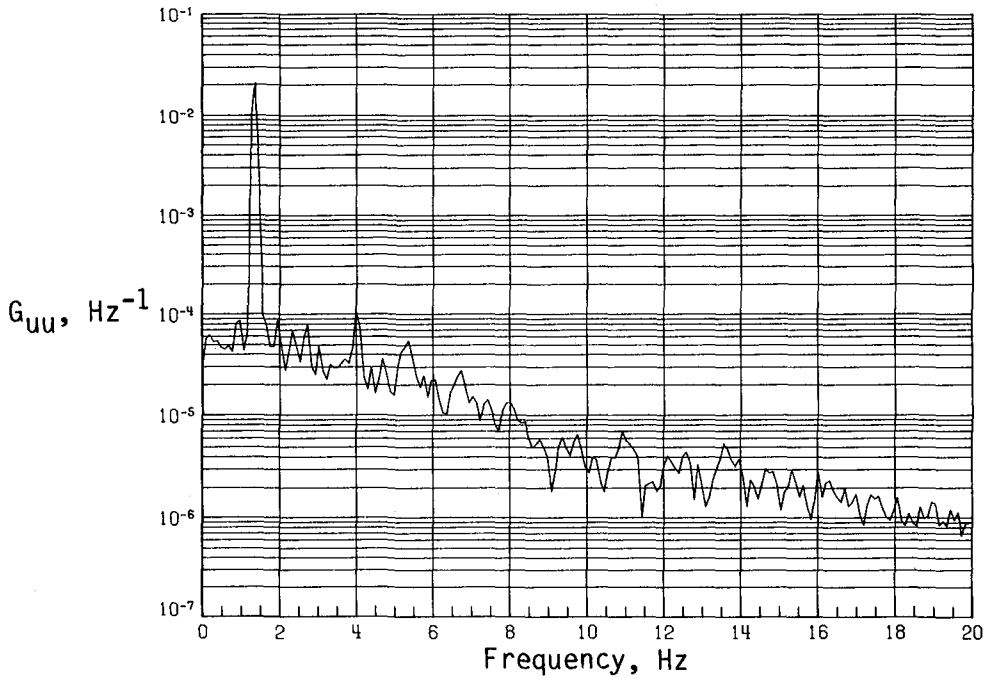

(c) PSD of streamwise velocity fluctuations.

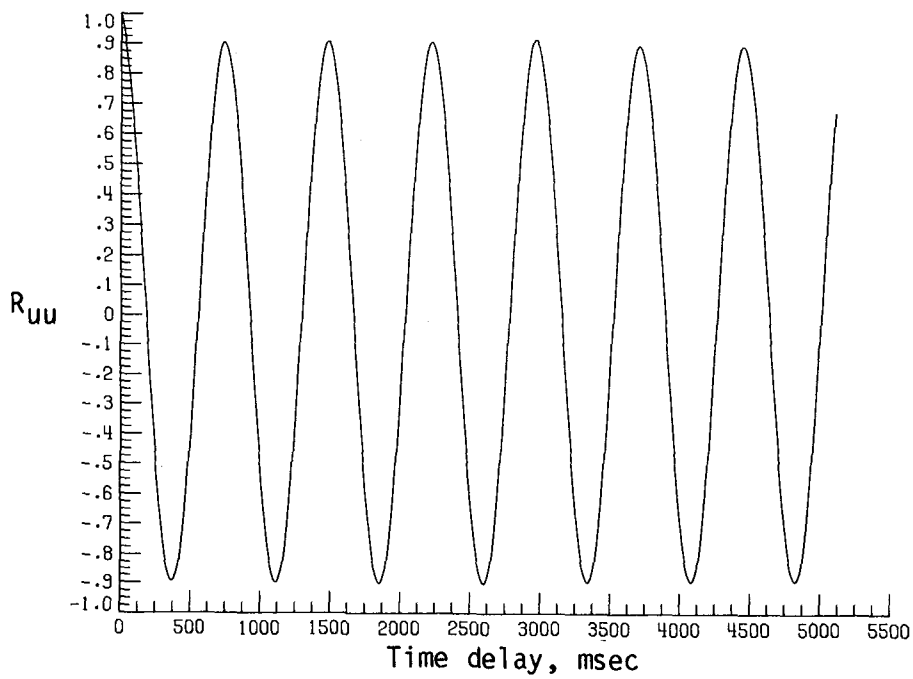

(d) Normalized autocorrelation of streamwise velocity fluctuations. $\sigma = 0.0599$.

Figure A6. Continued.

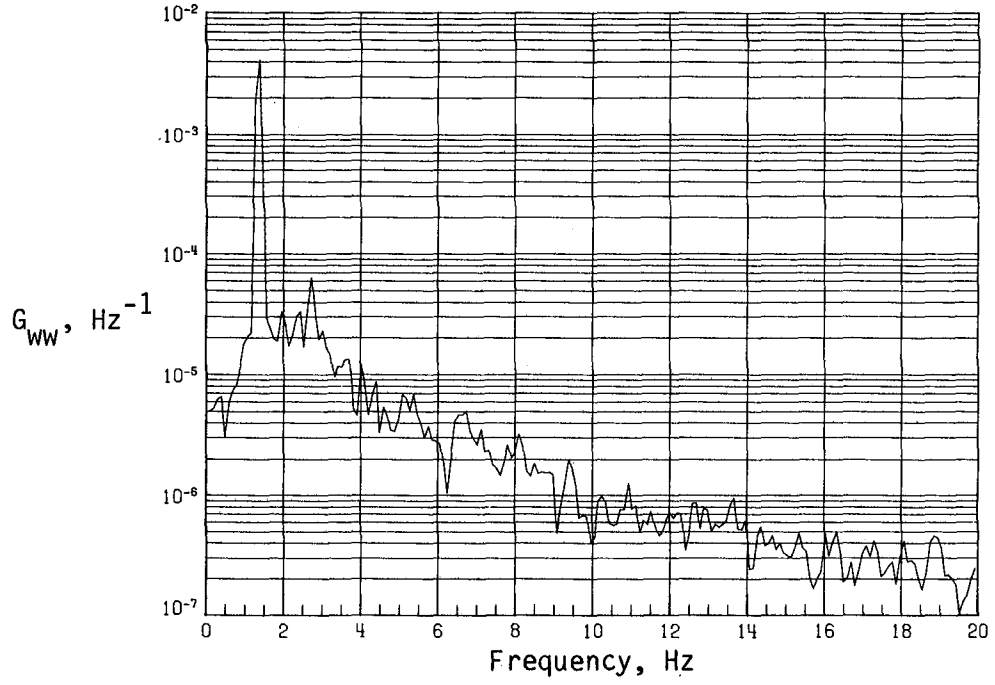

(e) PSD of vertical velocity fluctuations.

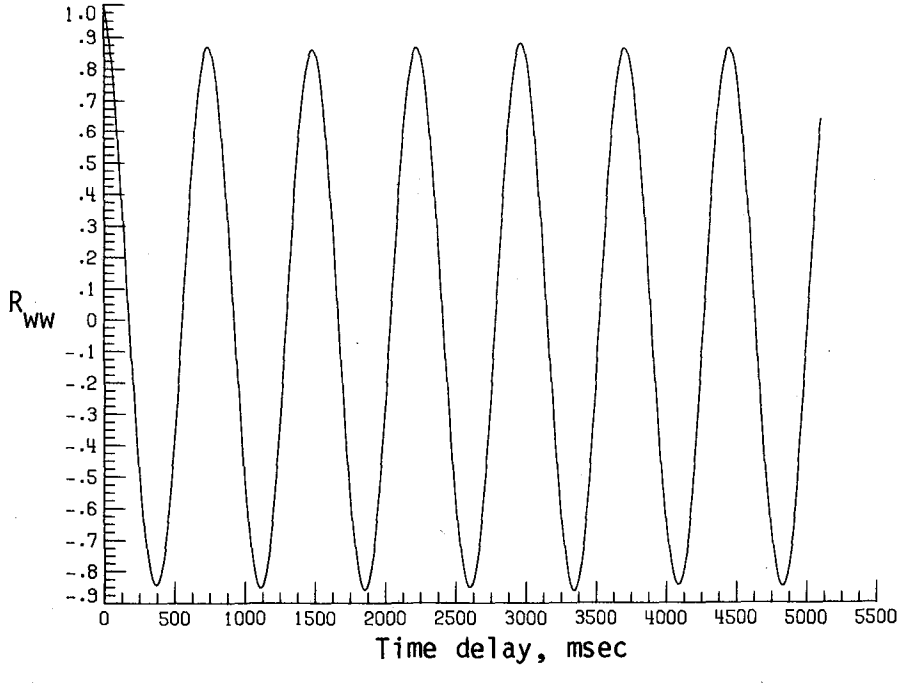

(f) Normalized autocorrelation of vertical velocity fluctuations. $\sigma = 0.0272$.

Figure A6. Concluded.

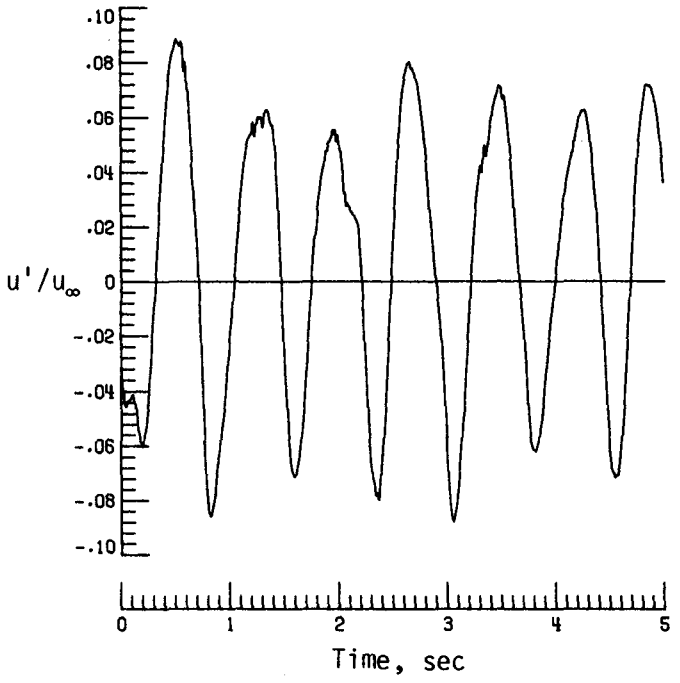

(a) Time history of streamwise velocity fluctuations.

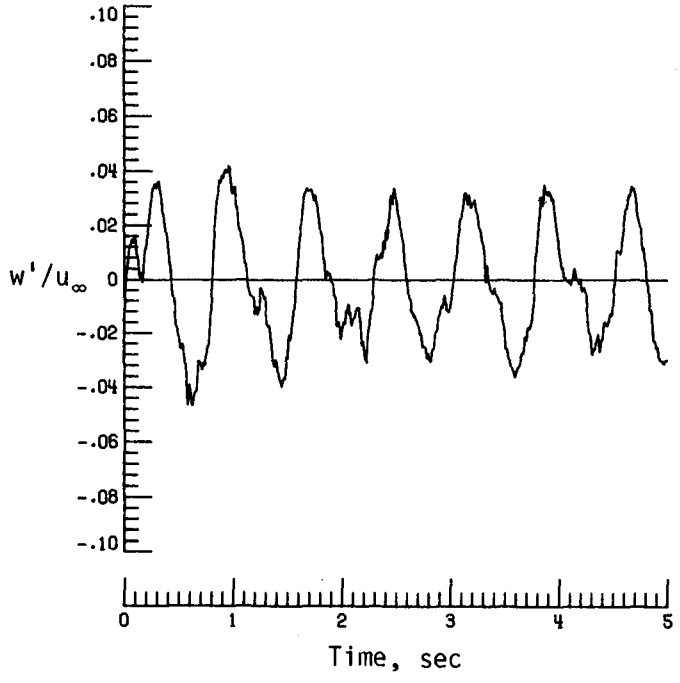

(b) Time history of vertical velocity fluctuations.

Figure A7. Dynamic-flow quality for baseline configuration at $q = 10.51$ lb/ft^2.

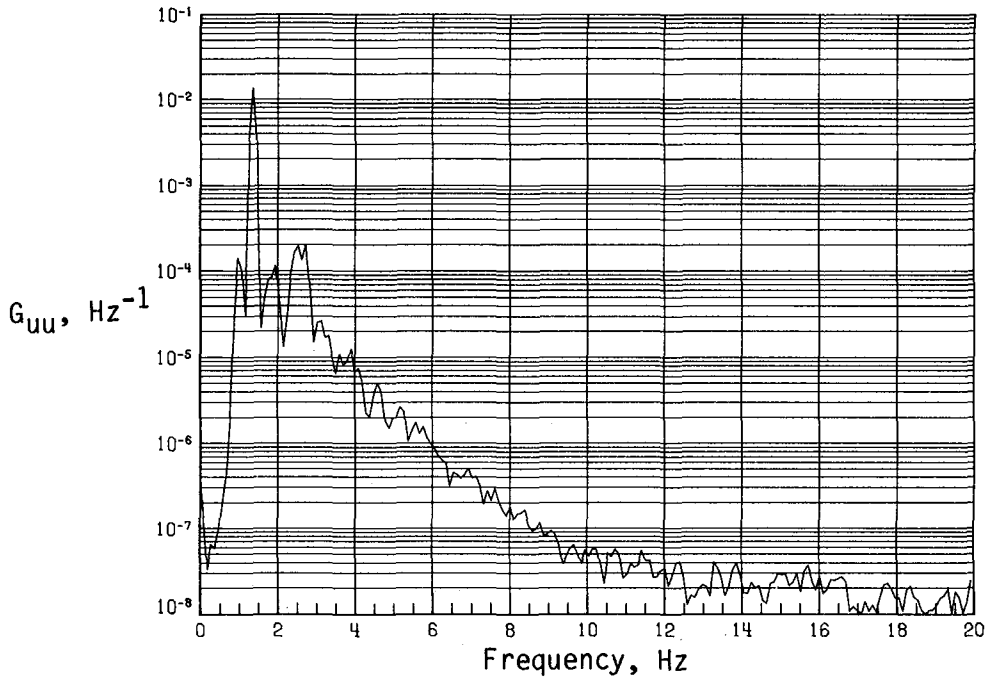

(c) PSD of streamwise velocity fluctuations.

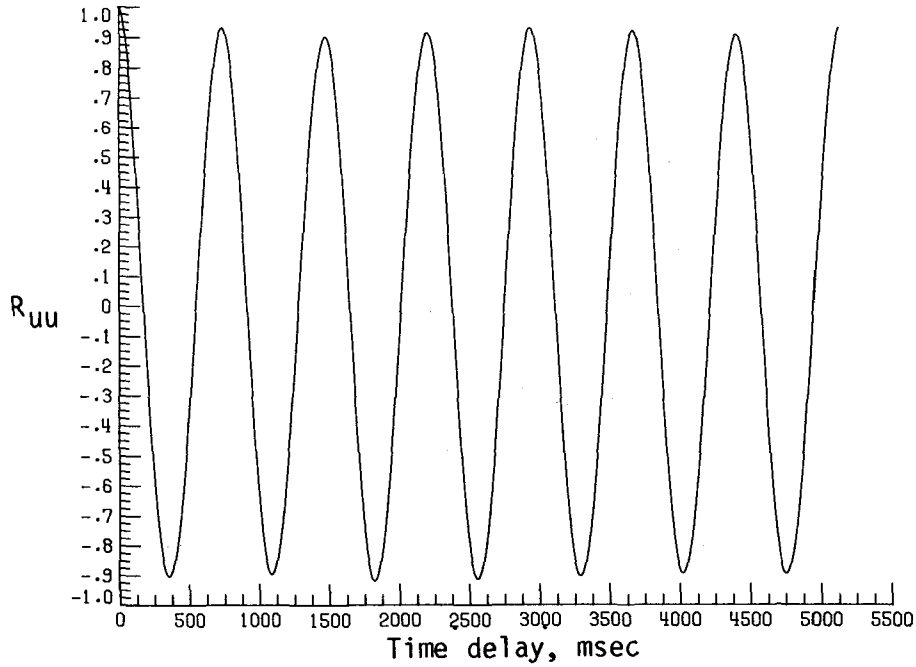

(d) Normalized autocorrelation of streamwise velocity fluctuations. $\sigma = 0.0470$.

Figure A7. Continued.

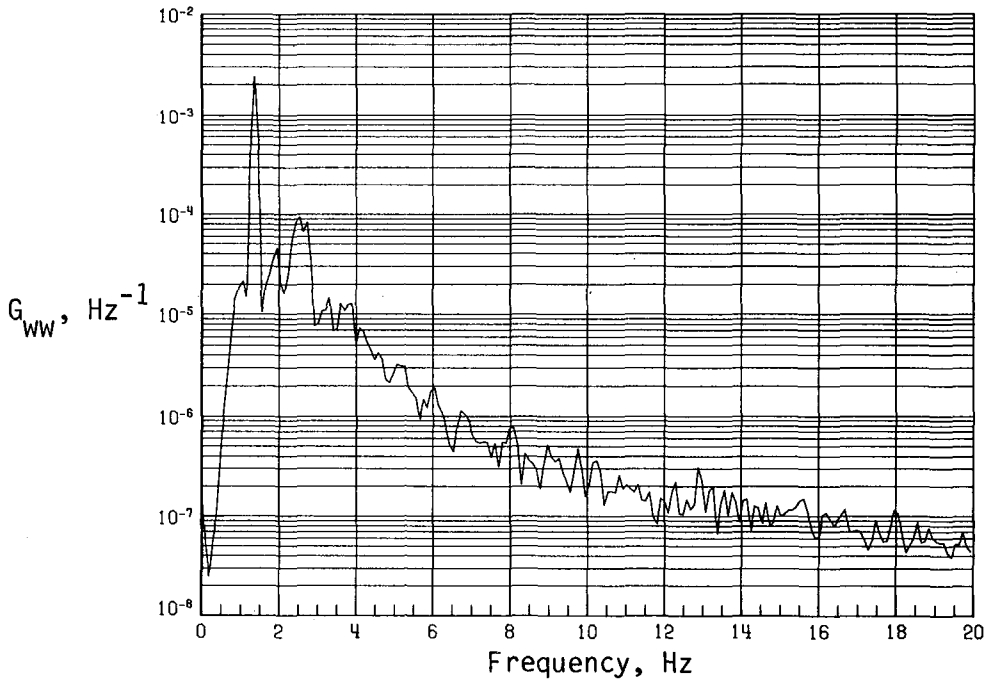

(e) PSD of vertical velocity fluctuations.

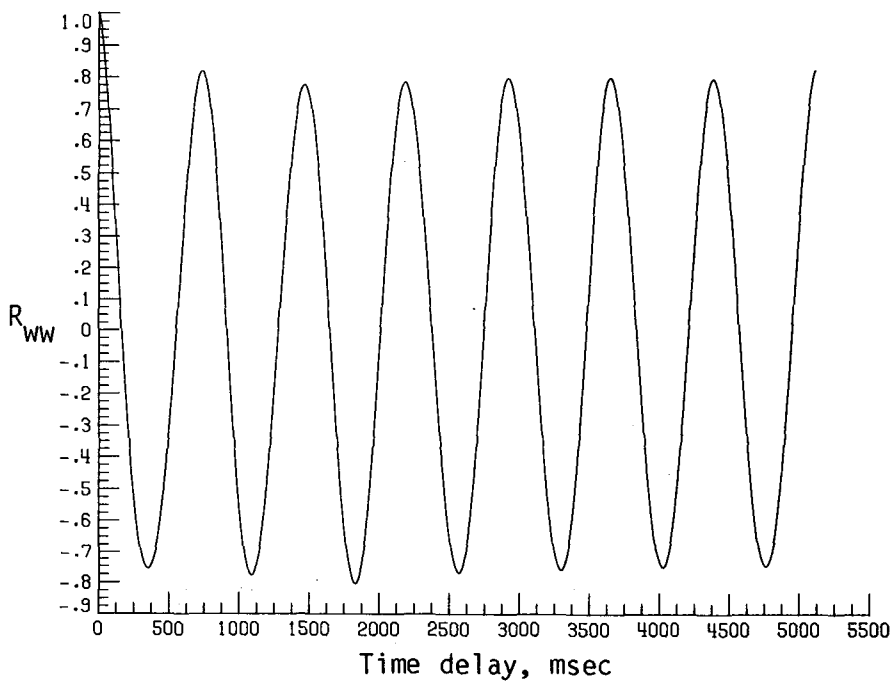

(f) Normalized autocorrelation of vertical velocity fluctuations. $\sigma = 0.0214$.

Figure A7. Concluded.

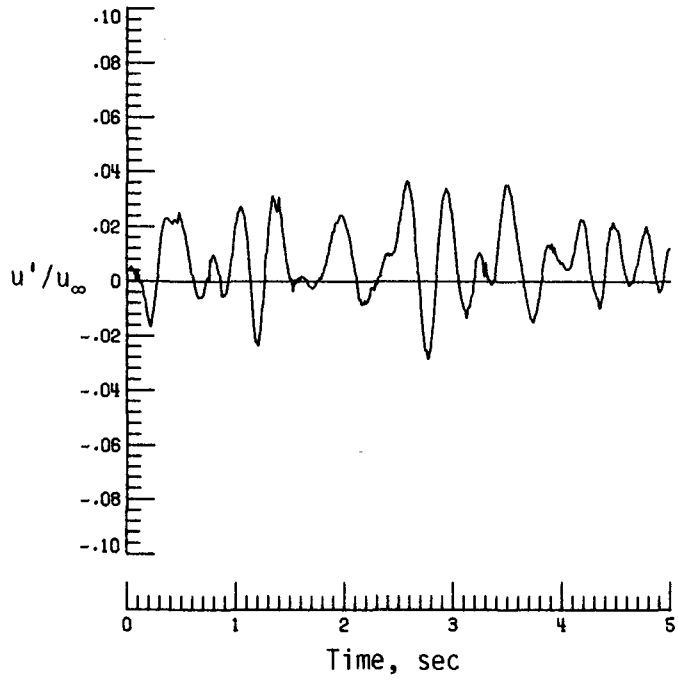

(a) Time history of streamwise velocity fluctuations.

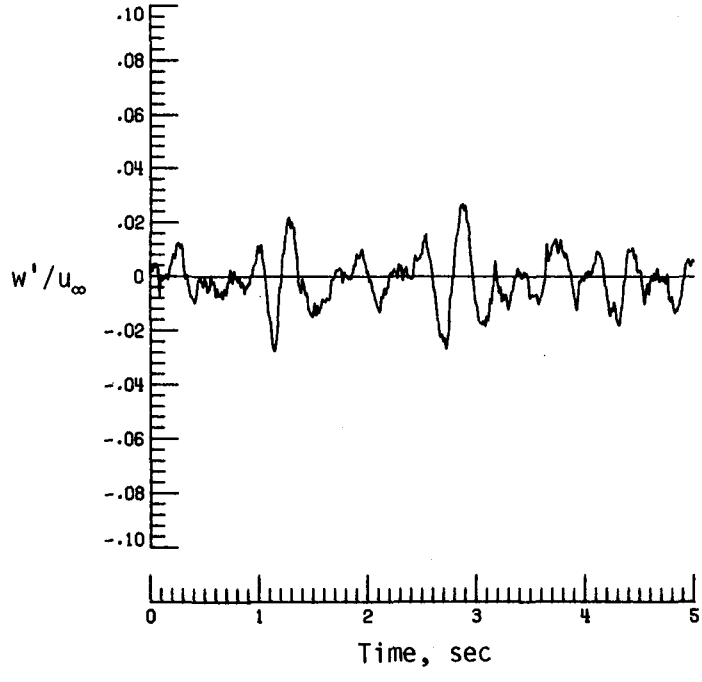

(b) Time history of vertical velocity fluctuations.

Figure A8. Dynamic-flow quality for baseline configuration at $q = 11.07$ lb/ft^2.

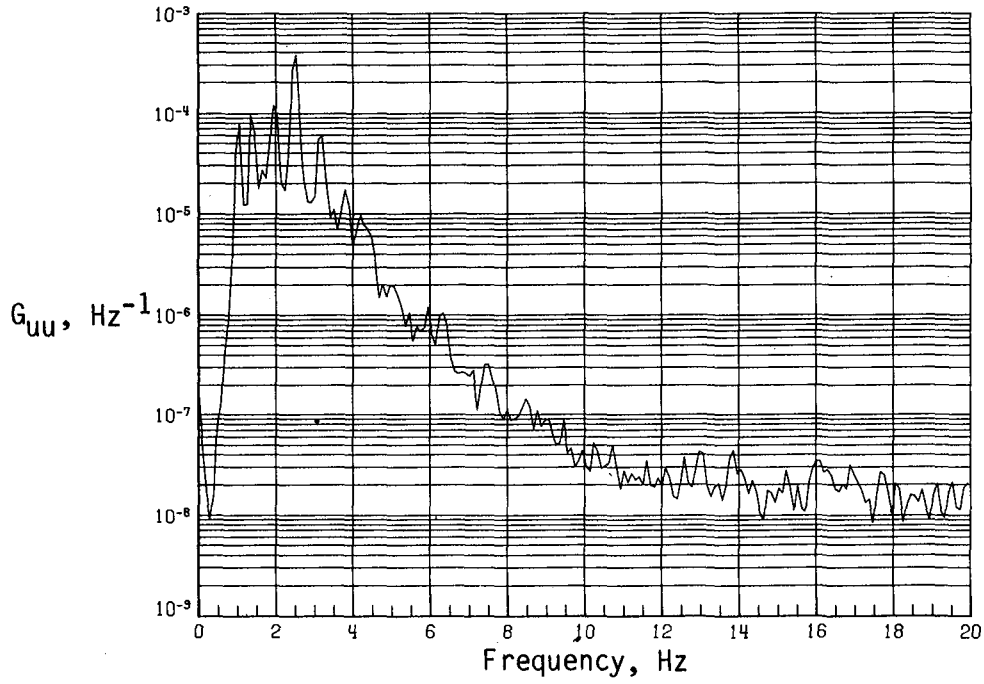

(c) PSD of streamwise velocity fluctuations.

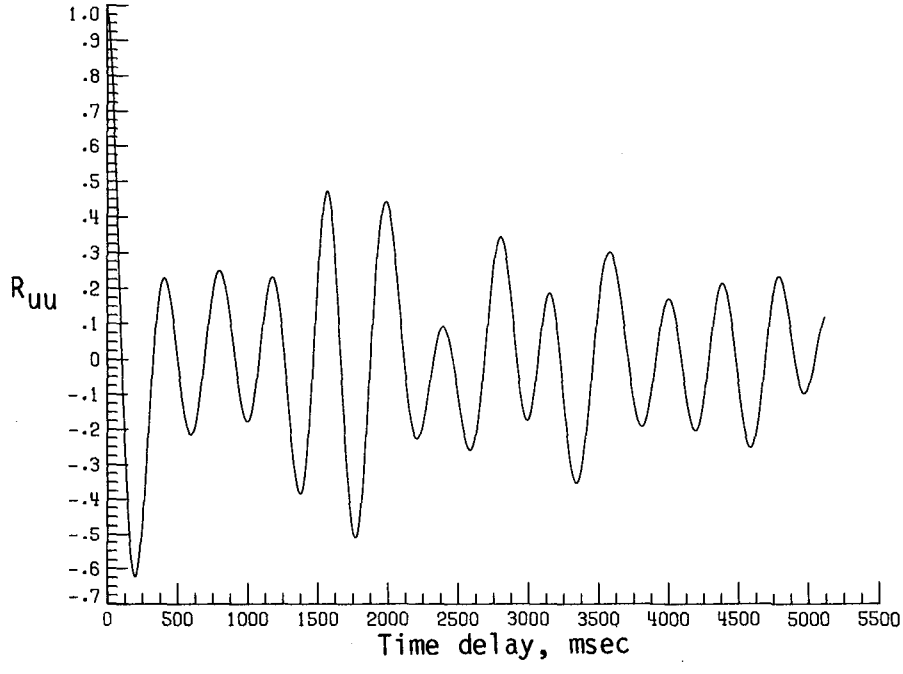

(d) Normalized autocorrelation of streamwise velocity fluctuations. $\sigma = 0.0134$.

Figure A8. Continued.

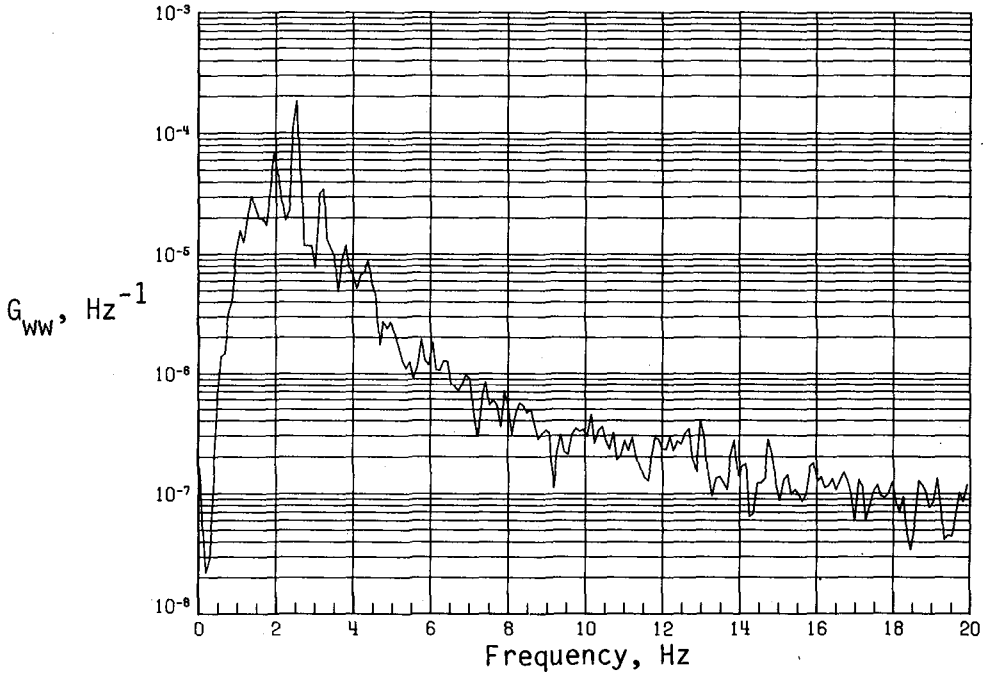

(e) PSD of vertical velocity fluctuations.

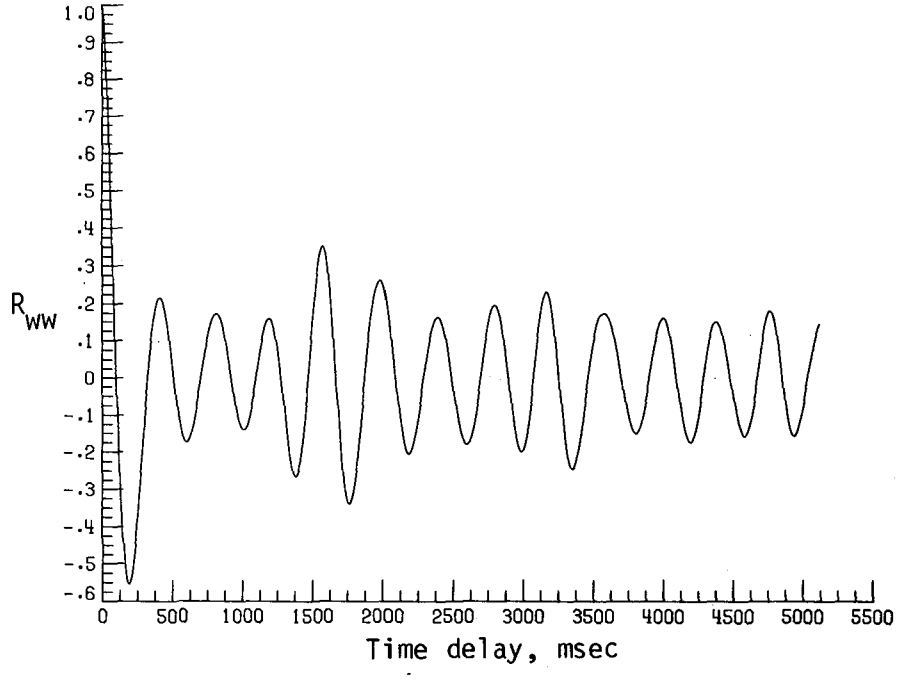

(f) Normalized autocorrelation of vertical velocity fluctuations. $\sigma = 0.0099$.

Figure A8. Concluded.

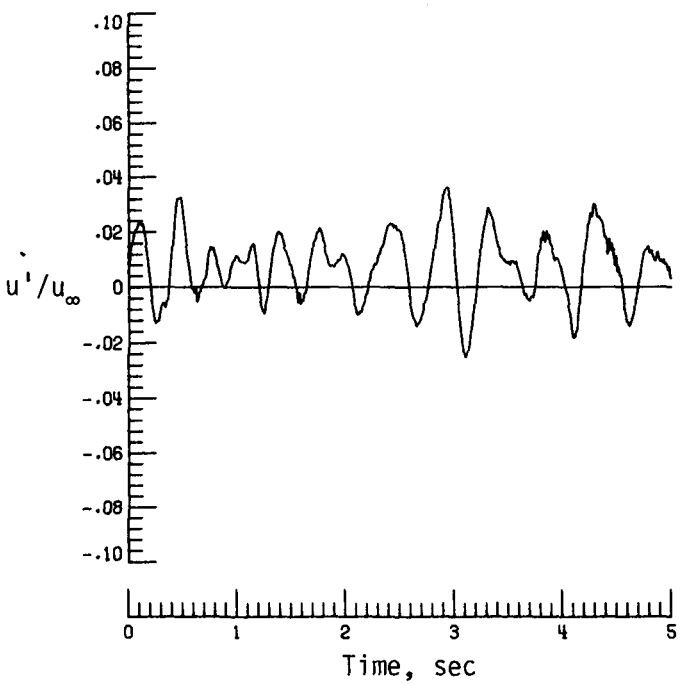

(a) Time history of streamwise velocity fluctuations.

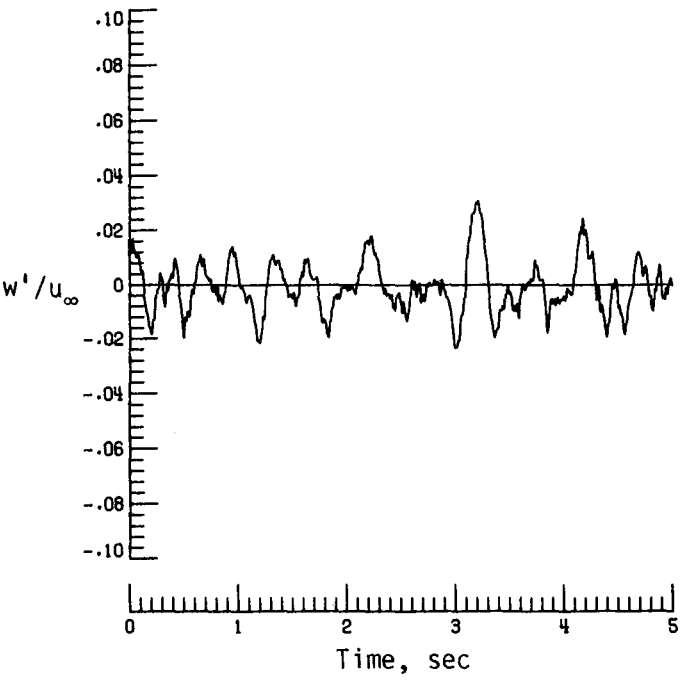

(b) Time history of vertical velocity fluctuations.

Figure A9. Dynamic-flow quality for baseline configuration at $q = 12.09$ lb/ft^2.

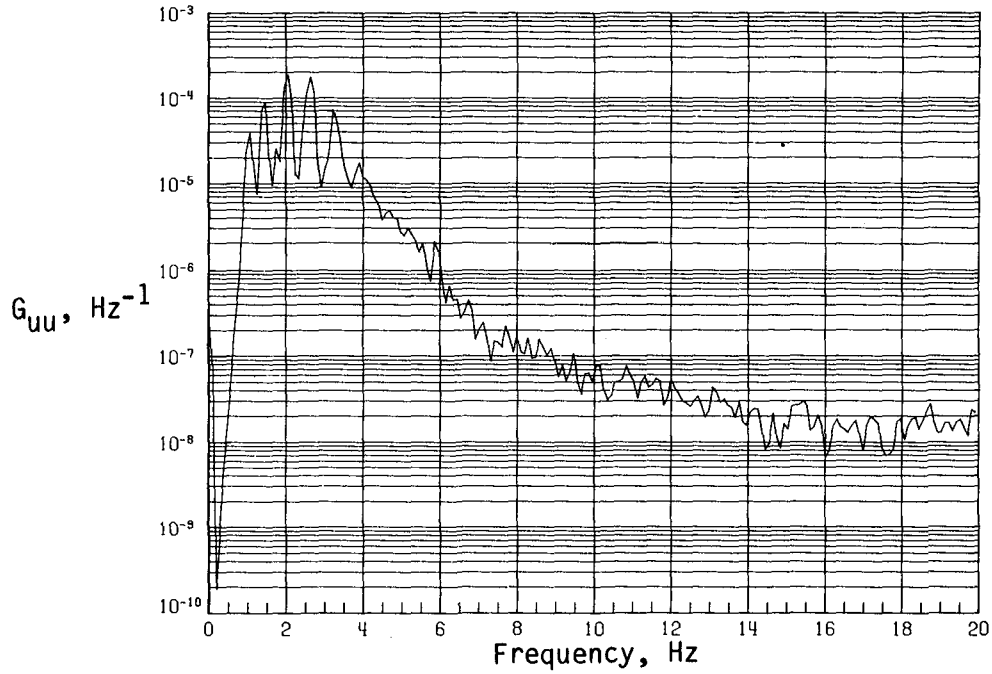

(c) PSD of streamwise velocity fluctuations.

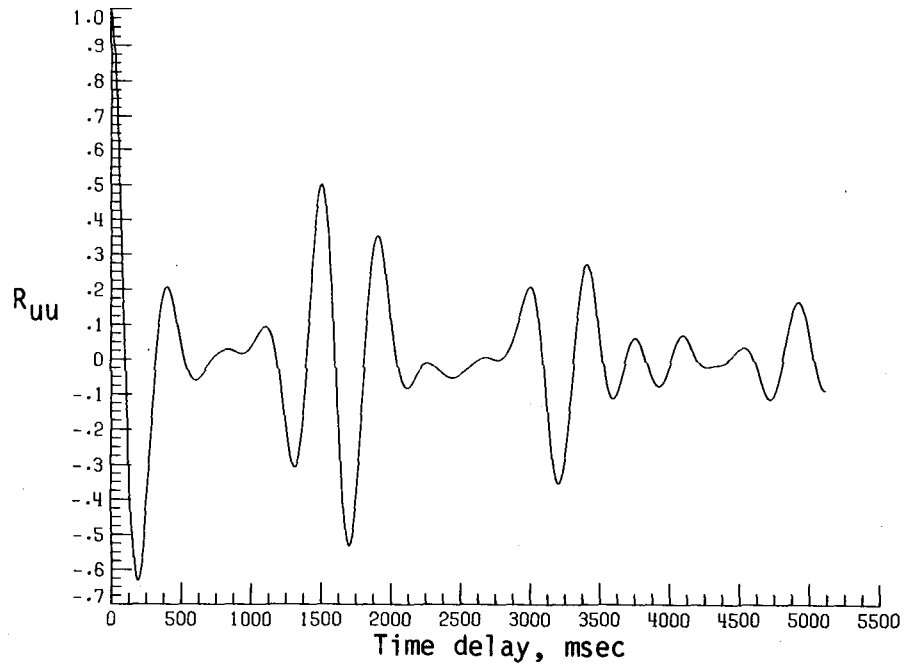

(d) Normalized autocorrelation of streamwise velocity fluctuations. $\sigma = 0.0127$.

Figure A9. Continued.

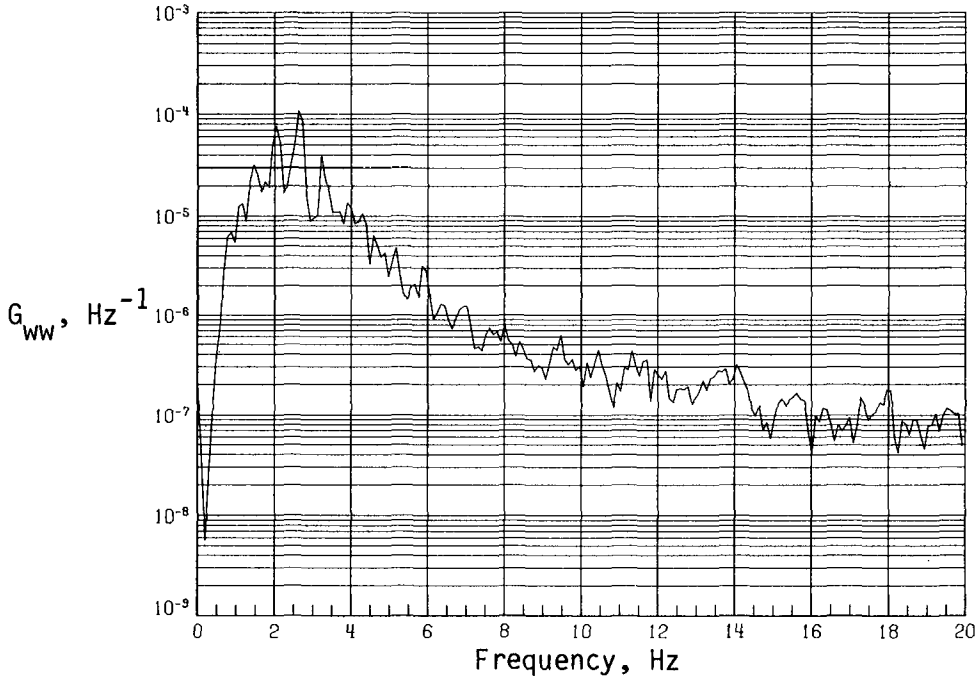

(e) PSD of vertical velocity fluctuations.

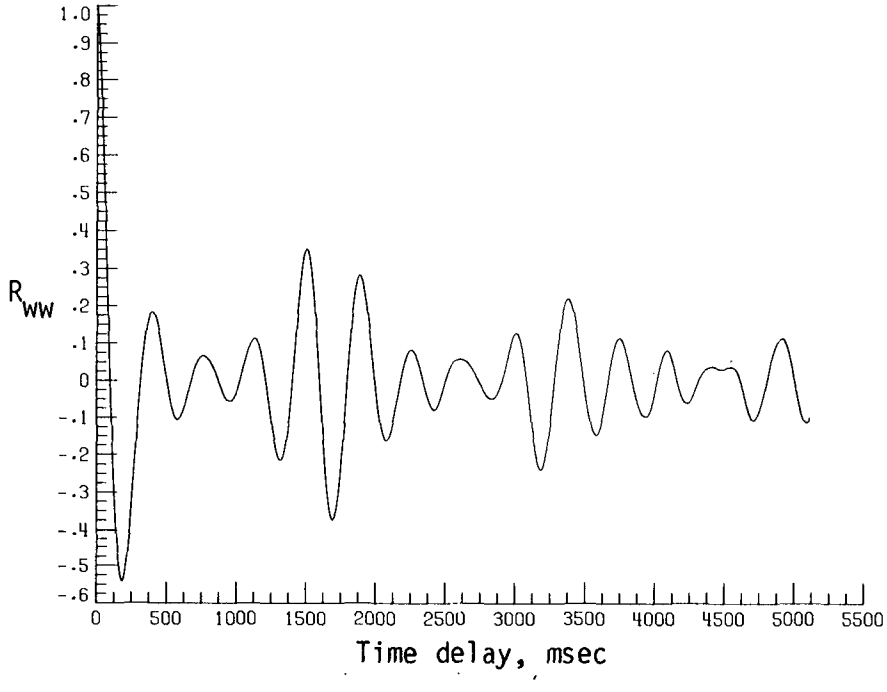

(f) Normalized autocorrelation of vertical velocity fluctuations. $\sigma = 0.0098$.

Figure A9. Concluded.

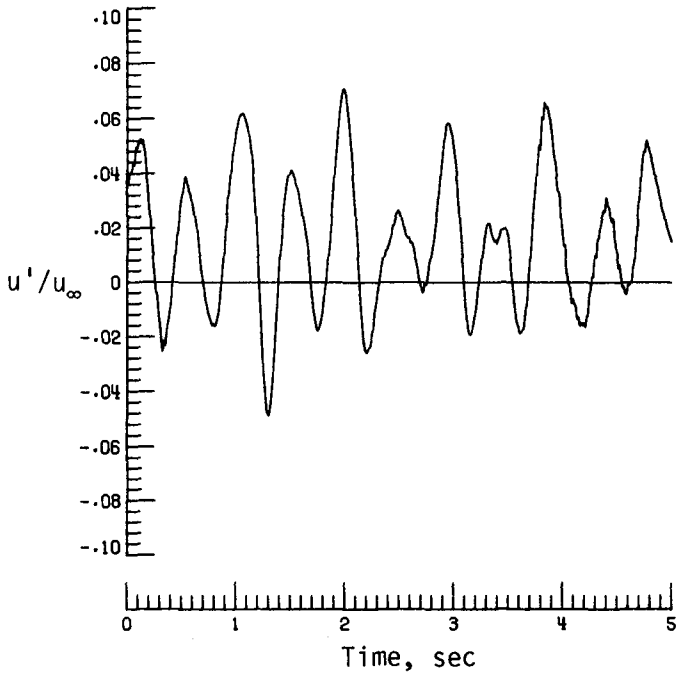

(a) Time history of streamwise velocity fluctuations.

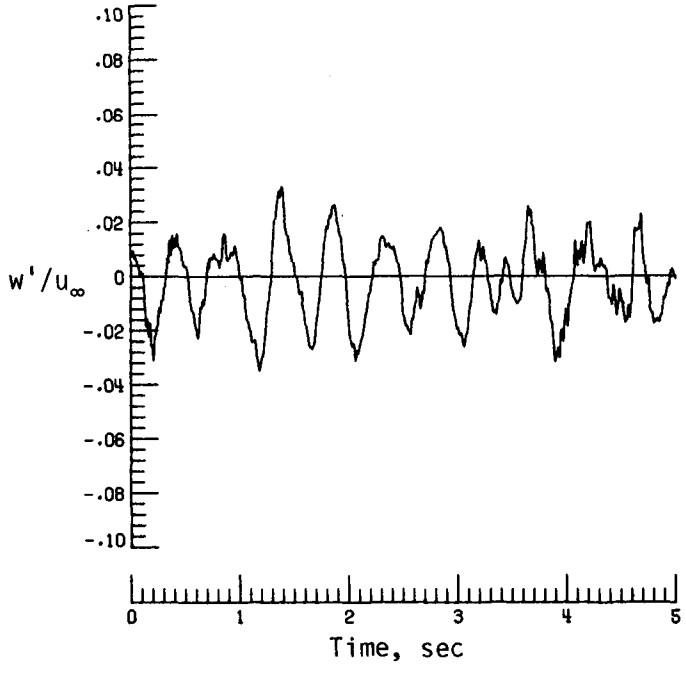

(b) Time history of vertical velocity fluctuations.

Figure A10. Dynamic-flow quality for baseline configuration at $q = 13.23$ lb/ft^2.

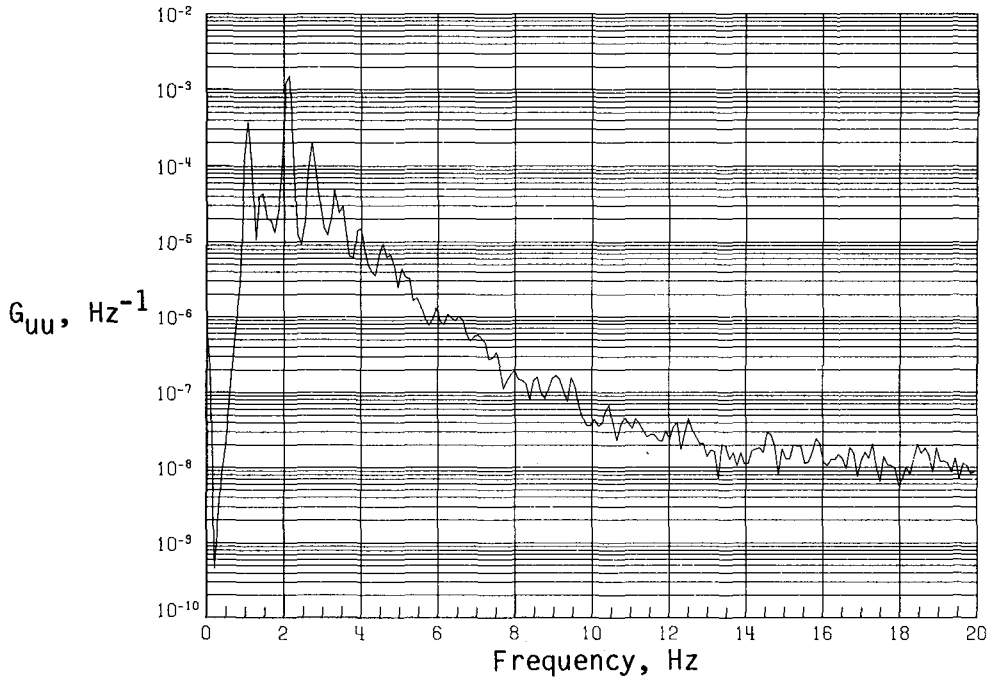

(c) PSD of streamwise velocity fluctuations.

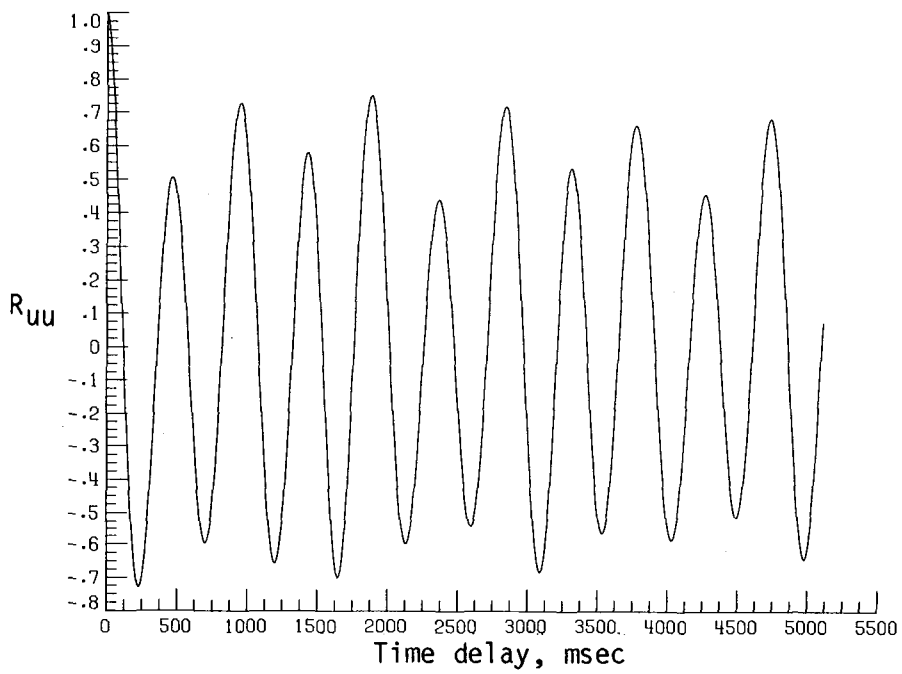

(d) Normalized autocorrelation of streamwise velocity fluctuations. $\sigma = 0.0210$.

Figure A10. Continued.

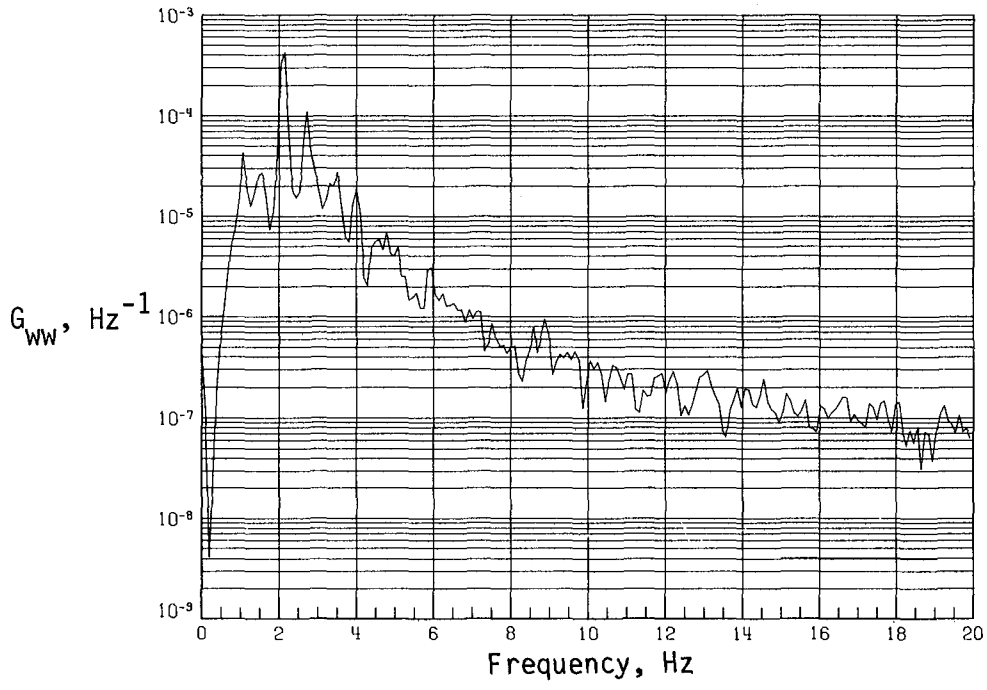

(e) PSD of vertical velocity fluctuations.

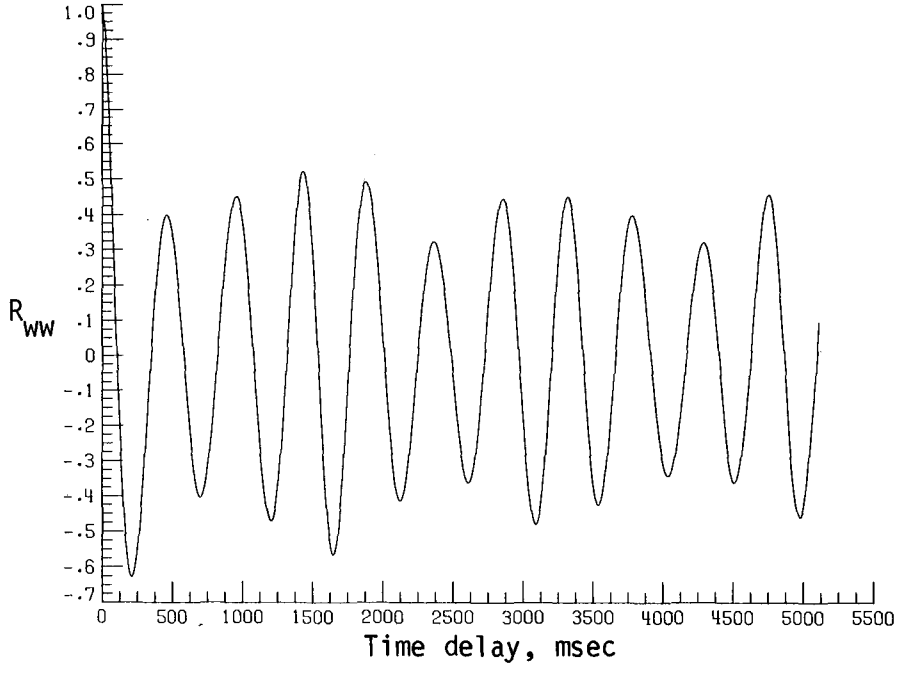

(f) Normalized autocorrelation of vertical velocity fluctuations. $\sigma = 0.0127$.

Figure A10. Concluded.

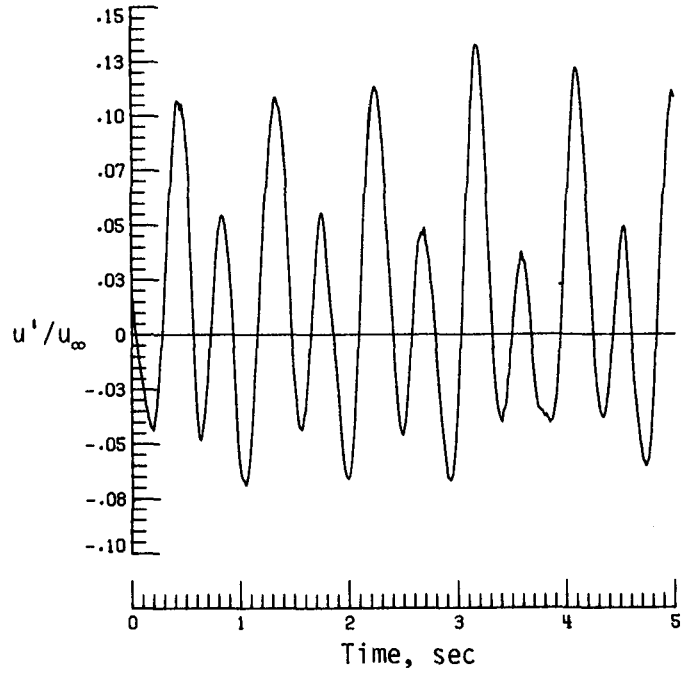

(a) Time history of streamwise velocity fluctuations.

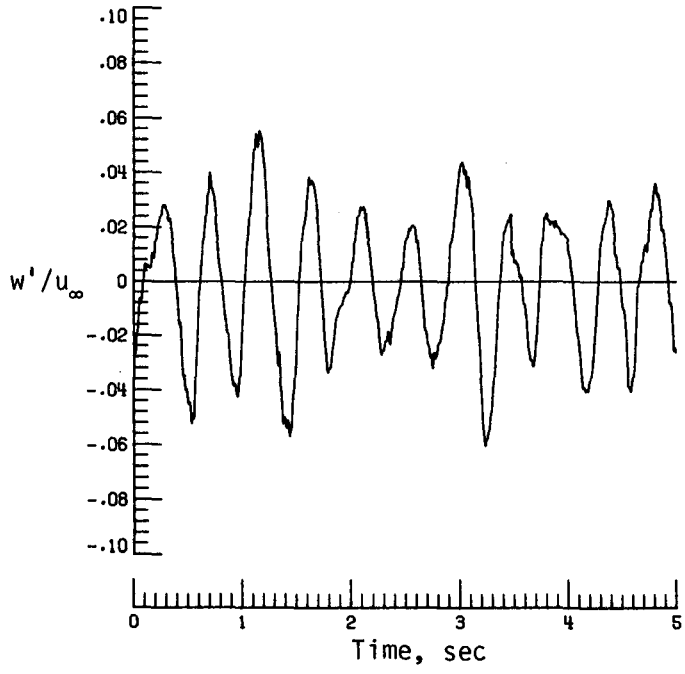

(b) Time history of vertical velocity fluctuations.

Figure A11. Dynamic-flow quality for baseline configuration at $q = 14.02$ lb/ft^2.

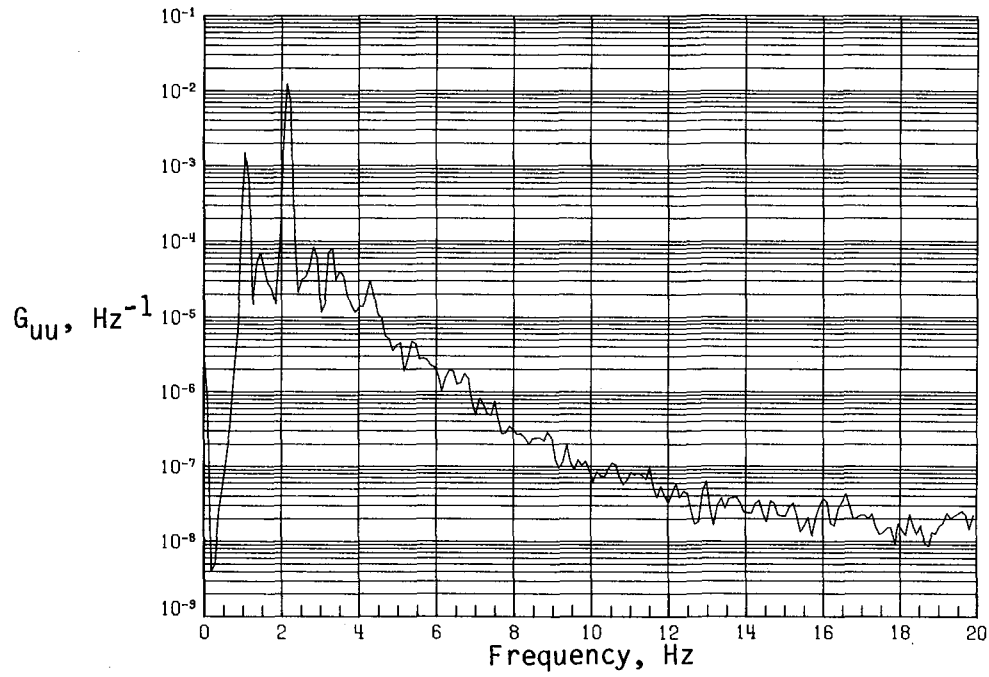

(c) PSD of streamwise velocity fluctuations.

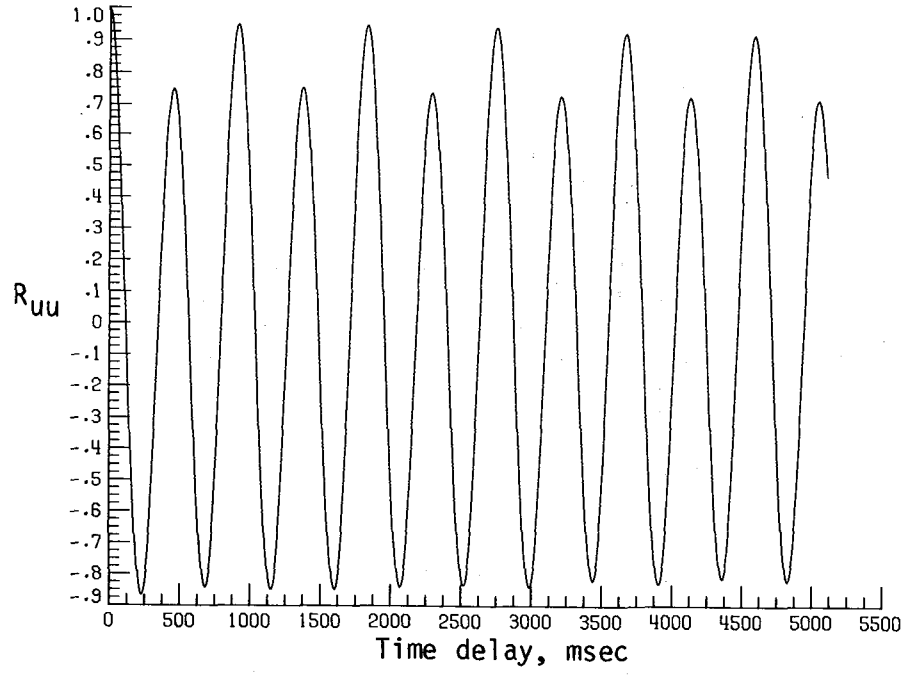

(d) Normalized autocorrelation of streamwise velocity fluctuations. $\sigma = 0.0489$.

Figure A11. Continued.

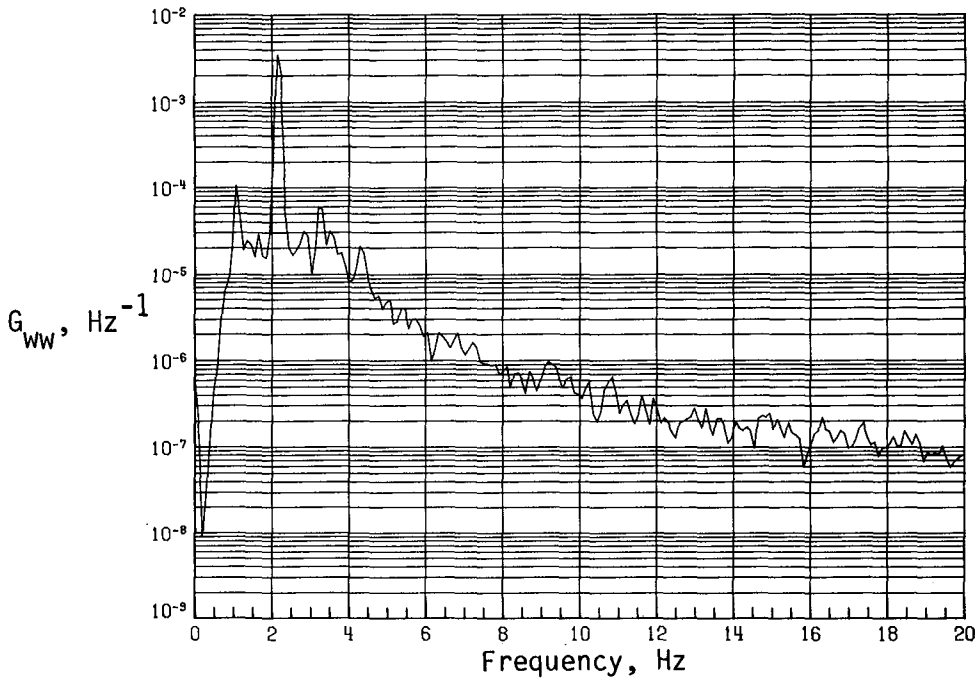

(e) PSD of vertical velocity fluctuations.

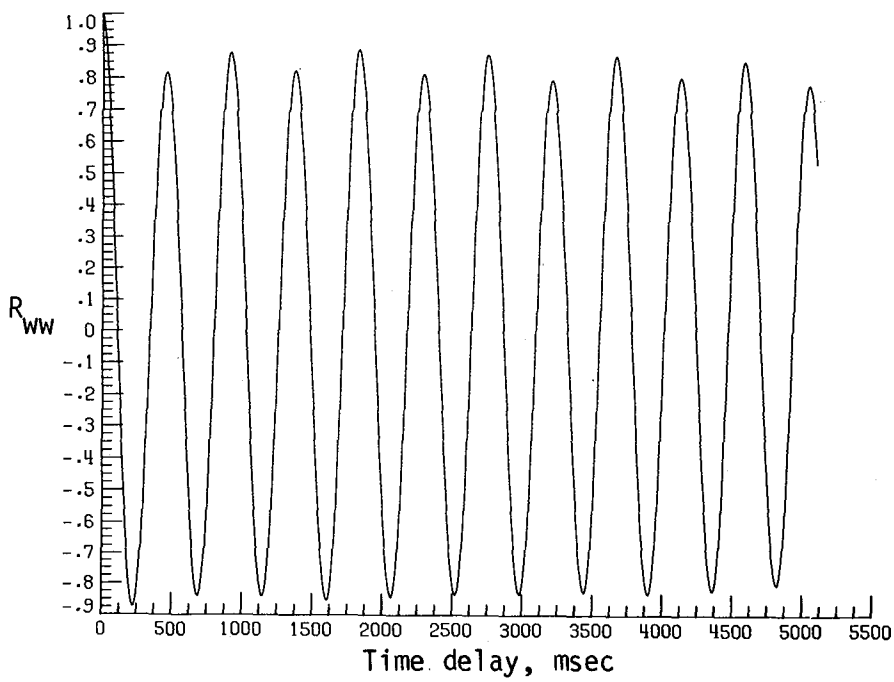

(f) Normalized autocorrelation of vertical velocity fluctuations. $\sigma = 0.0256$.

Figure A11. Concluded.

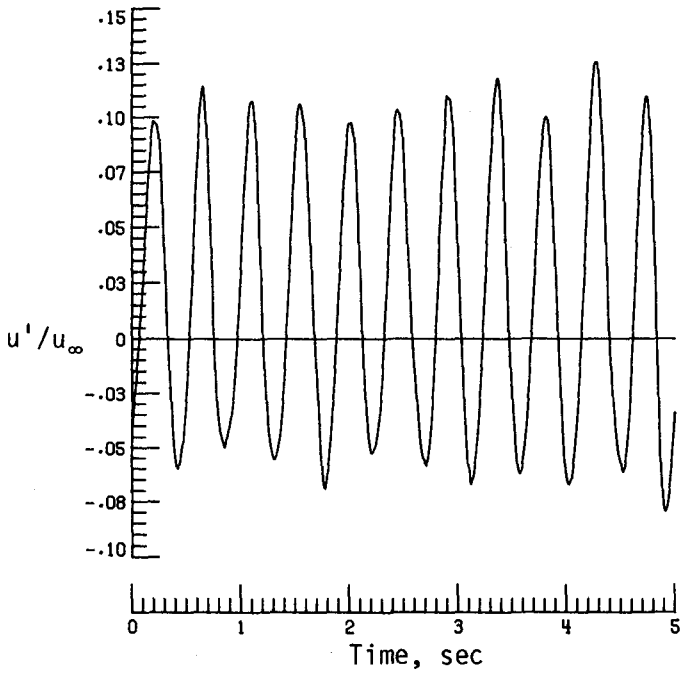

(a) Time history of streamwise velocity fluctuations.

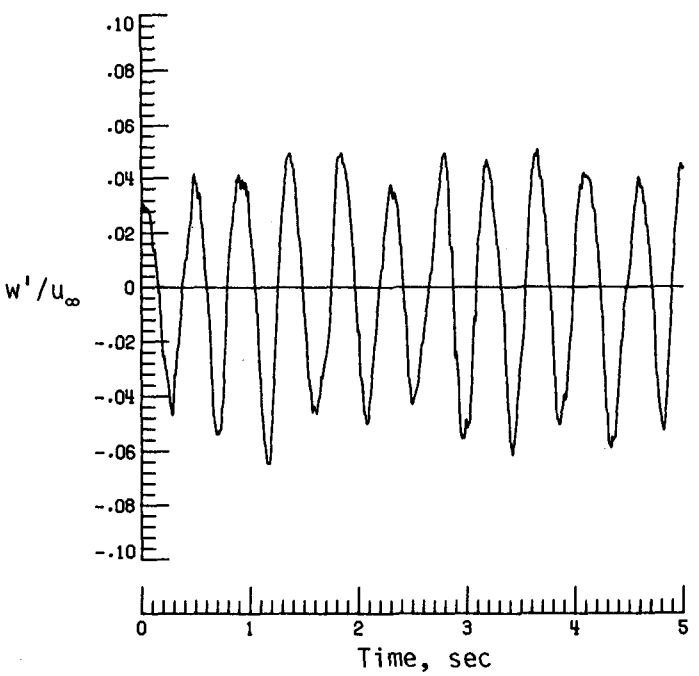

(b) Time history of vertical velocity fluctuations.

Figure A12. Dynamic-flow quality for baseline configuration at $q = 15.26$ lb/ft^2.

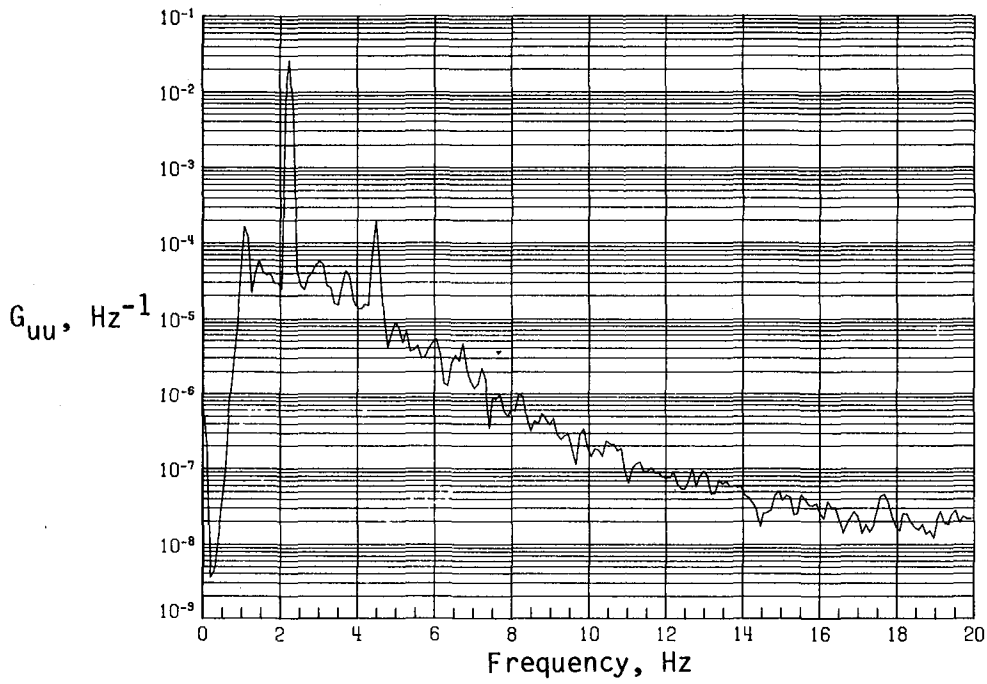

(c) PSD of streamwise velocity fluctuations.

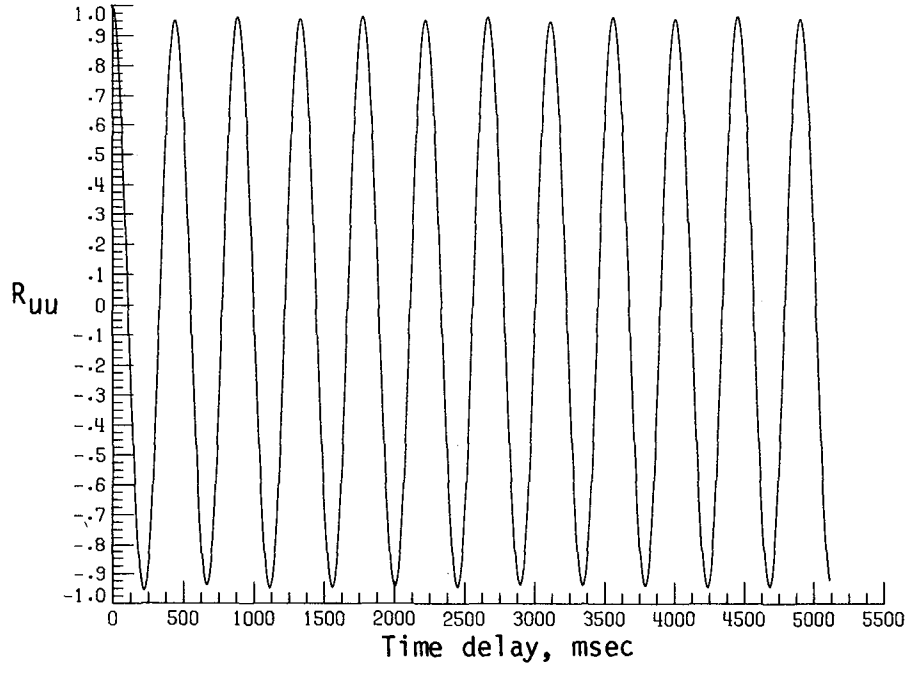

(d) Normalized autocorrelation of streamwise velocity fluctuations. $\sigma = 0.0642$.

Figure A12. Continued.

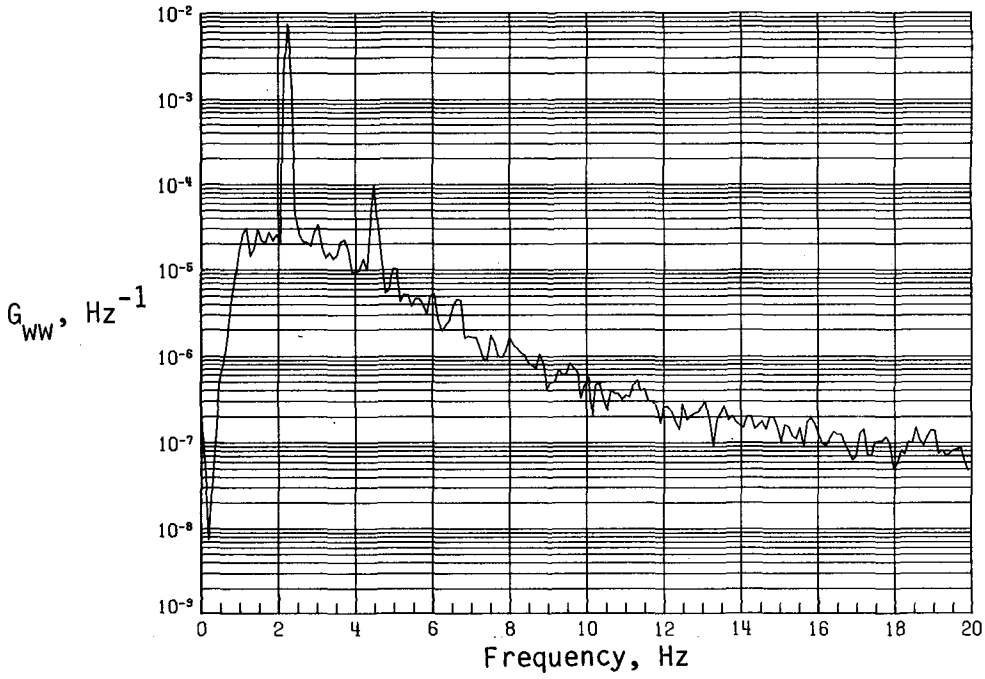

(e) PSD of vertical velocity fluctuations.

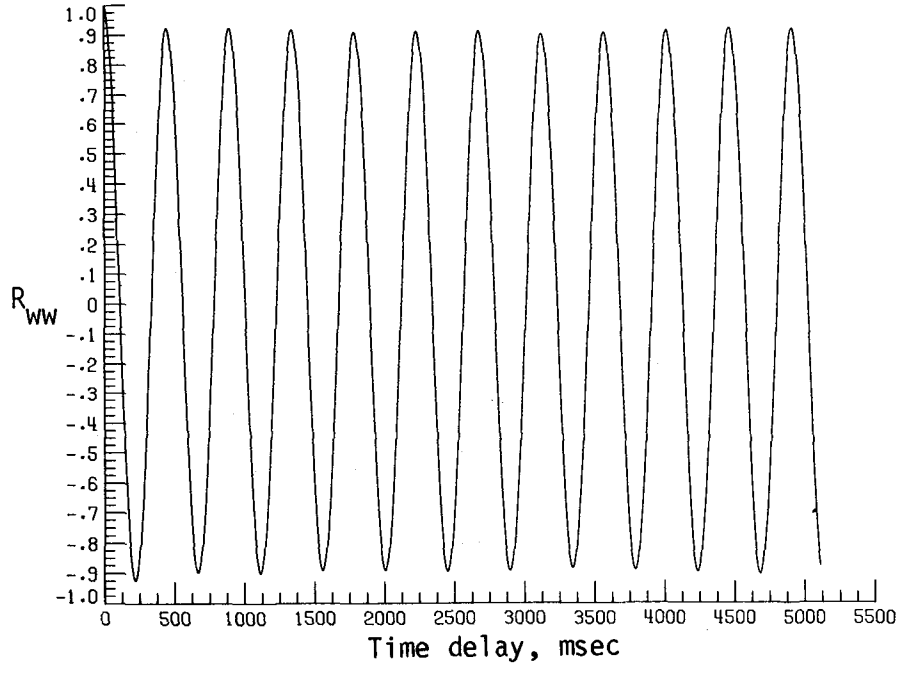

(f) Normalized autocorrelation of vertical velocity fluctuations. $\sigma = 0.0351$.

Figure A12. Concluded.

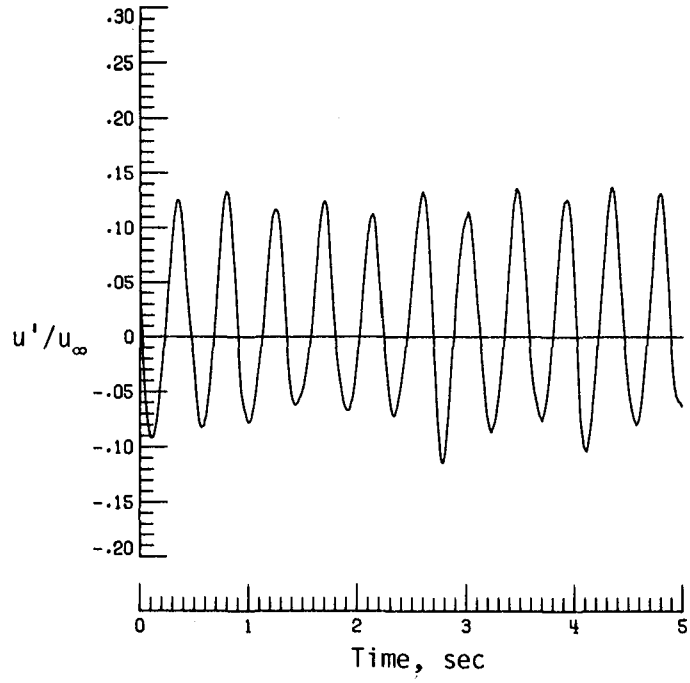

(a) Time history of streamwise velocity fluctuations.

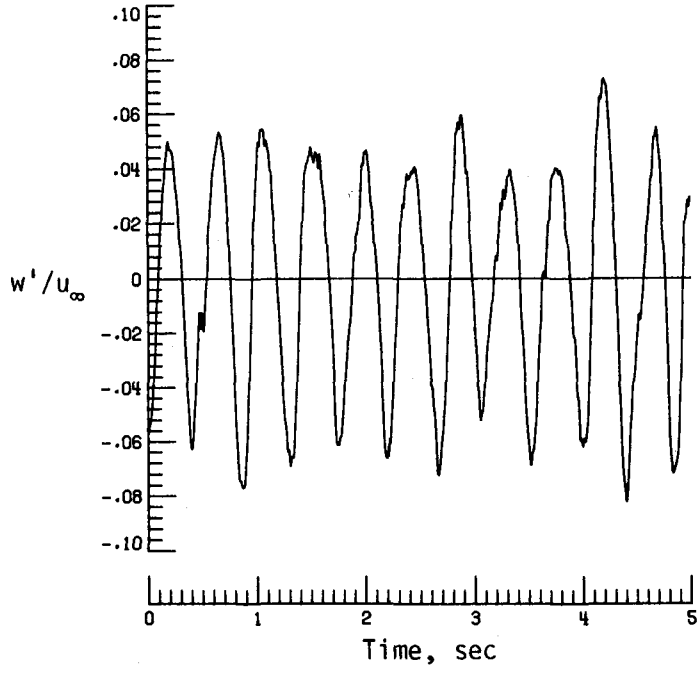

(b) Time history of vertical velocity fluctuations.

Figure A13. Dynamic-flow quality for baseline configuration at $q = 16.05$ lb/ft^2.

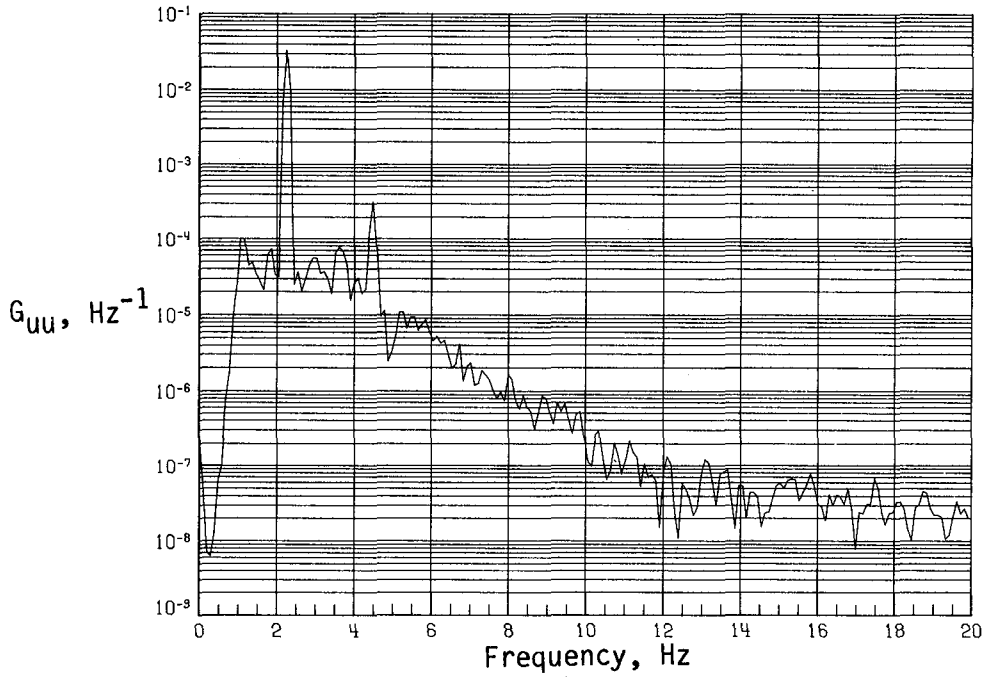

(c) PSD of streamwise velocity fluctuations.

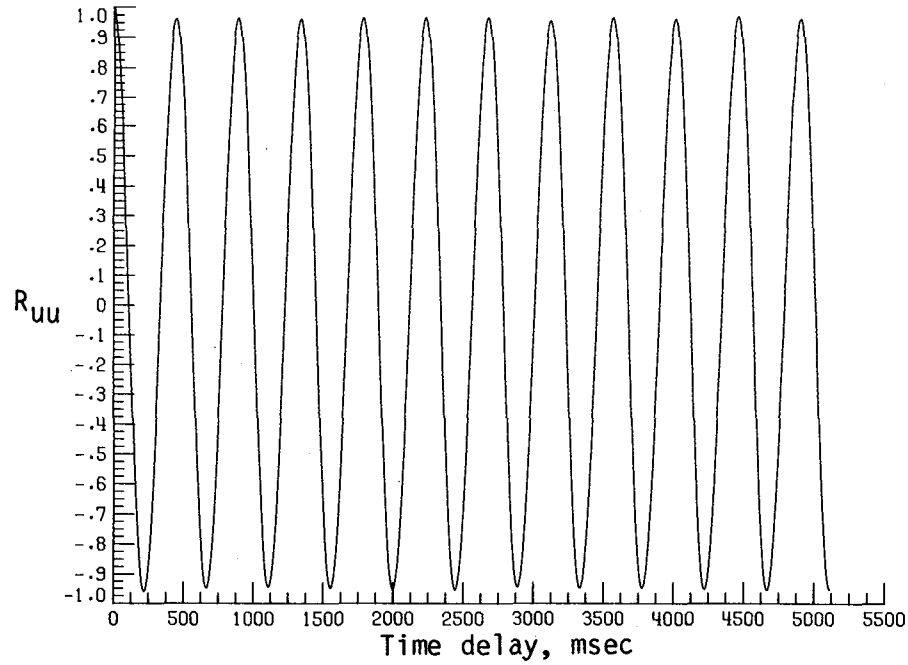

(d) Normalized autocorrelation of streamwise velocity fluctuations. $\sigma = 0.0715$.

Figure A13. Continued.

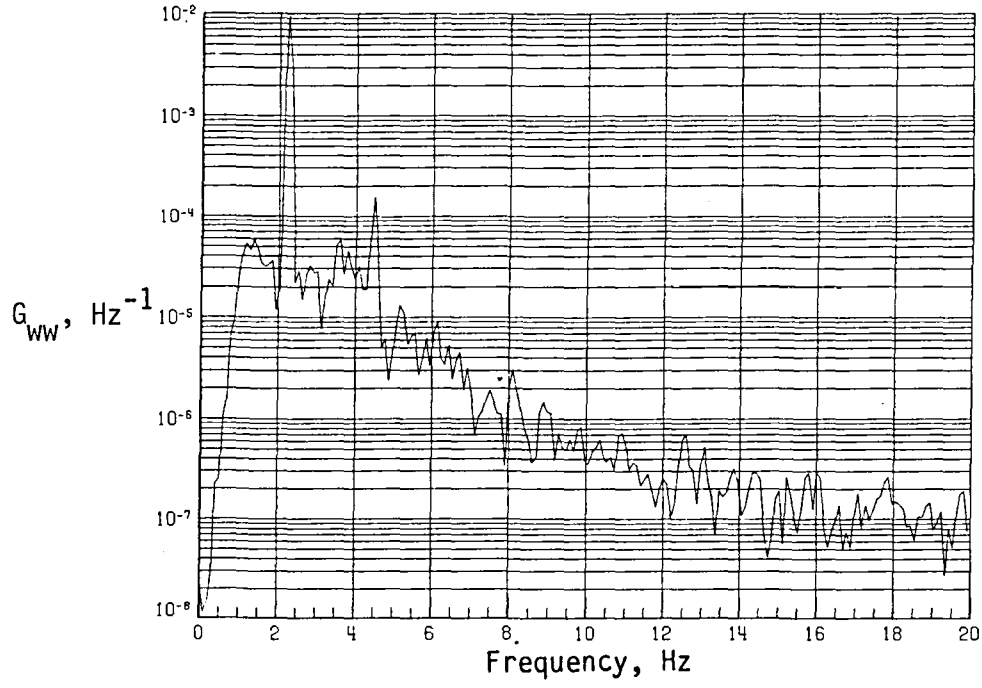

(e) PSD of vertical velocity fluctuations.

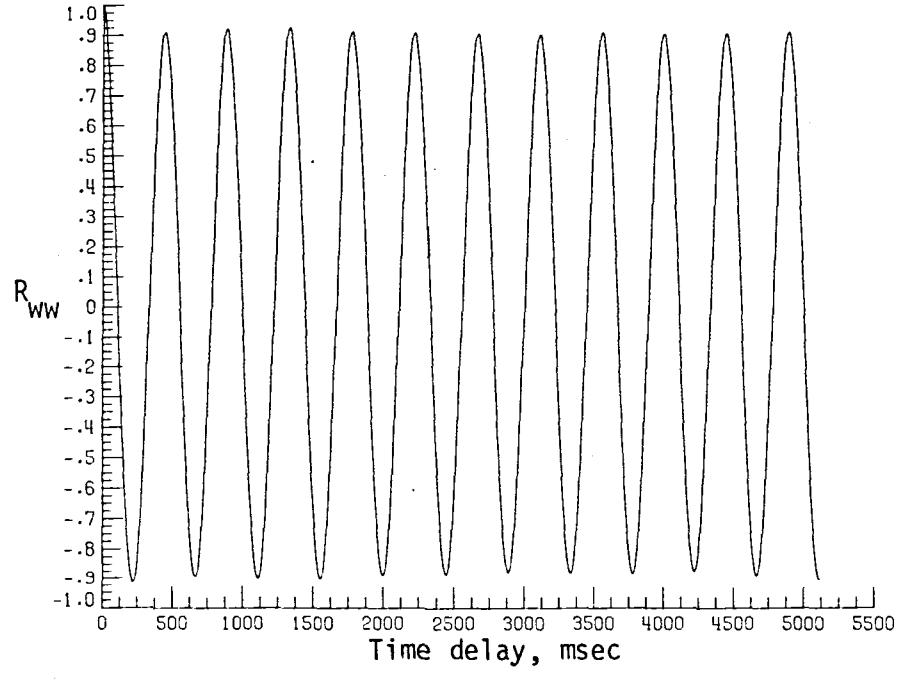

(f) Normalized autocorrelation of vertical velocity fluctuations. $\sigma = 0.0396$.

Figure A13. Concluded.

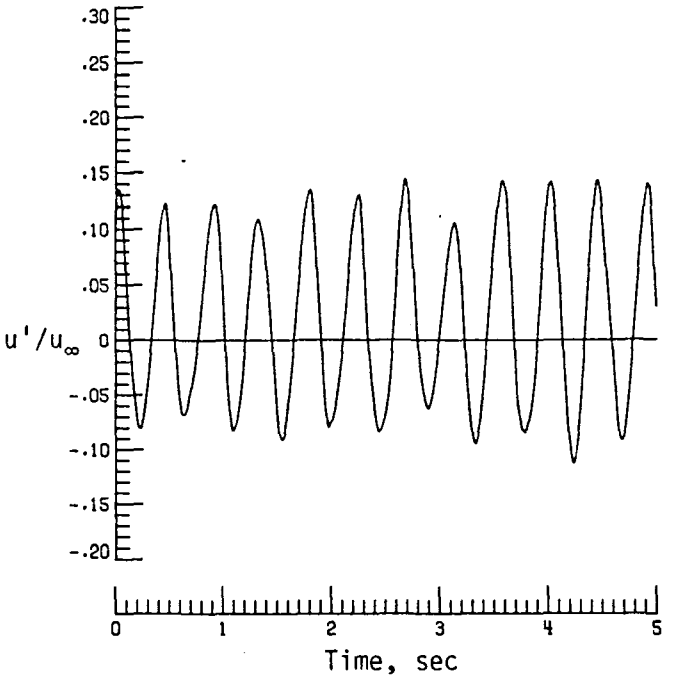

(a) Time history of streamwise velocity fluctuations.

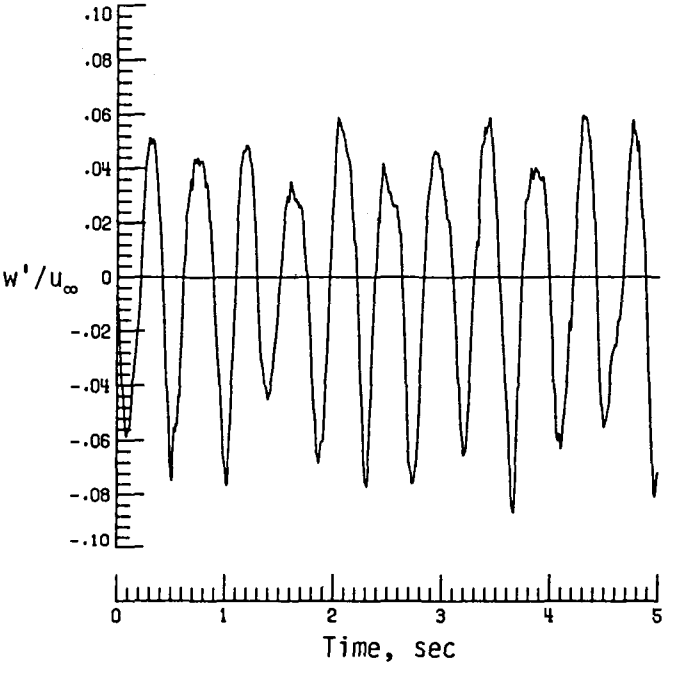

(b) Time history of vertical velocity fluctuations.

Figure A14. Dynamic-flow quality for baseline configuration at $q = 16.16$ lb/ft^2.

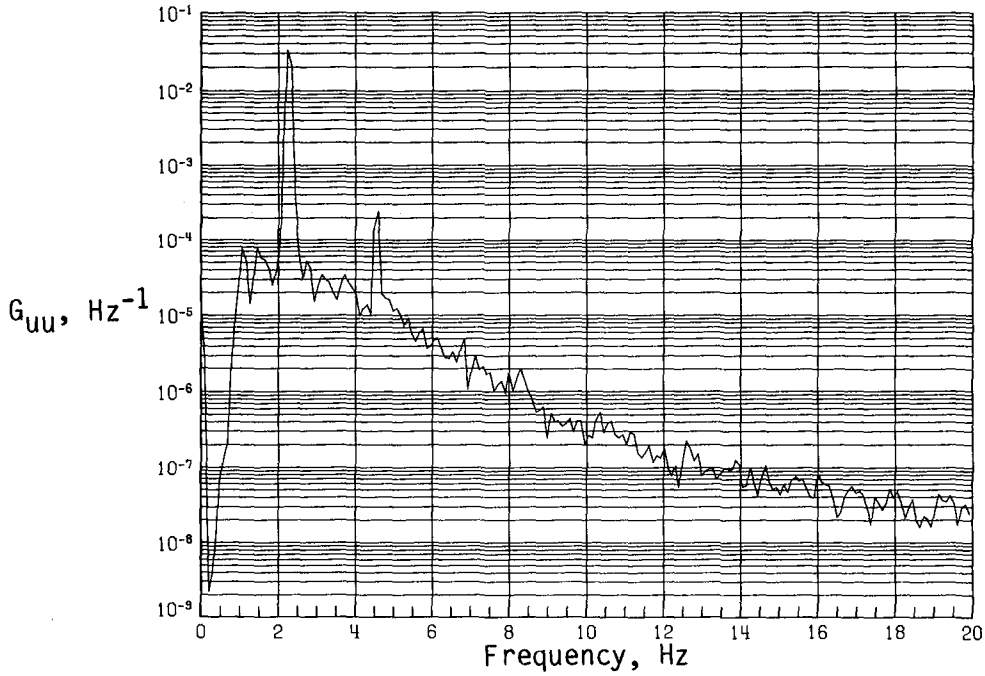

(c) PSD of streamwise velocity fluctuations.

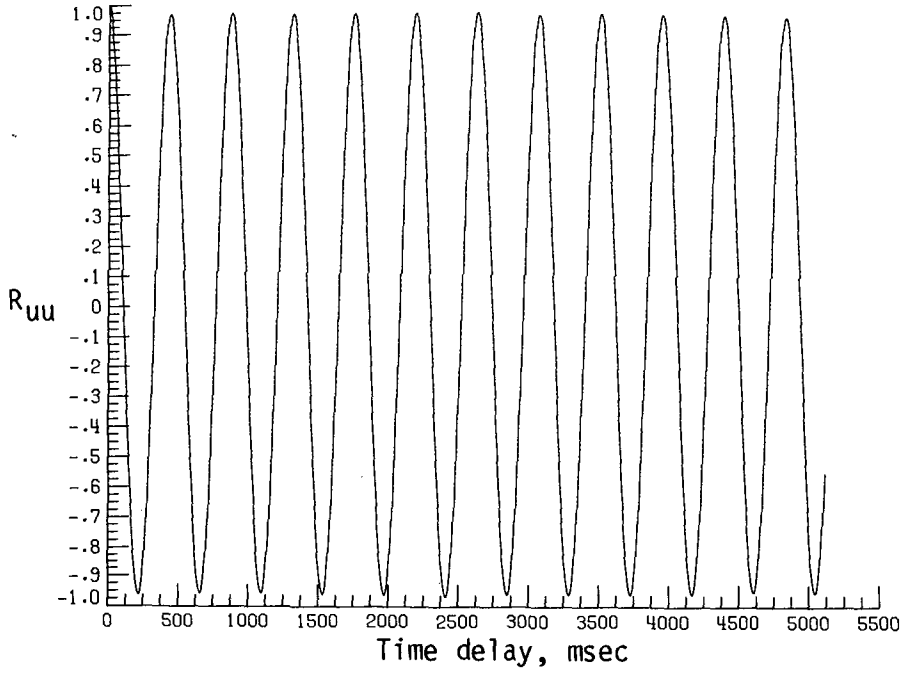

(d) Normalized autocorrelation of streamwise velocity fluctuations. $\sigma = 0.0749$.

Figure A14. Continued.

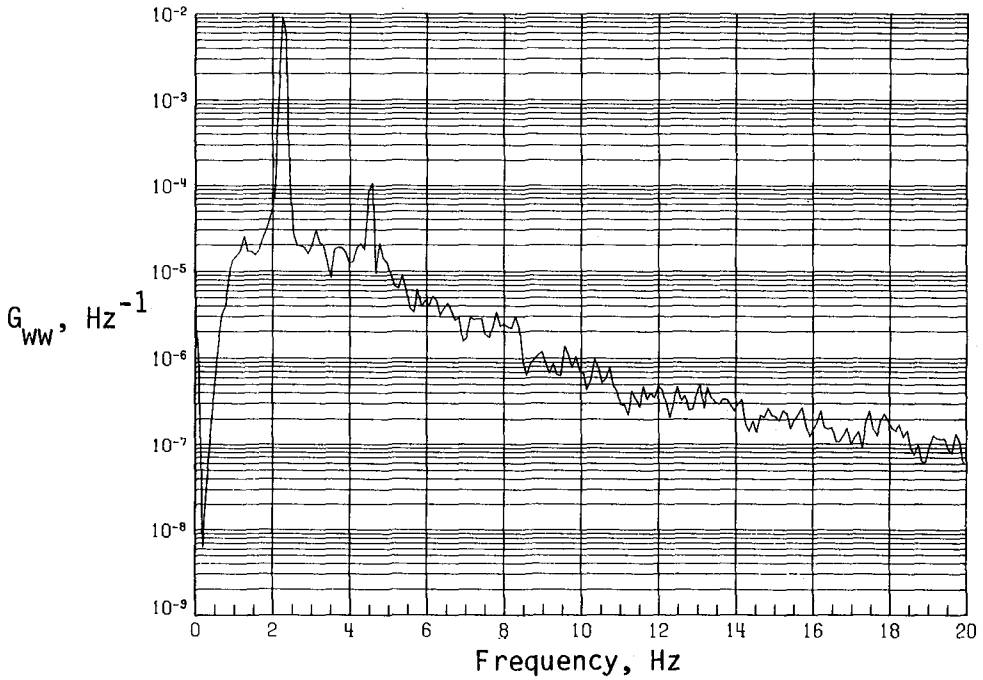

(e) PSD of vertical velocity fluctuations.

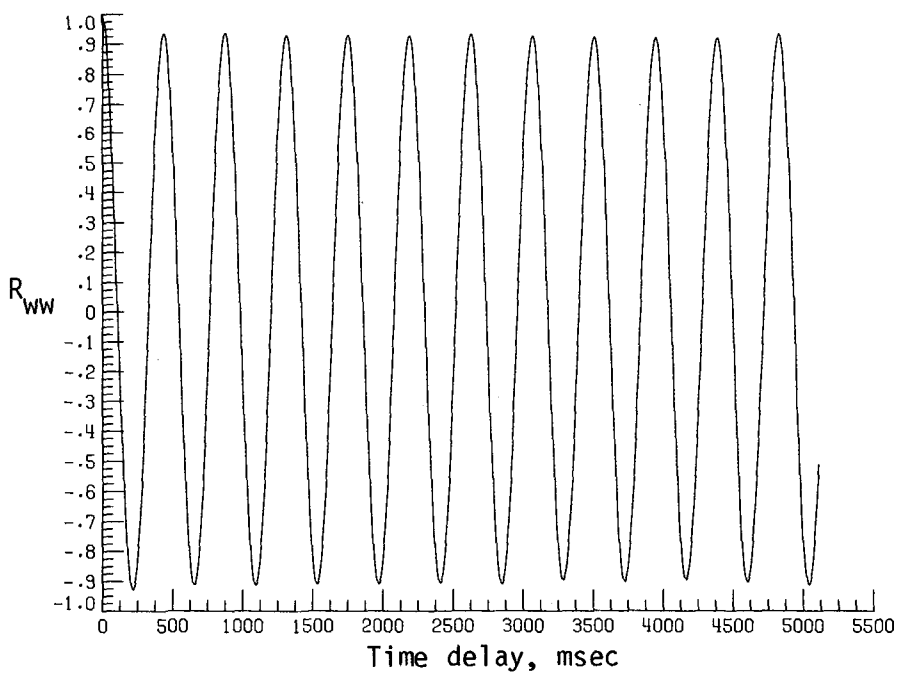

(f) Normalized autocorrelation of vertical velocity fluctuations. $\sigma = 0.0409$.

Figure A14. Concluded.

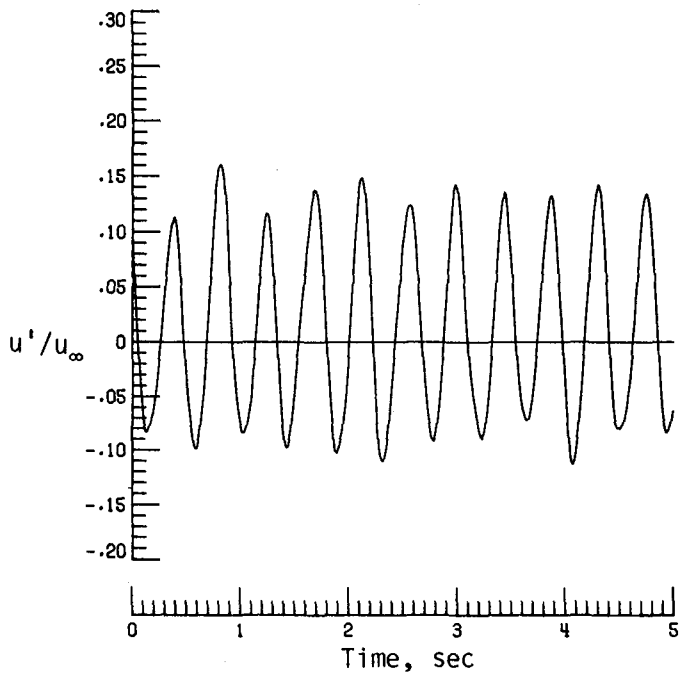

(a) Time history of streamwise velocity fluctuations.

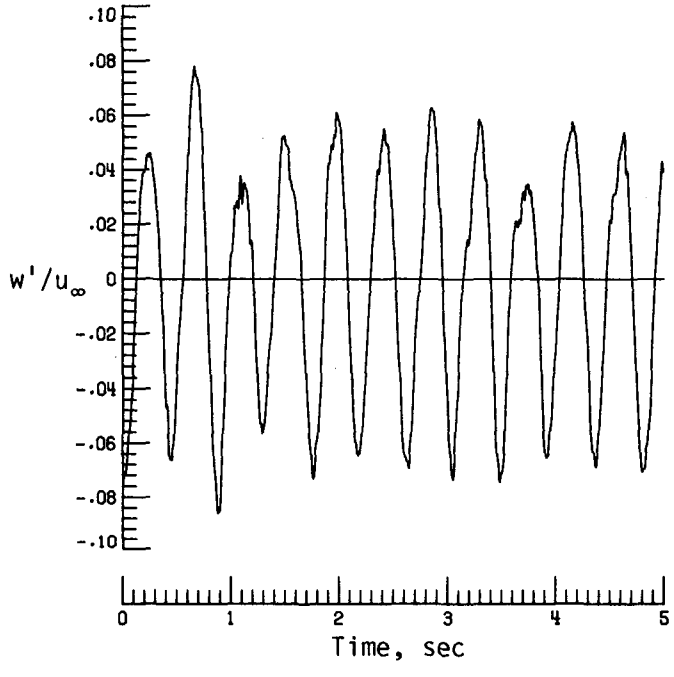

(b) Time history of vertical velocity fluctuations.

Figure A15. Dynamic-flow quality for baseline configuration at $q = 18.08$ lb/ft^2.

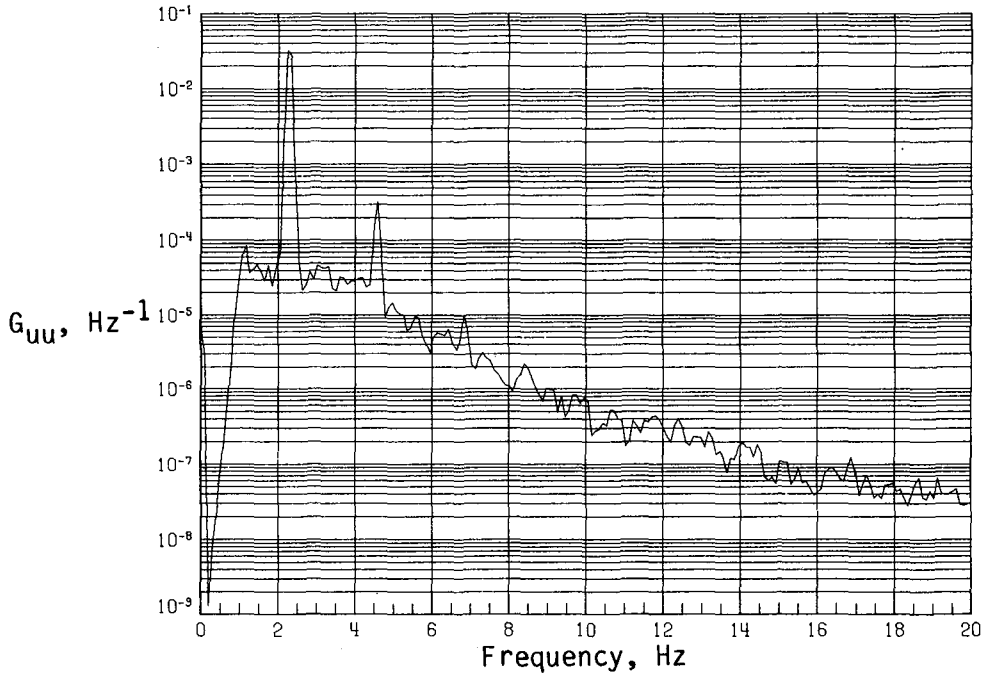

(c) PSD of streamwise velocity fluctuations.

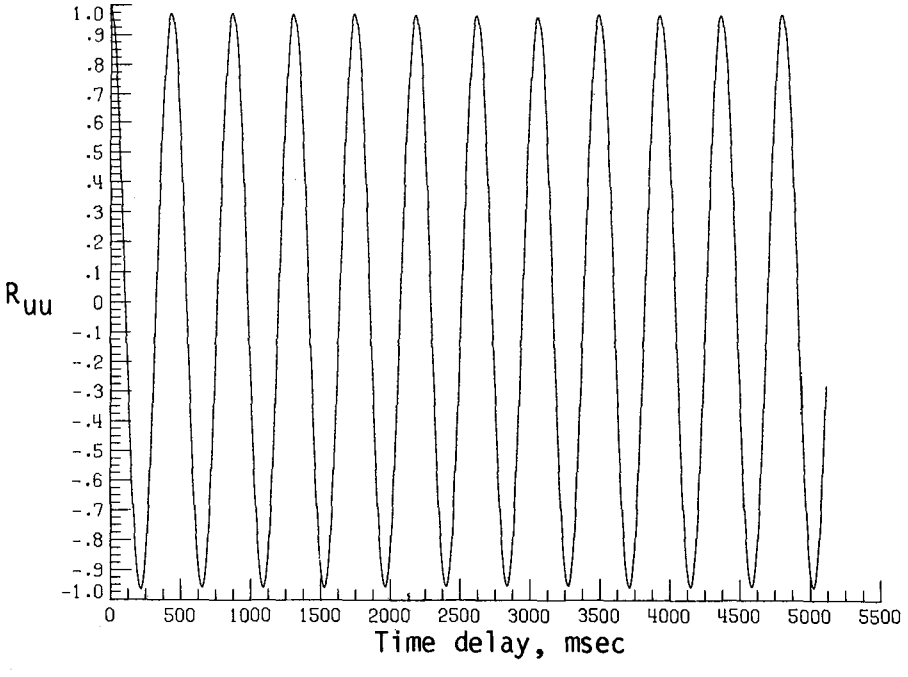

(d) Normalized autocorrelation of streamwise velocity fluctuations. $\sigma = 0.0789$.

Figure A15. Continued.

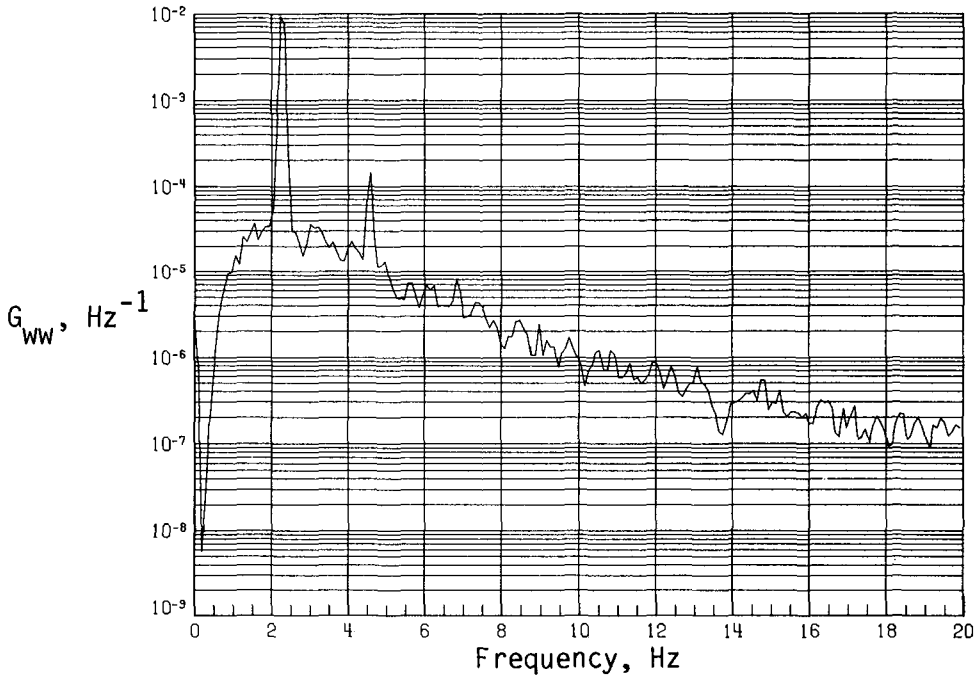

(e) PSD of vertical velocity fluctuations.

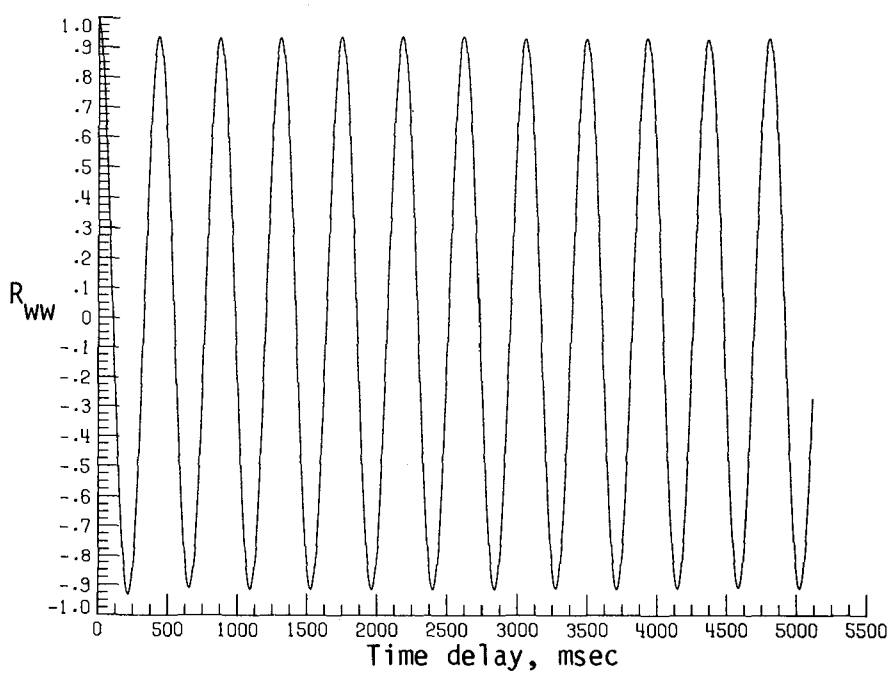

(f) Normalized autocorrelation of vertical velocity fluctuations. $\sigma = 0.0433$.

Figure A15. Concluded.

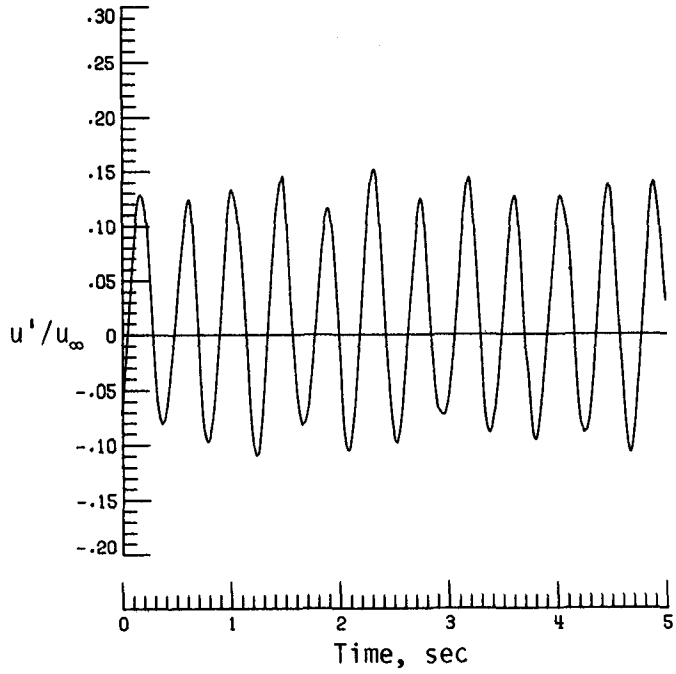

(a) Time history of streamwise velocity fluctuations.

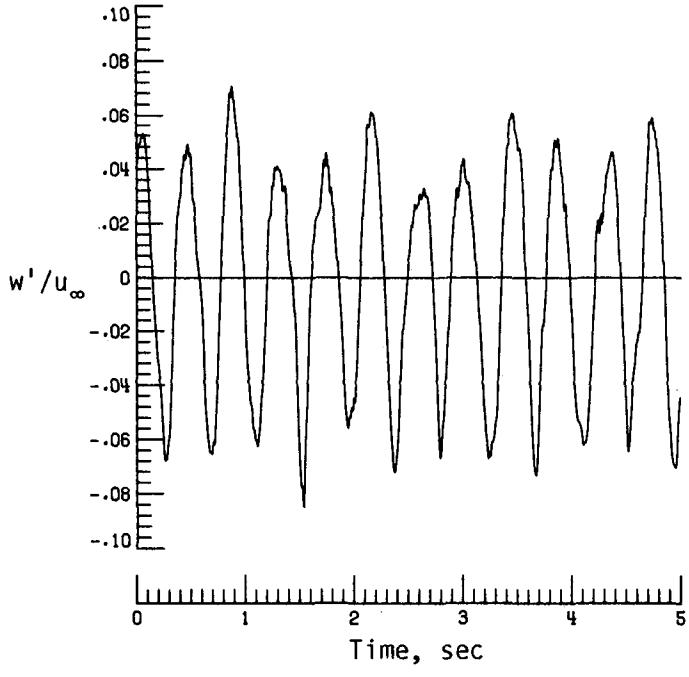

(b) Time history of vertical velocity fluctuations.

Figure A16. Dynamic-flow quality for baseline configuration at $q = 20.12$ lb/ft^2.

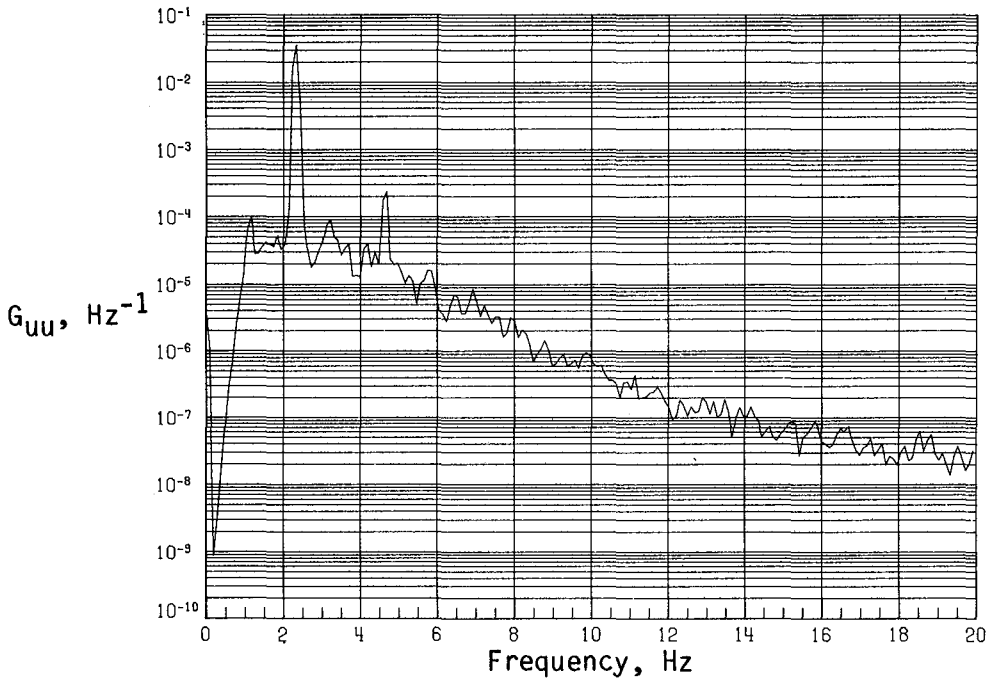

(c) PSD of streamwise velocity fluctuations.

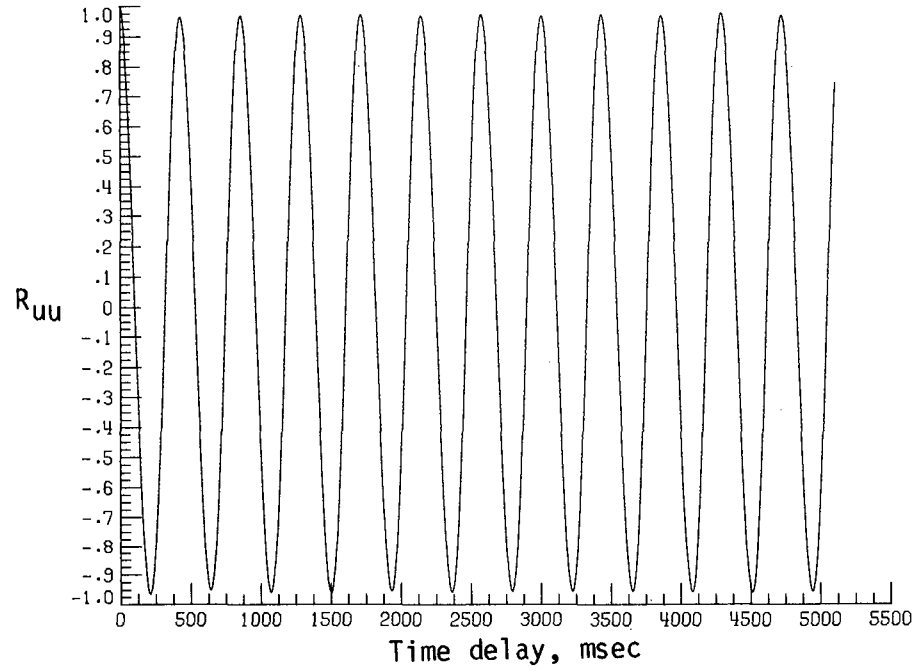

(d) Normalized autocorrelation of streamwise velocity fluctuations. $\sigma = 0.0764$.

Figure A16. Continued.

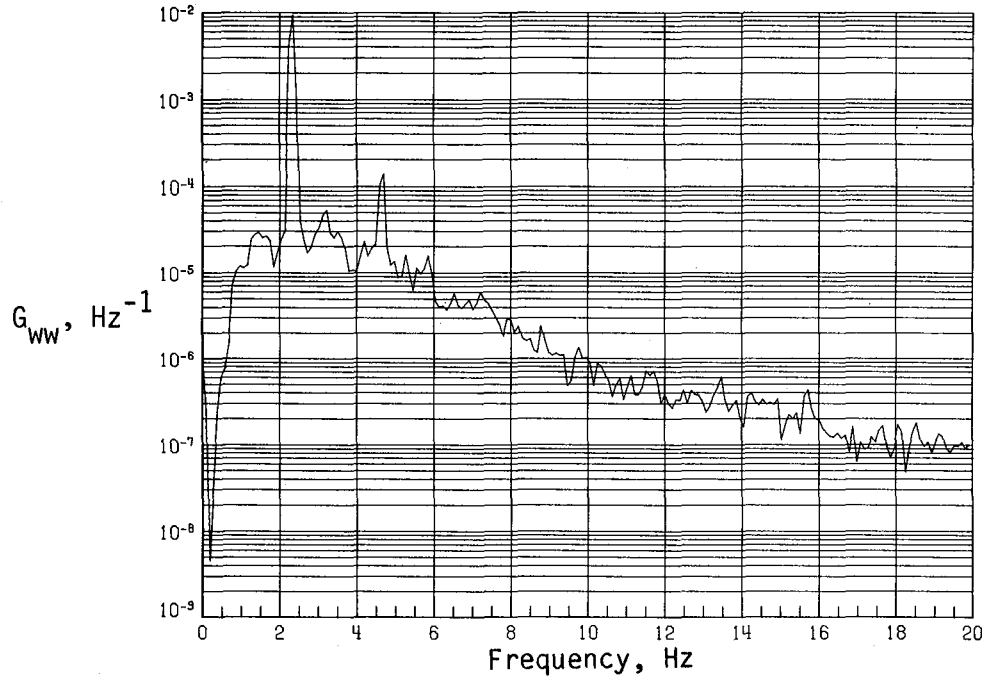

(e) PSD of vertical velocity fluctuations.

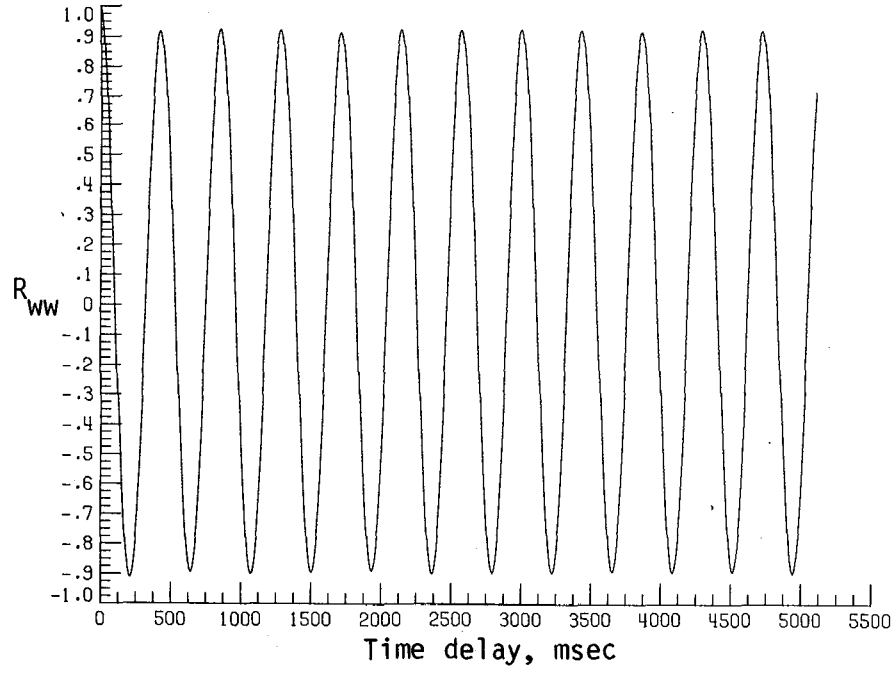

(f) Normalized autocorrelation of vertical velocity fluctuations. $\sigma = 0.0399$.

Figure A16. Concluded.

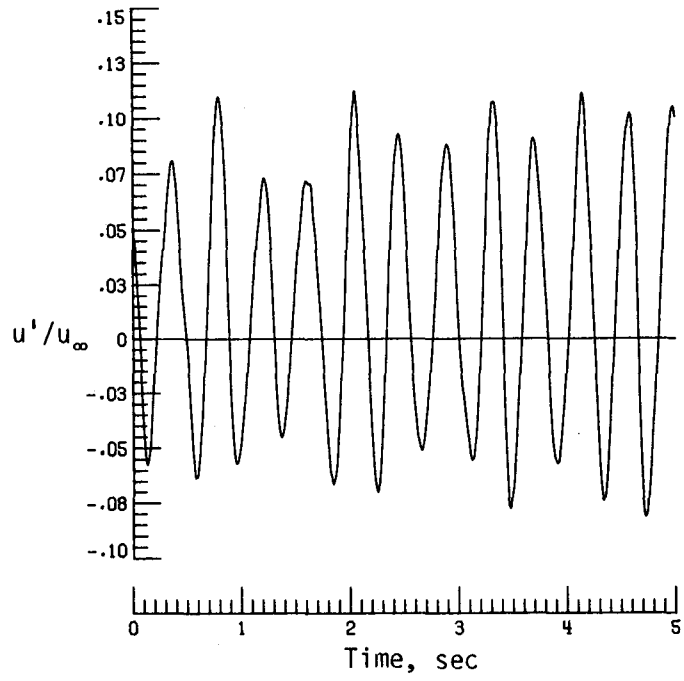

(a) Time history of streamwise velocity fluctuations.

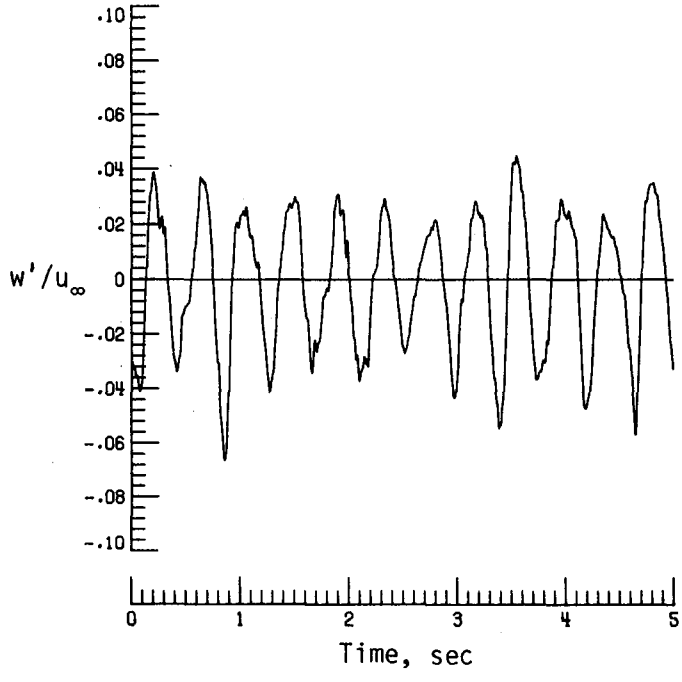

(b) Time history of vertical velocity fluctuations.

Figure A17. Dynamic-flow quality for baseline configuration at $q = 22.16$ lb/ft^2.

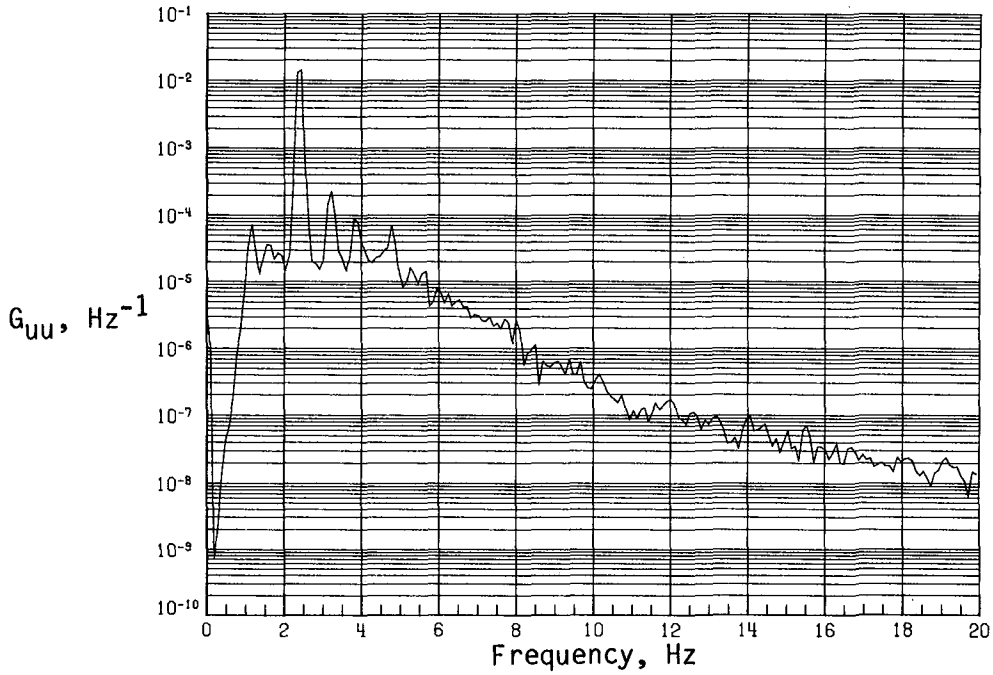

(c) PSD of streamwise velocity fluctuations.

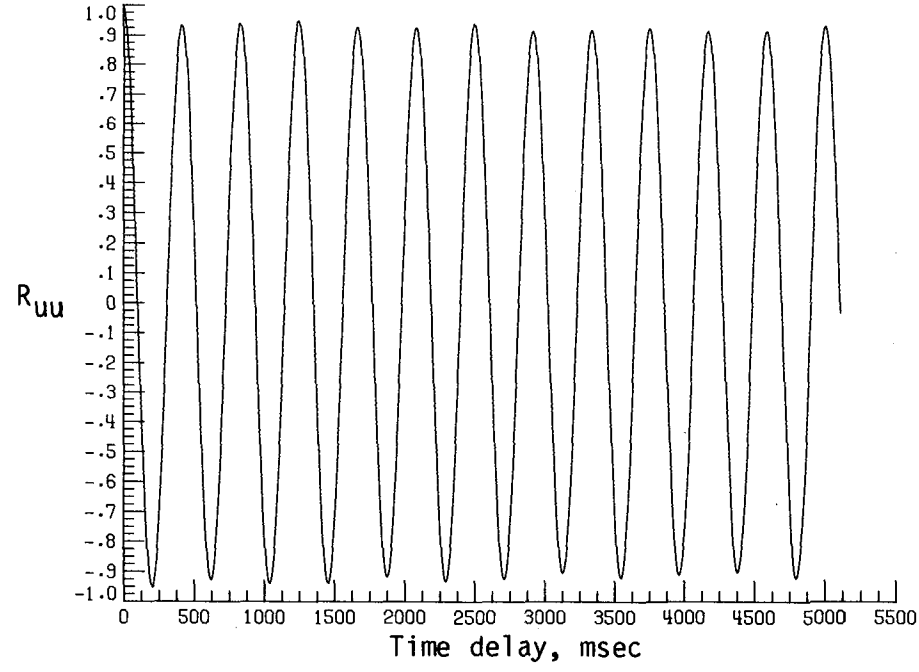

(d) Normalized autocorrelation of streamwise velocity fluctuations. $\sigma = 0.0551$.

Figure A17. Continued.

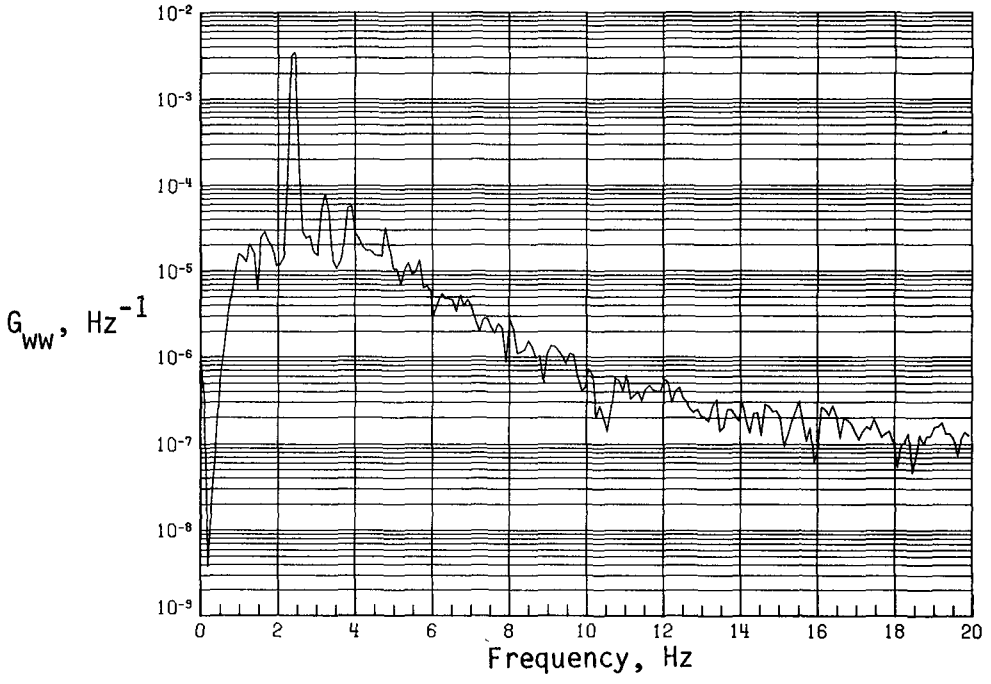

(e) PSD of vertical velocity fluctuations.

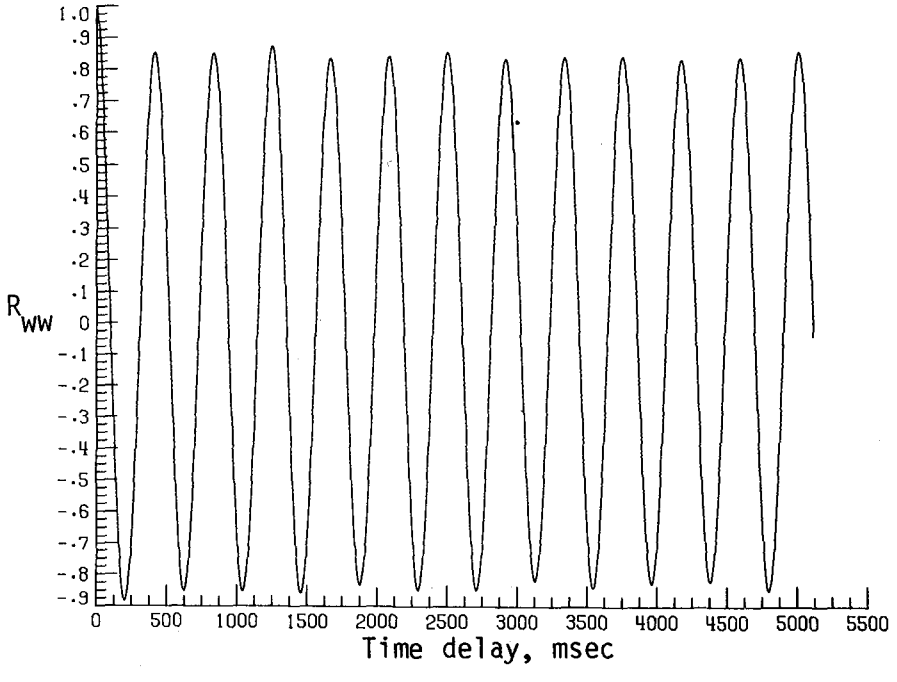

(f) Normalized autocorrelation of vertical velocity fluctuations. $\sigma = 0.0286$.

Figure A17. Concluded.

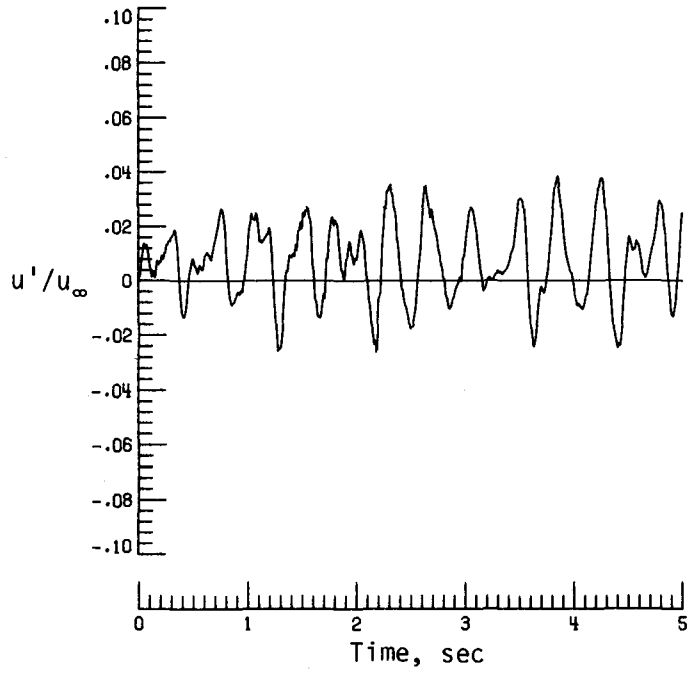

(a) Time history of streamwise velocity fluctuations.

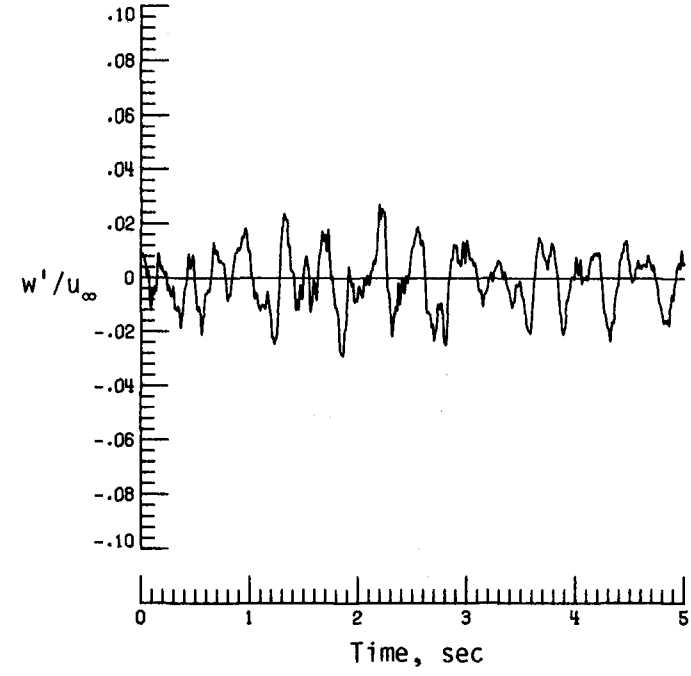

(b) Time history of vertical velocity fluctuations.

Figure A18. Dynamic-flow quality for baseline configuration at $q = 25.31$ lb/ft^2.

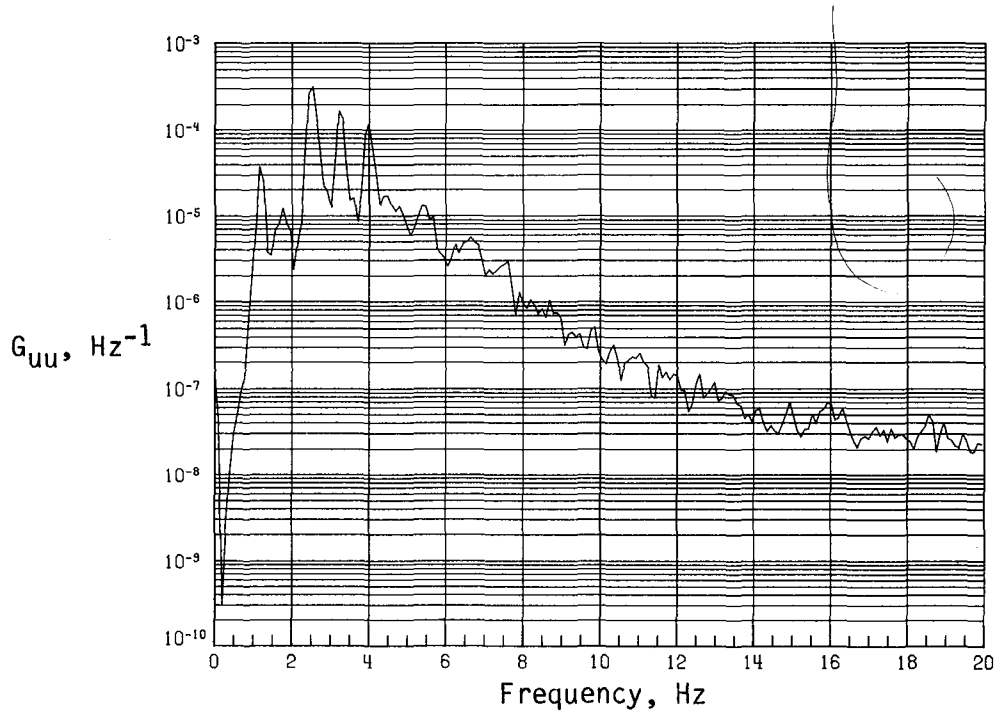

(c) PSD of streamwise velocity fluctuations.

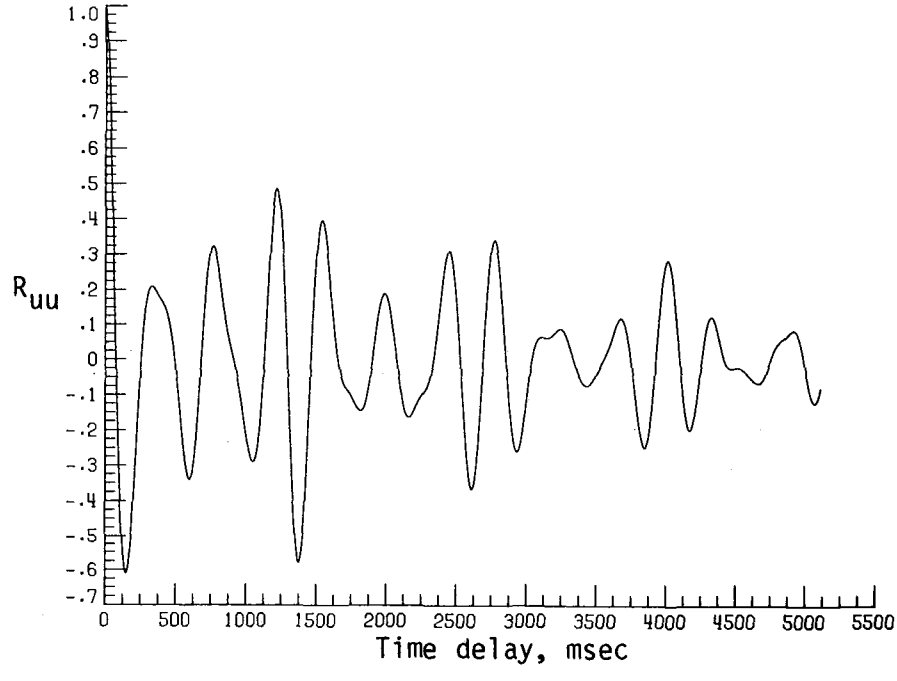

(d) Normalized autocorrelation of streamwise velocity fluctuations. $\sigma = 0.0142$.

Figure A18. Continued.

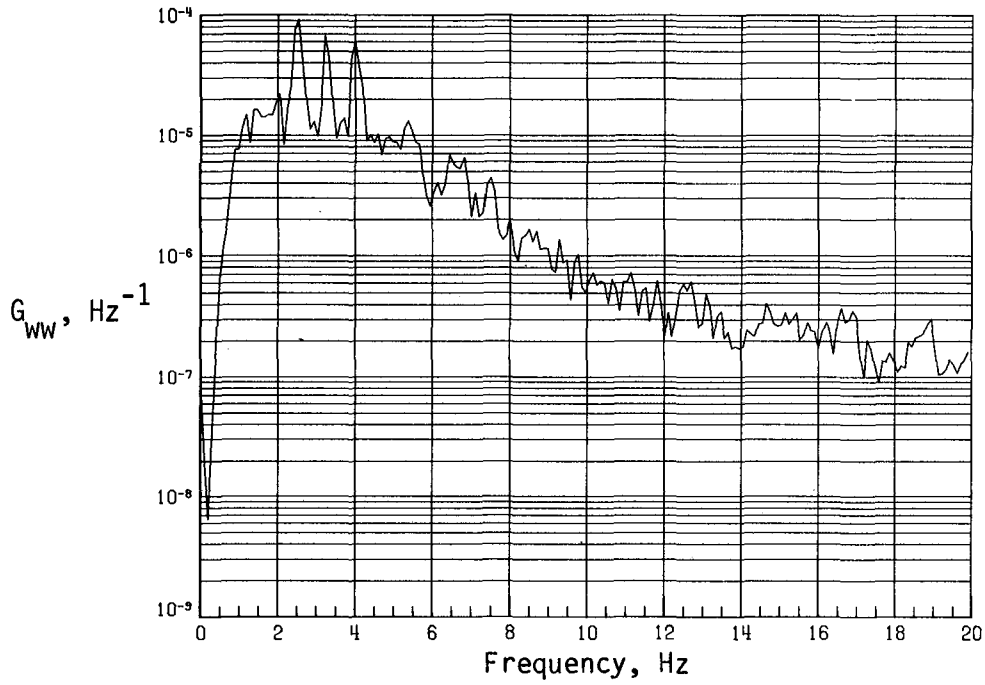

(e) PSD of vertical velocity fluctuations.

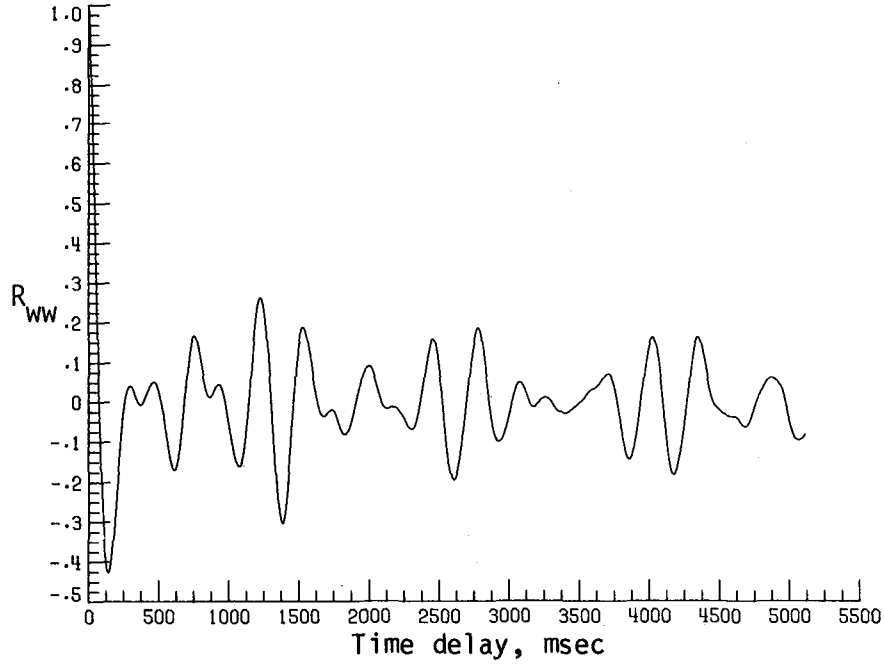

(f) Normalized autocorrelation of vertical velocity fluctuations. $\sigma = 0.0111$.

Figure A18. Concluded.

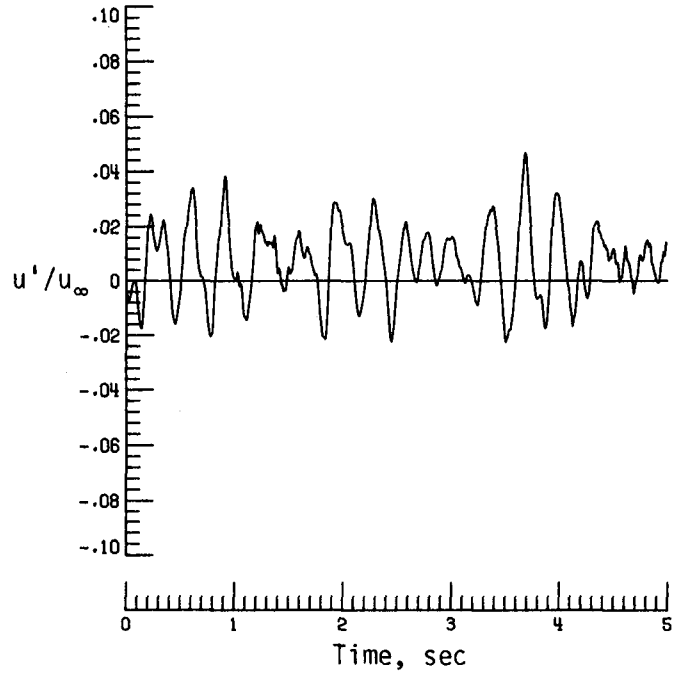

(a) Time history of streamwise velocity fluctuations.

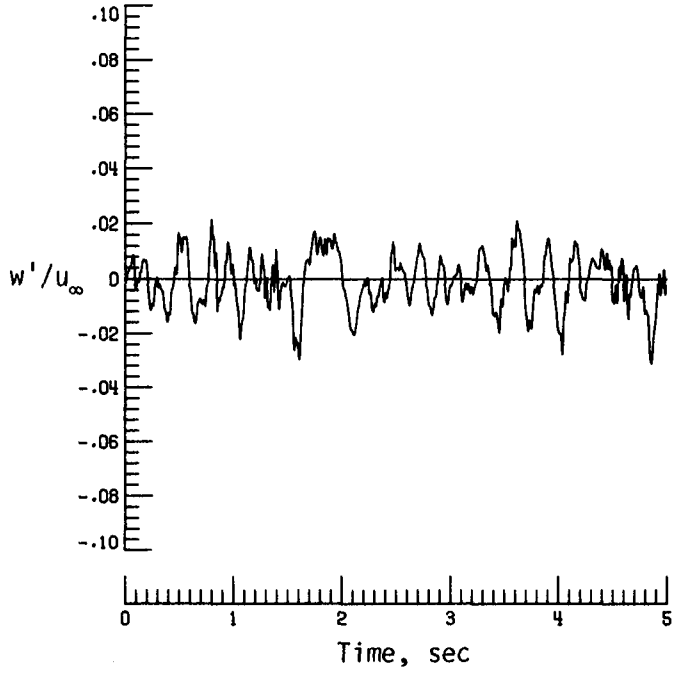

(b) Time history of vertical velocity fluctuations.

Figure A19. Dynamic-flow quality for baseline configuration at $q = 32.21$ lb/ft^2.

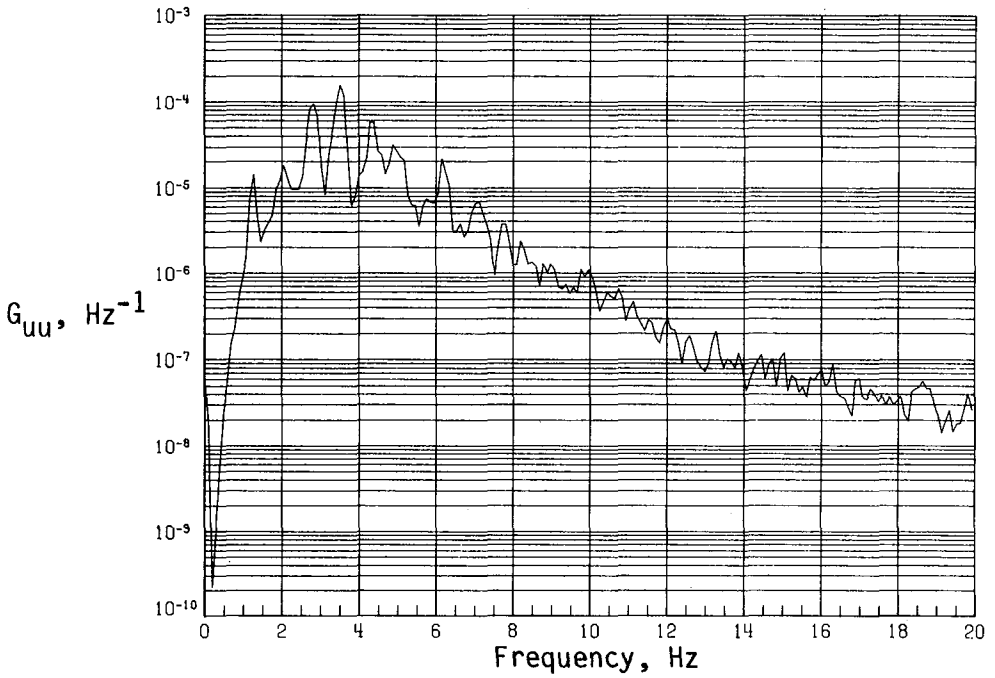

(c) PSD of streamwise velocity fluctuations.

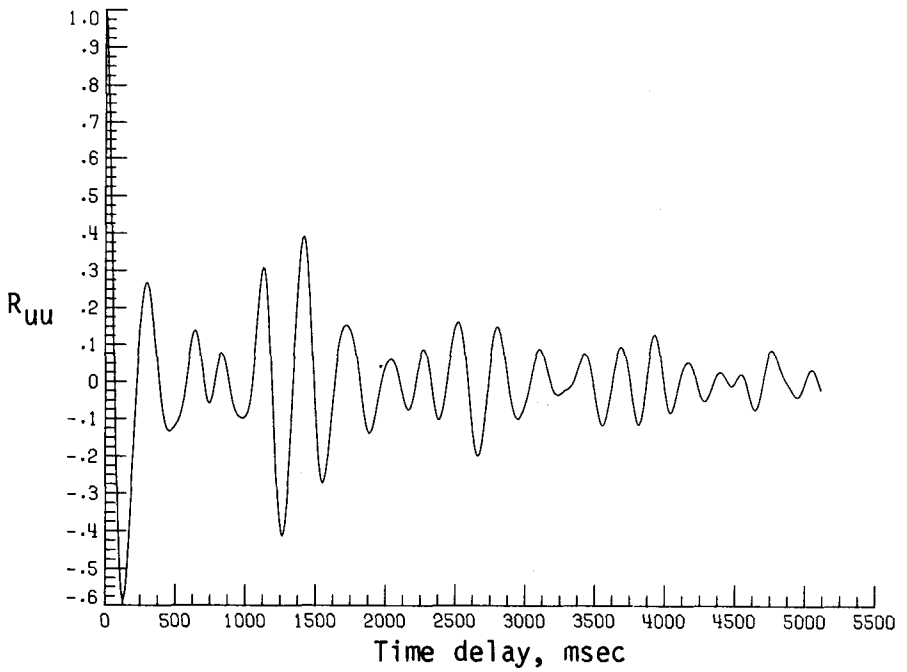

(d) Normalized autocorrelation of streamwise velocity fluctuations. $\sigma = 0.0122$.

Figure A19. Continued.

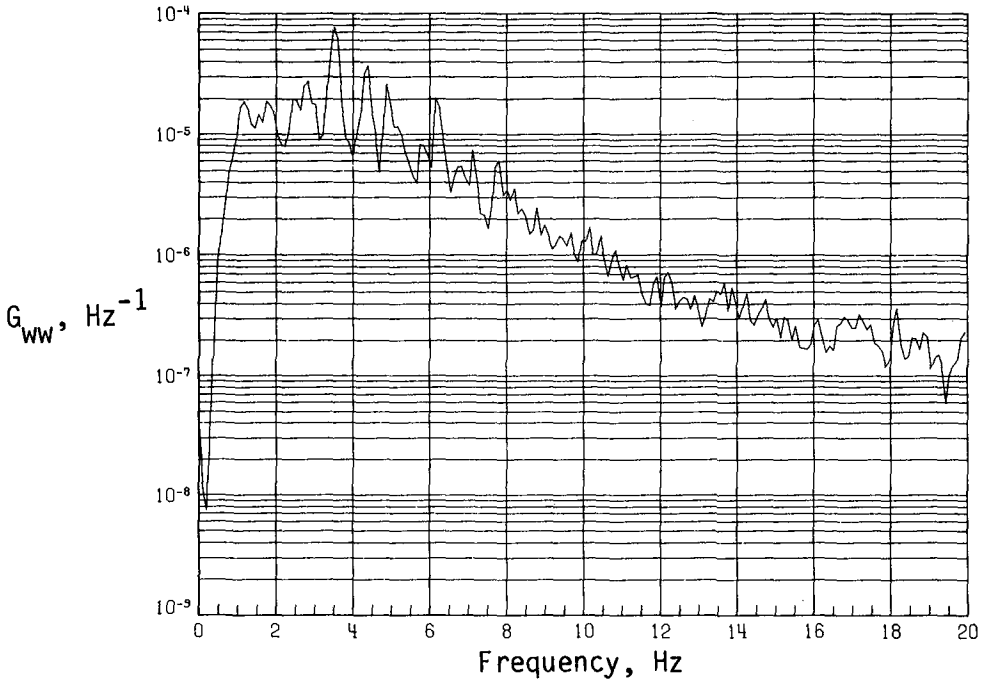

(e) PSD of vertical velocity fluctuations.

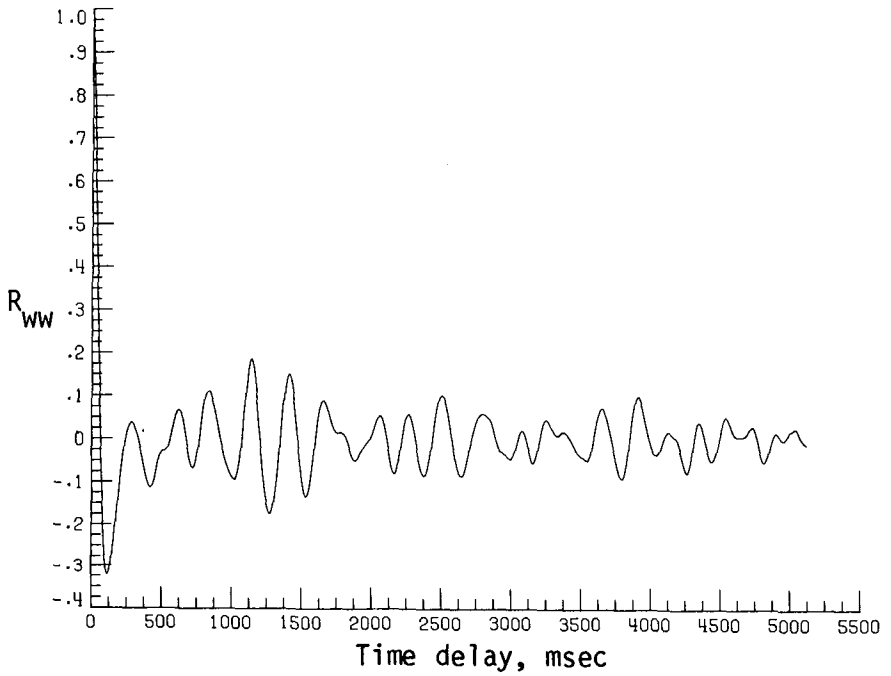

(f) Normalized autocorrelation of vertical velocity fluctuations. $\sigma = 0.0100$.

Figure A19. Concluded.

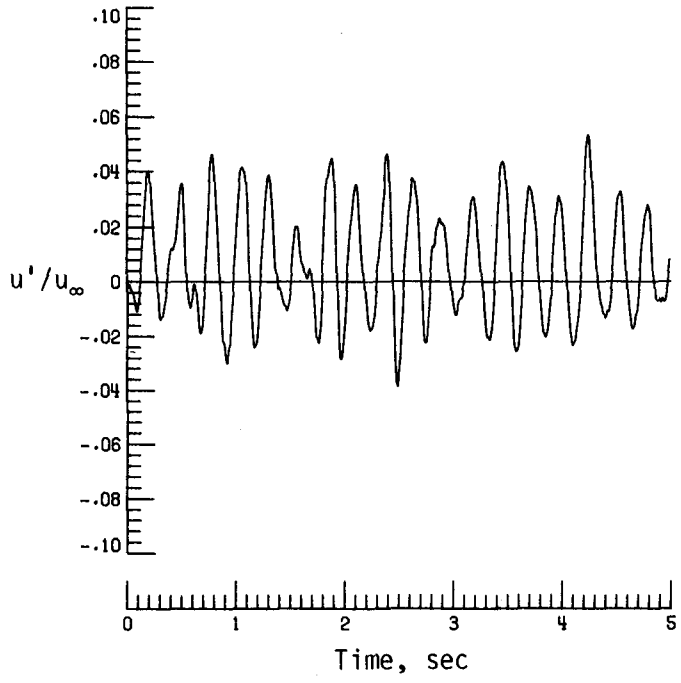

(a) Time history of streamwise velocity fluctuations.

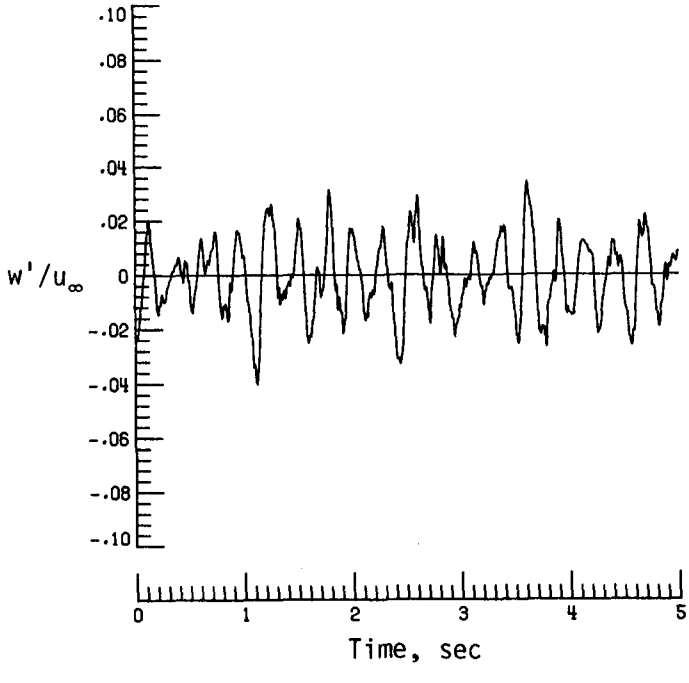

(b) Time history of vertical velocity fluctuations.

Figure A20. Dynamic-flow quality for baseline configuration at $q = 40.23$ lb/ft^2.

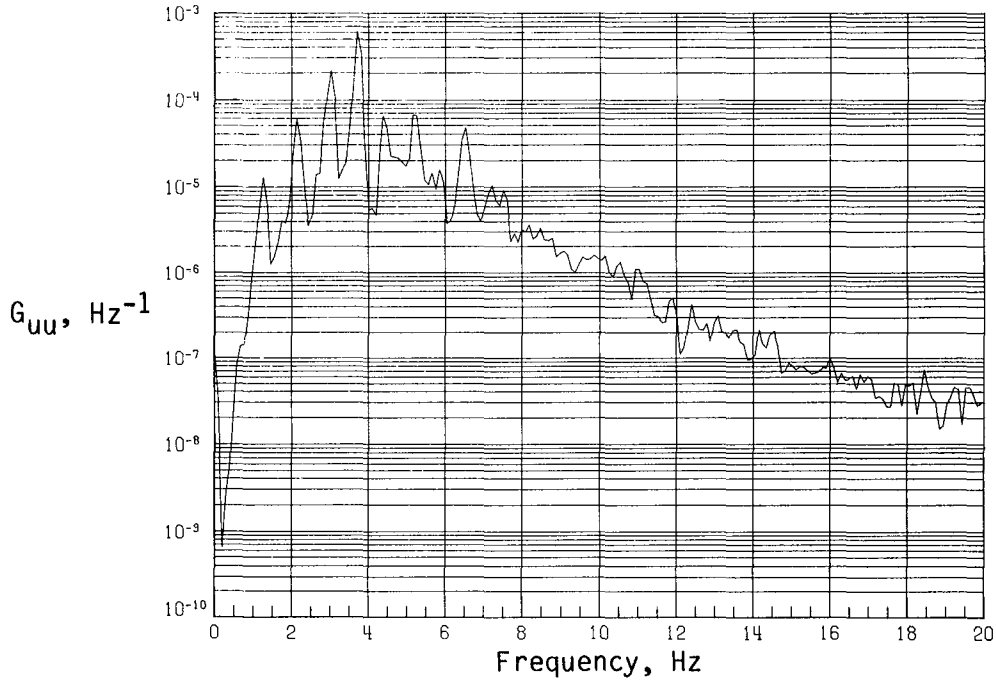

(c) PSD of vertical velocity fluctuations.

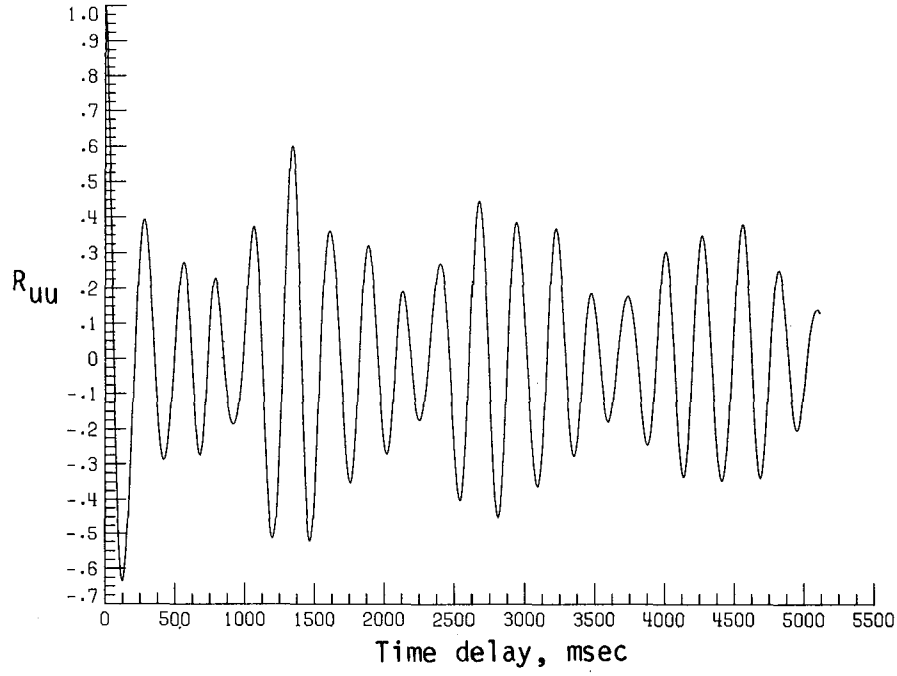

(d) Normalized autocorrelation of streamwise velocity fluctuations. $\sigma = 0.0157$.

Figure A20. Continued.

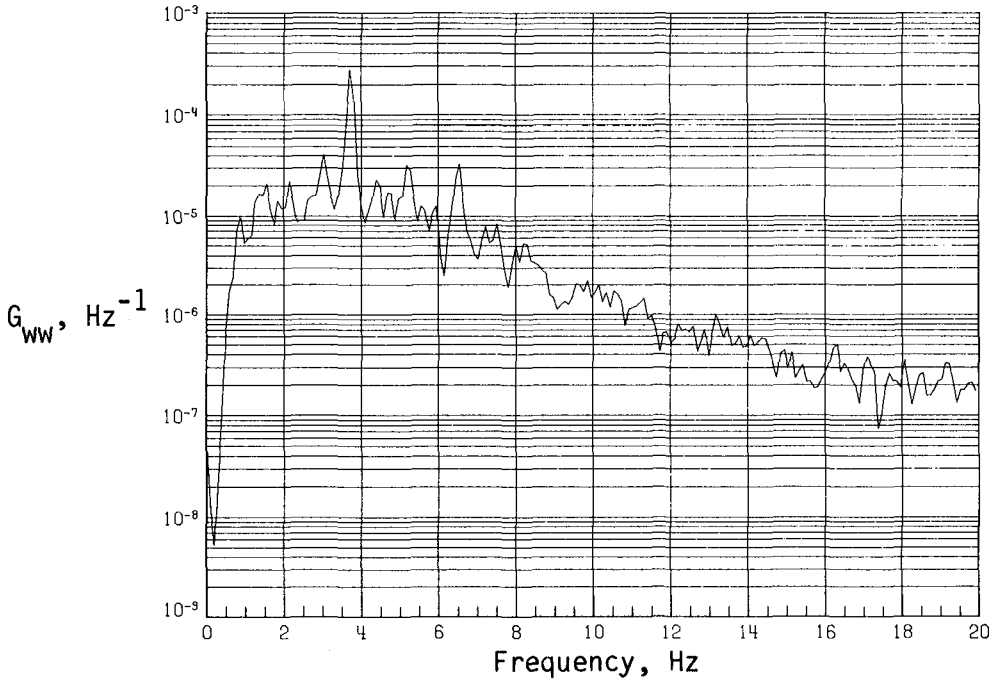

(e) PSD of vertical velocity fluctuations.

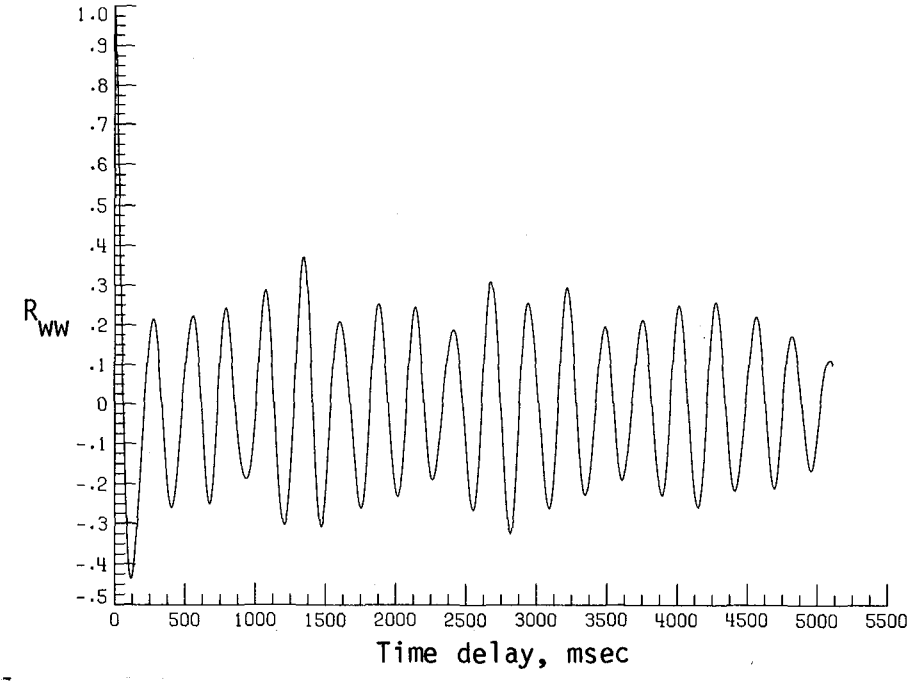

(f) Normalized autocorrelation of vertical velocity fluctuations. $\sigma = 0.0120$.

Figure A20. Concluded.

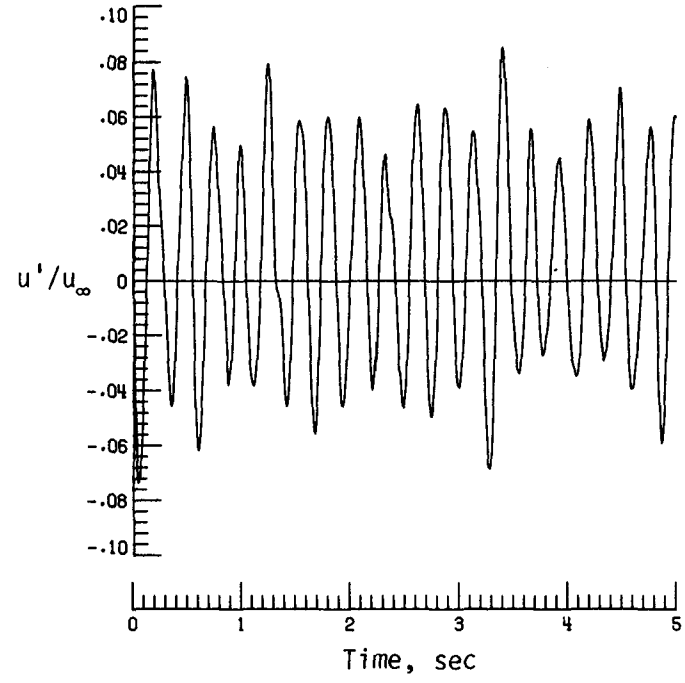

(a) Time history of streamwise velocity fluctuations.

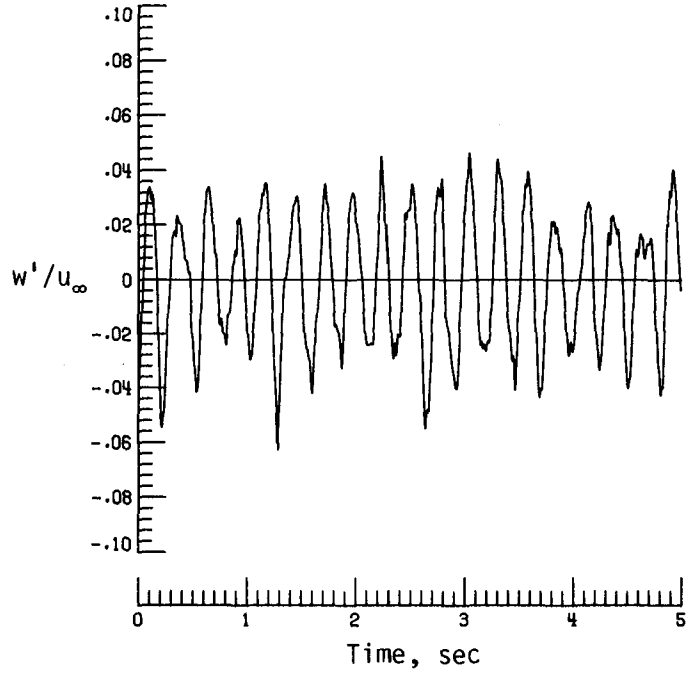

(b) Time history of vertical velocity fluctuations.

Figure A21. Dynamic-flow quality for baseline configuration at $q = 42.49$ lb/ft^2.

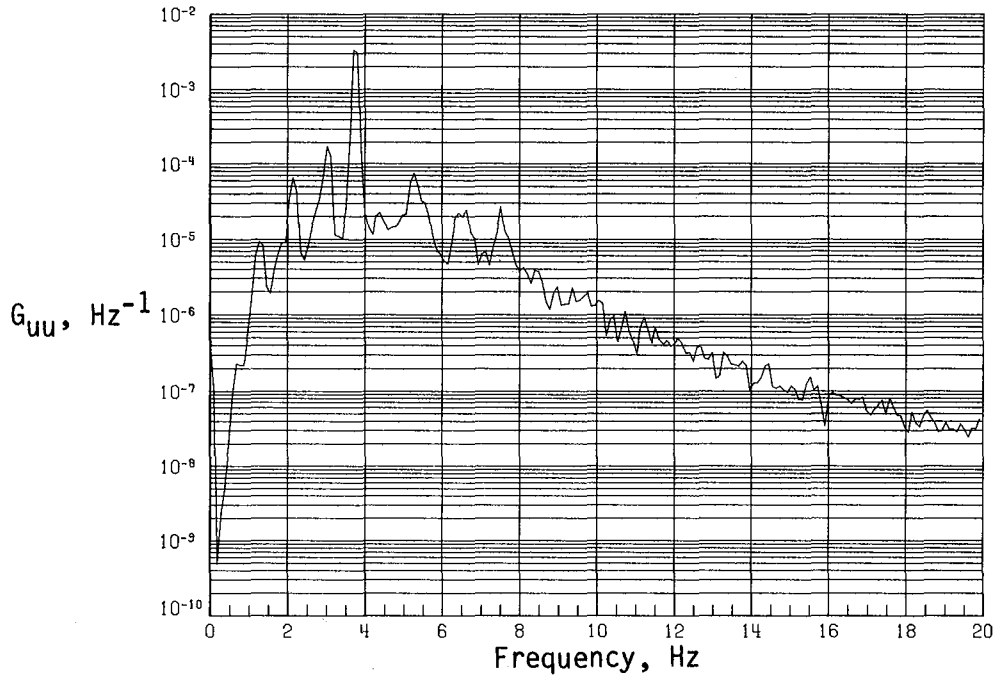

(c) PSD of streamwise velocity fluctuations.

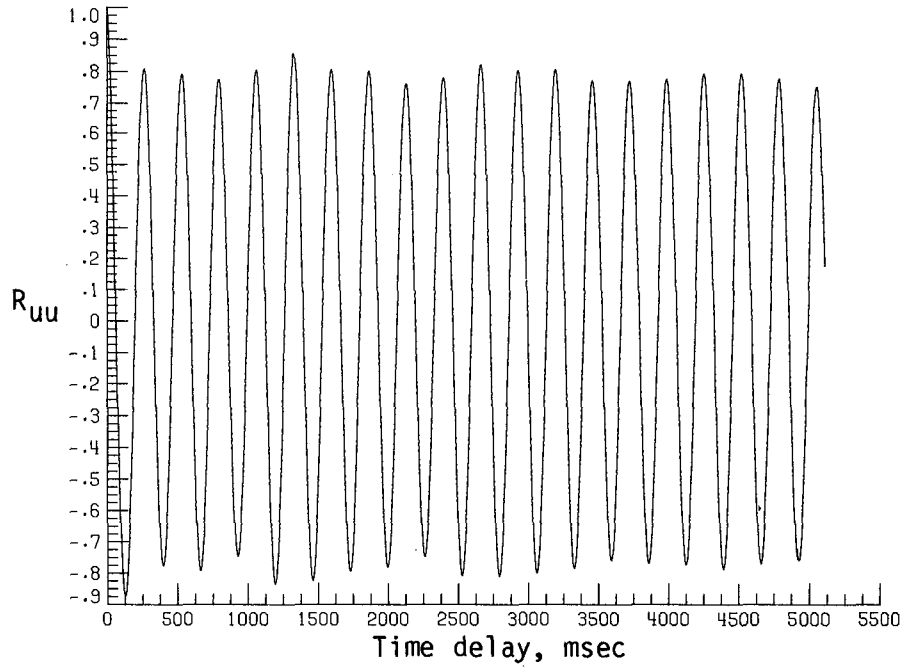

(d) Normalized autocorrelation of streamwise velocity fluctuations. $\sigma = 0.0284$.

Figure A21. Continued.

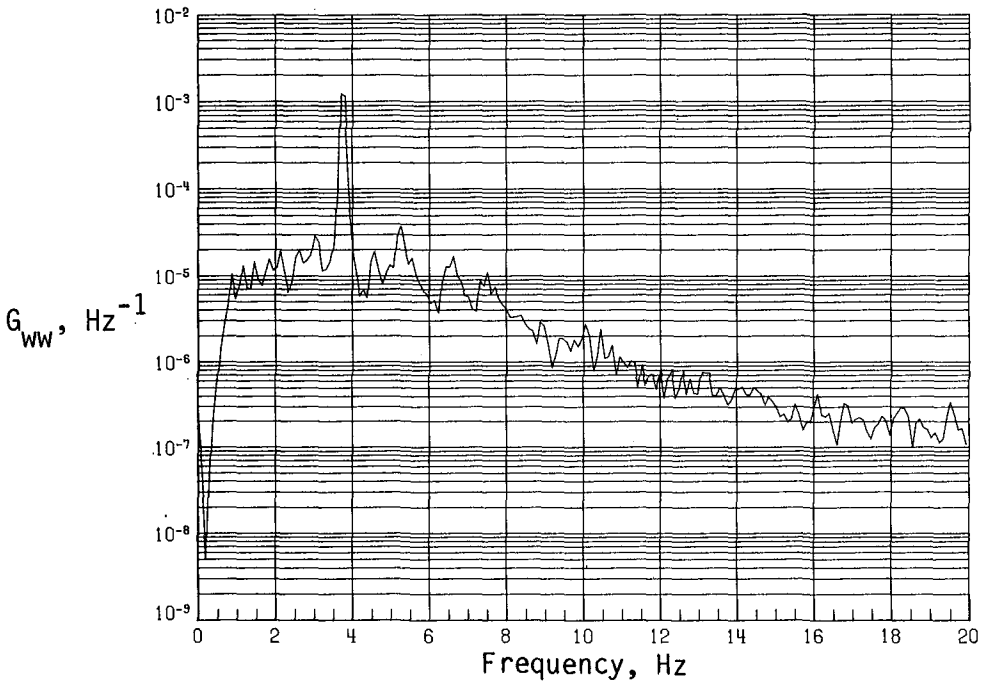

(e) PSD of vertical velocity fluctuations.

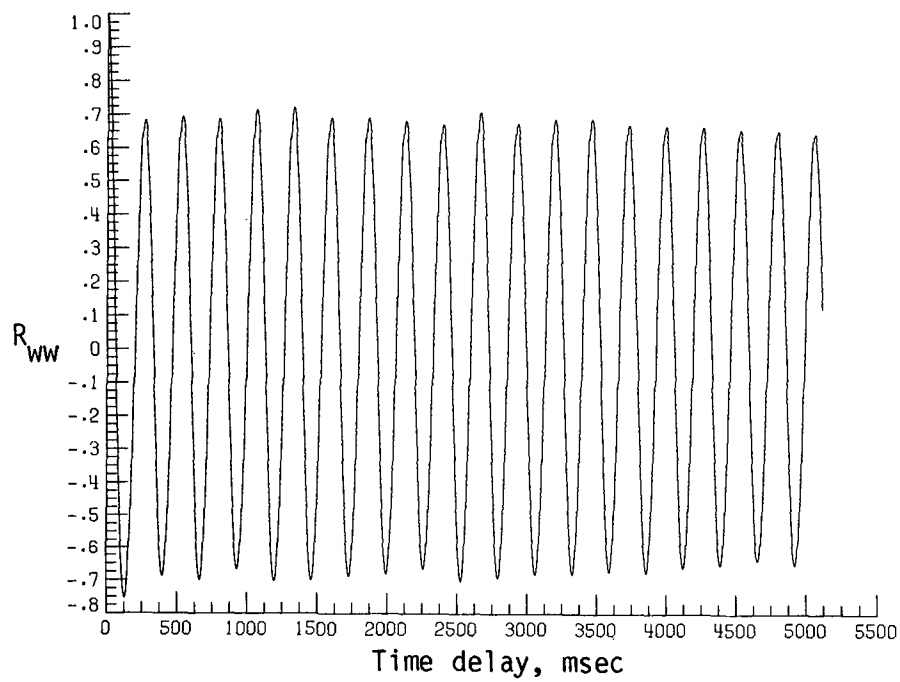

(f) Normalized autocorrelation of vertical velocity fluctuations. $\sigma = 0.0185$.

Figure A21. Concluded.

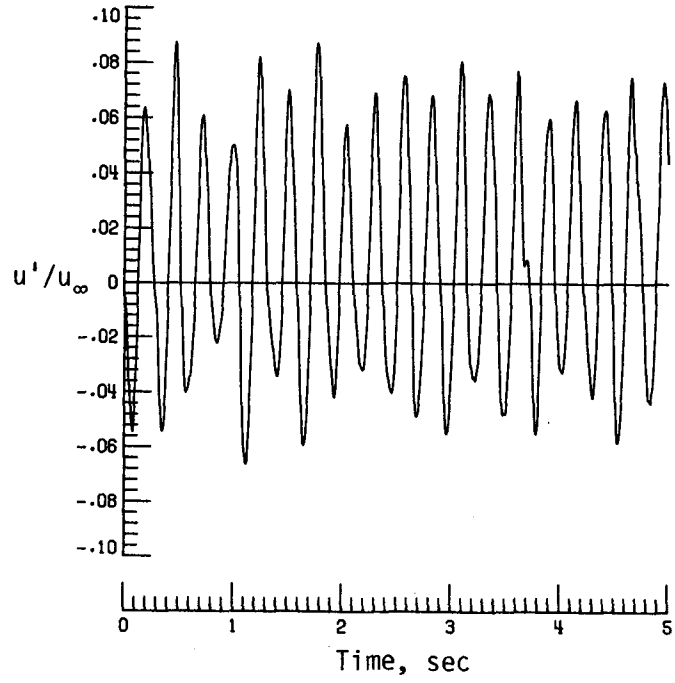

(a) Time history of streamwise velocity fluctuations.

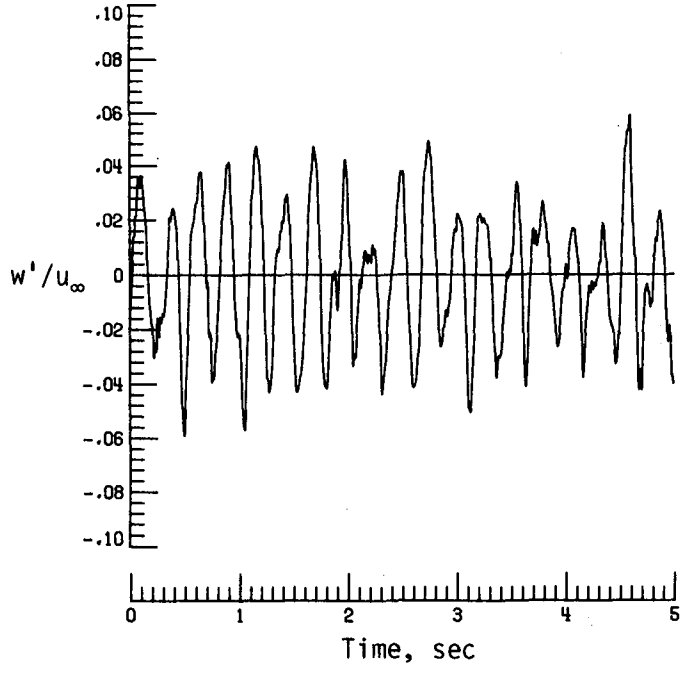

(b) Time history of vertical velocity fluctuations.

Figure A22. Dynamic-flow quality for baseline configuration at $q = 45.09$ lb/ft^2.

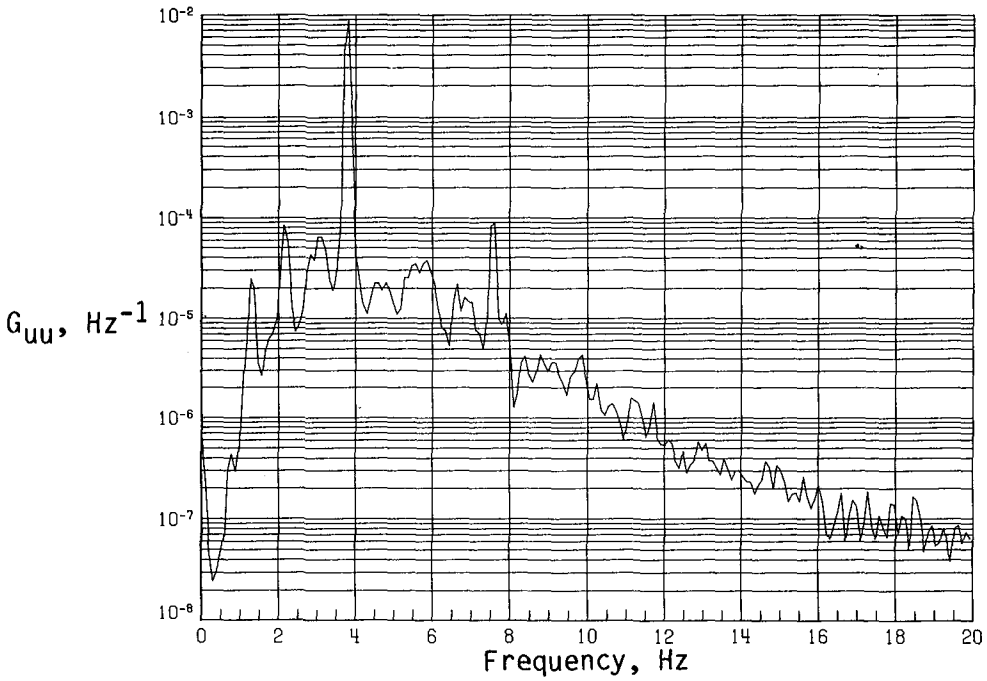

(c) PSD of streamwise velocity fluctuations.

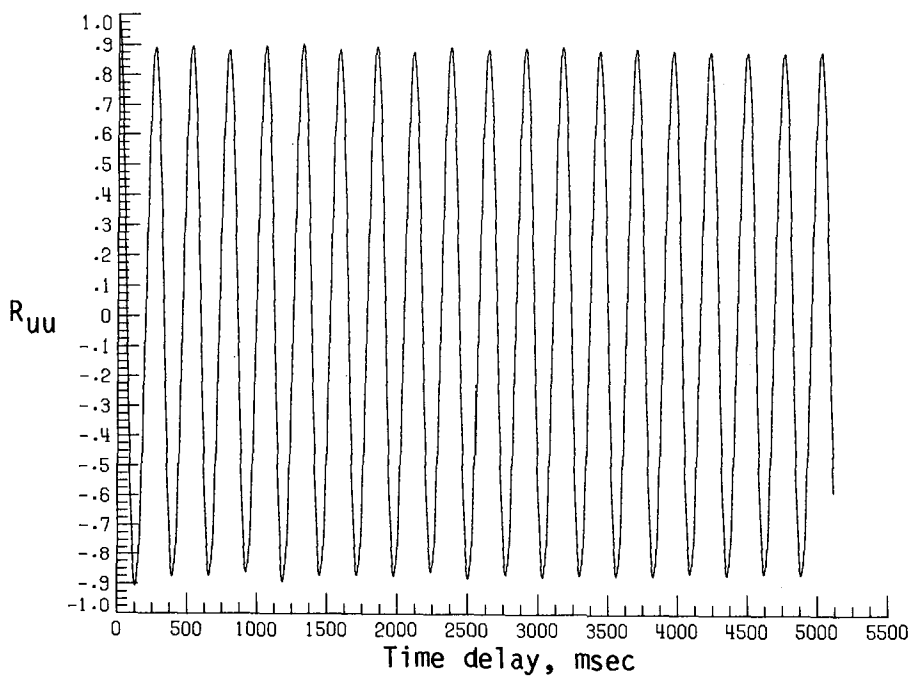

(d) Normalized autocorrelation of streamwise velocity fluctuations. $\sigma = 0.0393$.

Figure A22. Continued.

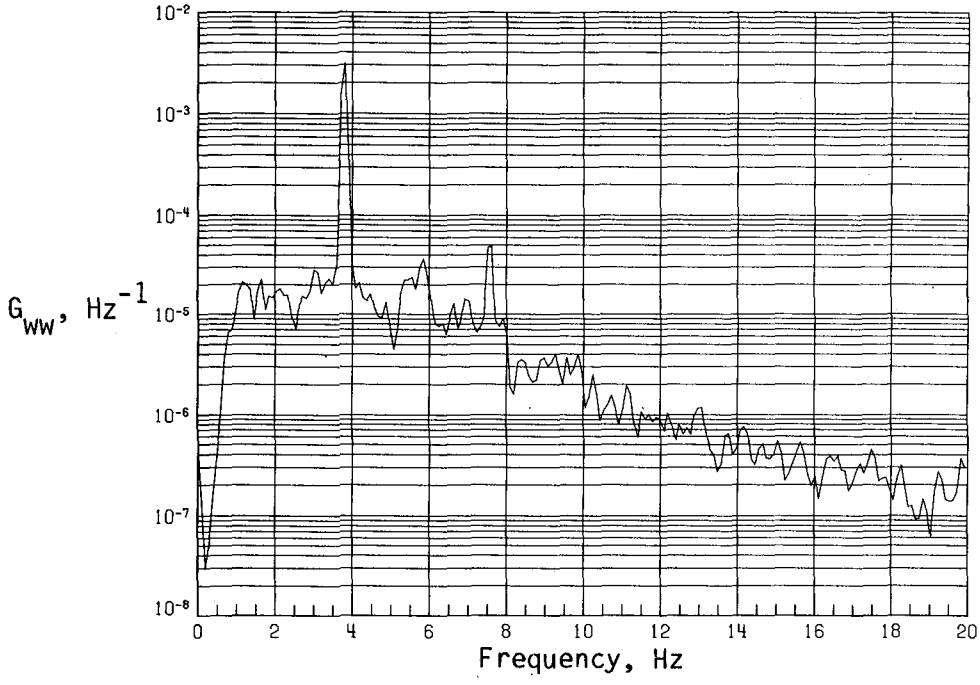

(e) PSD of vertical velocity fluctuations.

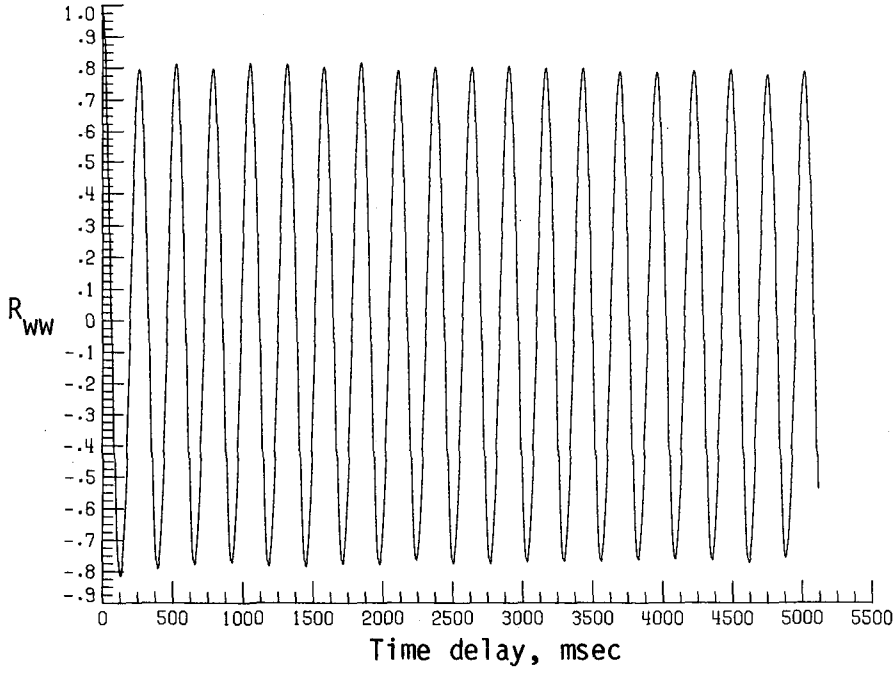

(f) Normalized autocorrelation of vertical velocity fluctuations. $\sigma = 0.0245$.

Figure A22. Concluded.

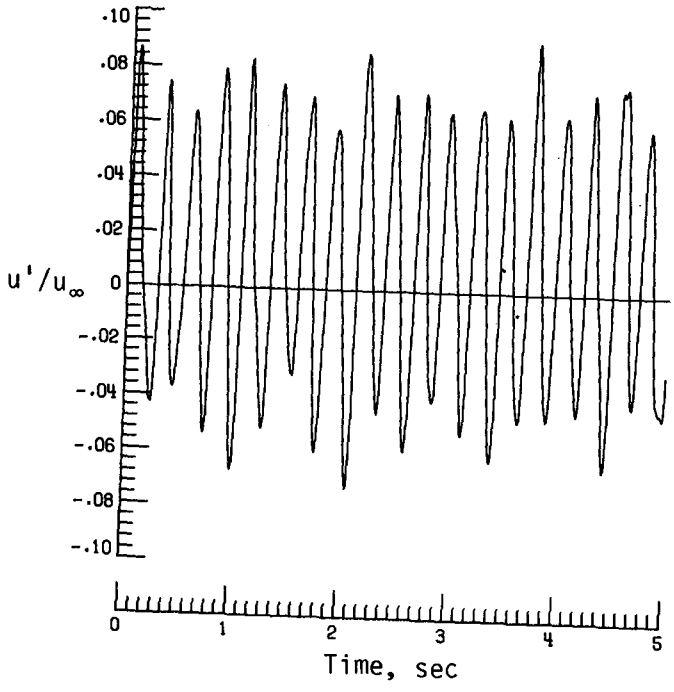

(a) Time history of streamwise velocity fluctuations.

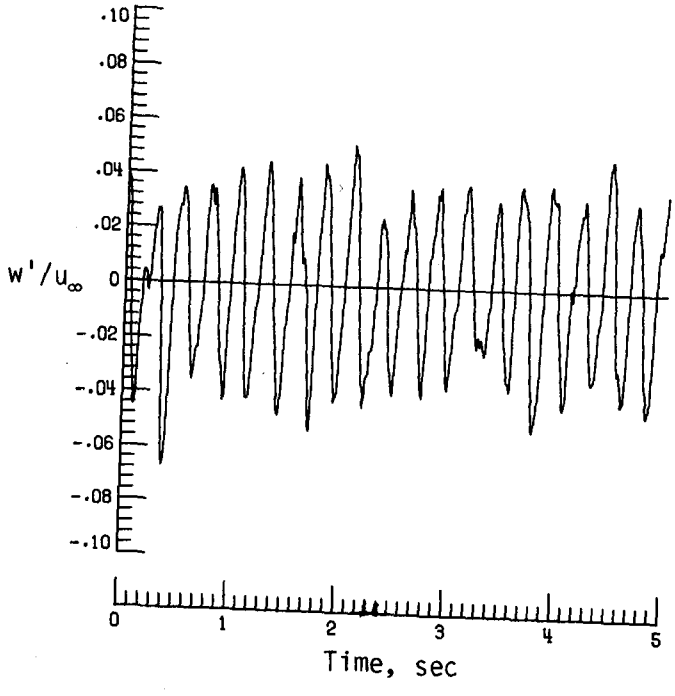

(b) Time history of vertical velocity fluctuations.

Figure A23. Dynamic-flow quality for baseline configuration at $q = 47.58$ lb/ft^2.

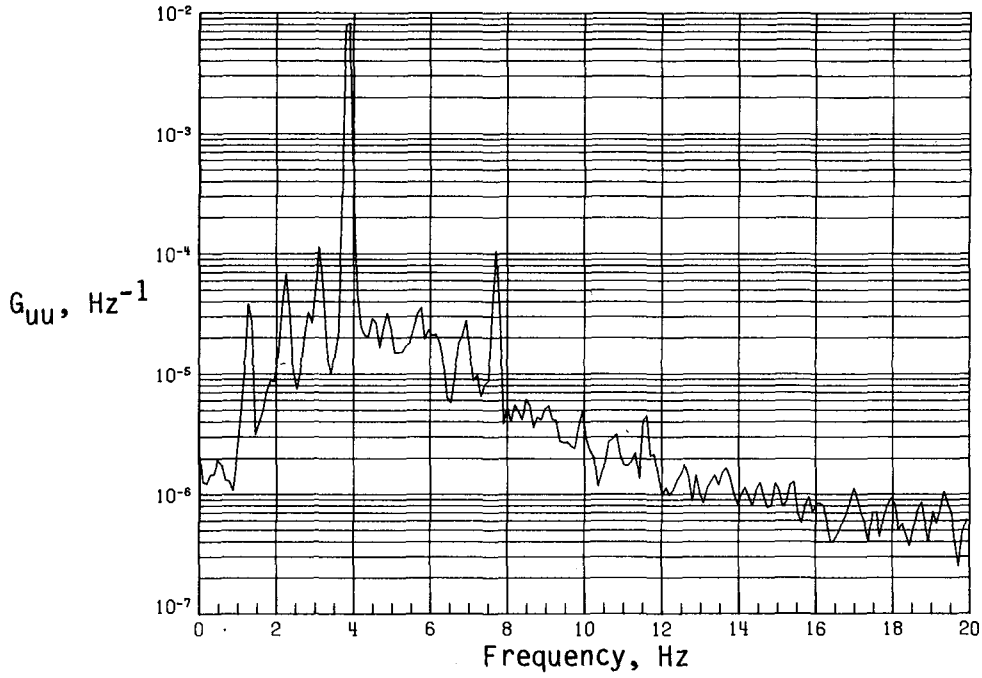

(c) PSD of streamwise velocity fluctuations.

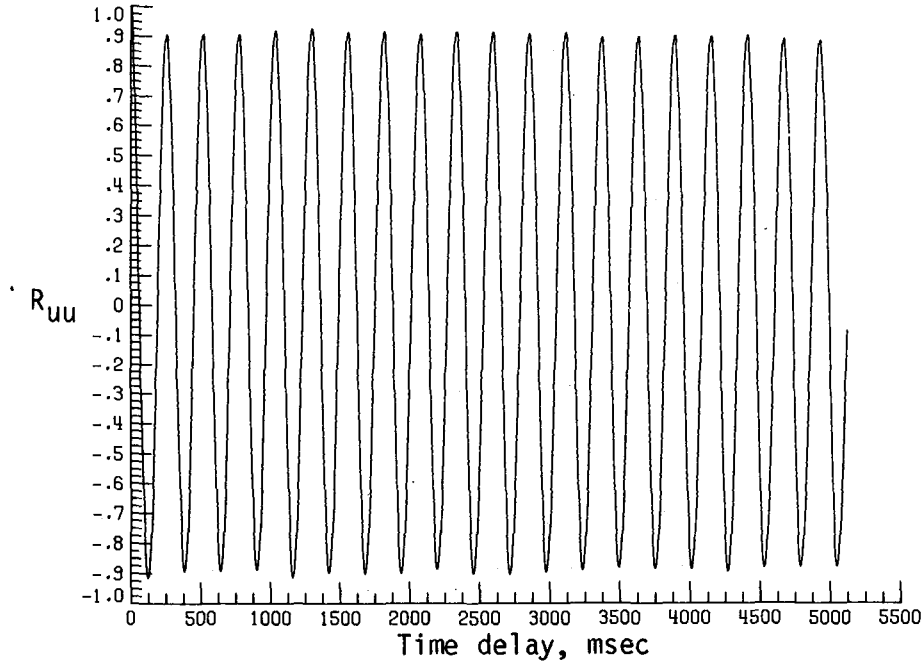

(d) Normalized autocorrelation of streamwise velocity fluctuations. $\sigma = 0.0421$.

Figure A23. Continued.

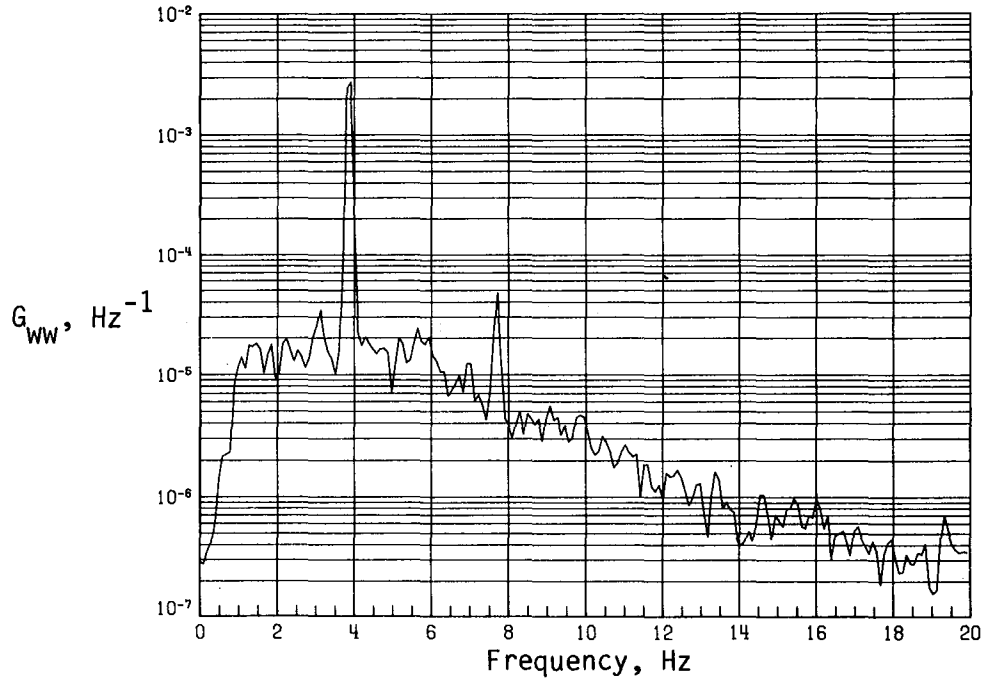

(e) PSD of vertical velocity fluctuations.

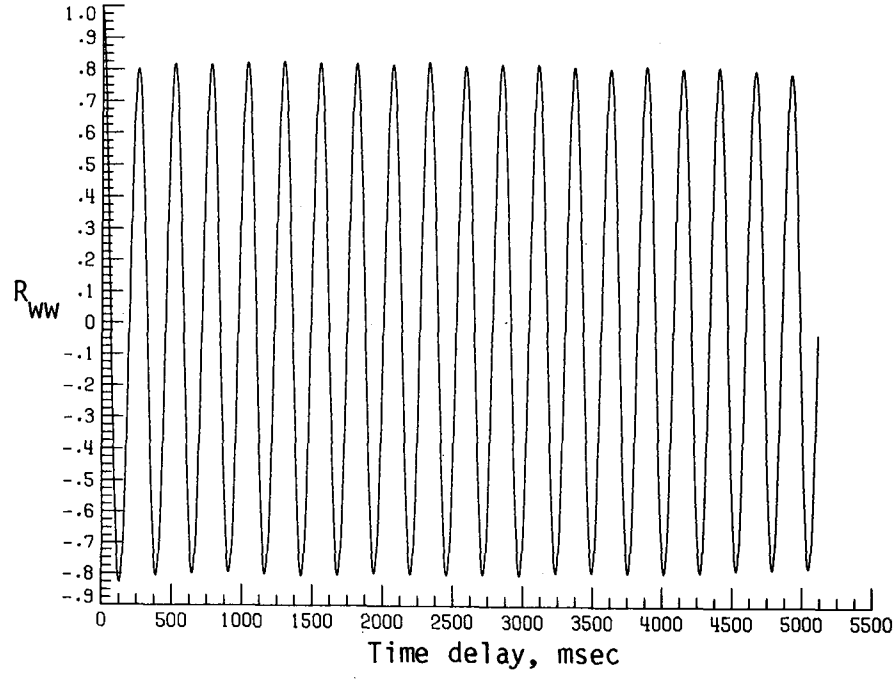

(f) Normalized autocorrelation of vertical velocity fluctuations. $\sigma = 0.0252$.

Figure A23. Concluded.

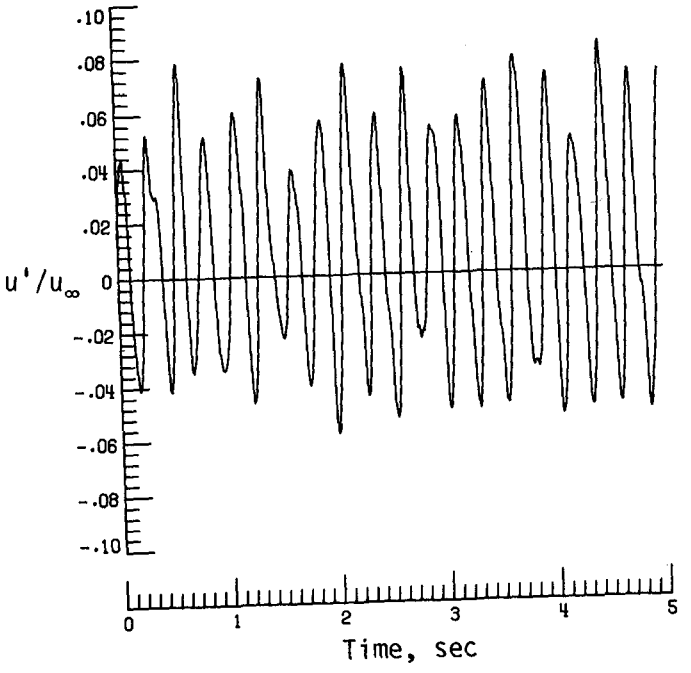

(a) Time history of streamwise velocity fluctuations.

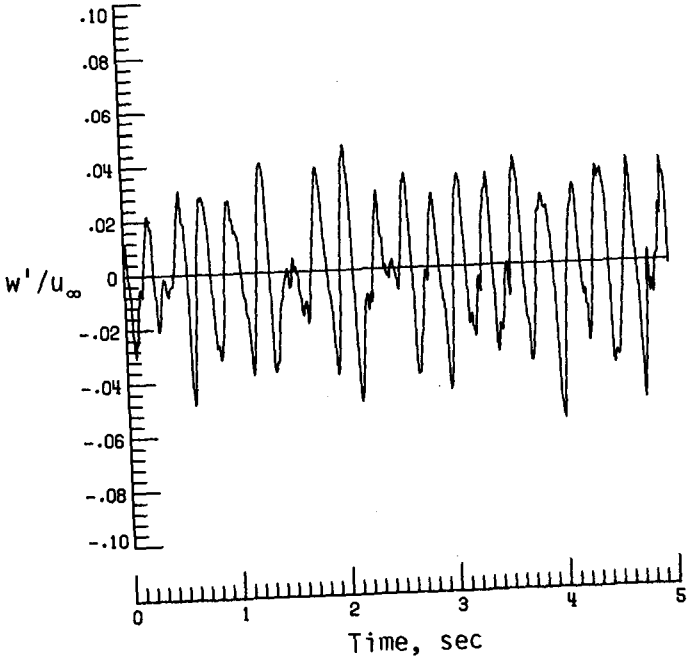

(b) Time history of vertical velocity fluctuations.

Figure A24. Dynamic-flow quality for baseline configuration at $q = 50.29$ lb/ft^2.

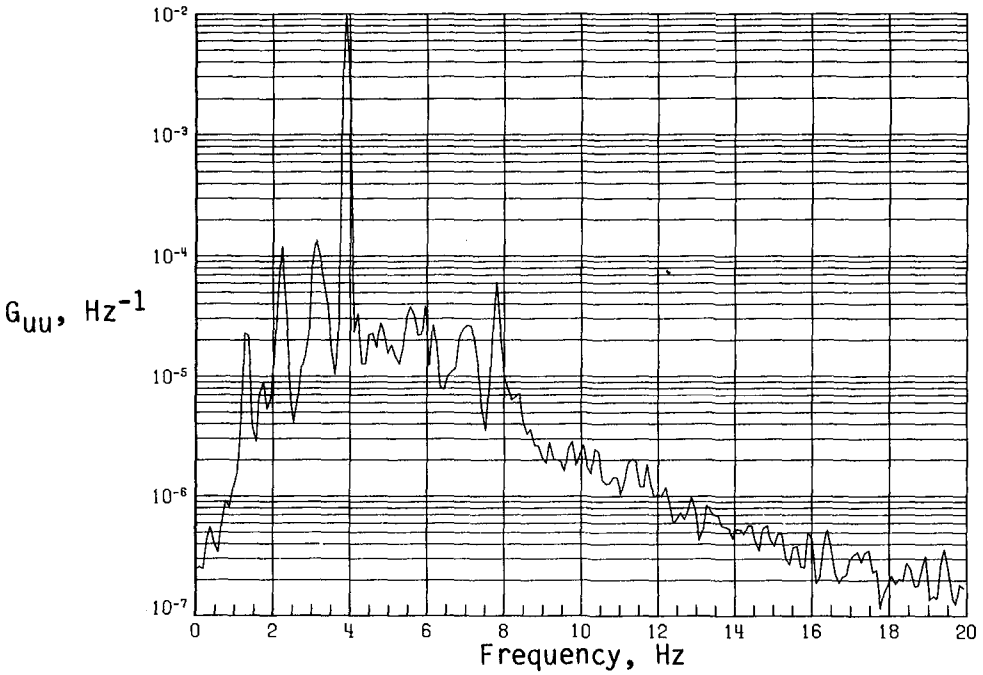

(c) PSD of streamwise velocity fluctuations.

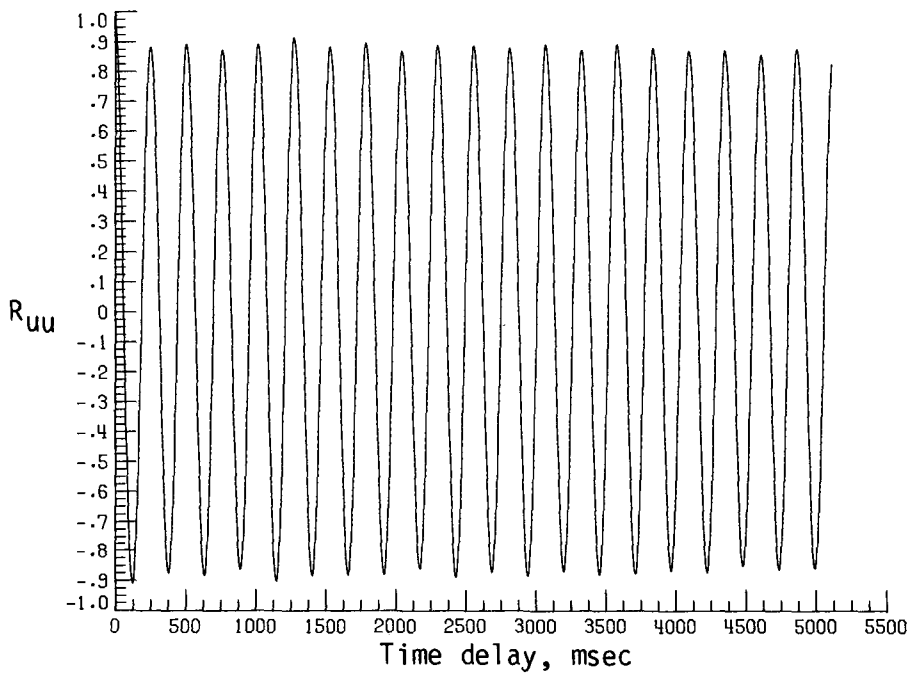

(d) Normalized autocorrelation of streamwise velocity fluctuations. $\sigma = 0.0396$.

Figure A24. Continued.

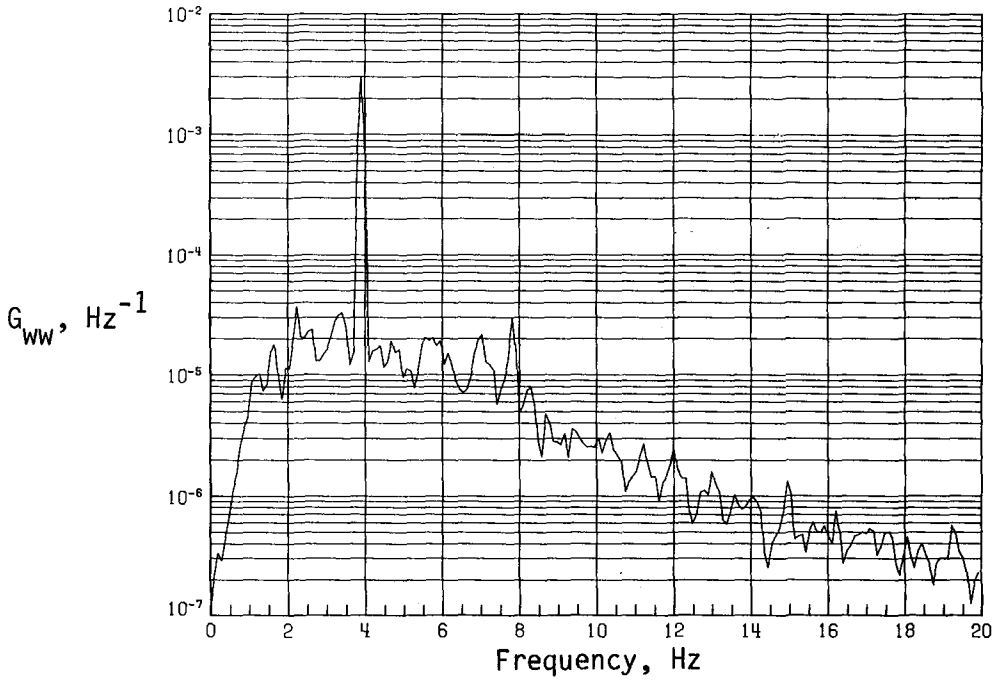

(e) PSD of vertical velocity fluctuations.

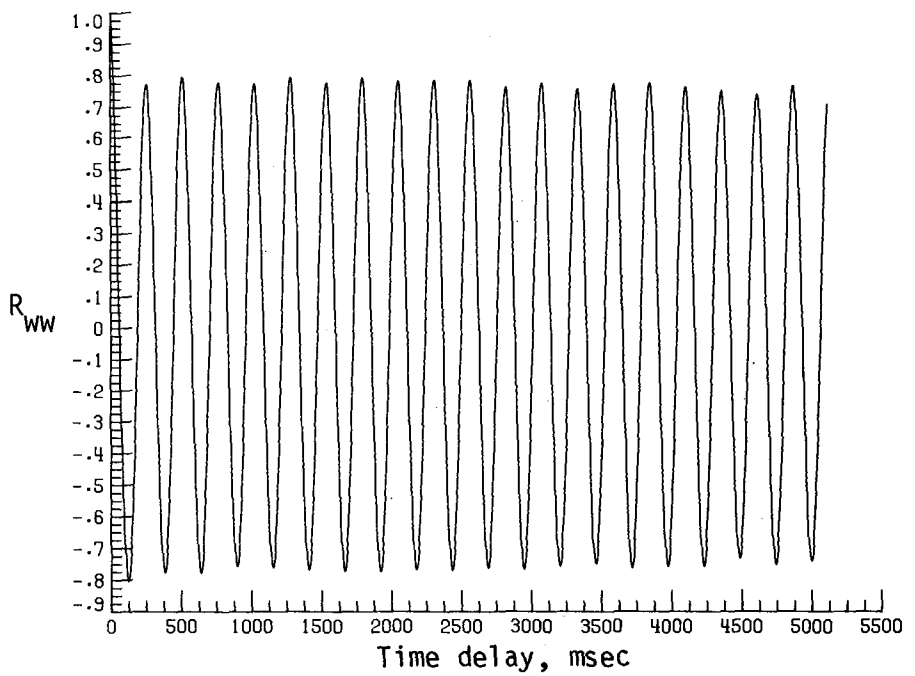

(f) Normalized autocorrelation of vertical velocity fluctuations. $\sigma = 0.0235$.

Figure A24. Concluded.

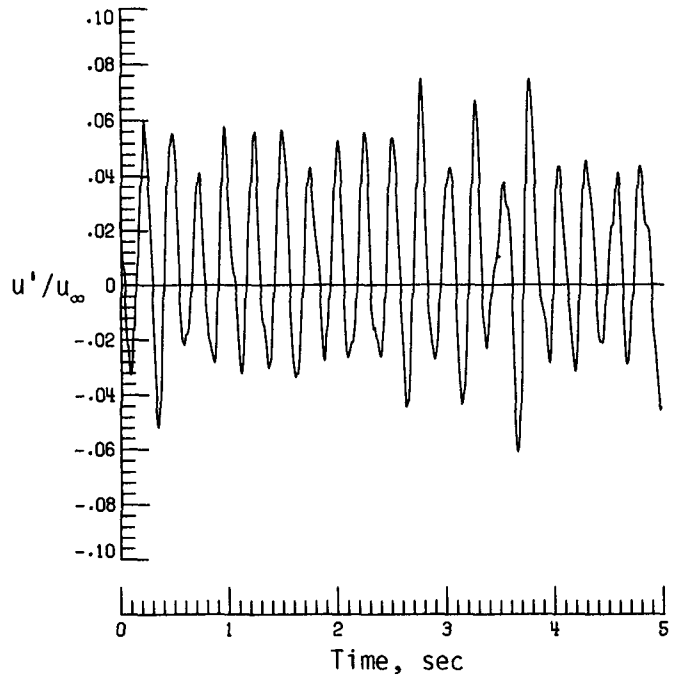

(a) Time history of streamwise velocity fluctuations.

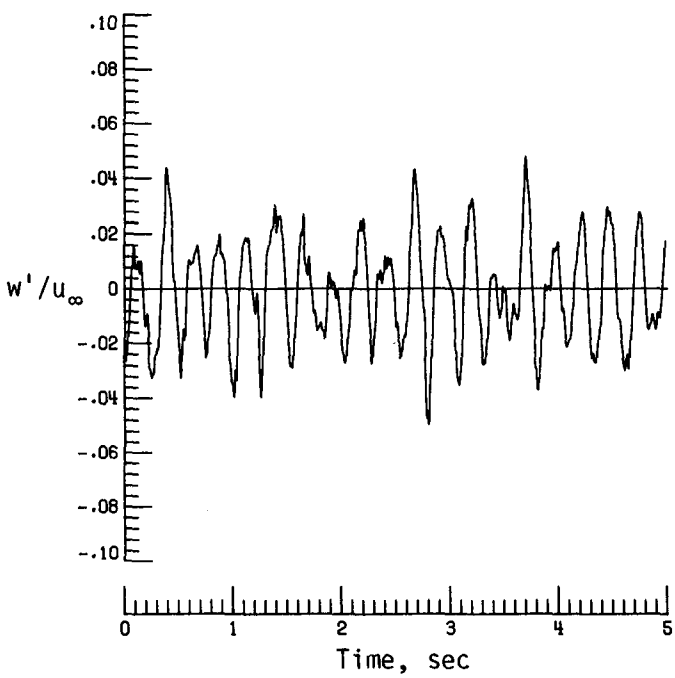

(b) Time history of vertical velocity fluctuations.

Figure A25. Dynamic-flow quality for baseline configuration at $q = 55.26$ lb/ft^2.

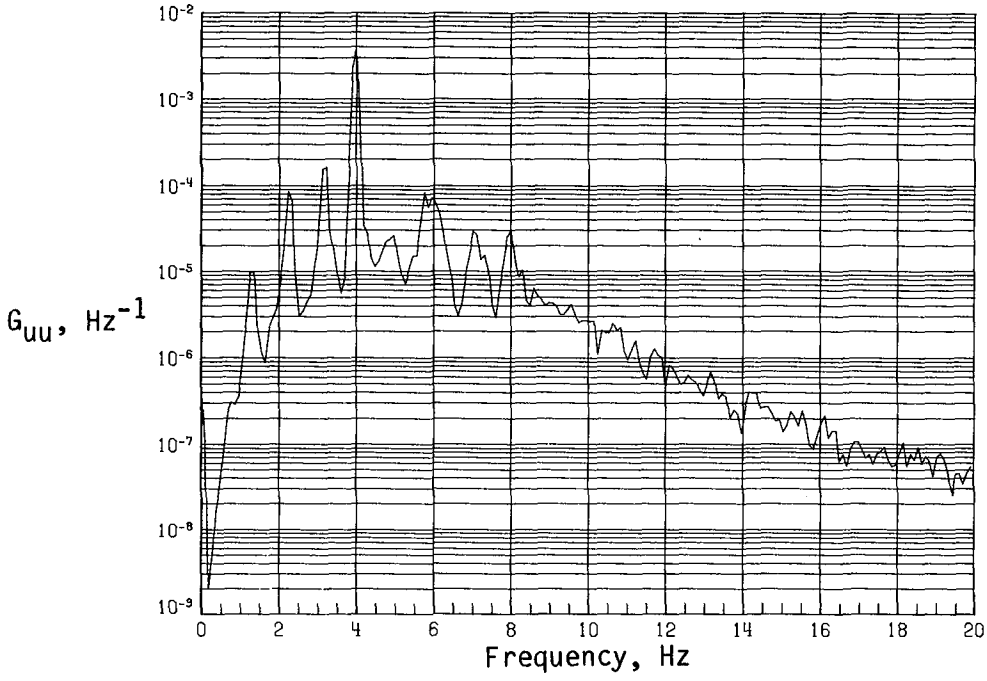

(c) PSD of streamwise velocity fluctuations.

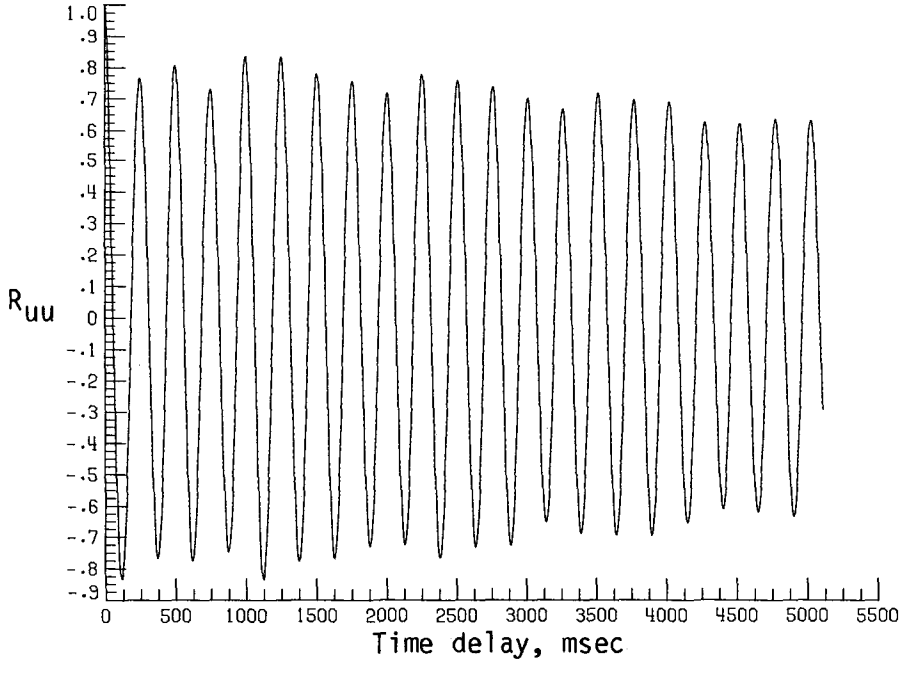

(d) Normalized autocorrelation of streamwise velocity fluctuations. $\sigma = 0.0282$.

Figure A25. Continued.

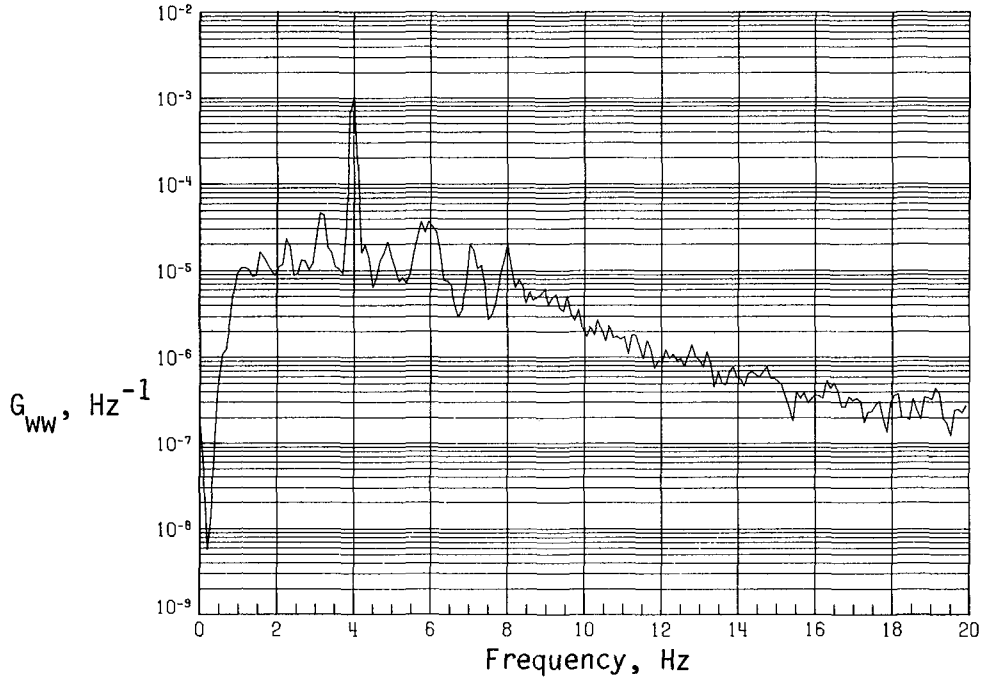

(e) PSD of vertical velocity fluctuations.

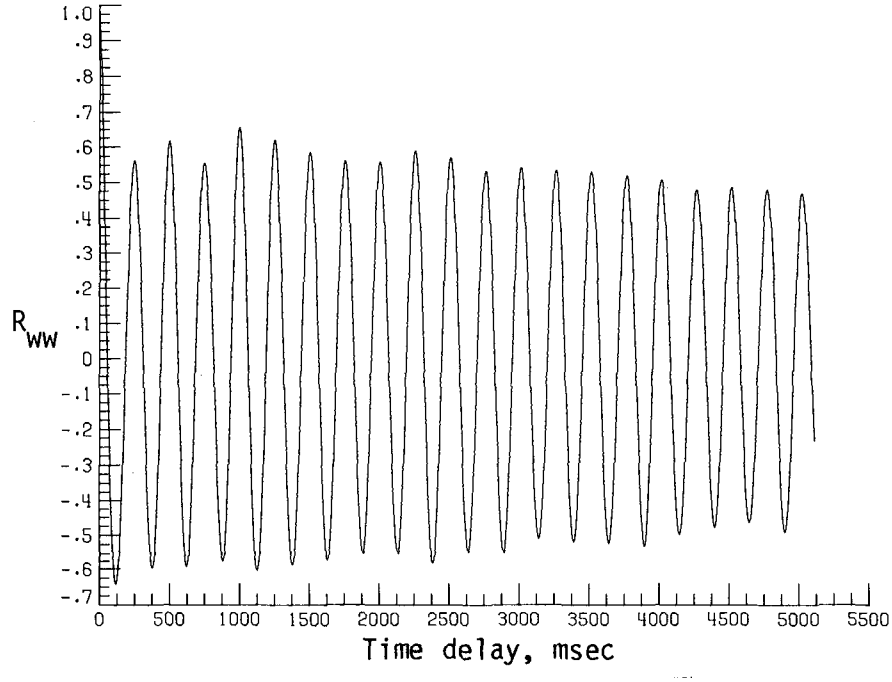

(f) Normalized autocorrelation of vertical velocity fluctuations. $\sigma = 0.0169$.

Figure A25. Concluded.

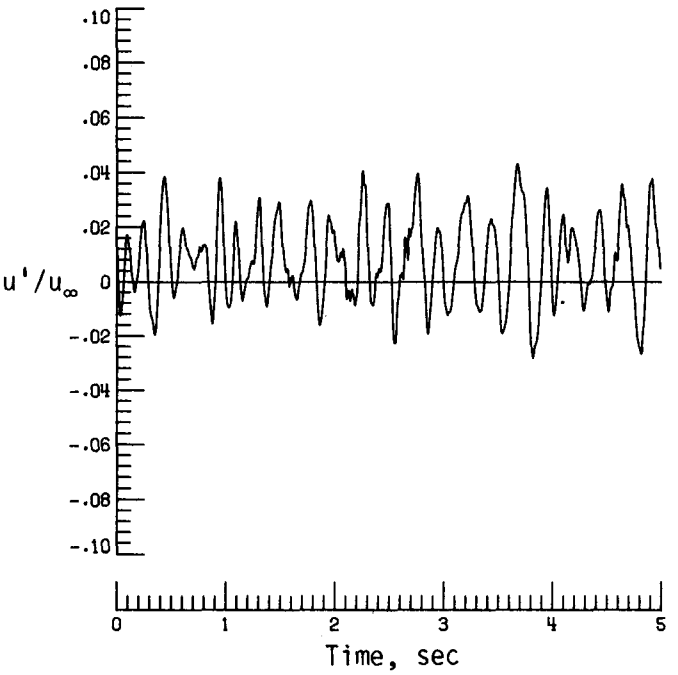

(a) Time history of streamwise velocity fluctuations.

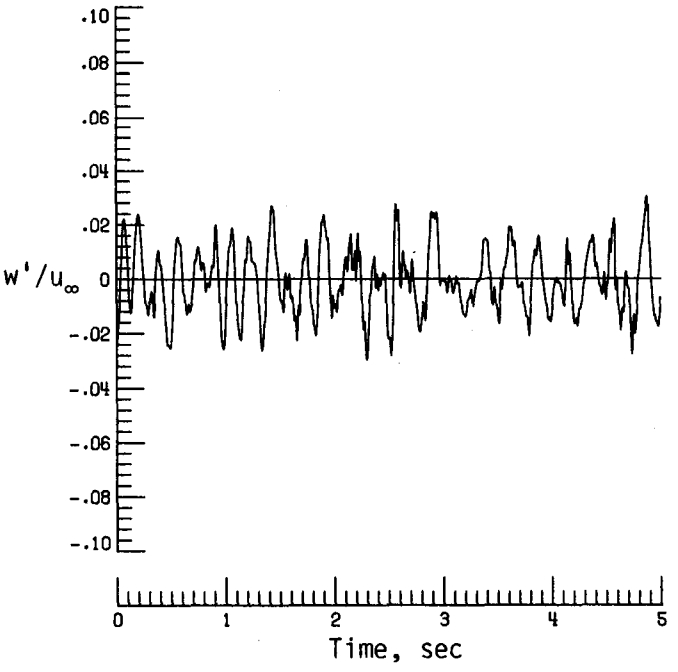

(b) Time history of vertical velocity fluctuations.

Figure A26. Dynamic-flow quality for baseline configuration at $q = 59.10$ lb/ft^2.

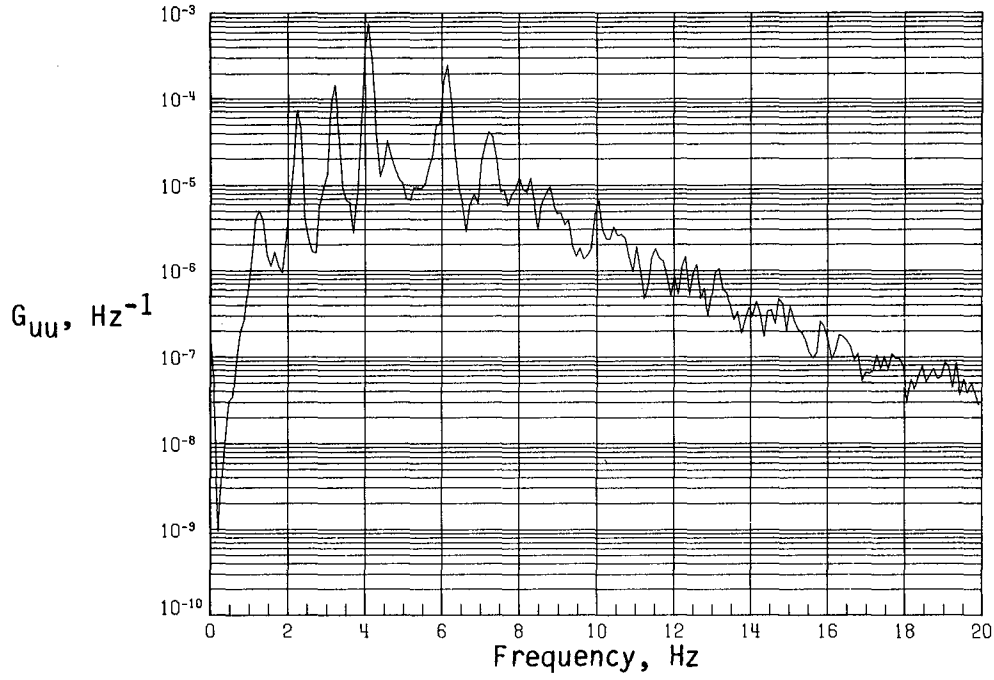

(c) PSD of streamwise velocity fluctuations.

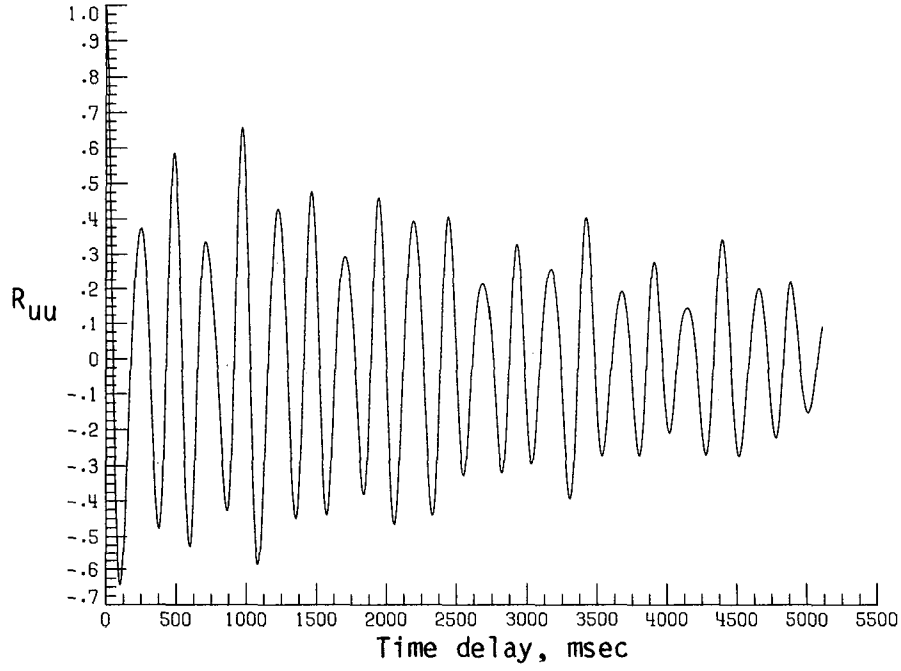

(d) Normalized autocorrelation of streamwise velocity fluctuations. $\sigma = 0.0181$.

Figure A26. Continued.

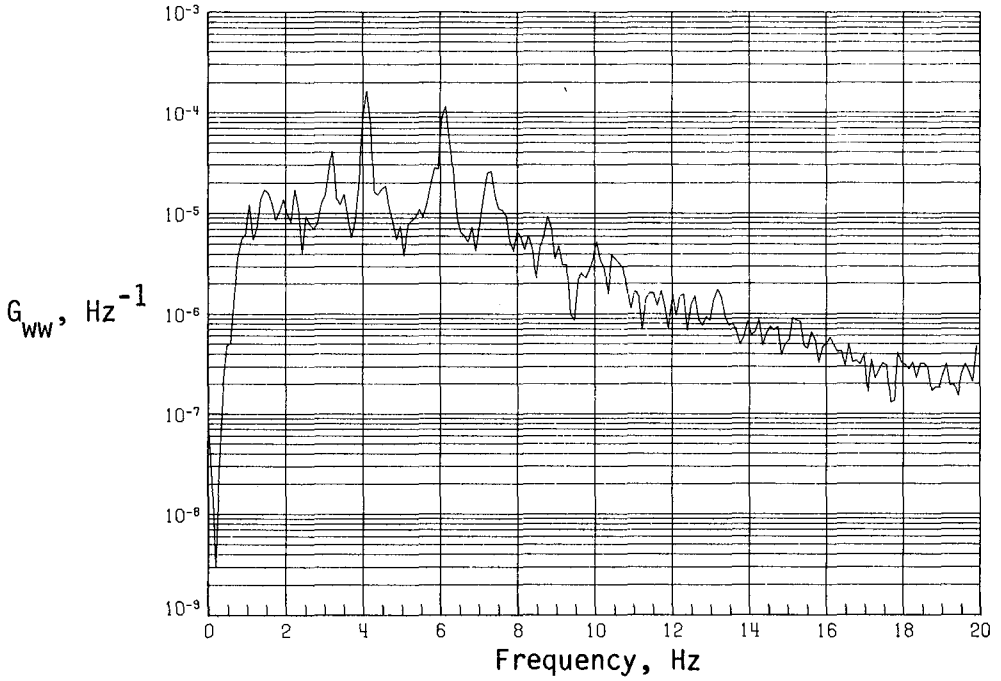

(e) PSD of vertical velocity fluctuations.

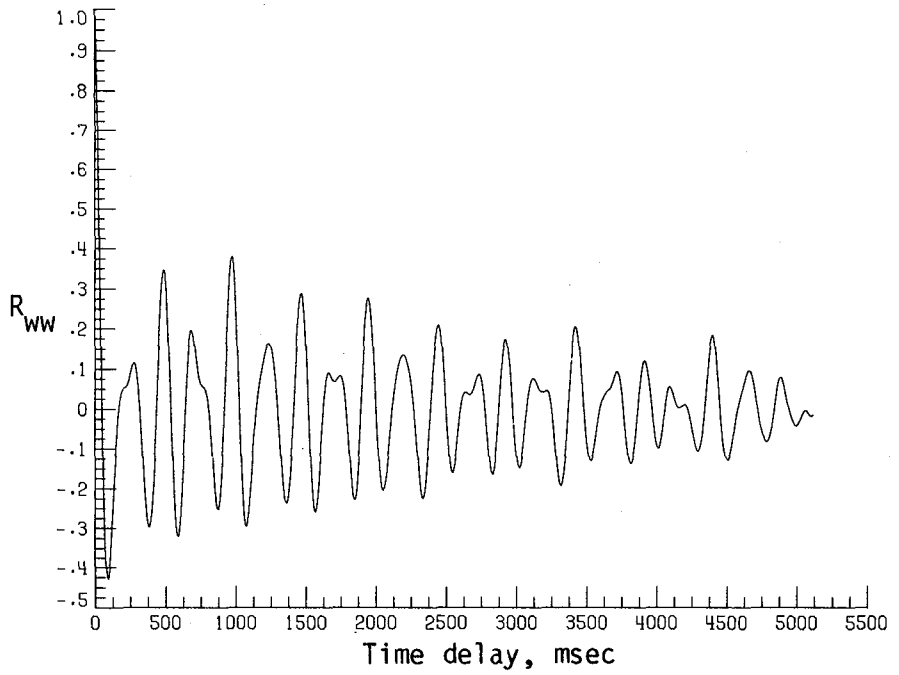

(f) Normalized autocorrelation of vertical velocity fluctuations. $\sigma = 0.0128$.

Figure A26. Concluded.

Appendix B

Dynamic-Flow Quality for Jet Exit Configuration 6

Appendix B presents the dynamic-flow-quality data for jet exit configuration 6. It includes the time histories and autopower spectral density (PSD) and autocorrelation functions of the velocity fluctuations corresponding to the RMS data points shown in figure 20. The time history plots show a typical 5-sec time slice of the streamwise (u') and vertical (w') velocity fluctuations. The data are presented in the following order:

Figure	q, lb/ft^2
B1	1.93
B2	2.94
B3	4.07
B4	4.53
B5	5.09
B6	5.54
B7	5.99
B8	6.56
B9	7.12
B10	8.03
B11	9.05
B12	10.06
B13	11.19
B14	13.11
B15	13.90
B16	15.03
B17	16.05
B18	16.98
B19	18.08
B20	20.00
B21	22.49
B22	25.09
B23	32.10
B24	40.01
B25	42.60
B26	44.98
B27	47.46
B28	50.17
B29	54.81
B30	59.55

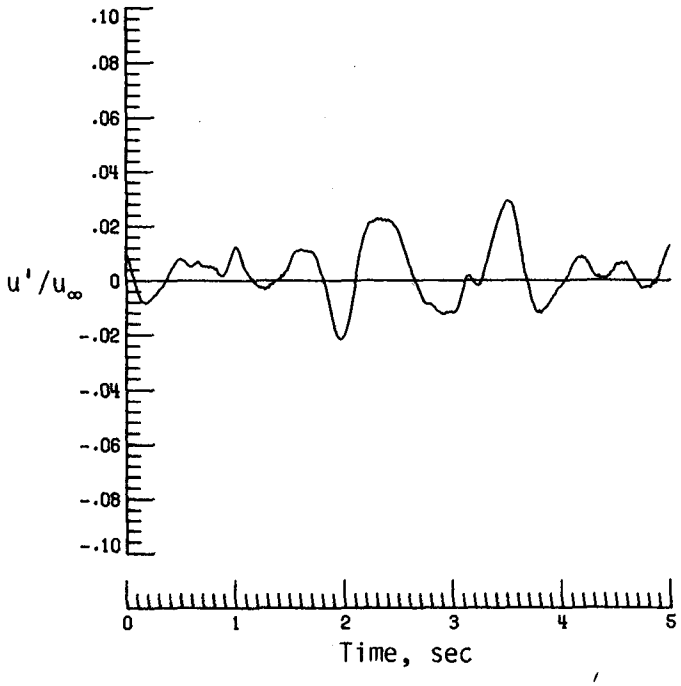

(a) Time history of streamwise velocity fluctuations.

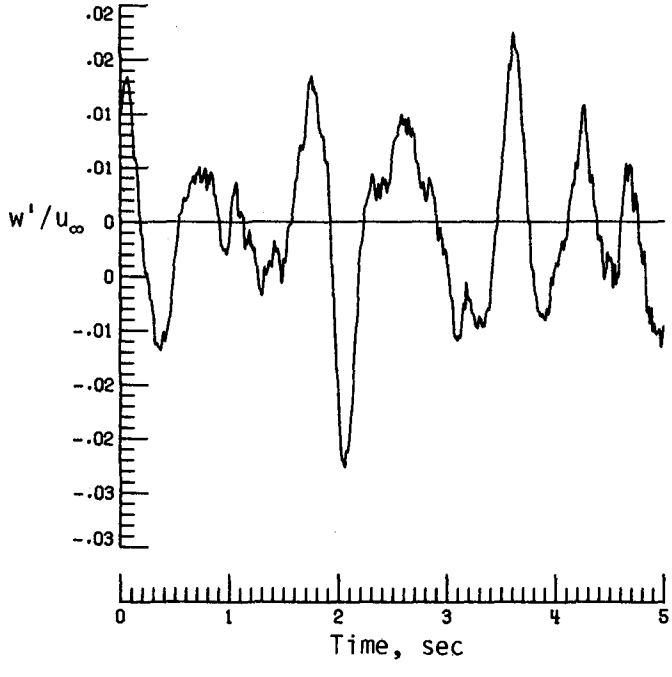

(b) Time history of vertical velocity fluctuations.

Figure B1. Dynamic-flow quality for configuration 6 at $q = 1.93$ lb/ft^2.

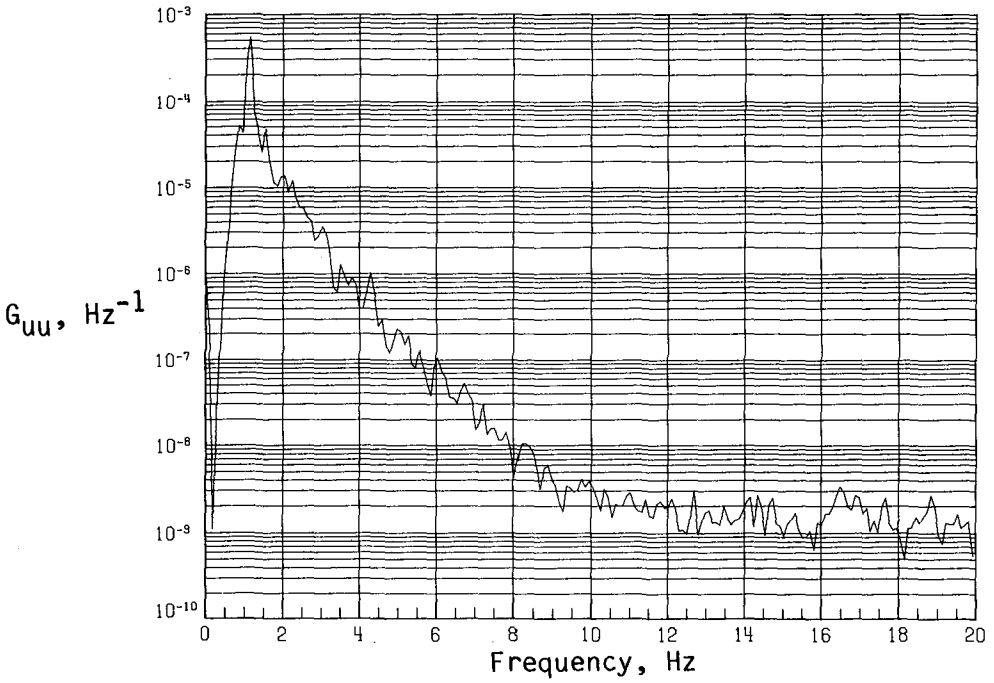

(c) PSD of streamwise velocity fluctuations.

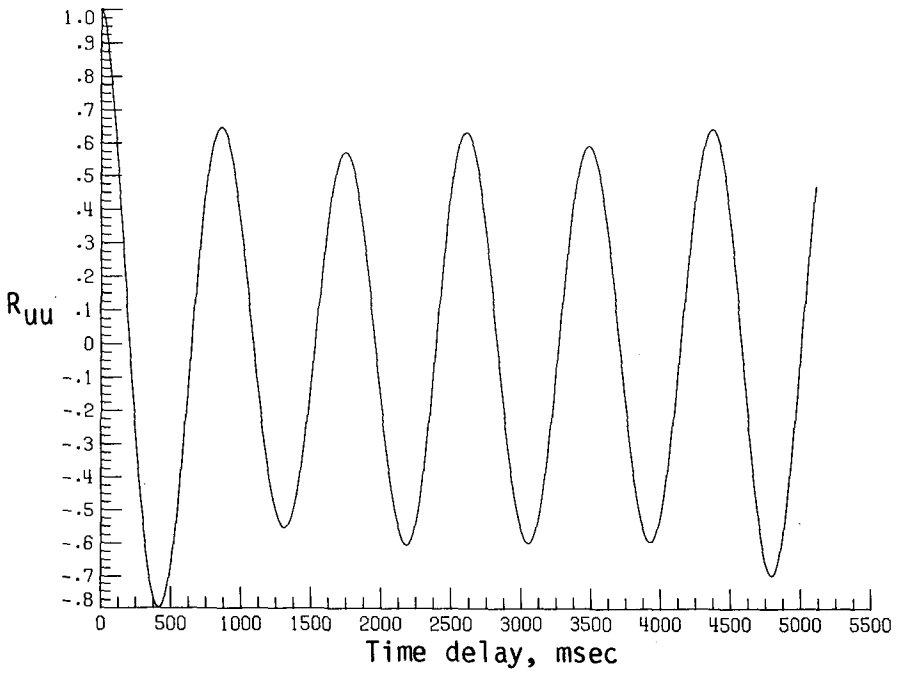

(d) Normalized autocorrelation of streamwise velocity fluctuations. $\sigma = 0.0120$.

Figure B1. Continued.

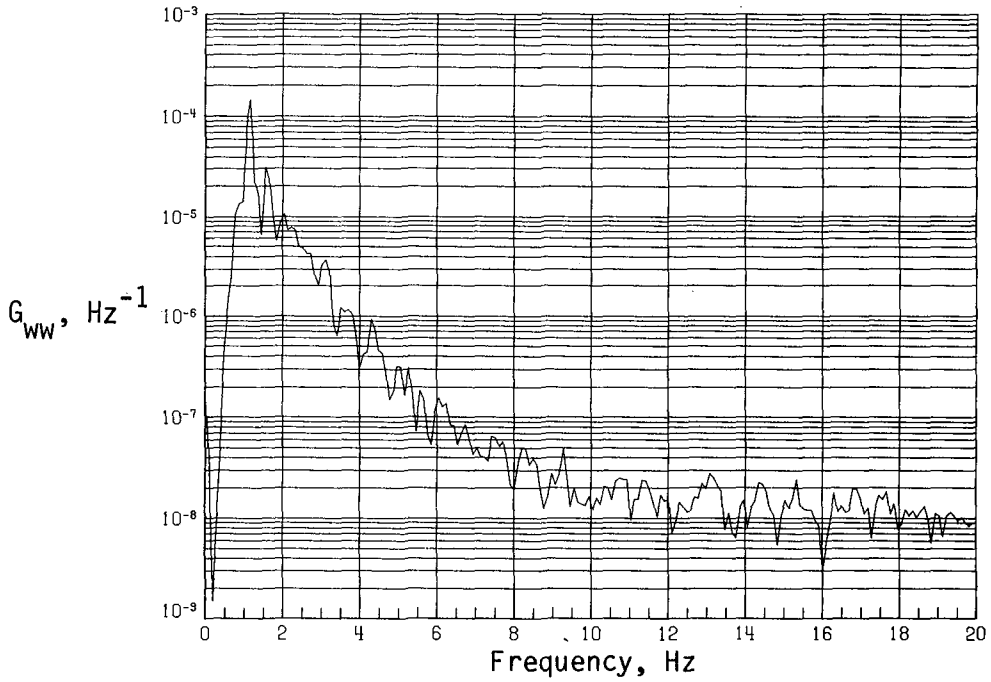

(e) PSD of vertical velocity fluctuations.

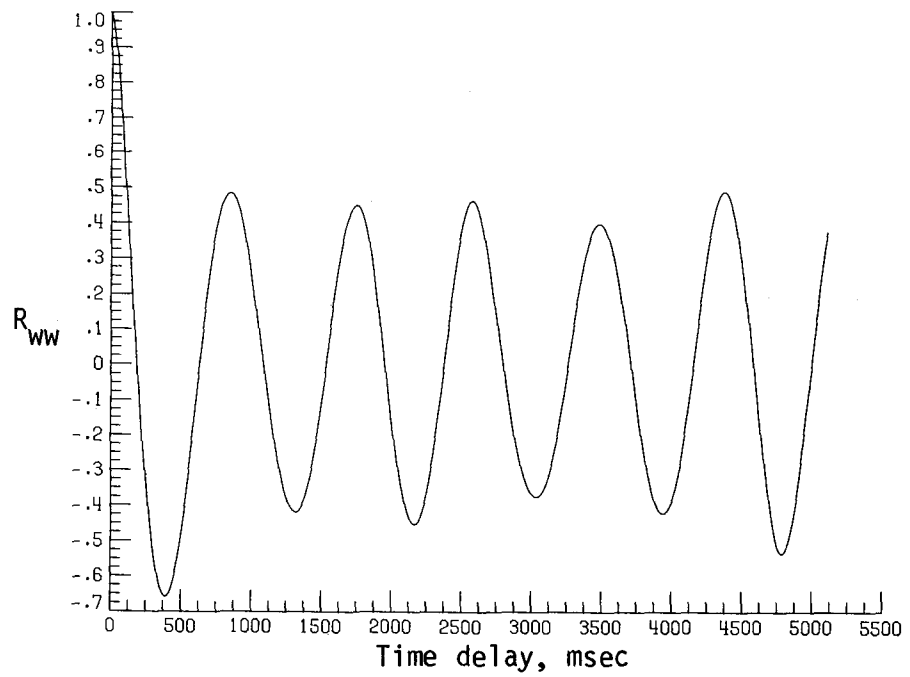

(f) Normalized autocorrelation of vertical velocity fluctuations. $\sigma = 0.0075$.

Figure B1. Concluded.

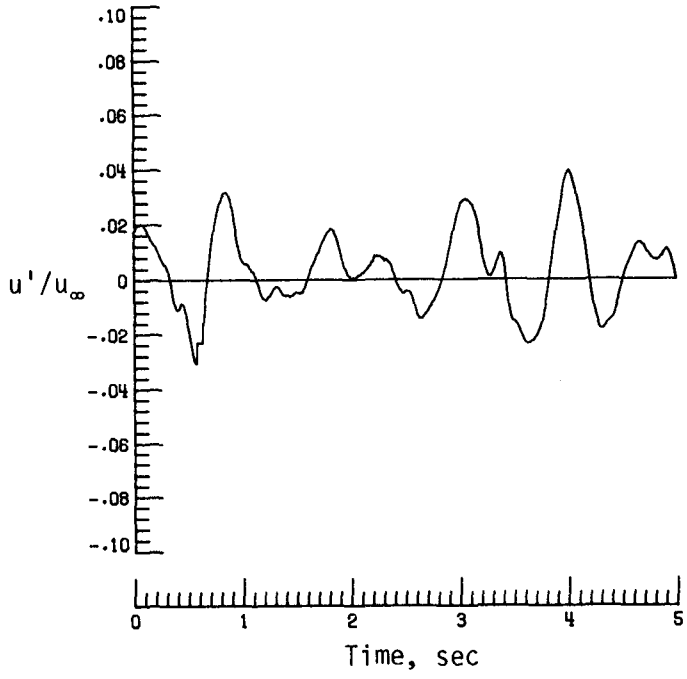

(a) Time history of streamwise velocity fluctuations.

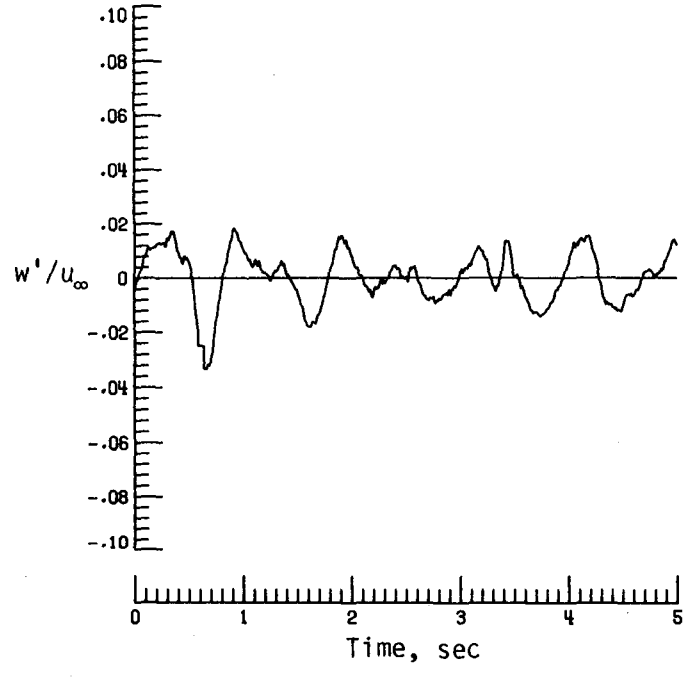

(b) Time history of vertical velocity fluctuations.

Figure B2. Dynamic-flow quality for configuration 6 at $q = 2.94$ lb/ft^2.

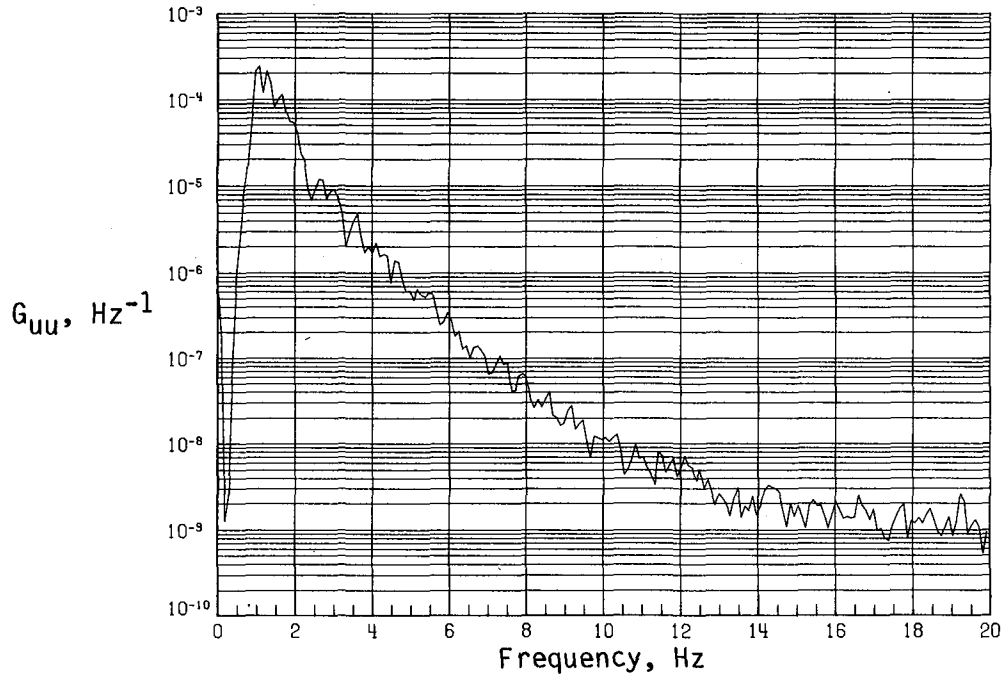

(c) PSD of streamwise velocity fluctuations.

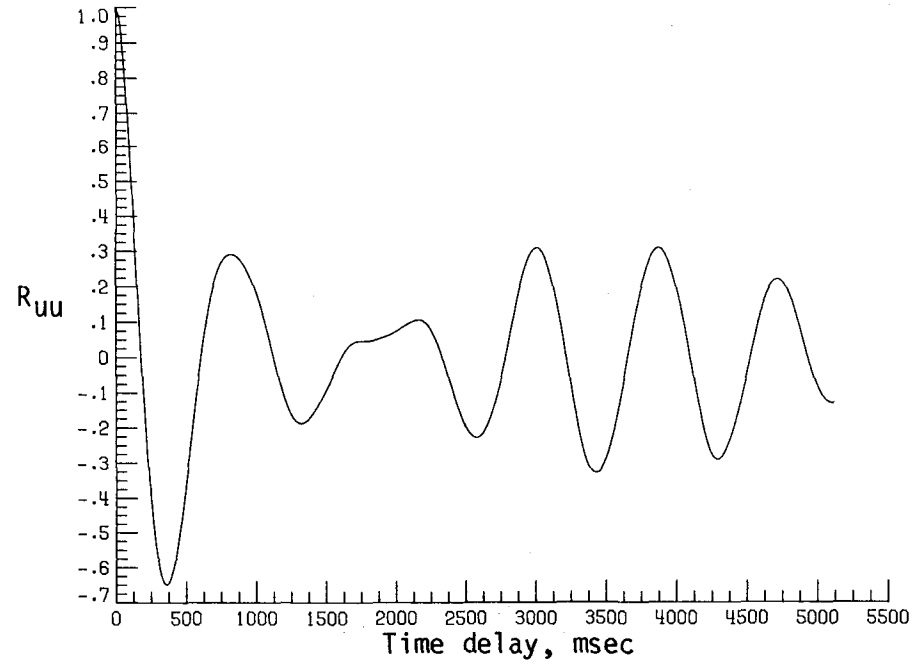

(d) Normalized autocorrelation of streamwise velocity fluctuations. $\sigma = 0.0121$.

Figure B2. Continued.

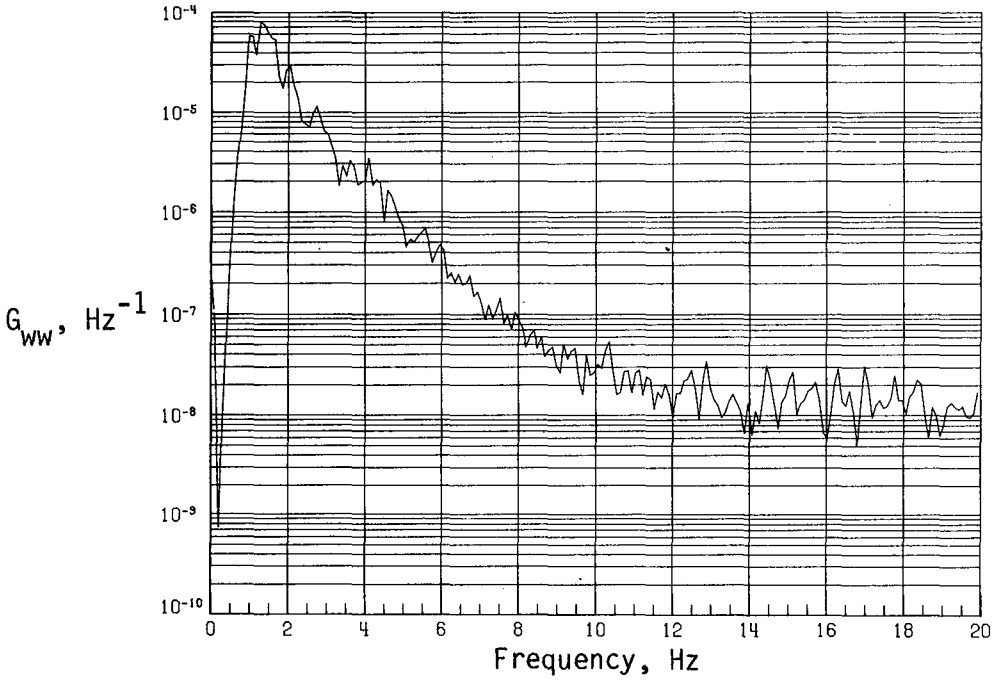

(e) PSD of vertical velocity fluctuations.

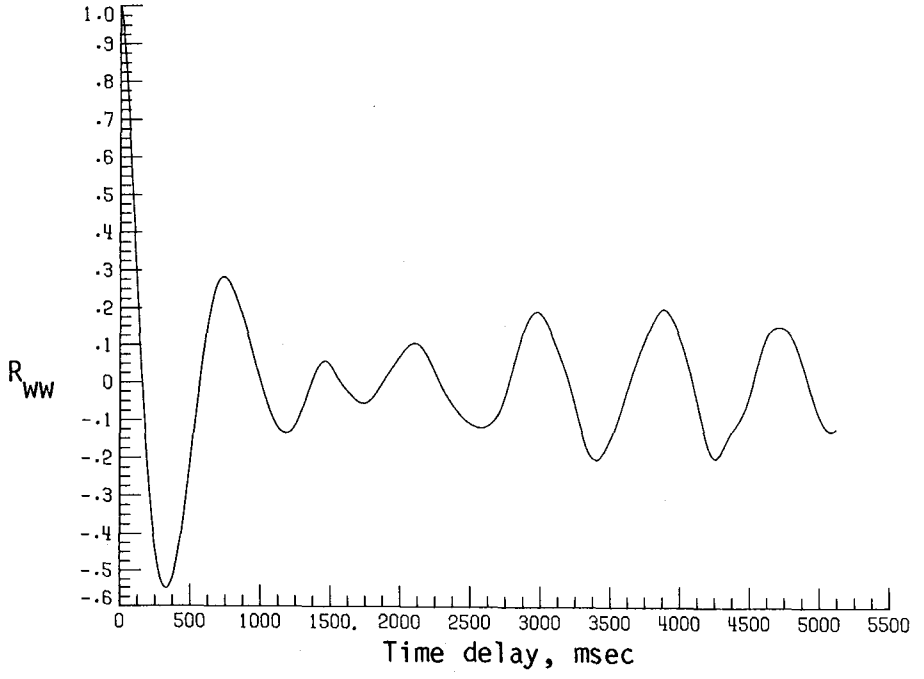

(f) Normalized autocorrelation of vertical velocity fluctuations. $\sigma = 0.0080$.

Figure B2. Concluded.

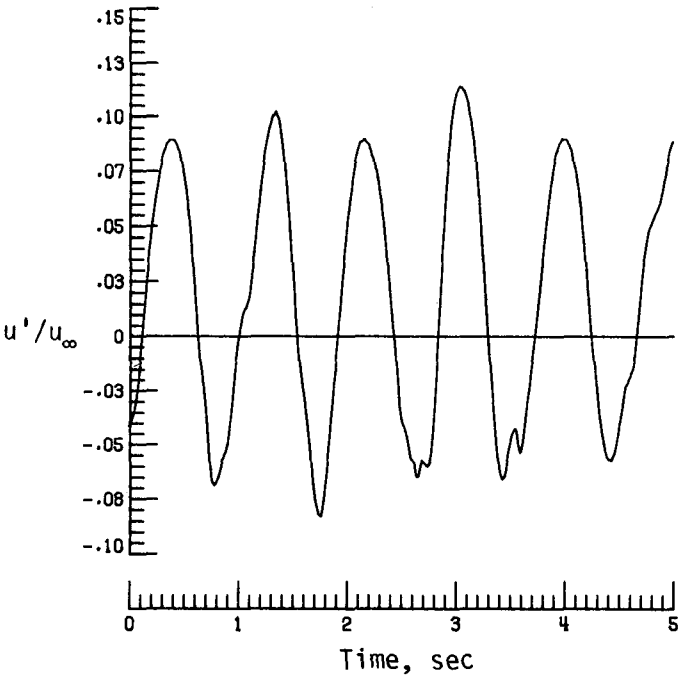

(a) Time history of streamwise velocity fluctuations.

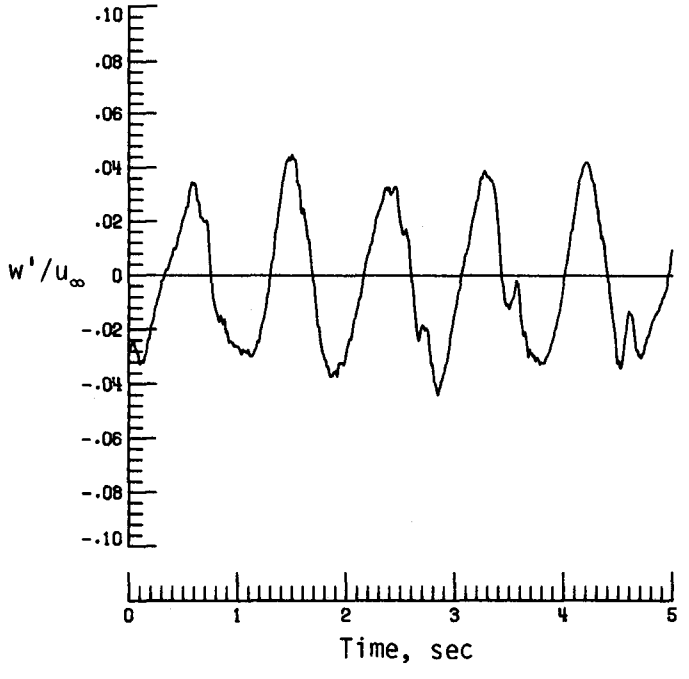

(b) Time history of vertical velocity fluctuations.

Figure B3. Dynamic-flow quality for configuration 6 at $q = 4.07$ lb/ft^2.

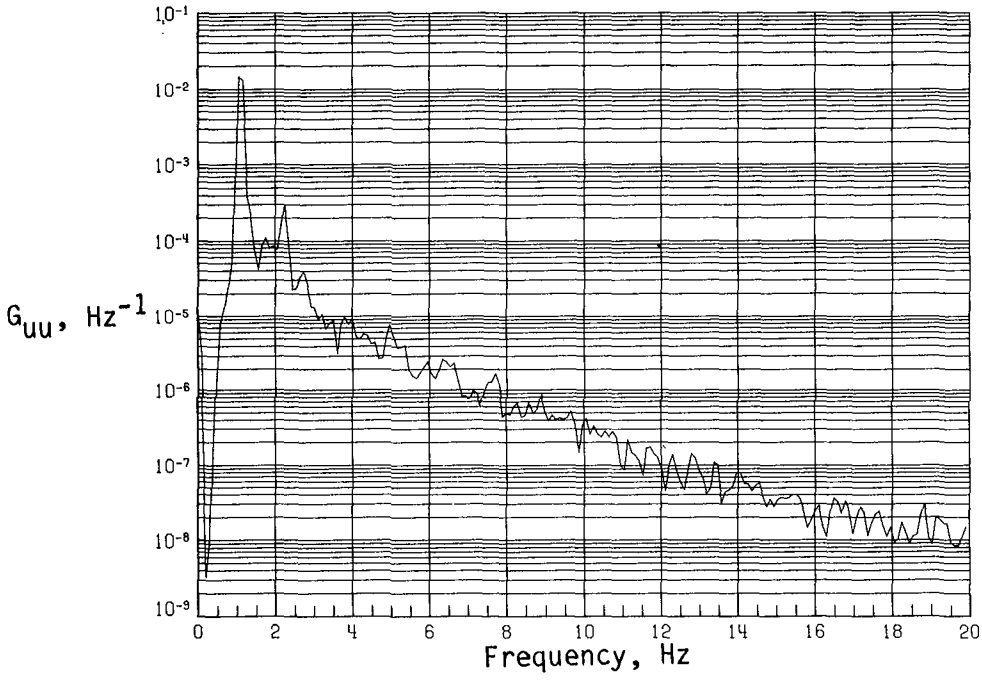

(c) PSD of streamwise velocity fluctuations.

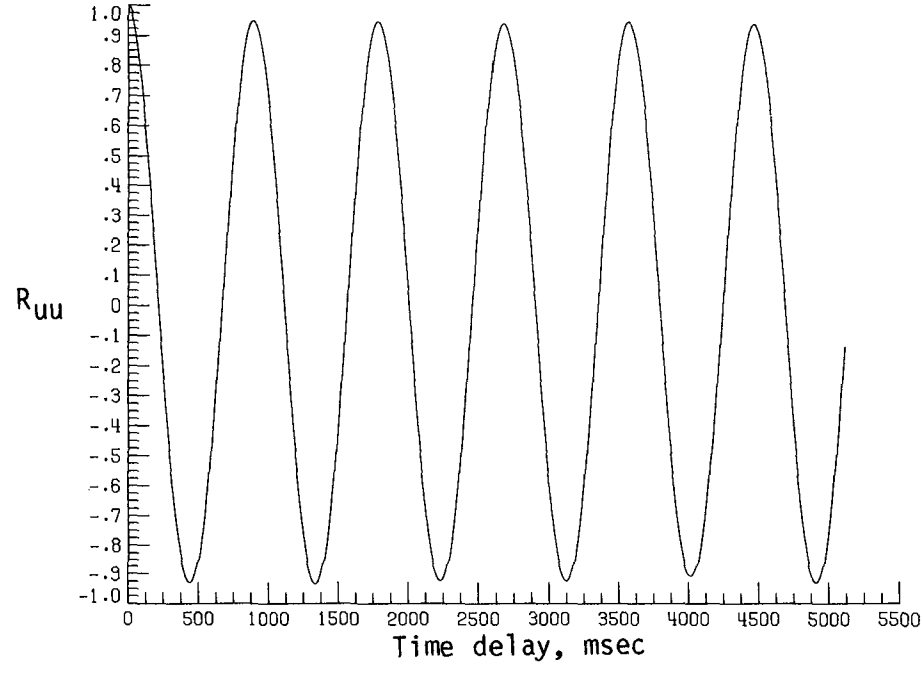

(d) Normalized autocorrelation of streamwise velocity fluctuations. $\sigma = 0.0551$.

Figure B3. Continued.

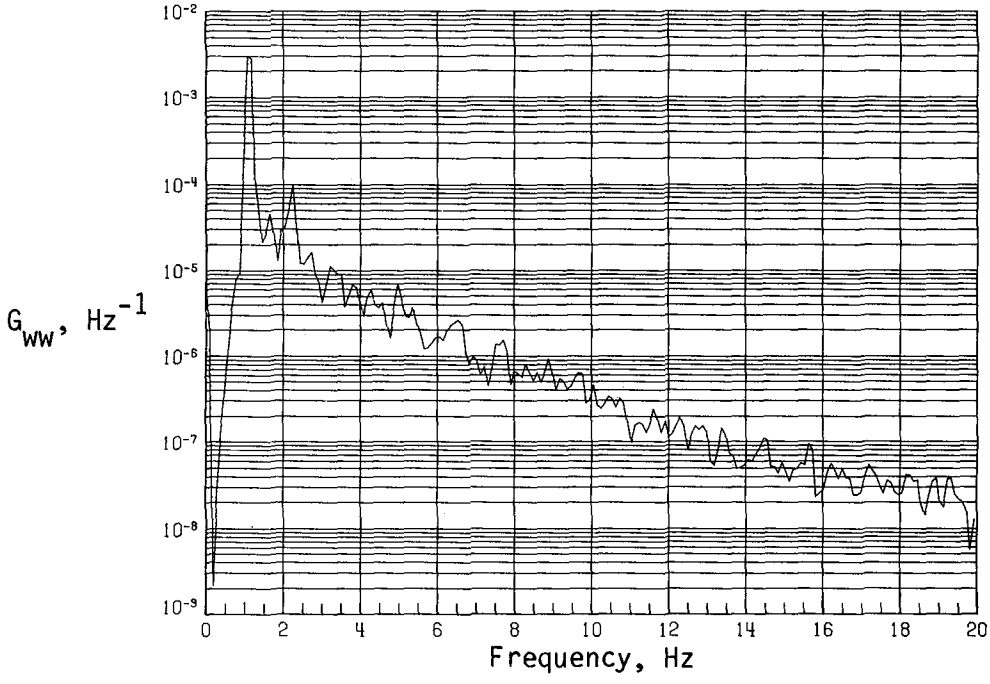

(e) PSD of vertical velocity fluctuations.

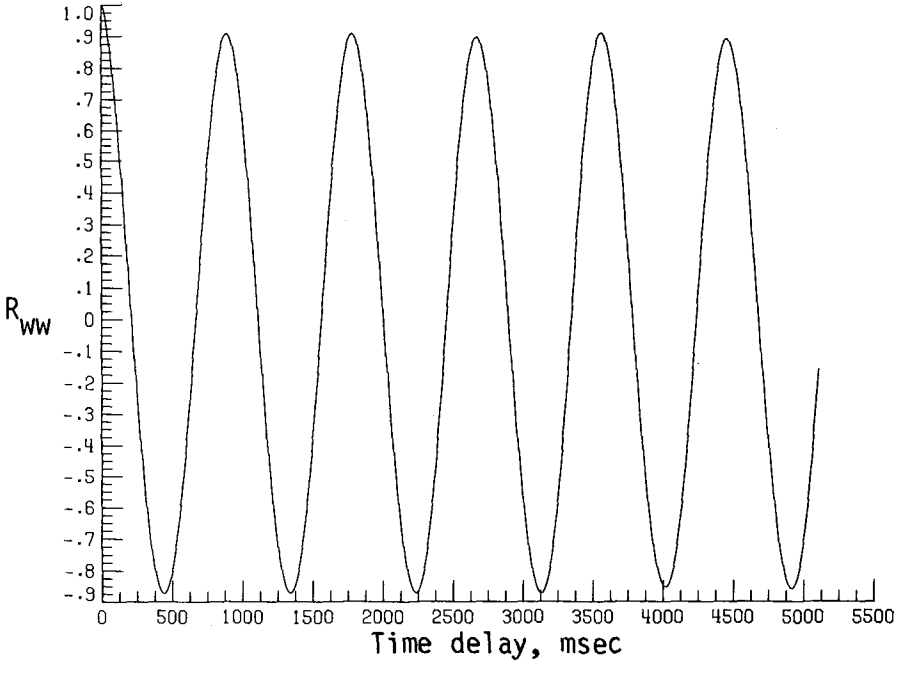

(f) Normalized autocorrelation of vertical velocity fluctuations. $\sigma = 0.0254$.

Figure B3. Concluded.

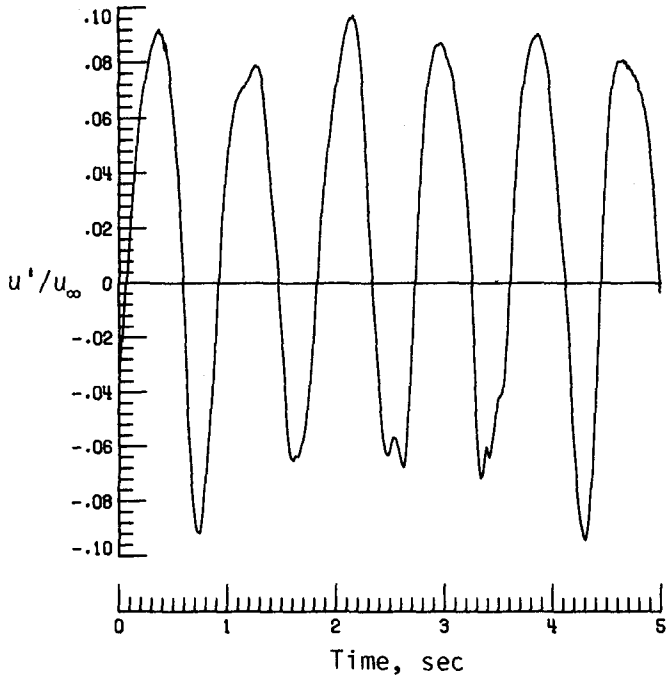

(a) Time history of streamwise velocity fluctuations.

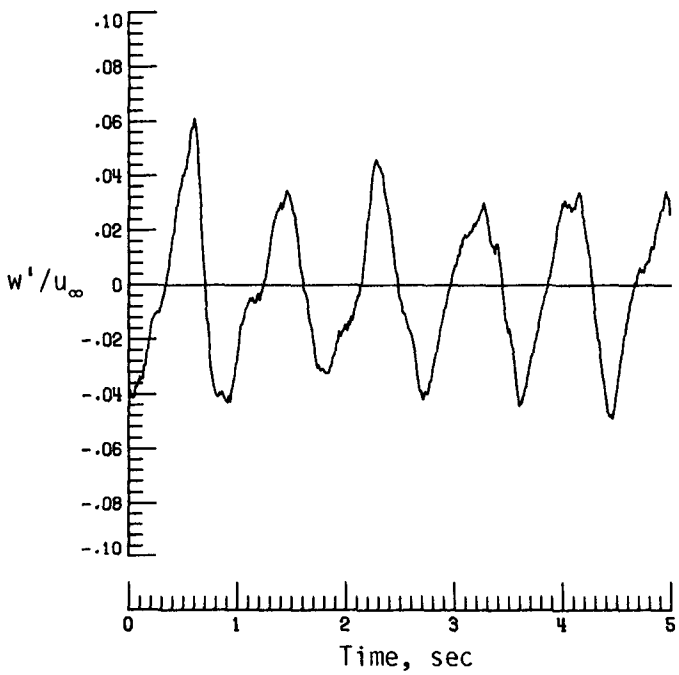

(b) Time history of vertical velocity fluctuations.

Figure B4. Dynamic-flow quality for configuration 6 at $q = 4.53$ lb/ft^2.

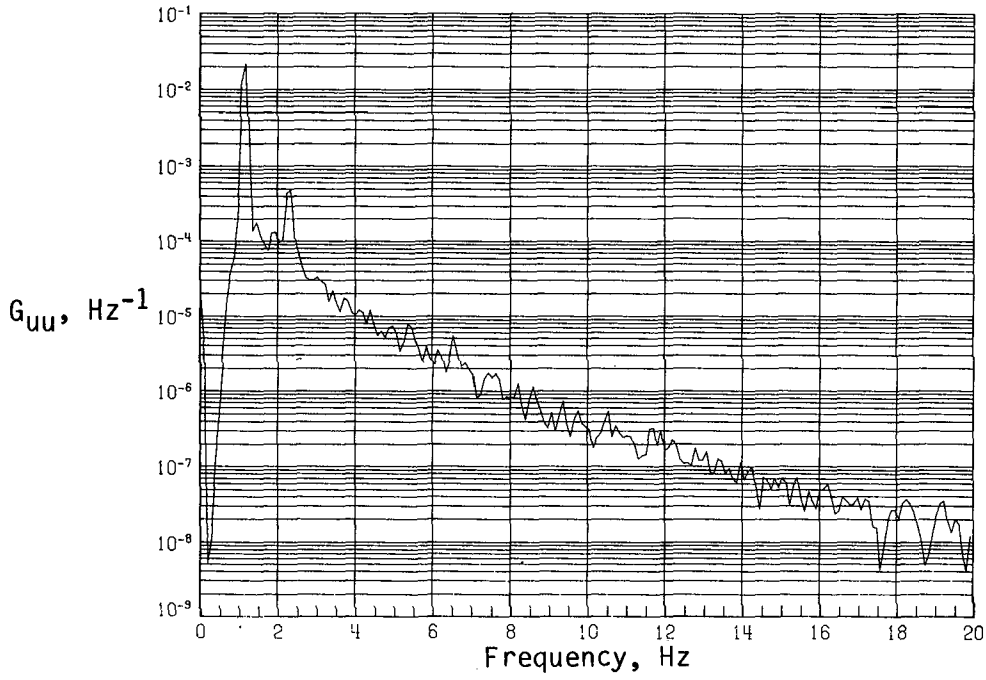

(c) PSD of streamwise velocity fluctuations.

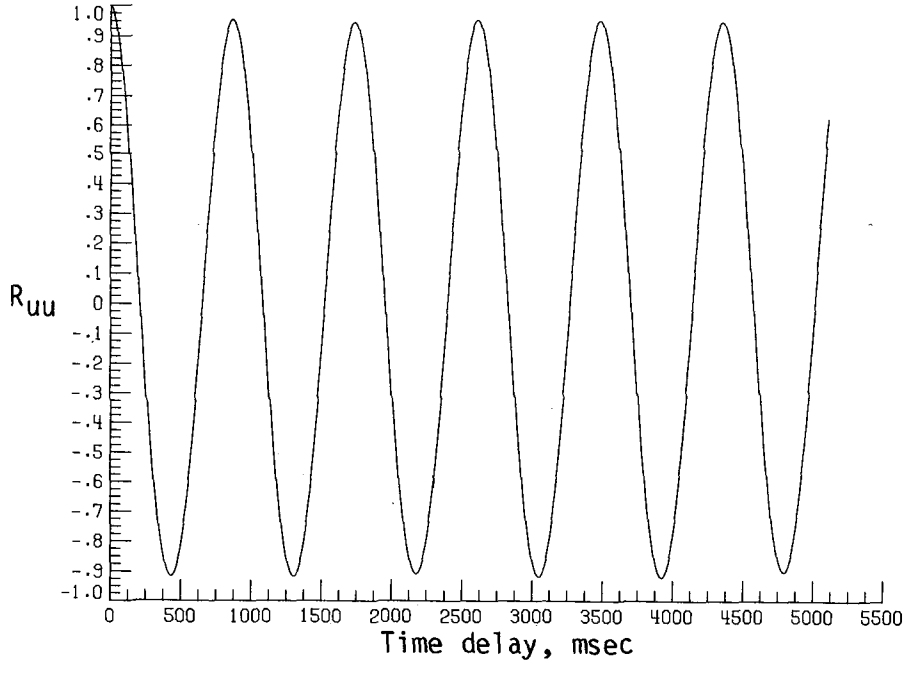

(d) Normalized autocorrelation of streamwise velocity fluctuations. $\sigma = 0.0609$.

Figure B4. Continued.

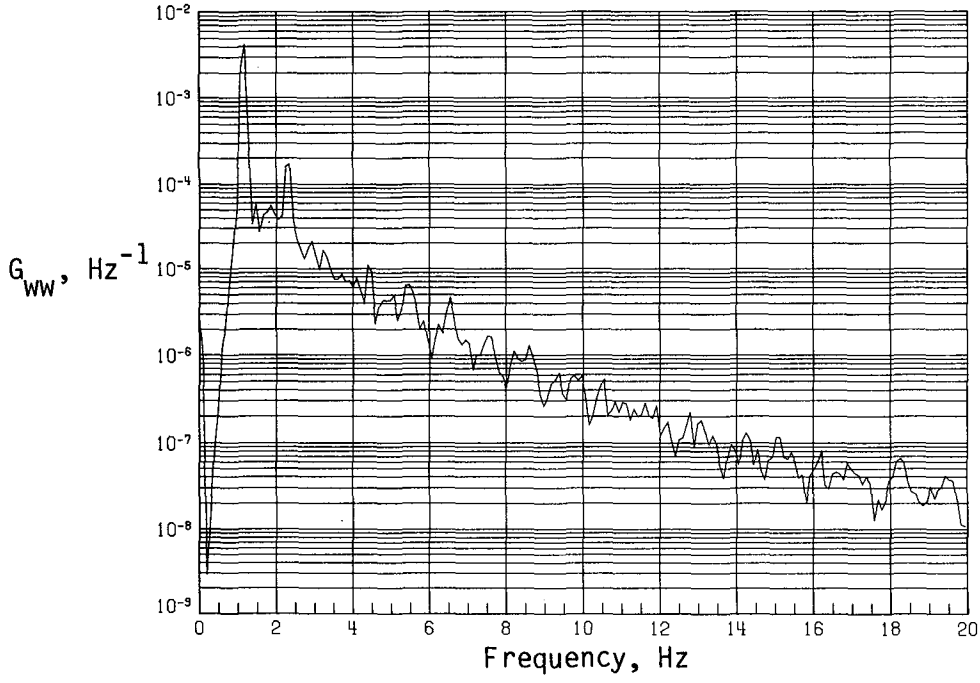

(e) PSD of vertical velocity fluctuations.

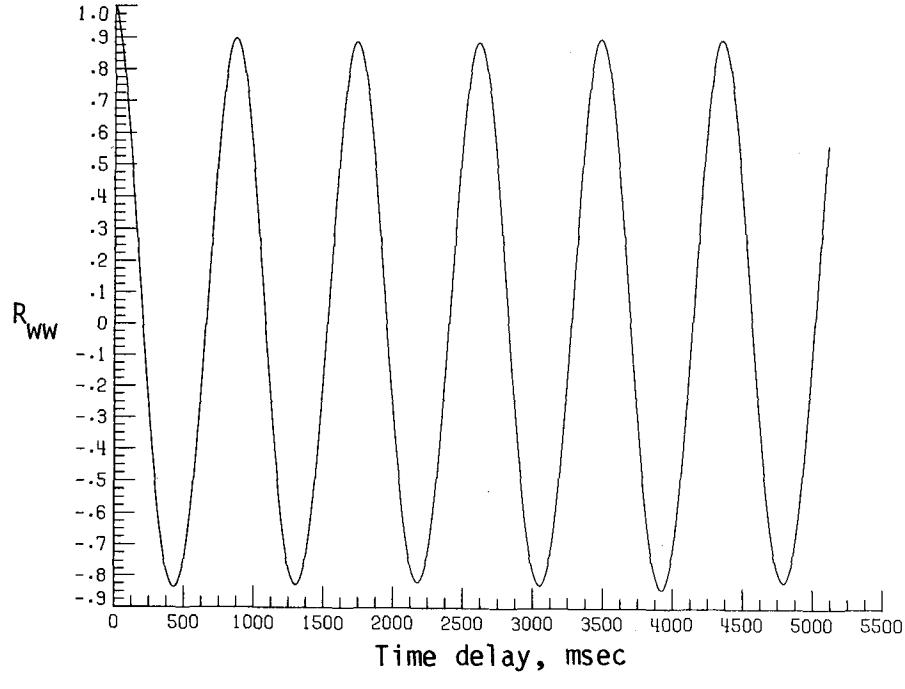

(f) Normalized autocorrelation of vertical velocity fluctuations. $\sigma = 0.0281$.

Figure B4. Concluded.

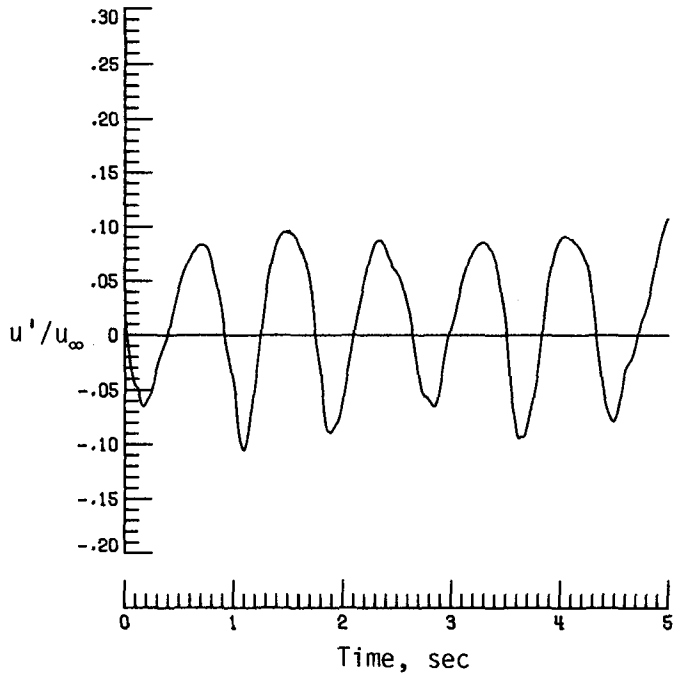

(a) Time history of streamwise velocity fluctuations.

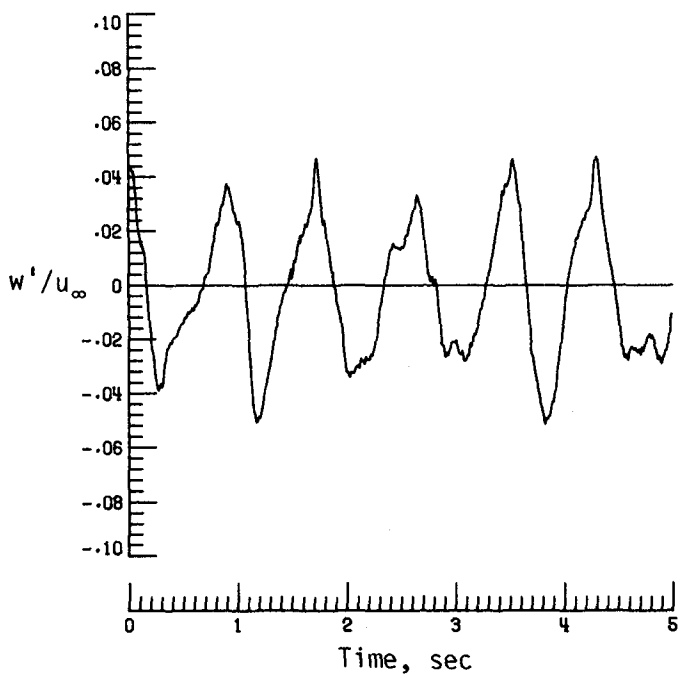

(b) Time history of vertical velocity fluctuations.

Figure B5. Dynamic-flow quality for configuration 6 at $q = 5.09$ lb/ft^2.

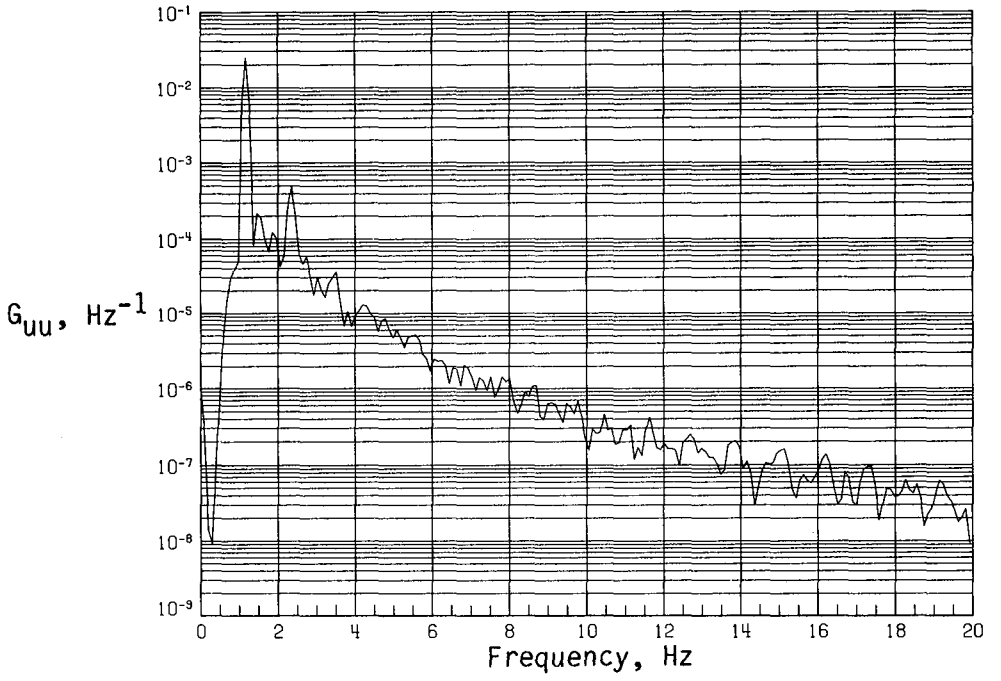

(c) PSD of streamwise velocity fluctuations.

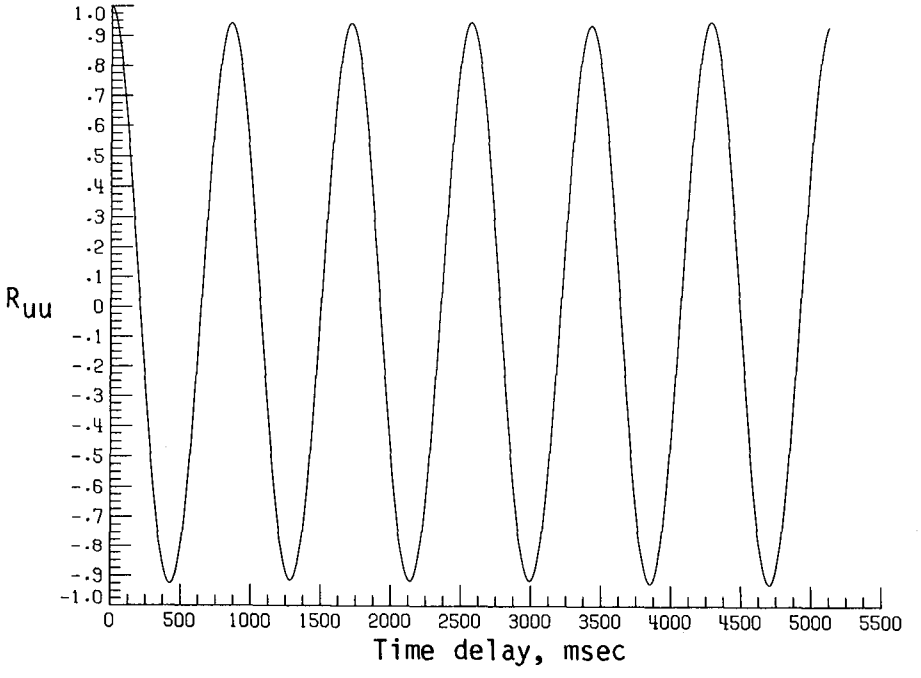

(d) Normalized autocorrelation of streamwise velocity fluctuations. $\sigma = 0.0629$.

Figure B5. Continued.

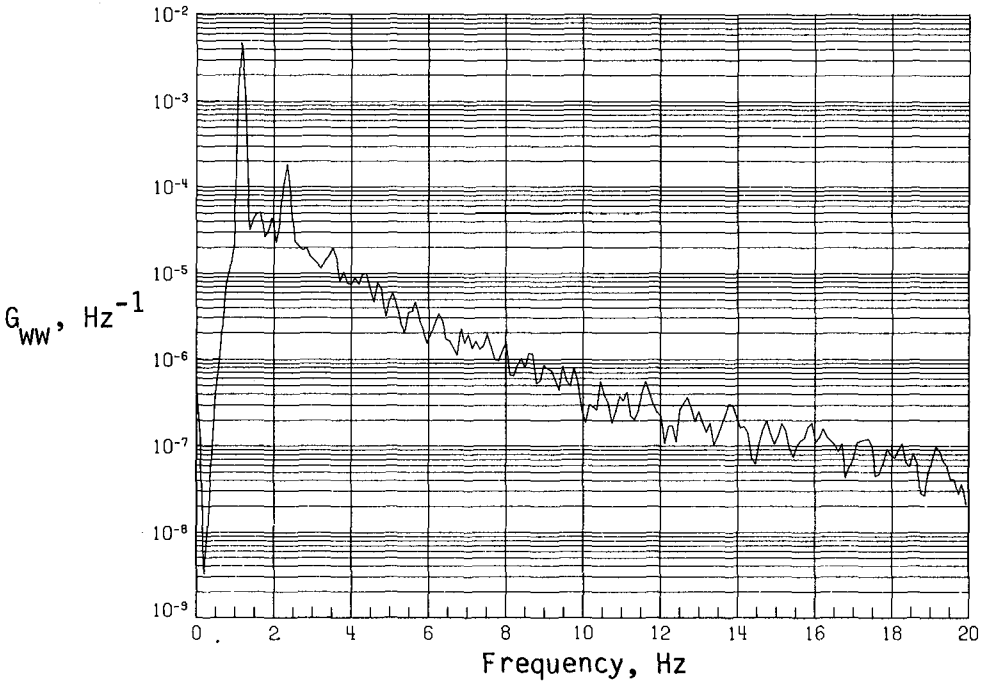

(e) PSD of vertical velocity fluctuations.

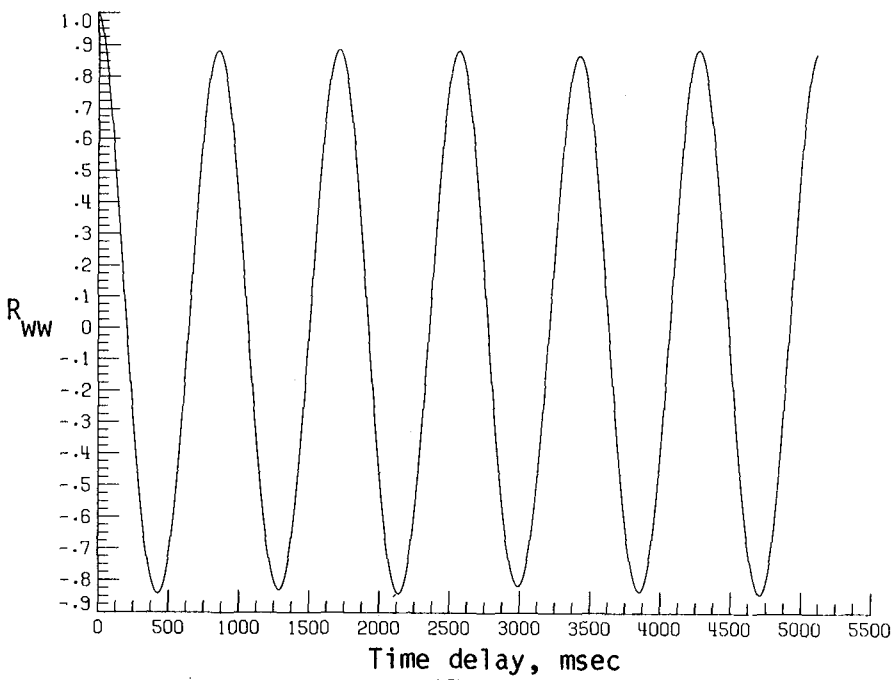

(f) Normalized autocorrelation of vertical velocity fluctuations. $\sigma = 0.0284$.

Figure B5. Concluded.

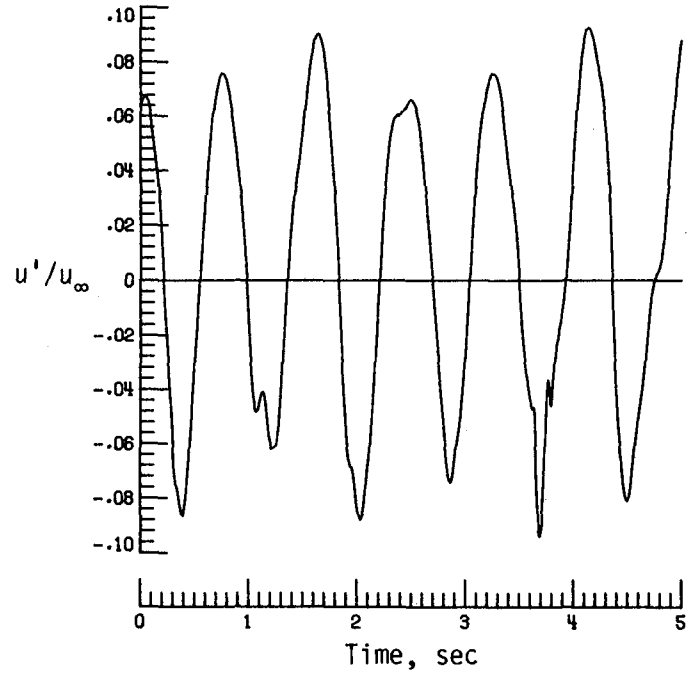

(a) Time history of streamwise velocity fluctuations.

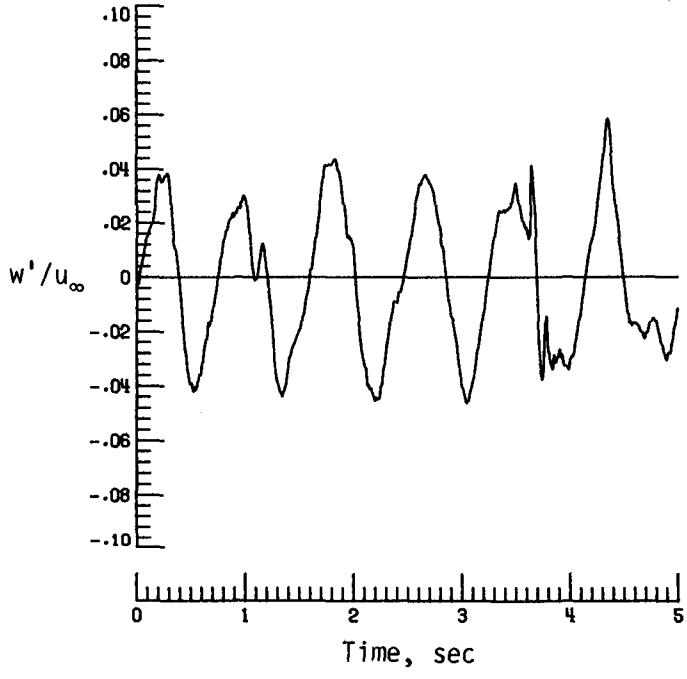

(b) Time history of vertical velocity fluctuations.

Figure B6. Dynamic-flow quality for configuration 6 at $q = 5.54$ lb/ft^2.

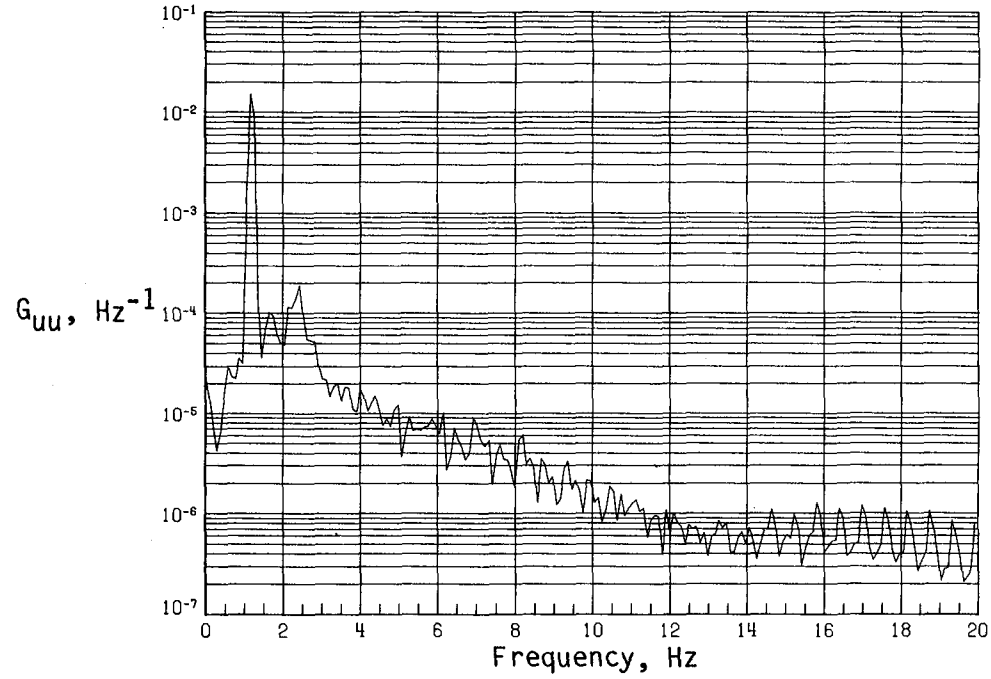

(c) PSD of streamwise velocity fluctuations.

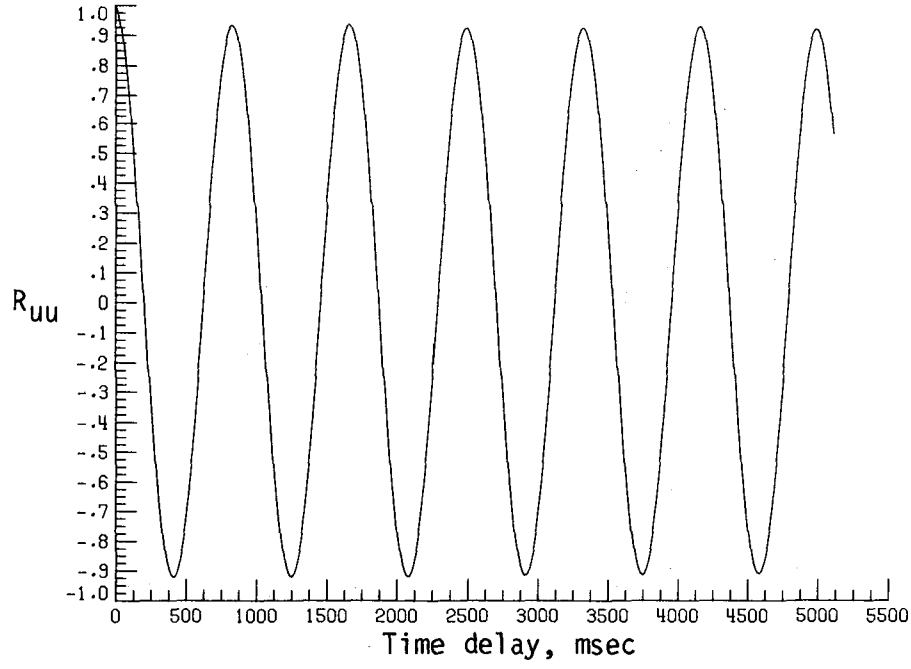

(d) Normalized autocorrelation of streamwise velocity fluctuations. $\sigma = 0.0519$.

Figure B6. Continued.

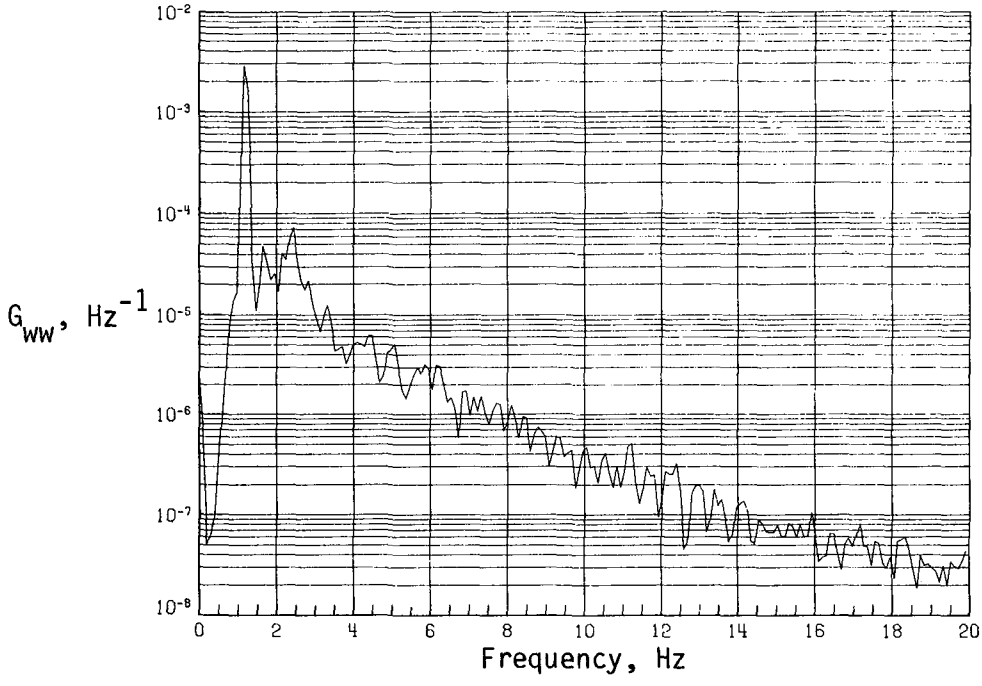

(e) PSD of vertical velocity fluctuations.

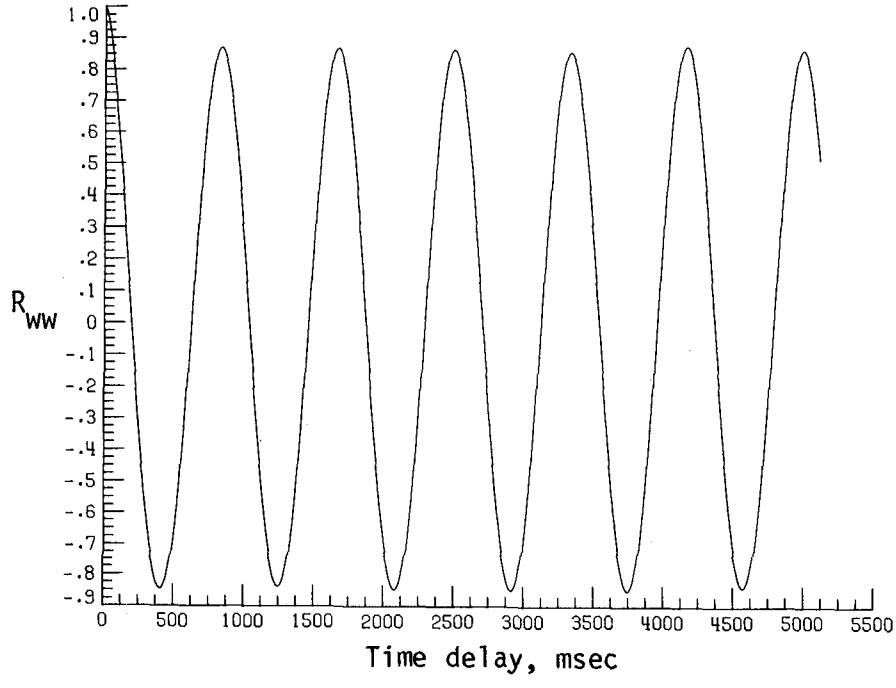

(f) Normalized autocorrelation of vertical velocity fluctuations. $\sigma = 0.0232$.

Figure B6. Concluded.

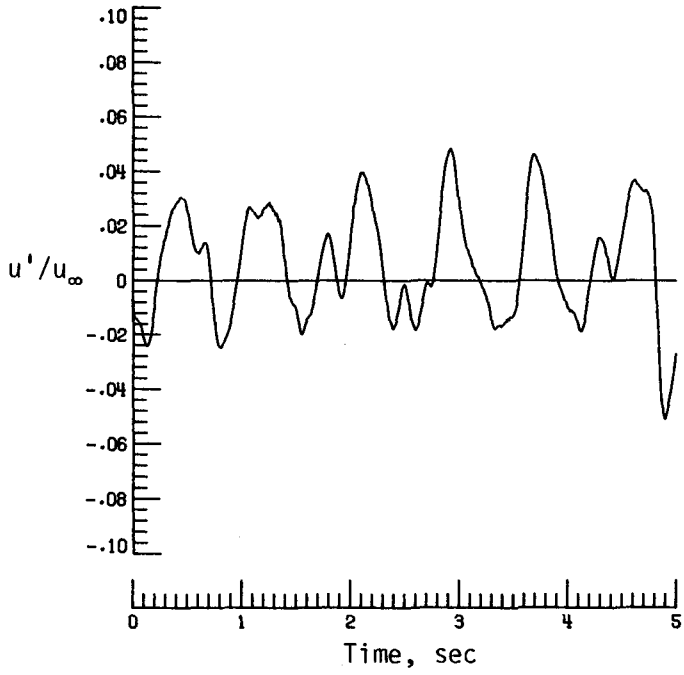

(a) Time history of streamwise velocity fluctuations.

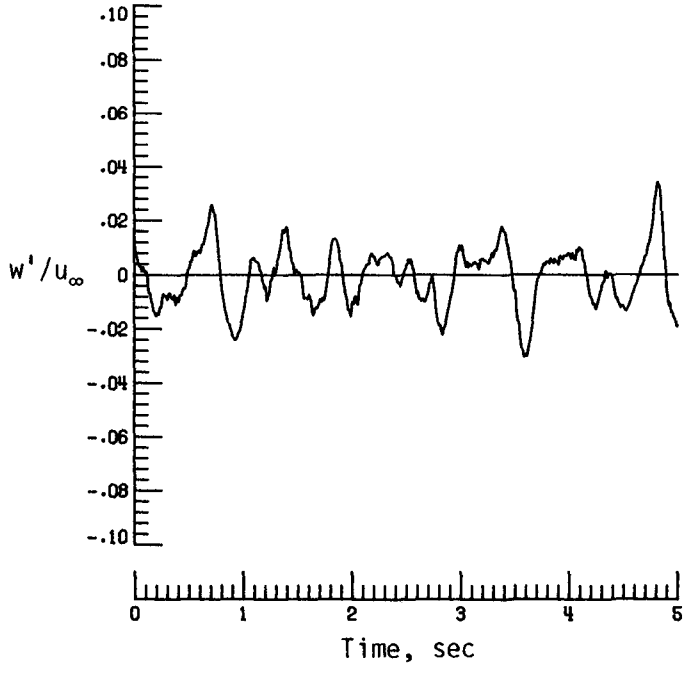

(b) Time history of vertical velocity fluctuations.

Figure B7. Dynamic-flow quality for configuration 6 at $q = 5.99$ lb/ft^2.

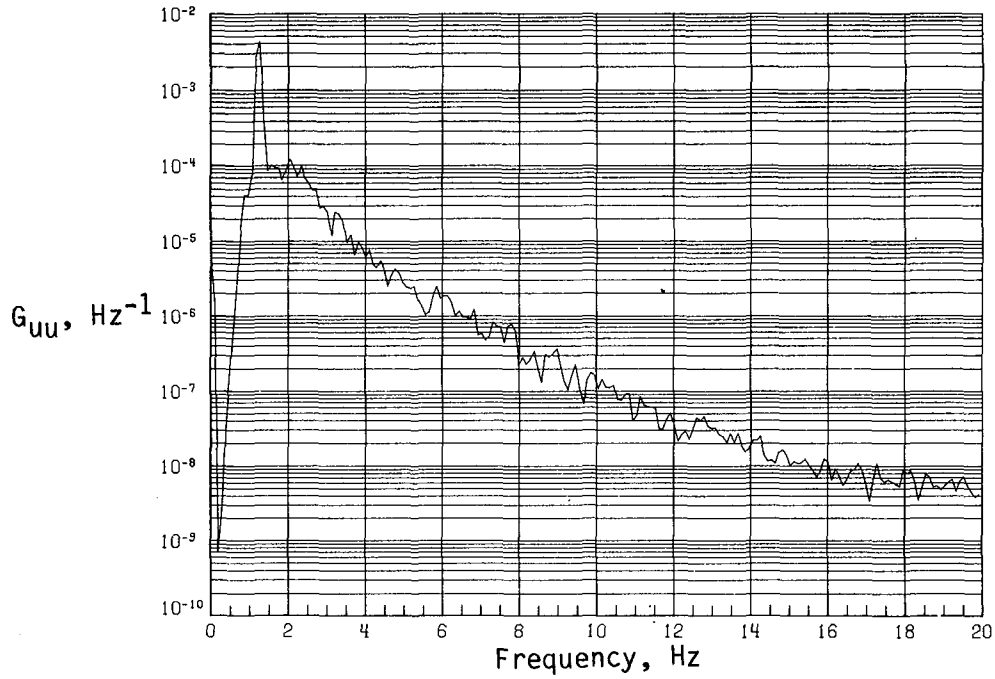

(c) PSD of streamwise velocity fluctuations.

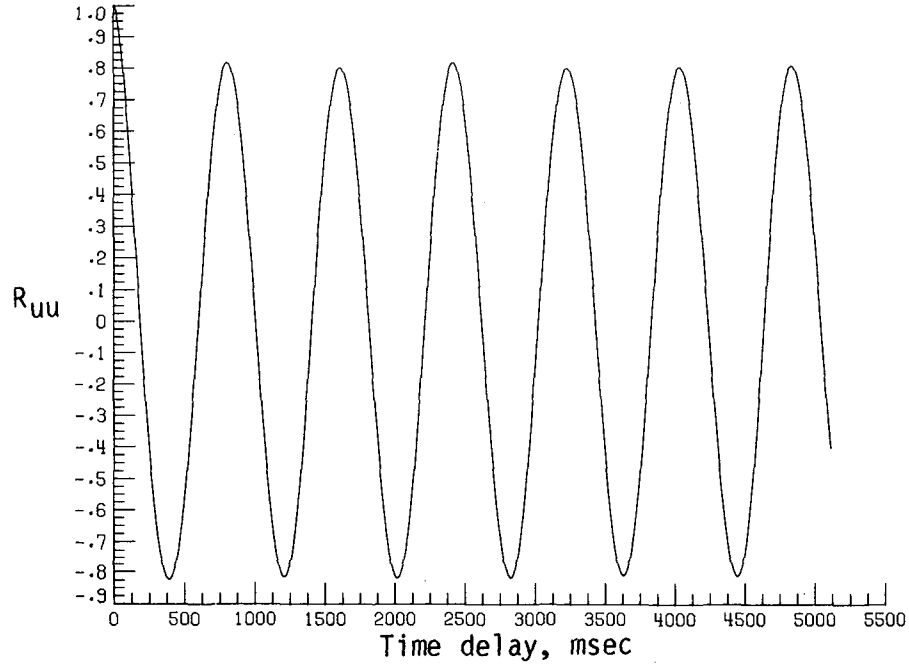

(d) Normalized autocorrelation of streamwise velocity fluctuations. $\sigma = 0.0300$.

Figure B7. Continued.

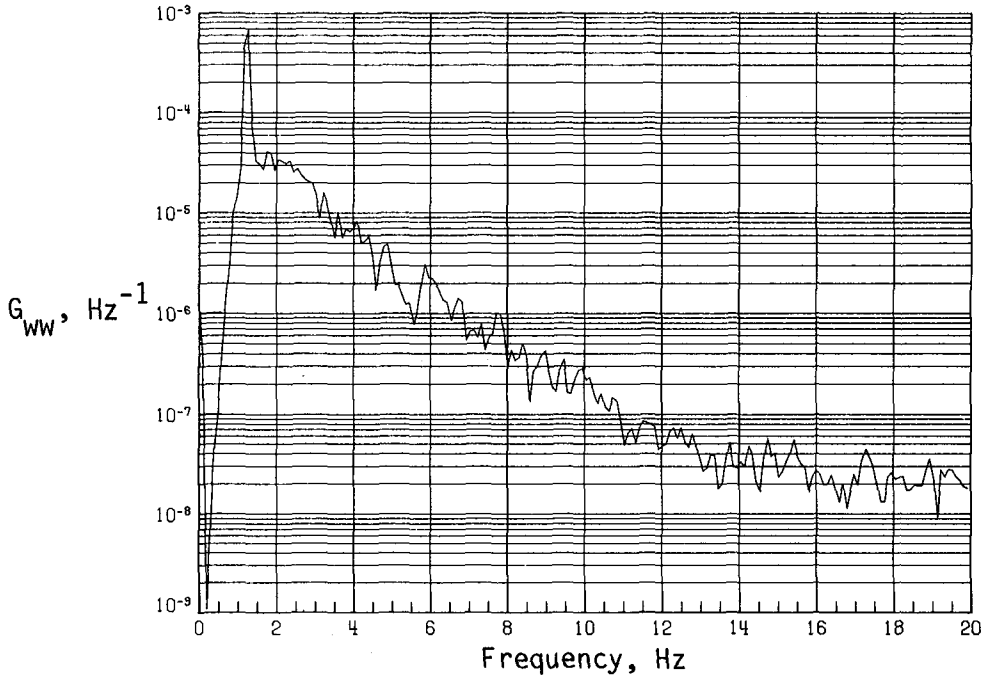

(e) PSD of vertical velocity fluctuations.

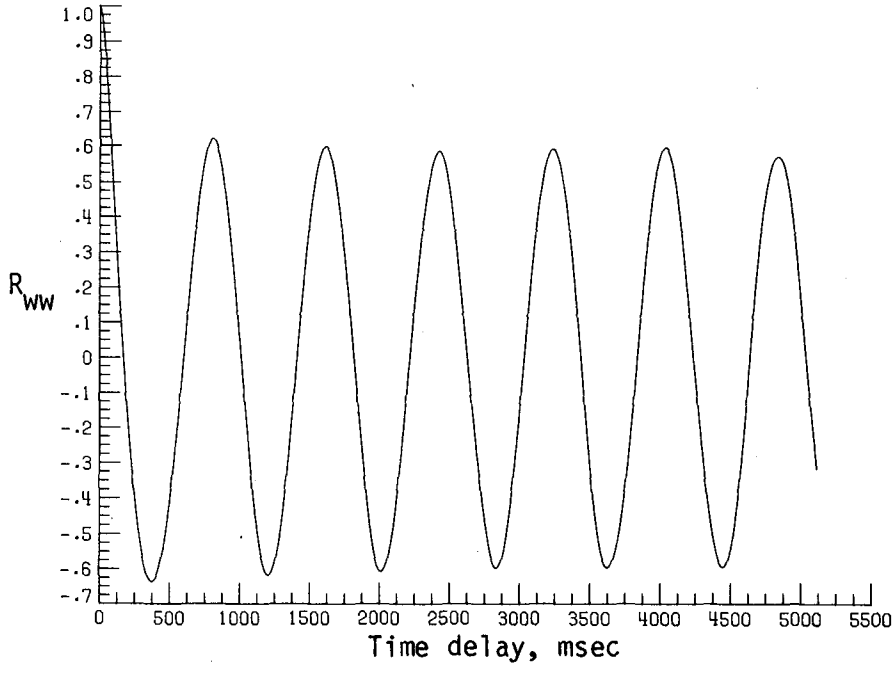

(f) Normalized autocorrelation of vertical velocity fluctuations. $\sigma = 0.0139$.

Figure B7. Concluded.

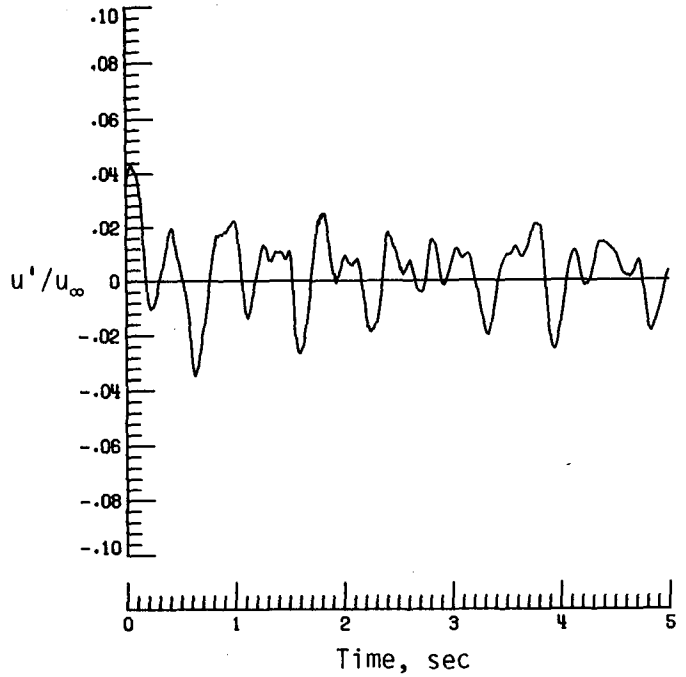

(a) Time history of streamwise velocity fluctuations.

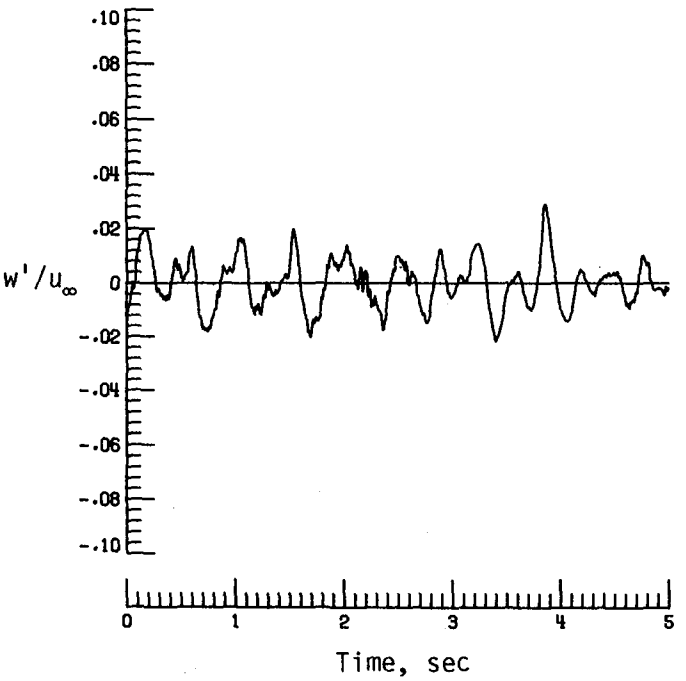

(b) Time history of vertical velocity fluctuations.

Figure B8. Dynamic-flow quality for configuration 6 at $q = 6.56$ lb/ft^2.

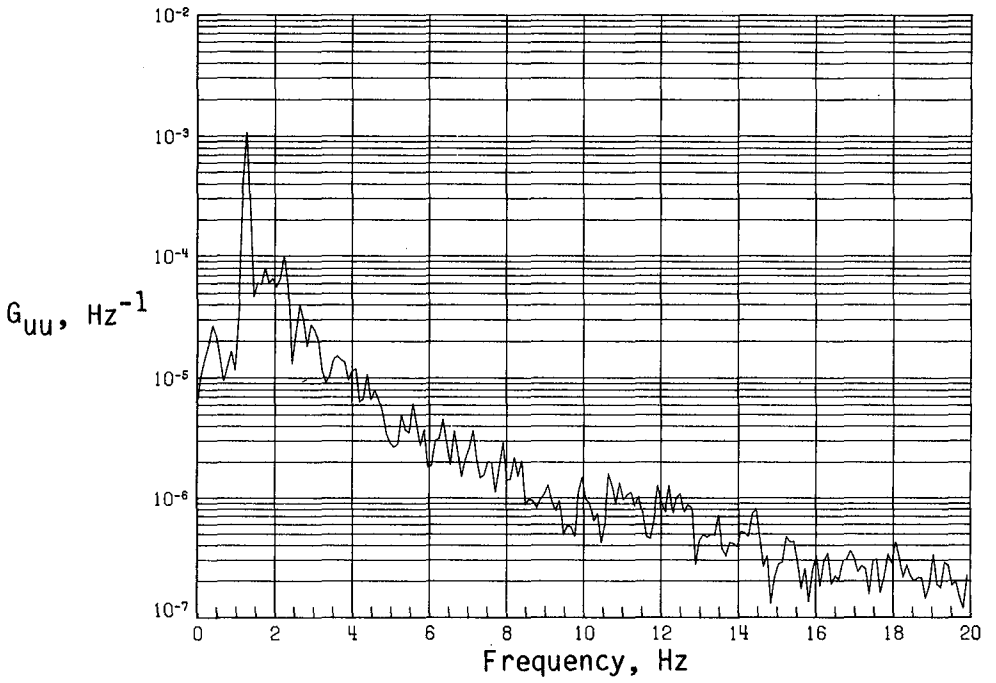

(c) PSD of streamwise velocity fluctuations.

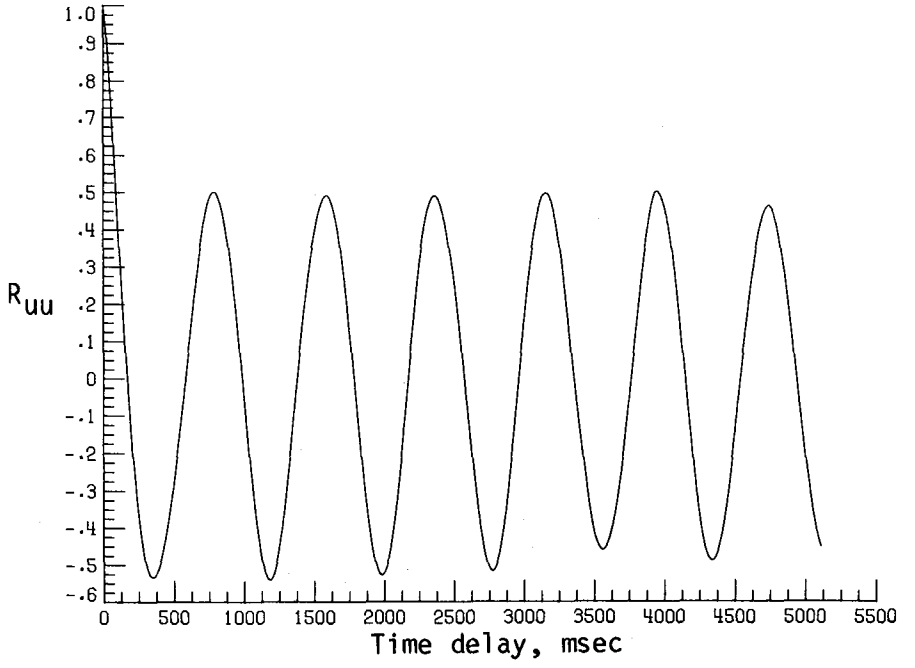

(d) Normalized autocorrelation of streamwise velocity fluctuations. $\sigma = 0.0176$.

Figure B8. Continued.

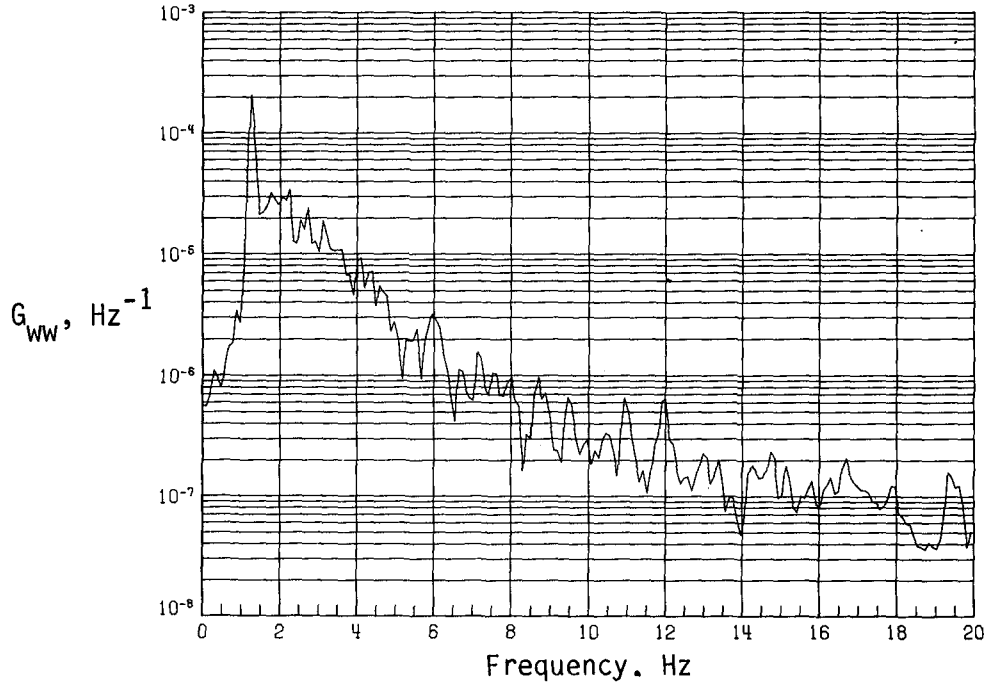

(e) PSD of vertical velocity fluctuations.

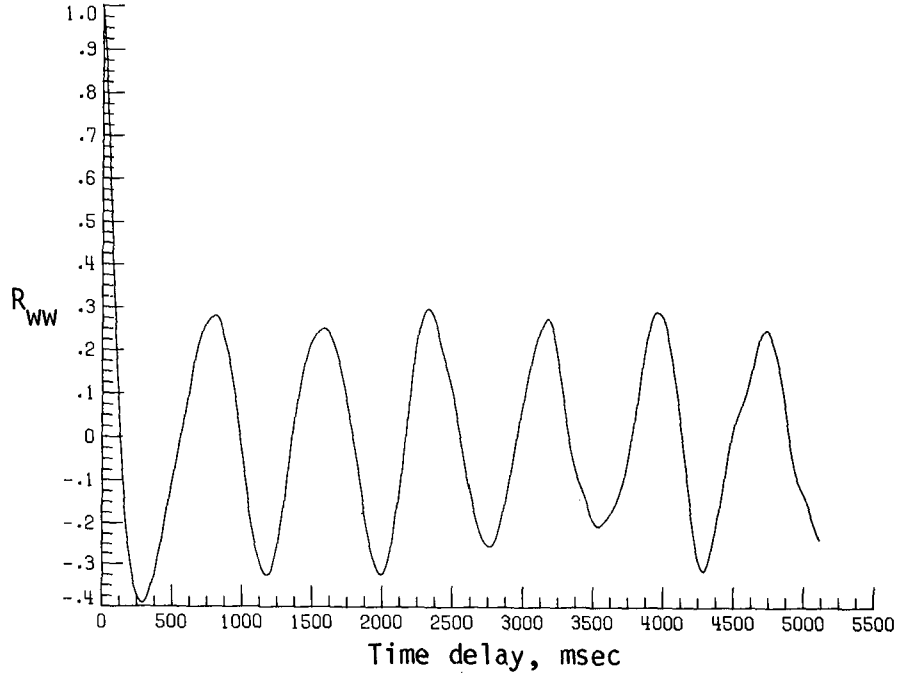

(f) Normalized autocorrelation of vertical velocity fluctuations. $\sigma = 0.0097$.

Figure B8. Concluded.

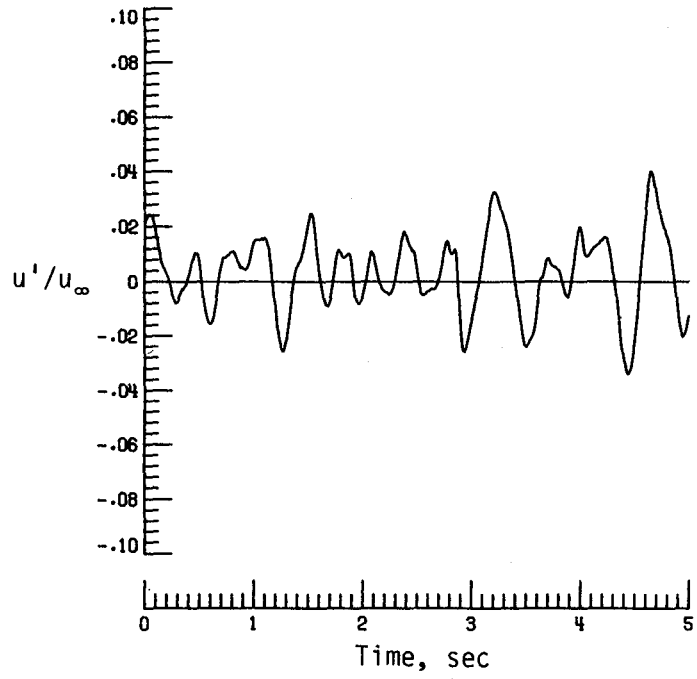

(a) Time history of streamwise velocity fluctuations.

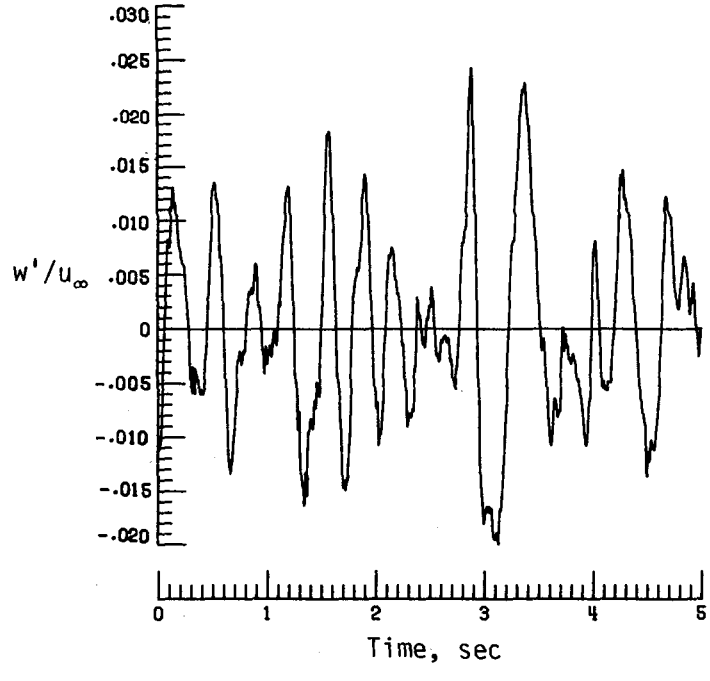

(b) Time history of vertical velocity fluctuations.

Figure B9. Dynamic-flow quality for configuration 6 at $q = 7.12$ lb/ft^2.

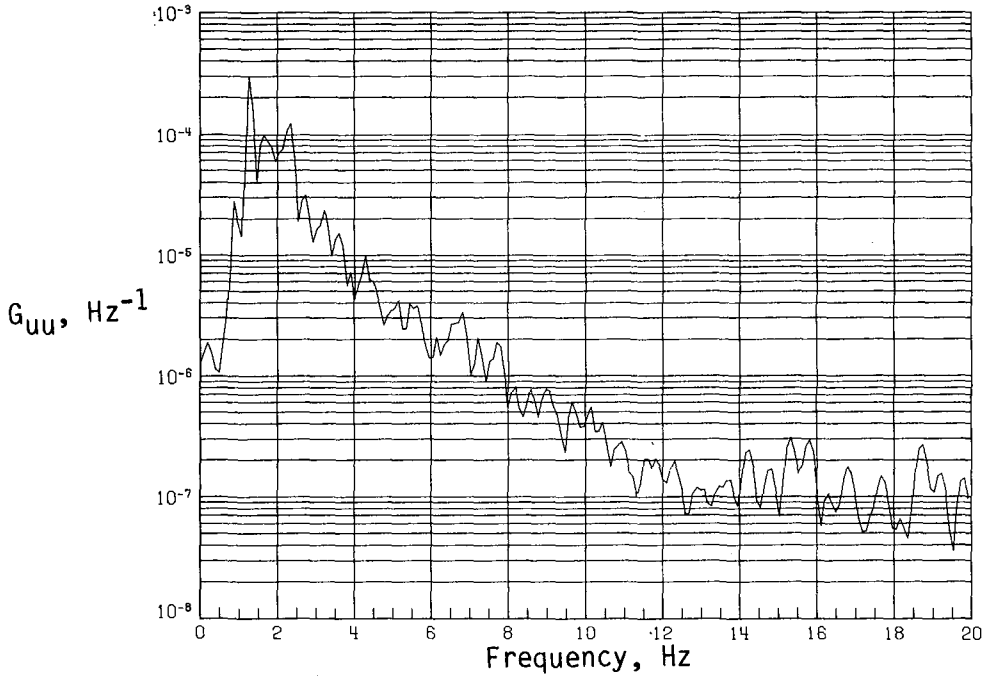

(c) PSD of streamwise velocity fluctuations.

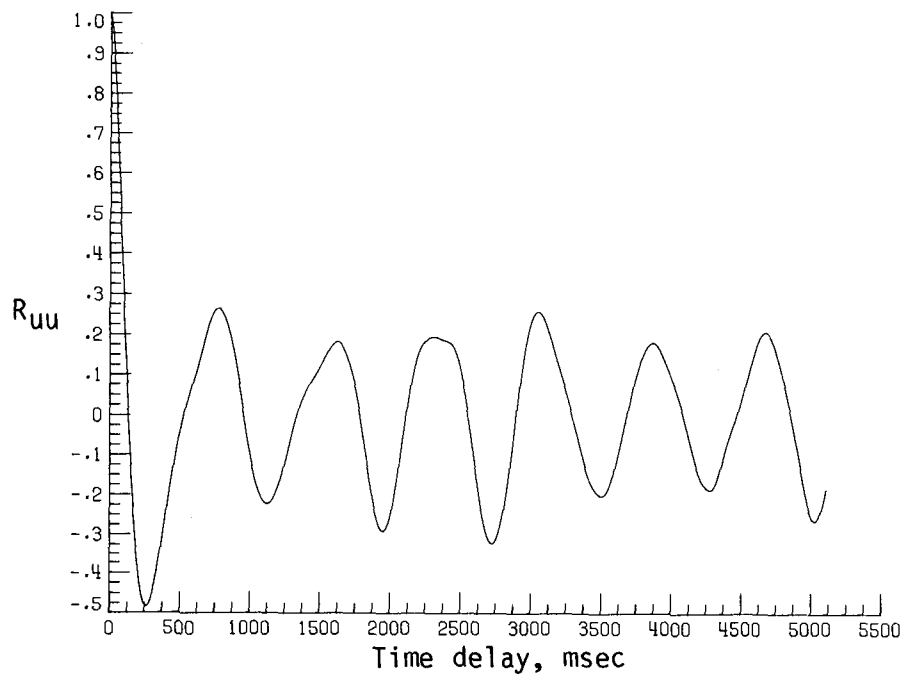

(d) Normalized autocorrelation of streamwise velocity fluctuations. $\sigma = 0.0135$.

Figure B9. Continued.

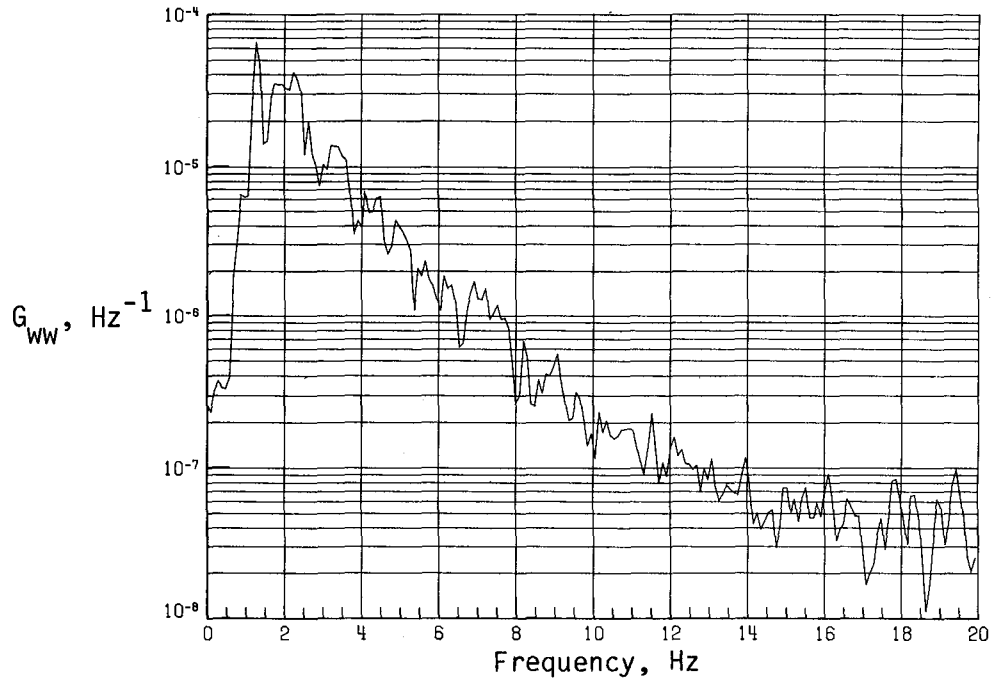

(e) PSD of vertical velocity fluctuations.

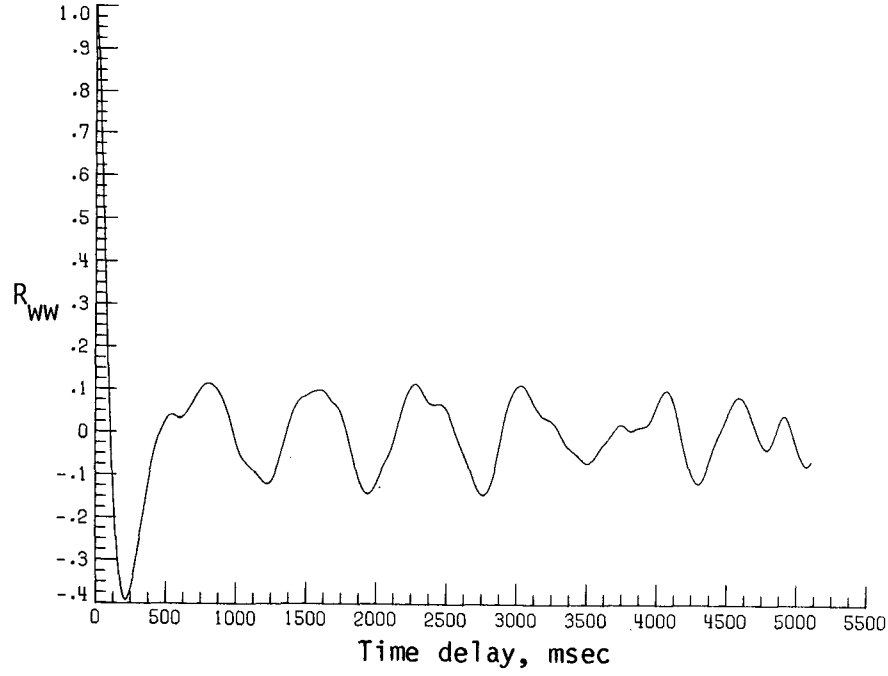

(f) Normalized autocorrelation of vertical velocity fluctuations. $\sigma = 0.0084$.

Figure B9. Concluded.

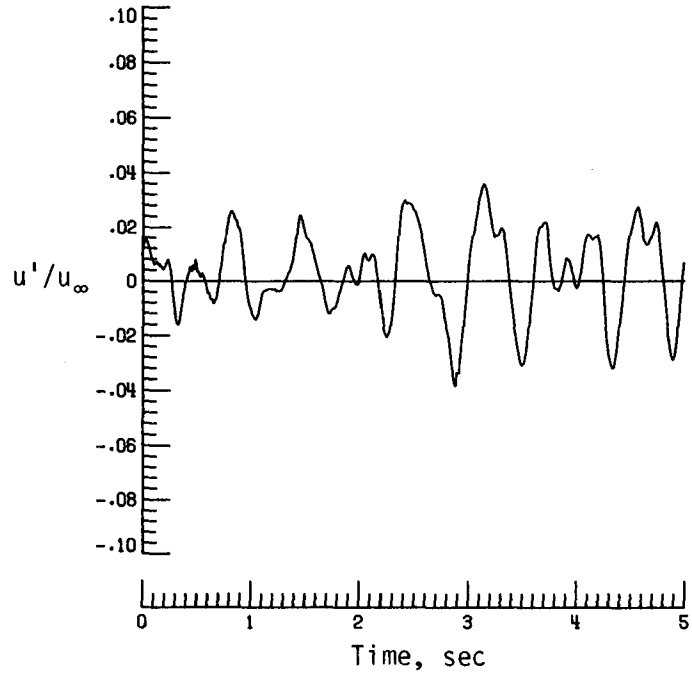

(a) Time history of streamwise velocity fluctuations.

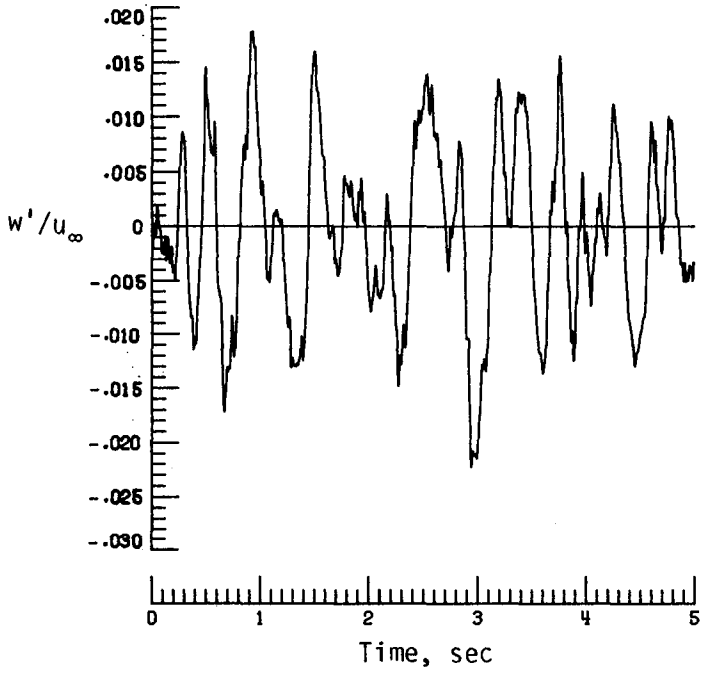

(b) Time history of vertical velocity fluctuations.

Figure B10. Dynamic-flow quality for configuration 6 at $q = 8.03$ lb/ft^2.

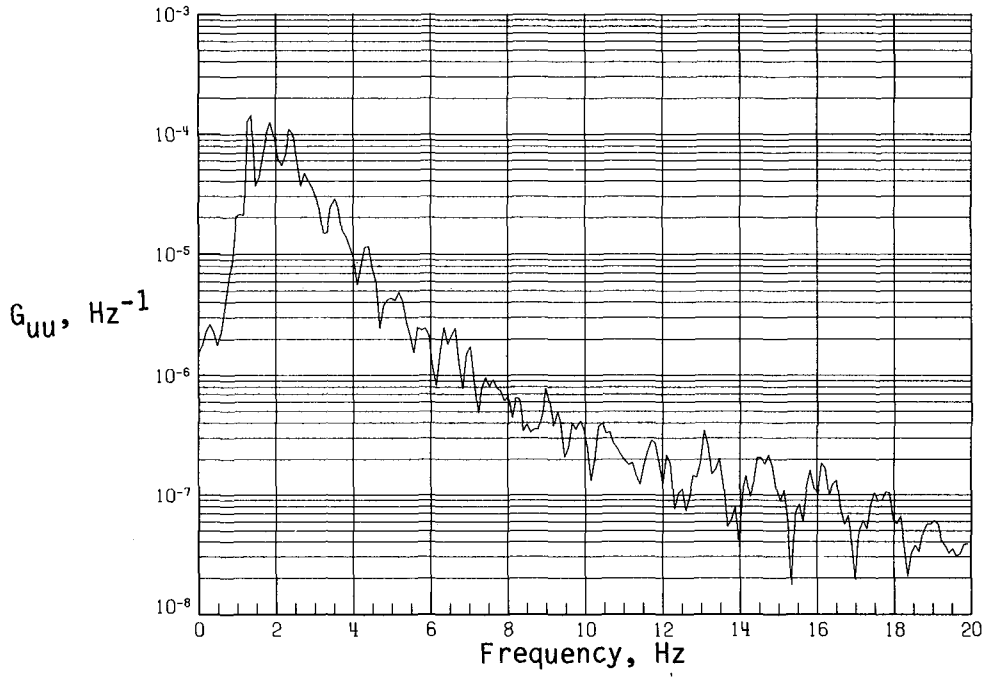

(c) PSD of streamwise velocity fluctuations.

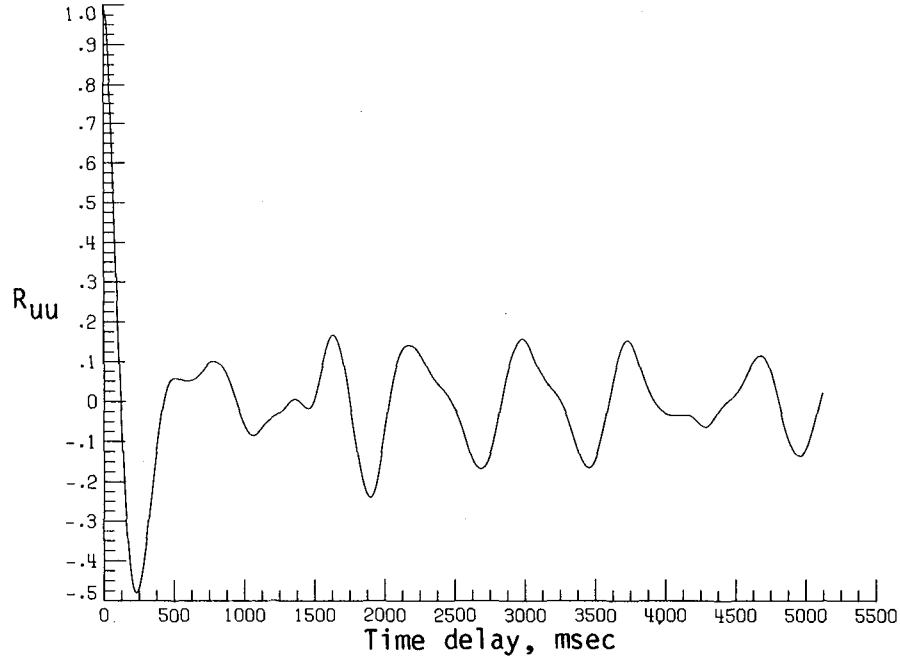

(d) Normalized autocorrelation of streamwise velocity fluctuations. $\sigma = 0.0132$.

Figure B10. Continued.

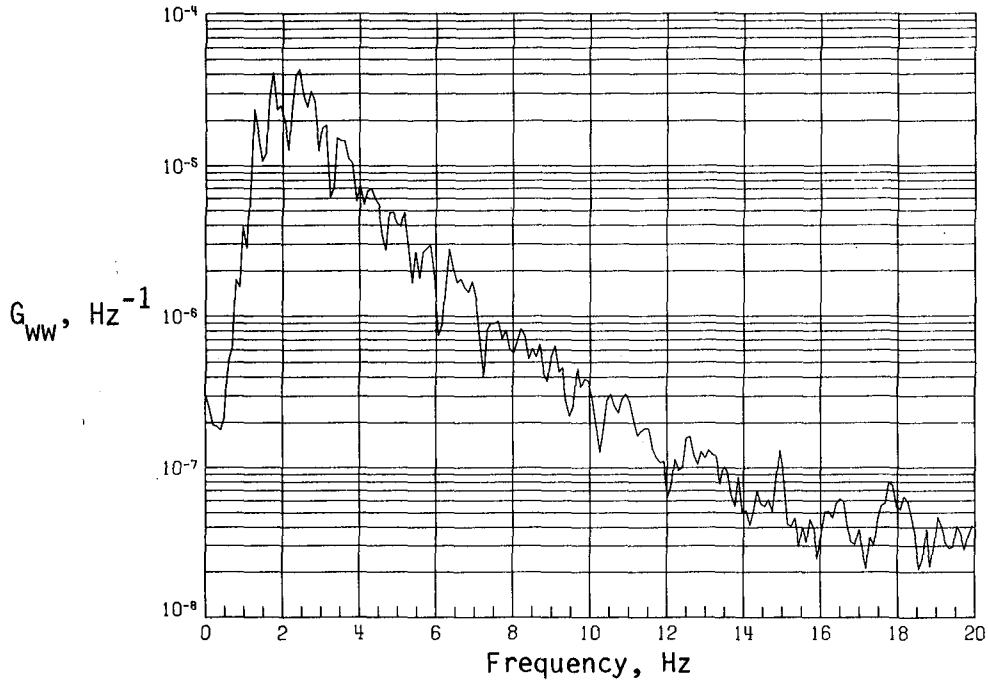

(e) PSD of vertical velocity fluctuations.

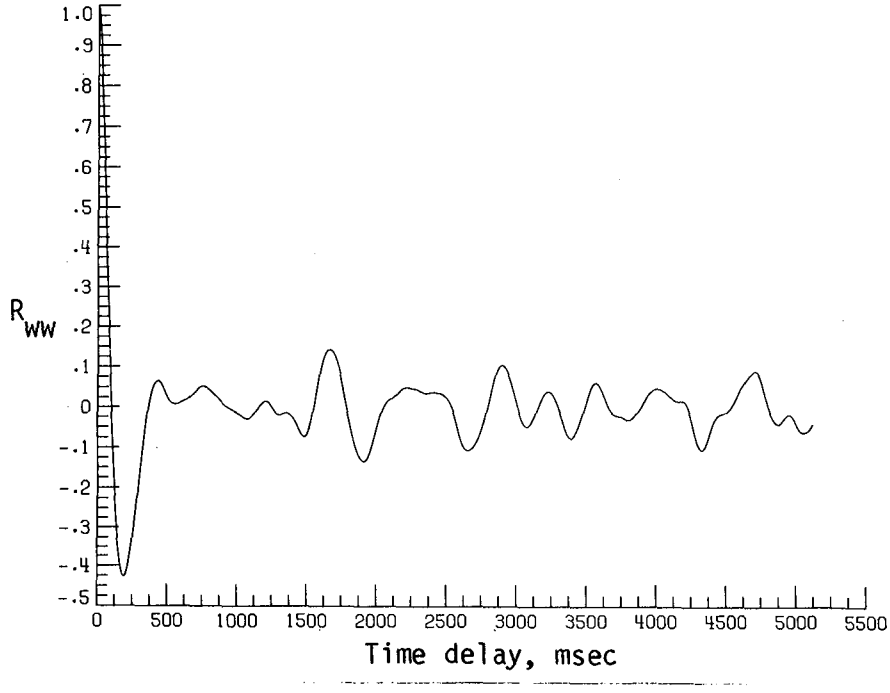

(f) Normalized autocorrelation of vertical velocity fluctuations. $\sigma = 0.0086$.

Figure B10. Concluded.

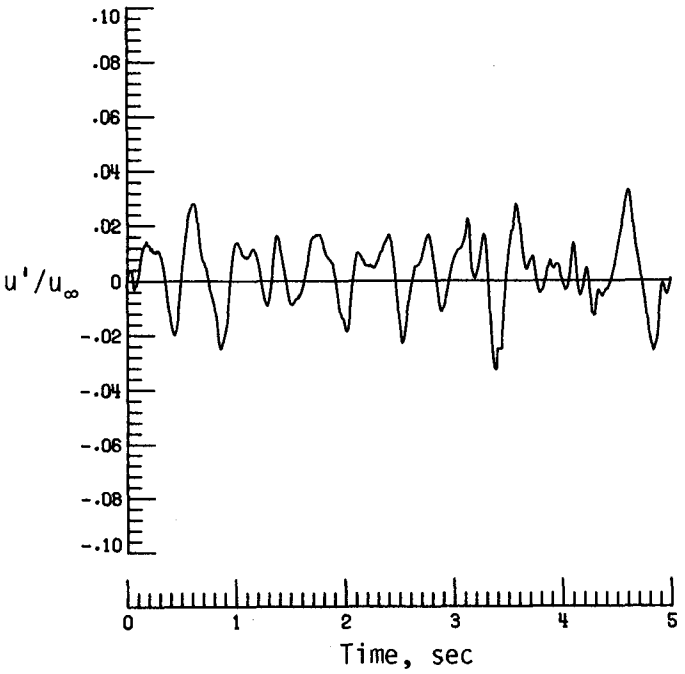

(a) Time history of streamwise velocity fluctuations.

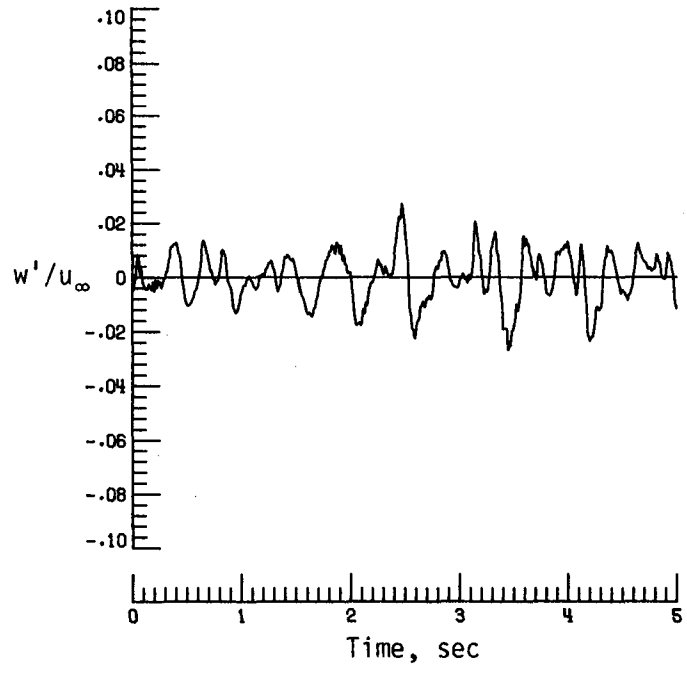

(b) Time history of vertical velocity fluctuations.

Figure B11. Dynamic-flow quality for configuration 6 at $q = 9.05$ lb/ft^2.

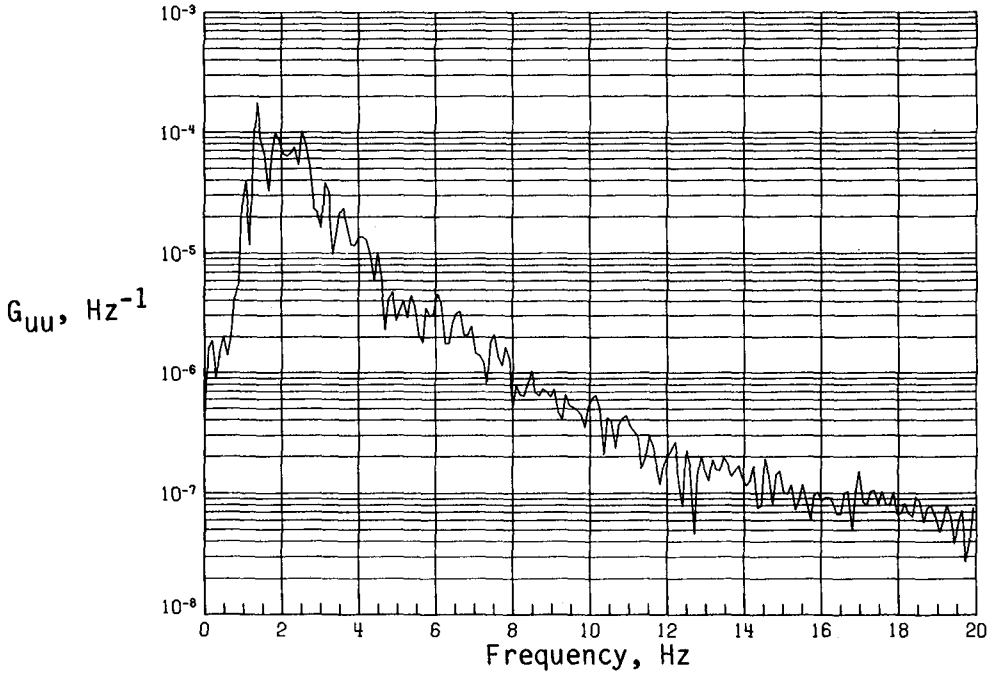

(c) PSD of streamwise velocity fluctuations.

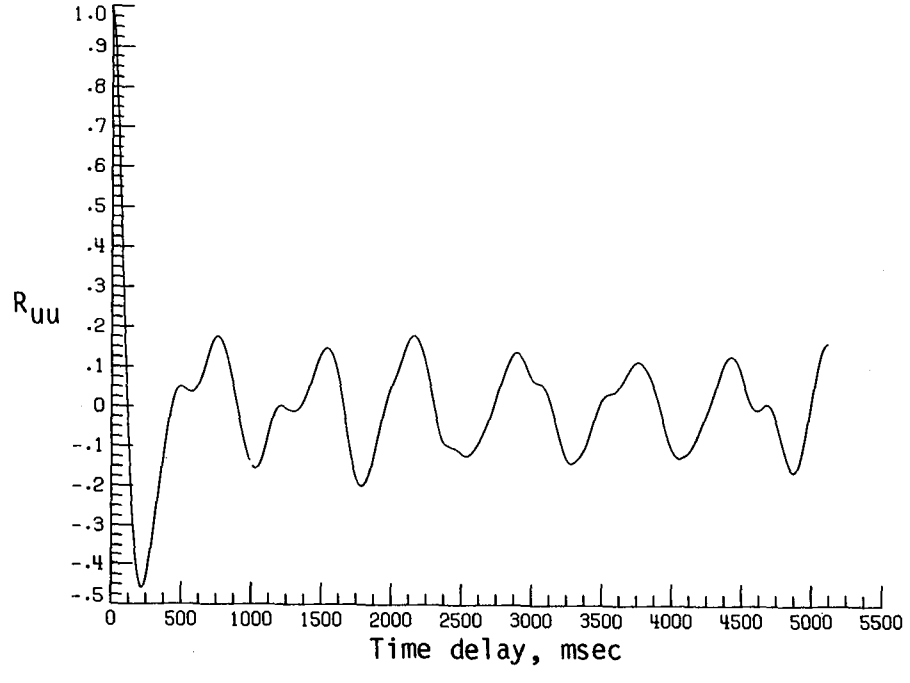

(d) Normalized autocorrelation of streamwise velocity fluctuations. $\sigma = 0.0126$.

Figure B11. Continued.

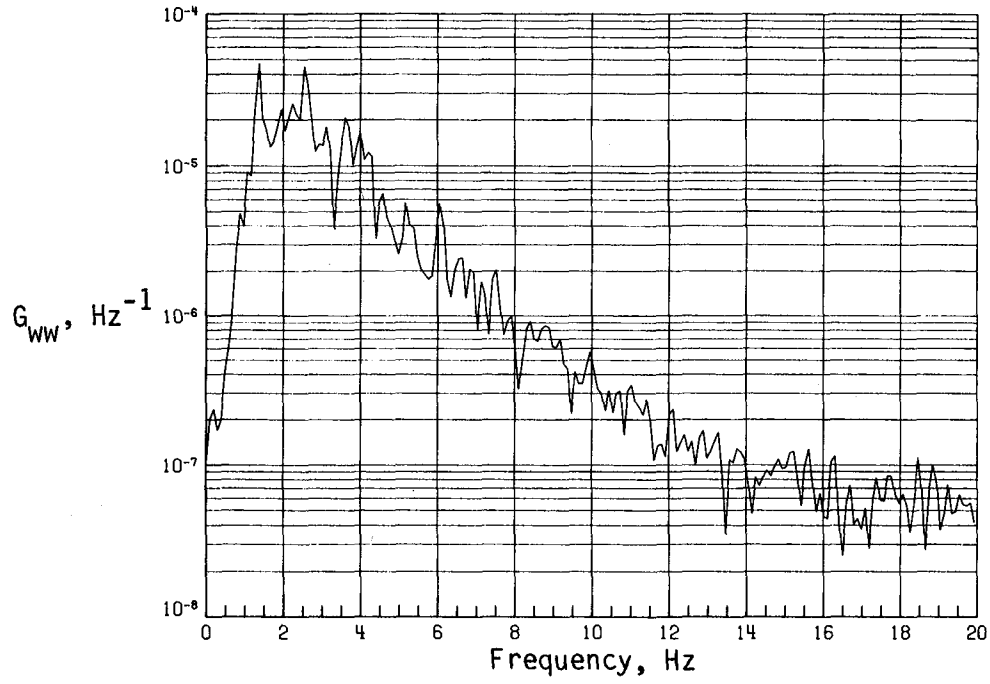

(e) PSD of vertical velocity fluctuations.

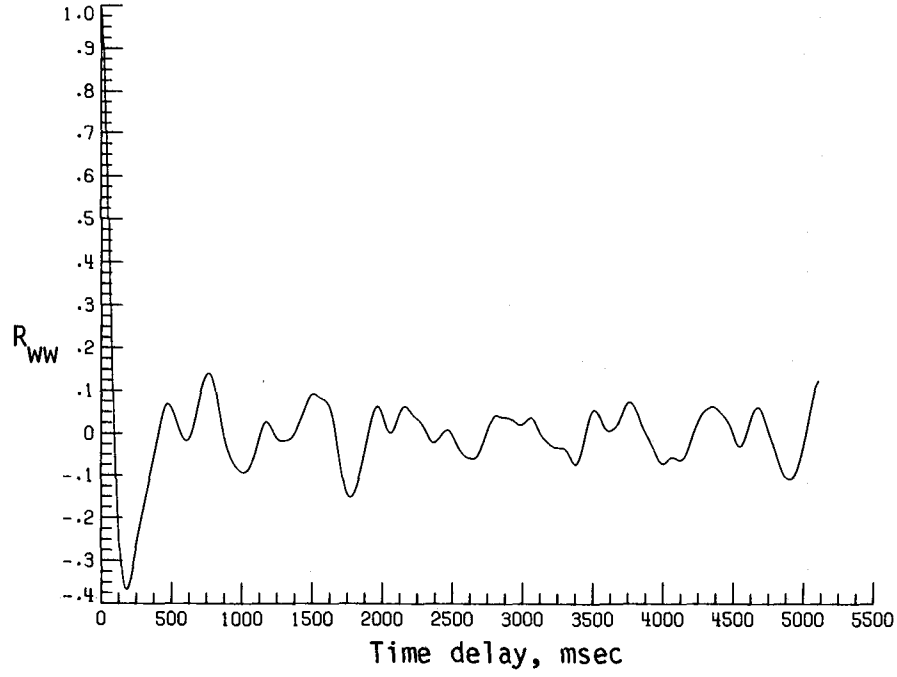

(f) Normalized autocorrelation of vertical velocity fluctuations. $\sigma = 0.0085$.

Figure B11. Concluded.

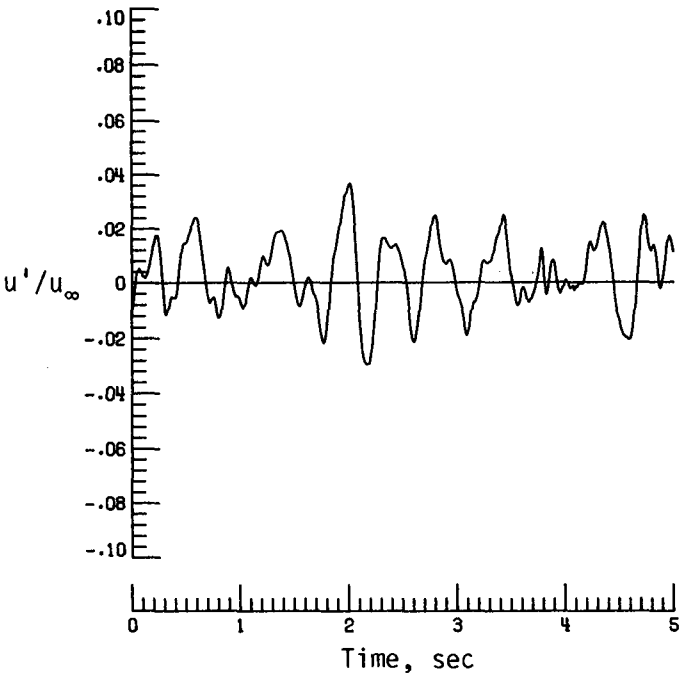

(a) Time history of streamwise velocity fluctuations.

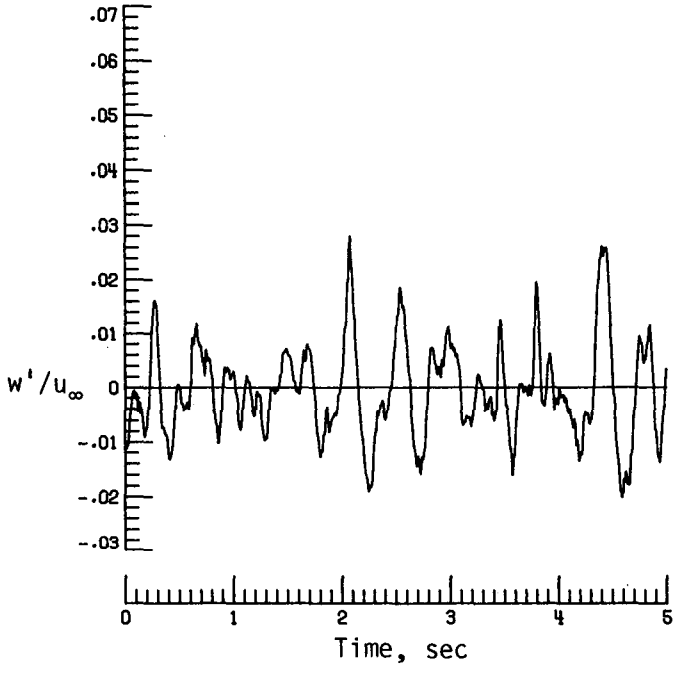

(b) Time history of vertical velocity fluctuations.

Figure B12. Dynamic-flow quality for configuration 6 at $q = 10.06$ lb/ft^2.

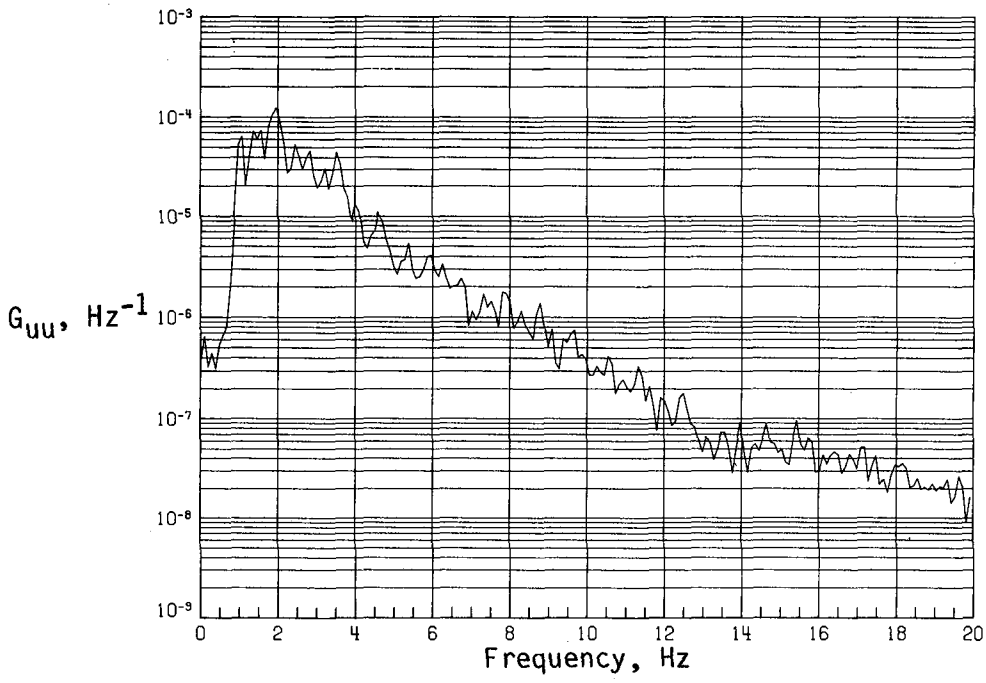

(c) PSD of streamwise velocity fluctuations.

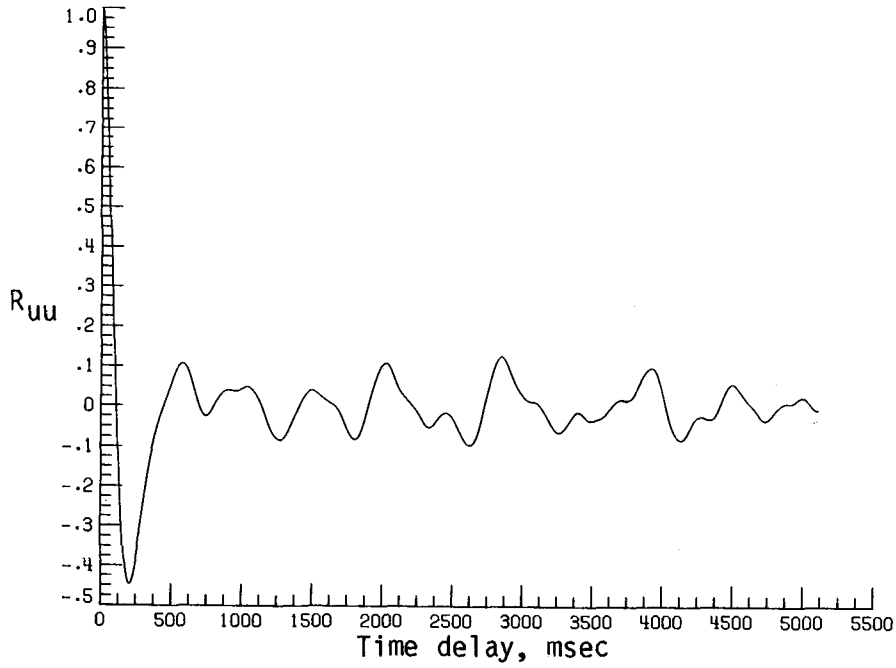

(d) Normalized autocorrelation of streamwise velocity fluctuations. $\sigma = 0.0124$.

Figure B12. Continued.

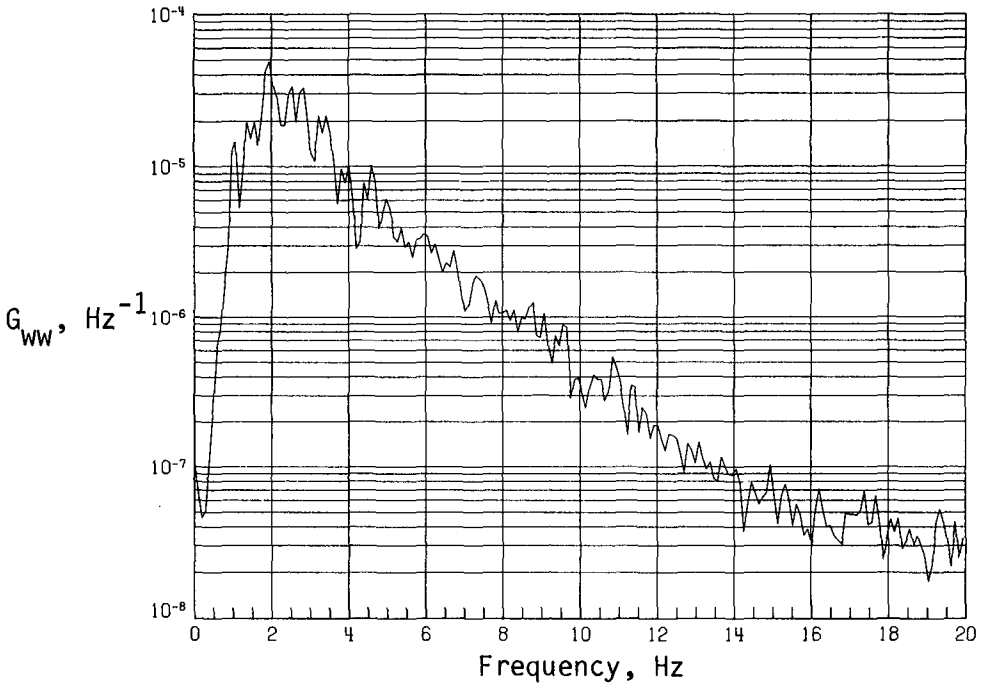

(e) PSD of vertical velocity fluctuations.

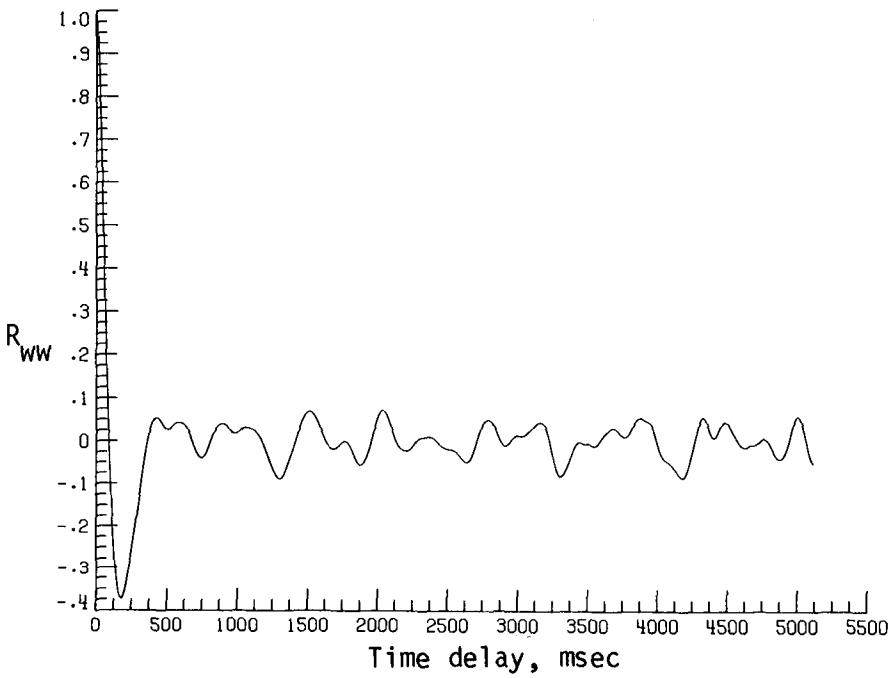

(f) Normalized autocorrelation of vertical velocity fluctuations. $\sigma = 0.0086$.

Figure B12. Concluded.

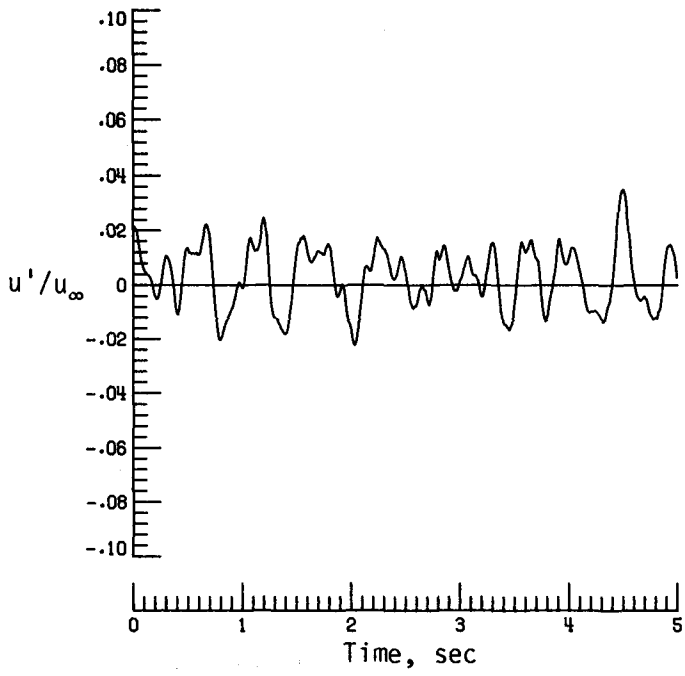

(a) Time history of streamwise velocity fluctuations.

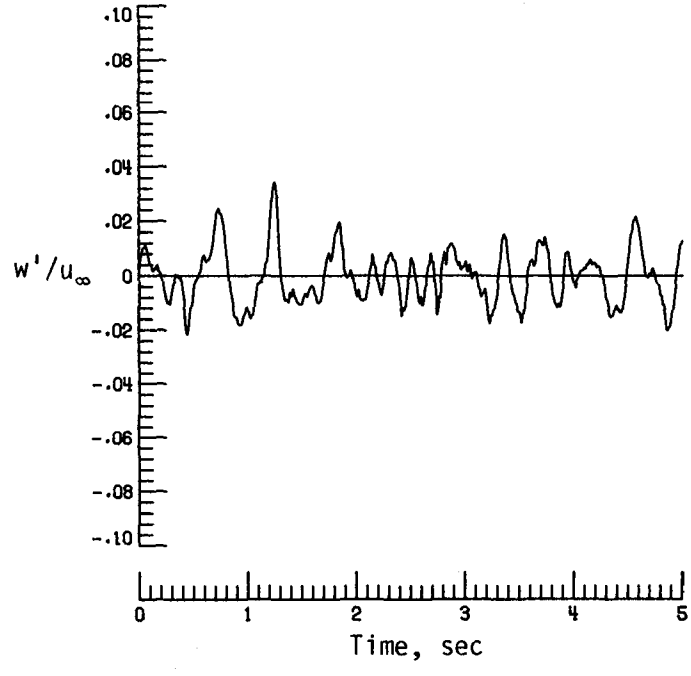

(b) Time history of vertical velocity fluctuations.

Figure B13. Dynamic-flow quality for configuration 6 at $q = 11.19$ lb/ft^2.

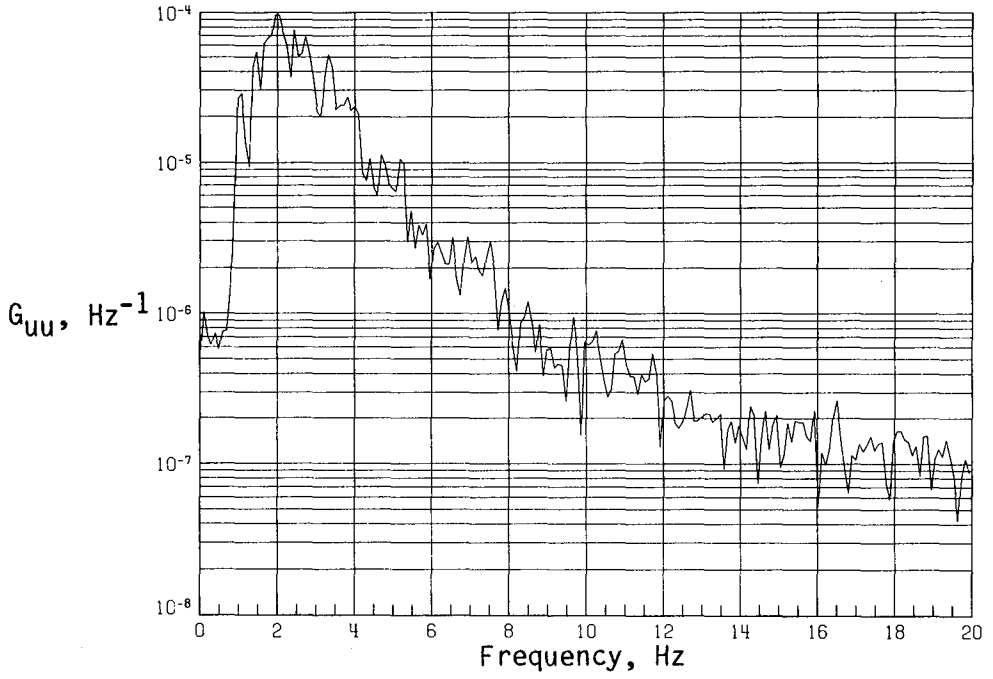

(c) PSD of streamwise velocity fluctuations.

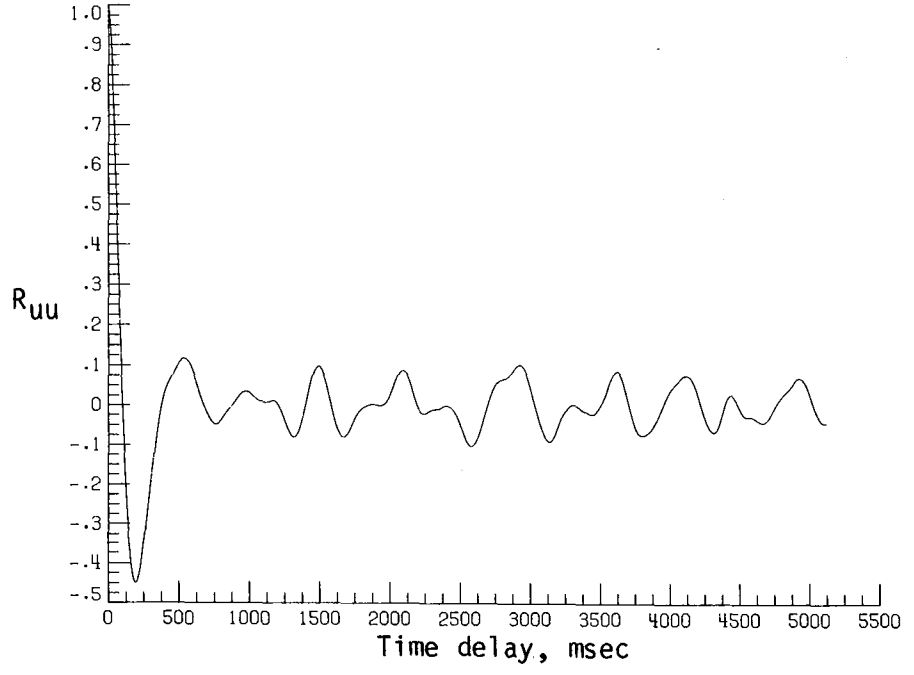

(d) Normalized autocorrelation of streamwise velocity fluctuations. $\sigma = 0.0128$.

Figure B13. Continued.

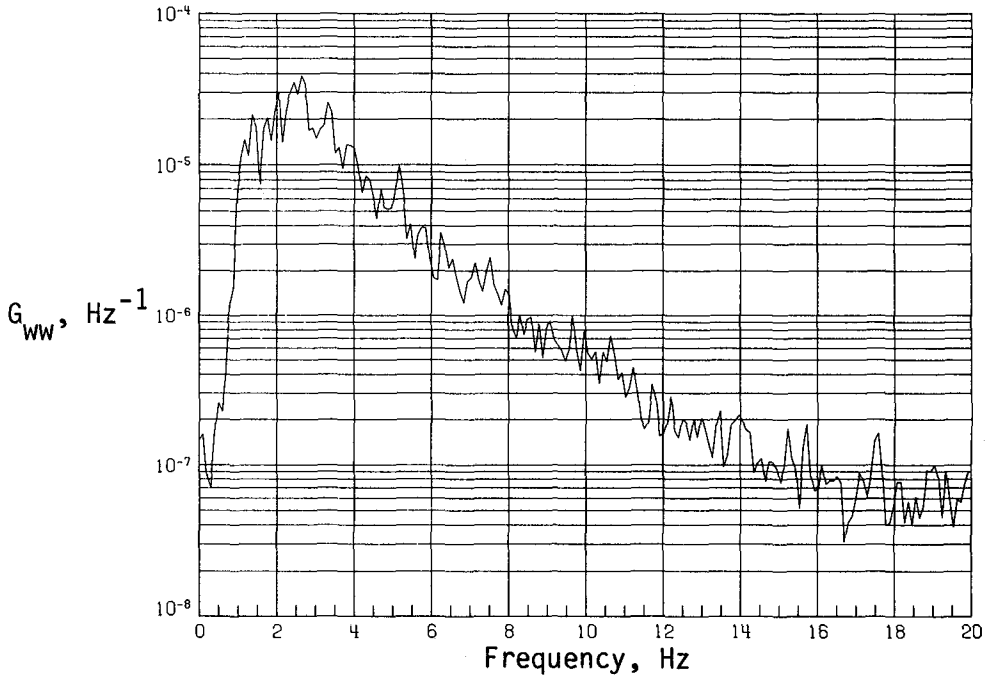

(e) PSD of vertical velocity fluctuations.

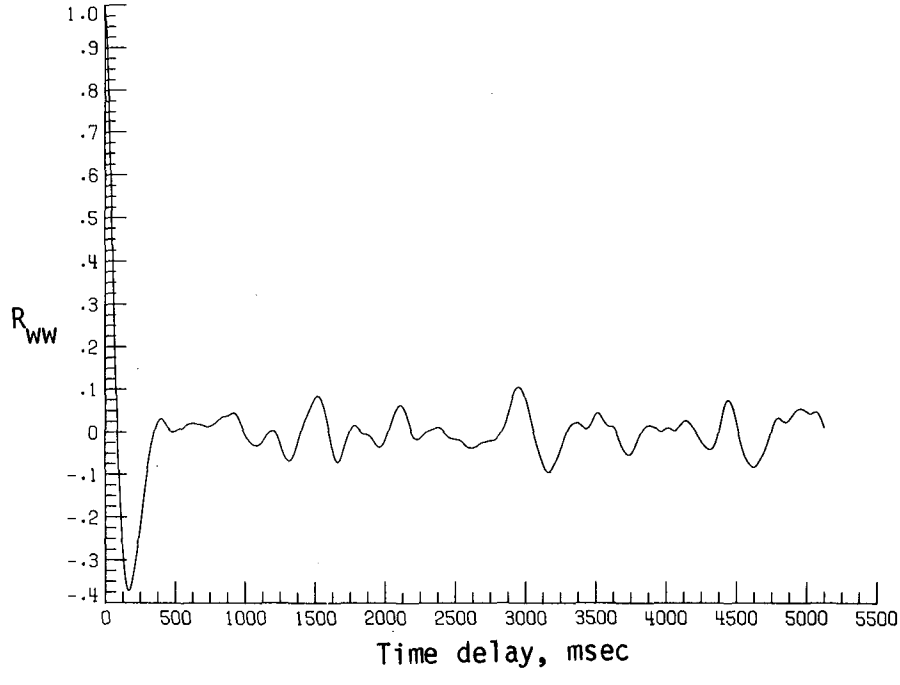

(f) Normalized autocorrelation of vertical velocity fluctuations. $\sigma = 0.0088$.

Figure B13. Concluded.

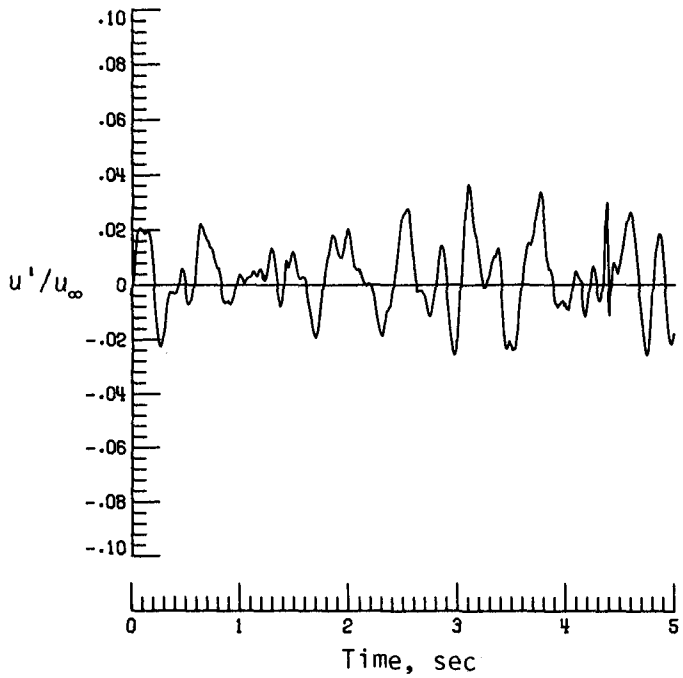

(a) Time history of streamwise velocity fluctuations.

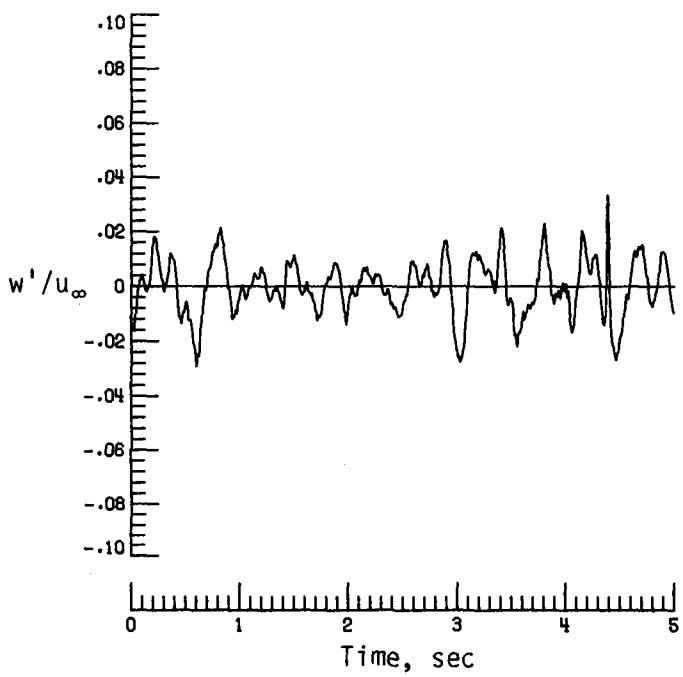

(b) Time history of vertical velocity fluctuations.

Figure B14. Dynamic-flow quality for configuration 6 at $q = 13.11$ lb/ft^2.

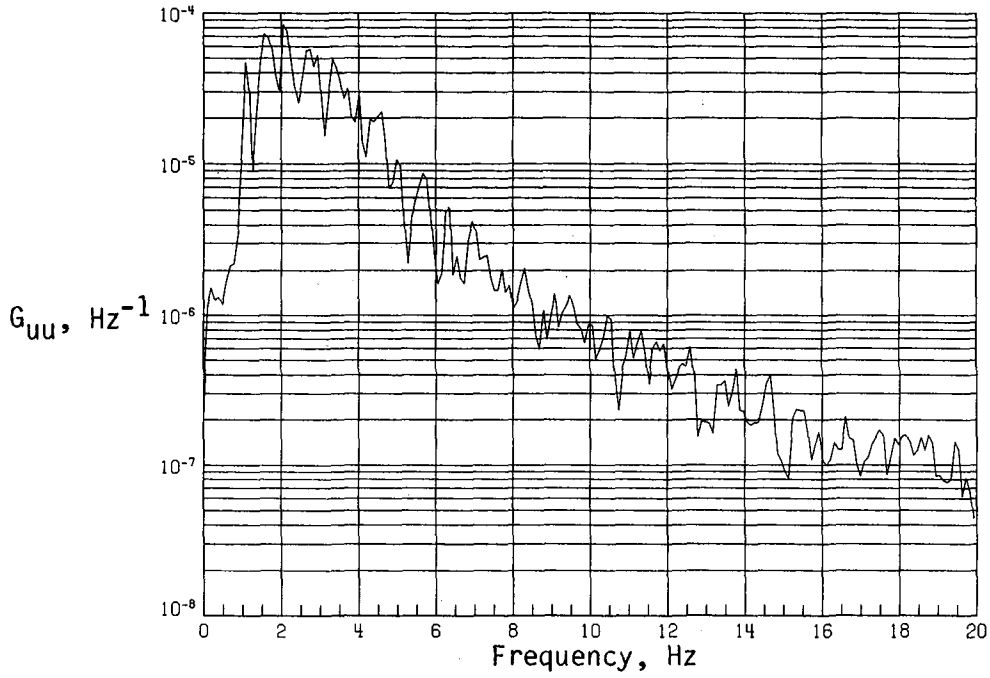

(c) PSD of streamwise velocity fluctuations.

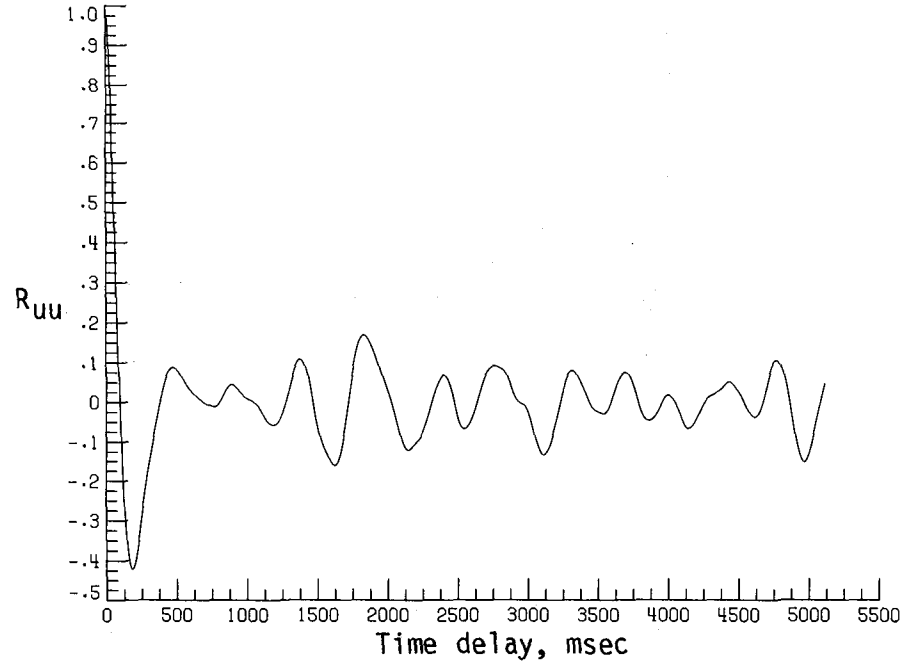

(d) Normalized autocorrelation of streamwise velocity fluctuations. $\sigma = 0.0127$.

Figure B14. Continued.

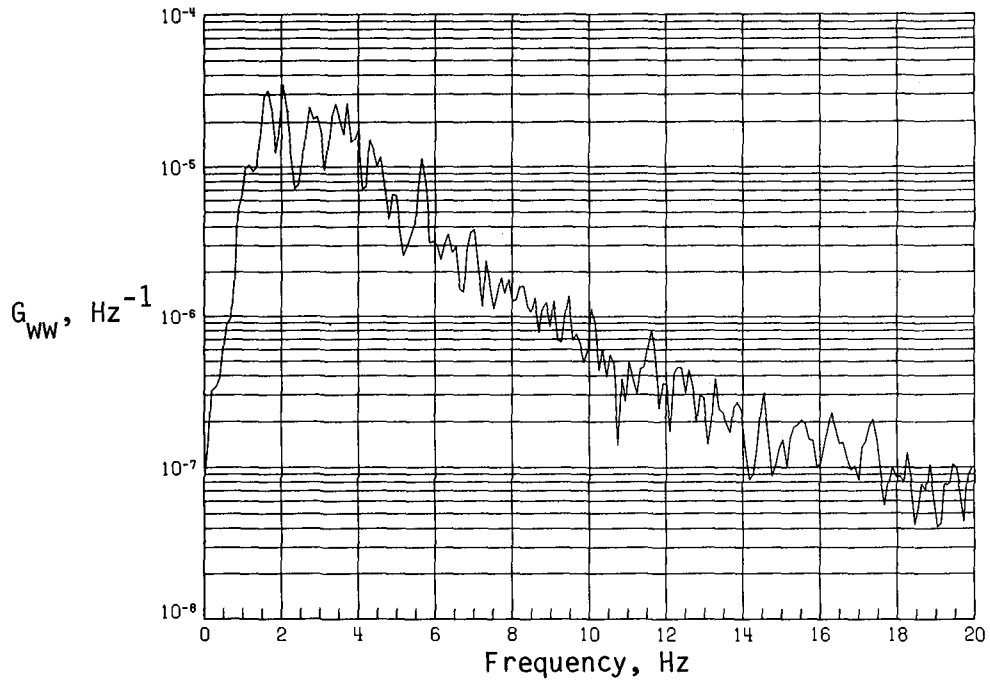

(e) PSD of vertical velocity fluctuations.

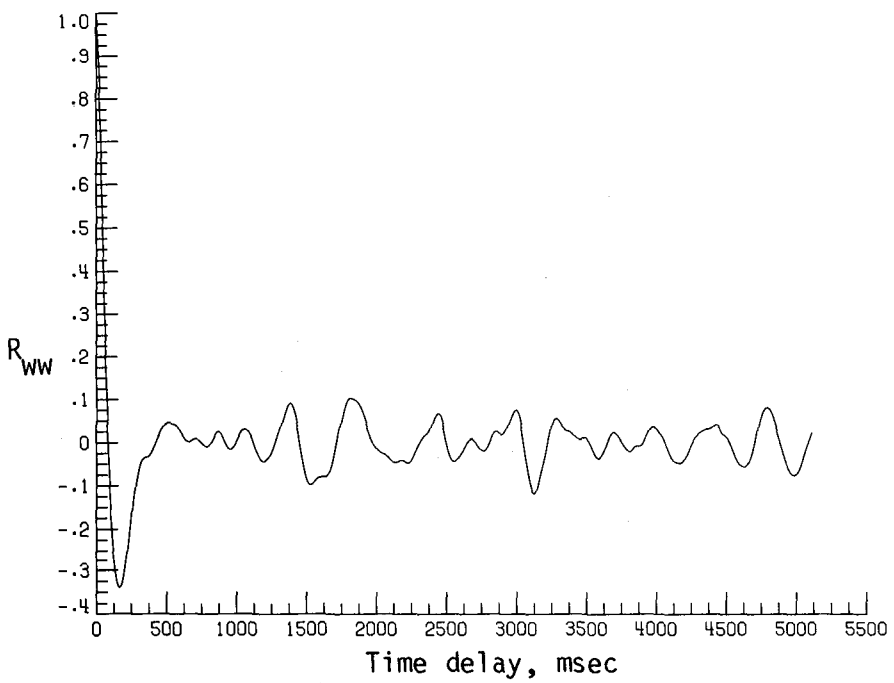

(f) Normalized autocorrelation of vertical velocity fluctuations. $\sigma = 0.0088$.

Figure B14. Concluded.

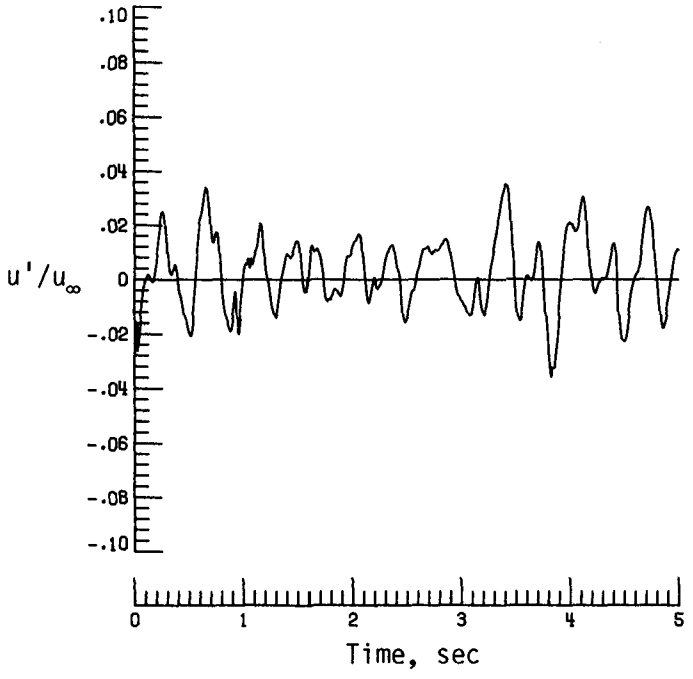

(a) Time history of streamwise velocity fluctuations.

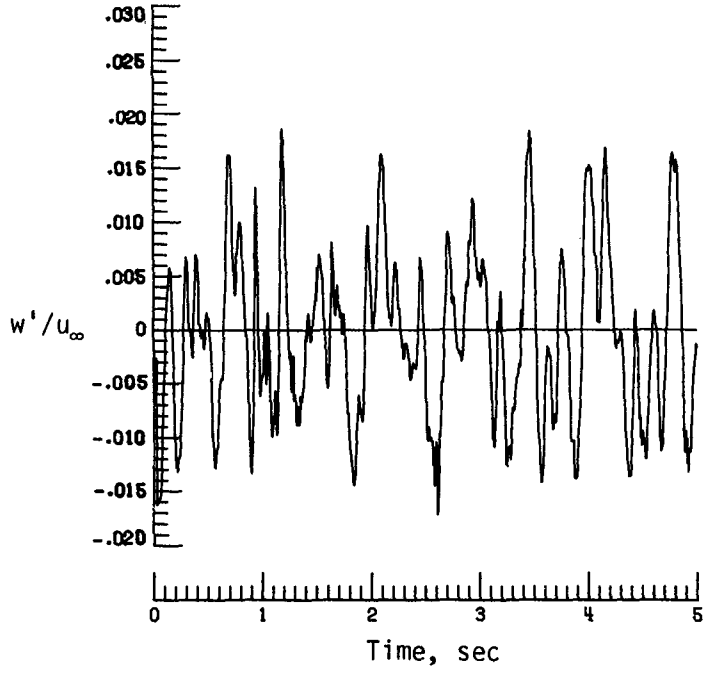

(b) Time history of vertical velocity fluctuations.

Figure B15. Dynamic-flow quality for configuration 6 at $q = 13.90$ lb/ft^2.

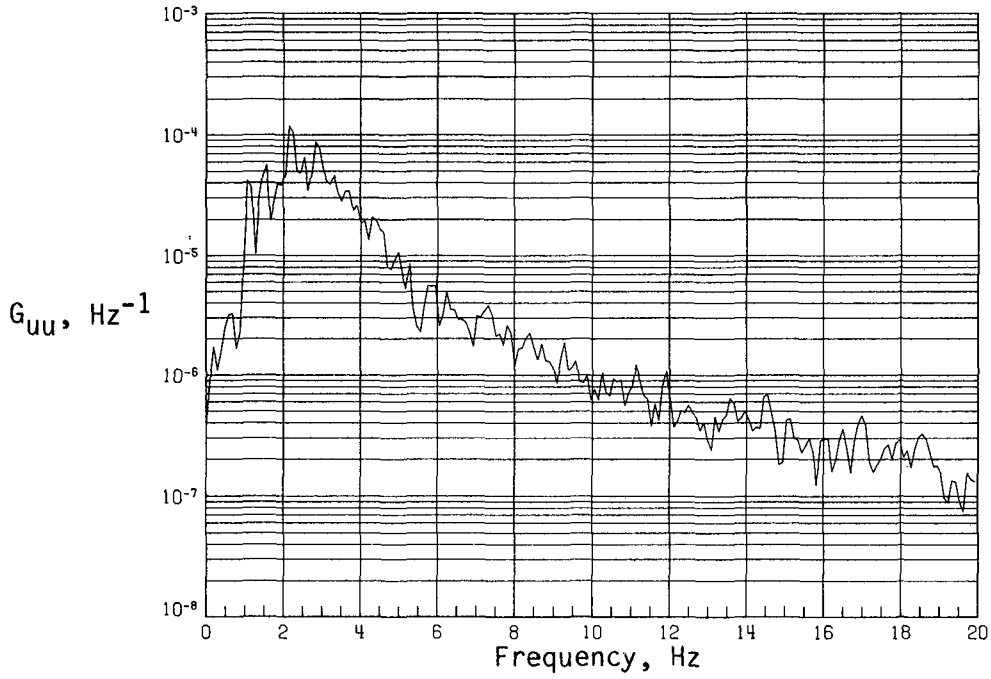

(c) PSD of streamwise velocity fluctuations.

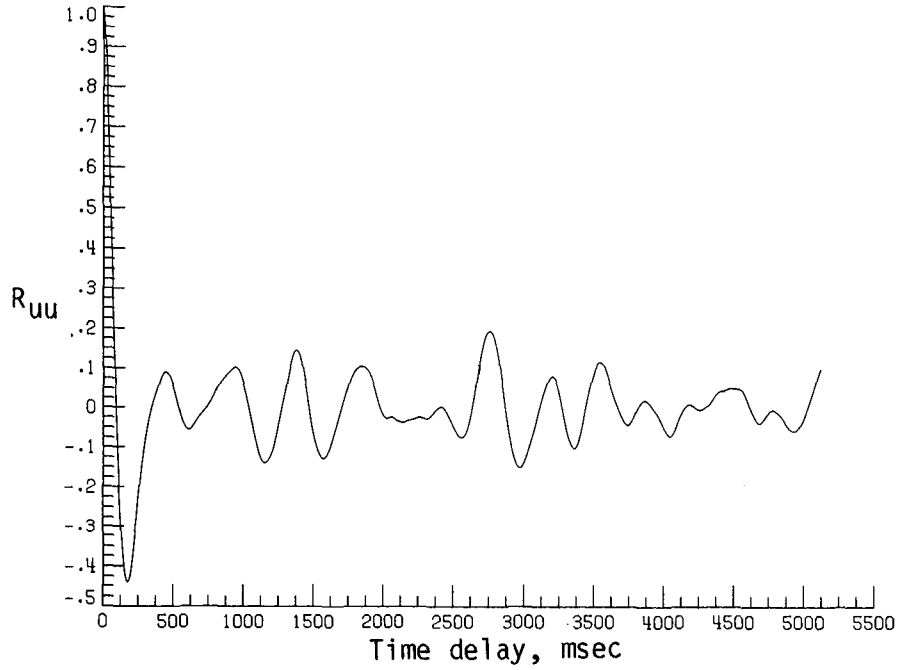

(d) Normalized autocorrelation of streamwise velocity fluctuations. $\sigma = 0.0130$.

Figure B15. Continued.

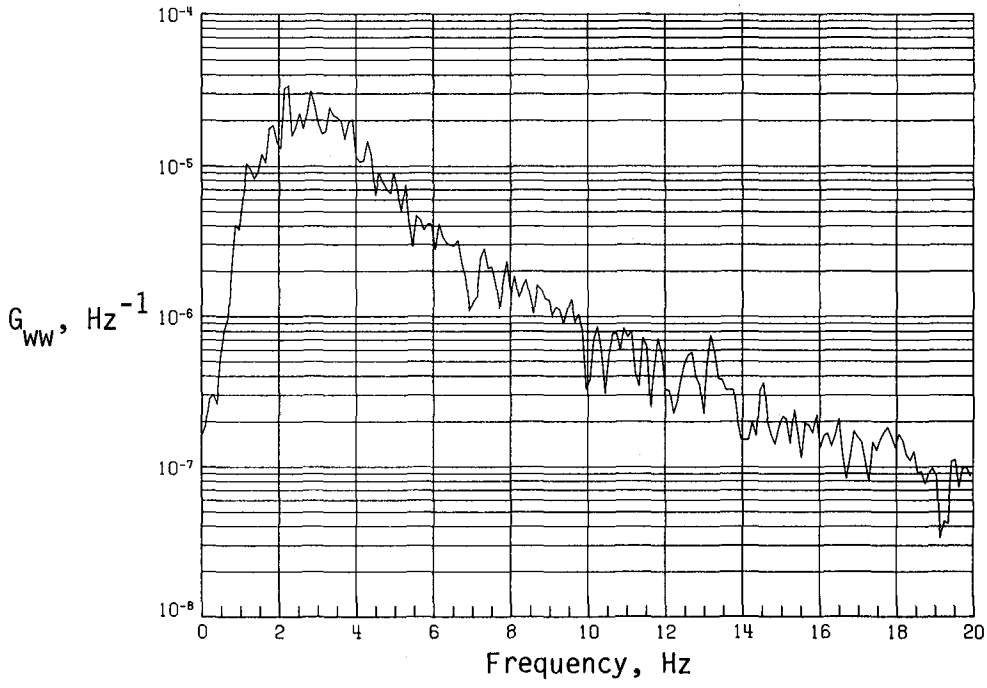

(e) PSD of vertical velocity fluctuations.

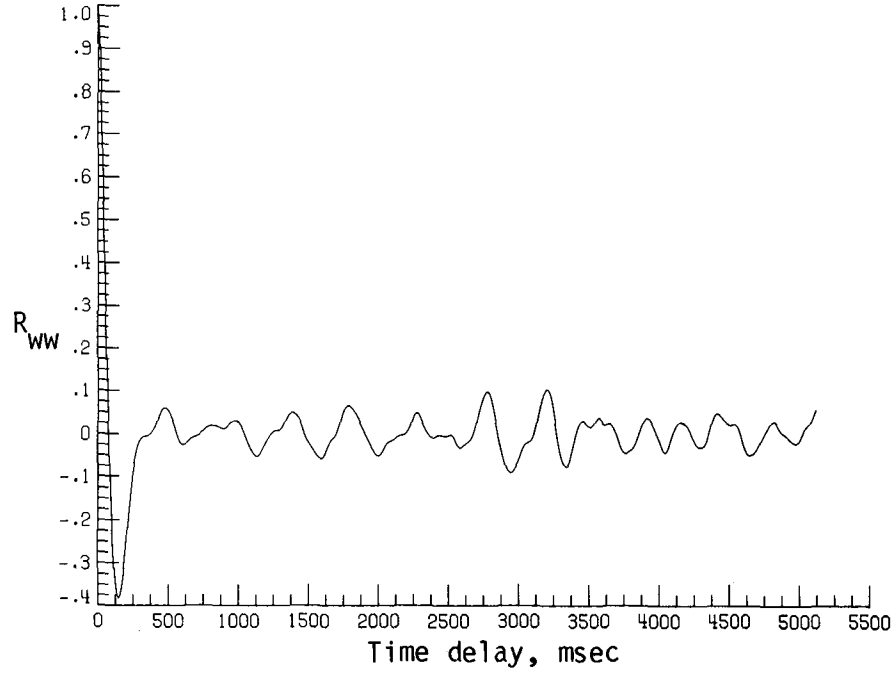

(f) Normalized autocorrelation of vertical velocity fluctuations. $\sigma = 0.0090$.

Figure B15. Concluded.

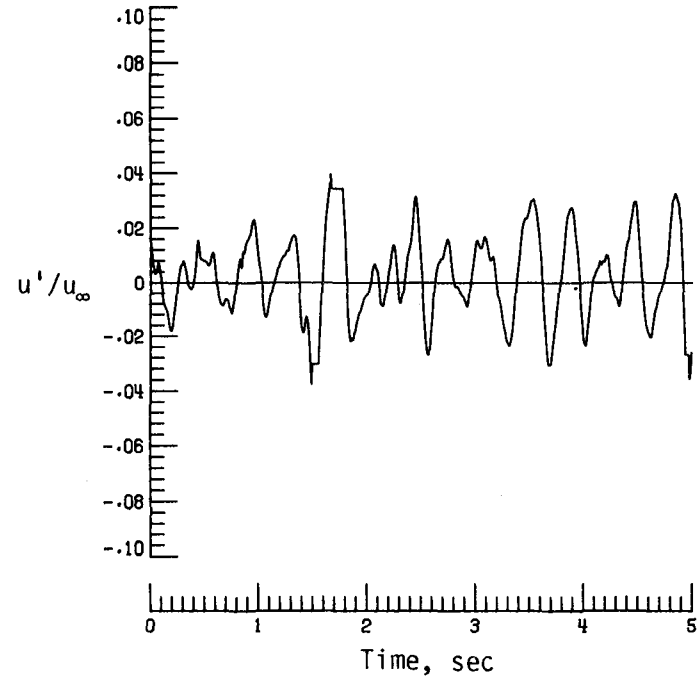

(a) Time history of streamwise velocity fluctuations.

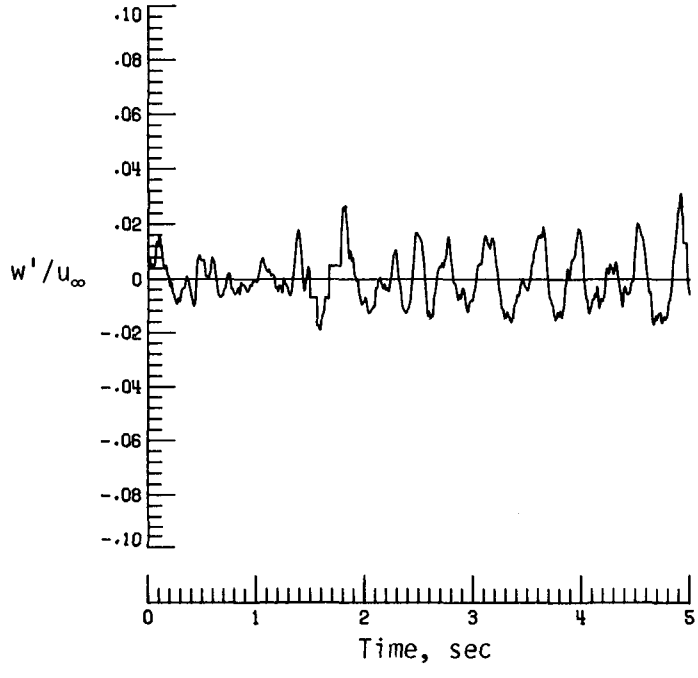

(b) Time history of vertical velocity fluctuations.

Figure B16. Dynamic-flow quality for configuration 6 at $q = 15.03$ lb/ft^2.

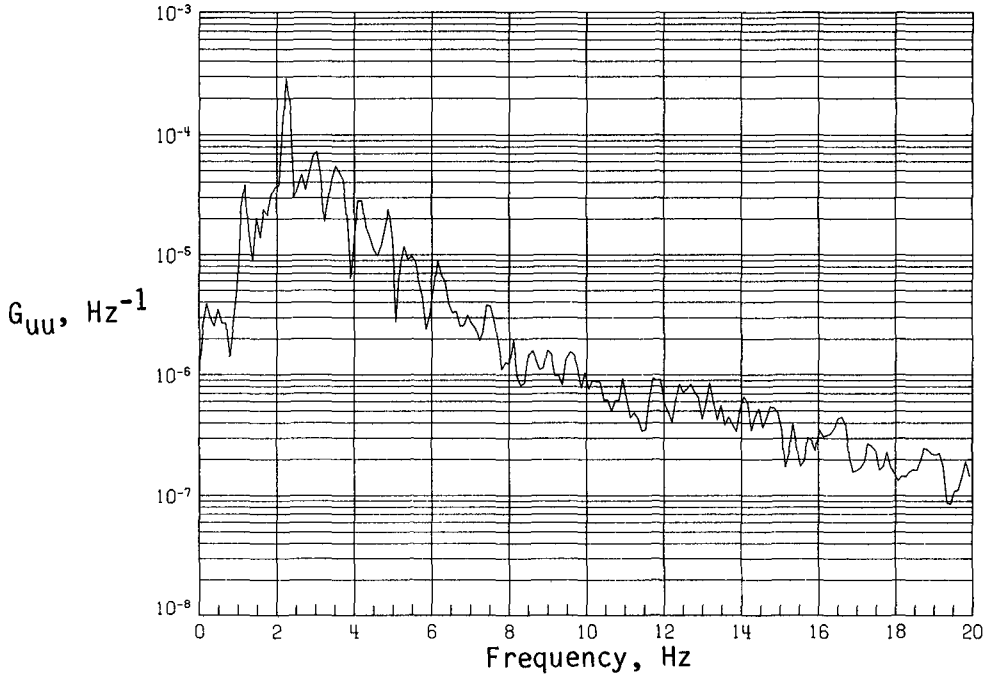

(c) PSD of streamwise velocity fluctuations.

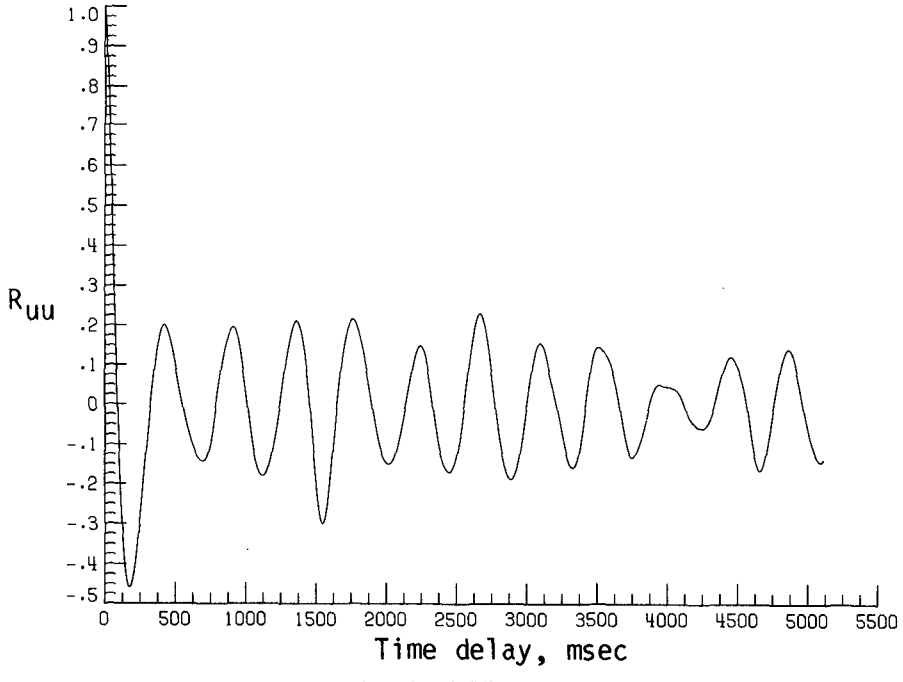

(d) Normalized autocorrelation of streamwise velocity fluctuations. $\sigma = 0.0136$.

Figure B16. Continued.

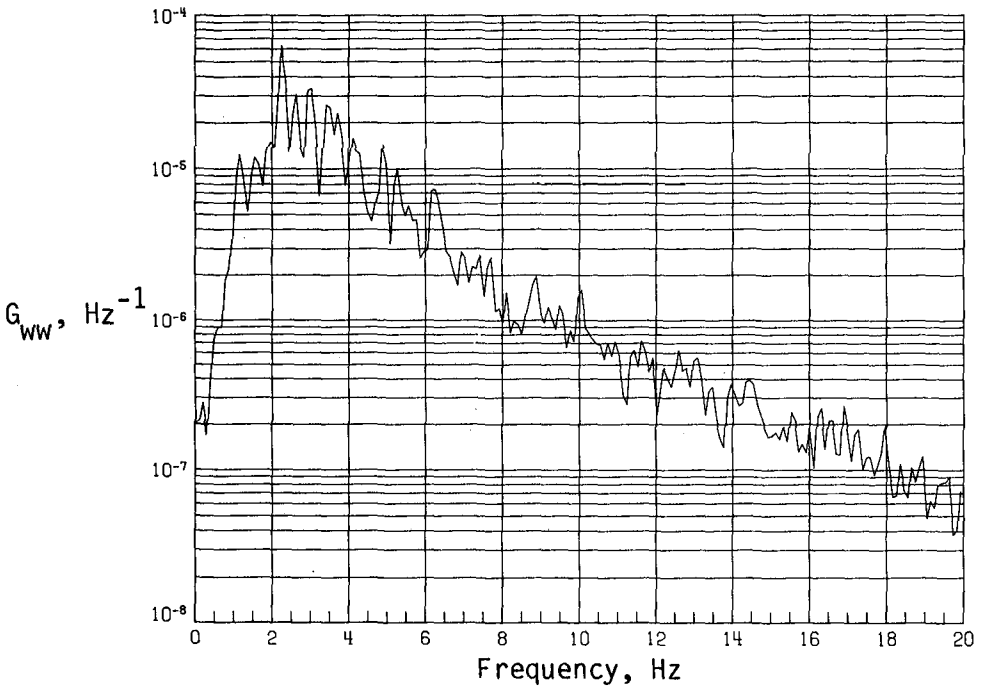

(e) PSD of vertical velocity fluctuations.

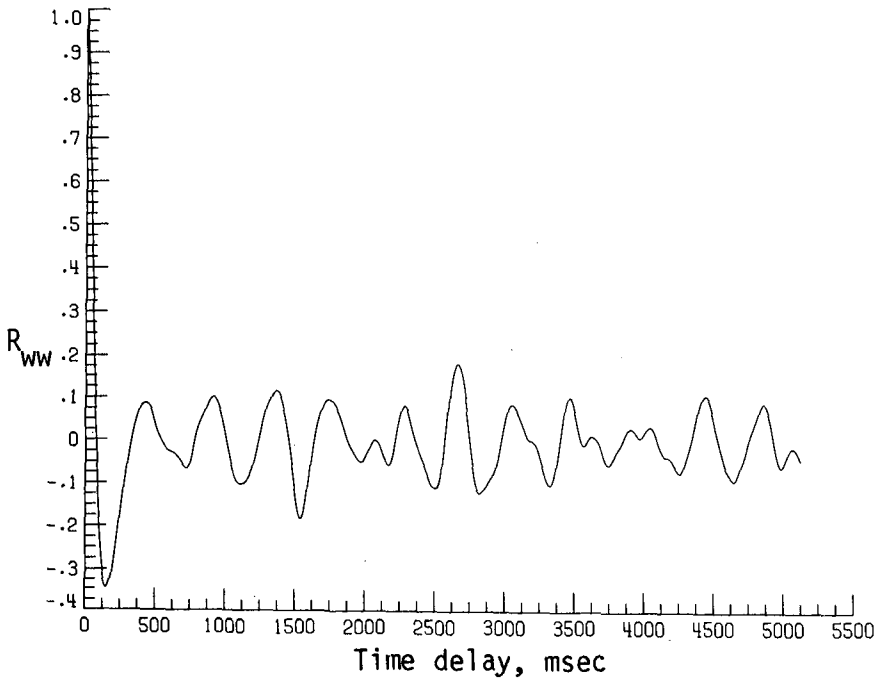

(f) Normalized autocorrelation of vertical velocity fluctuations. $\sigma = 0.0092$.

Figure B16. Concluded.

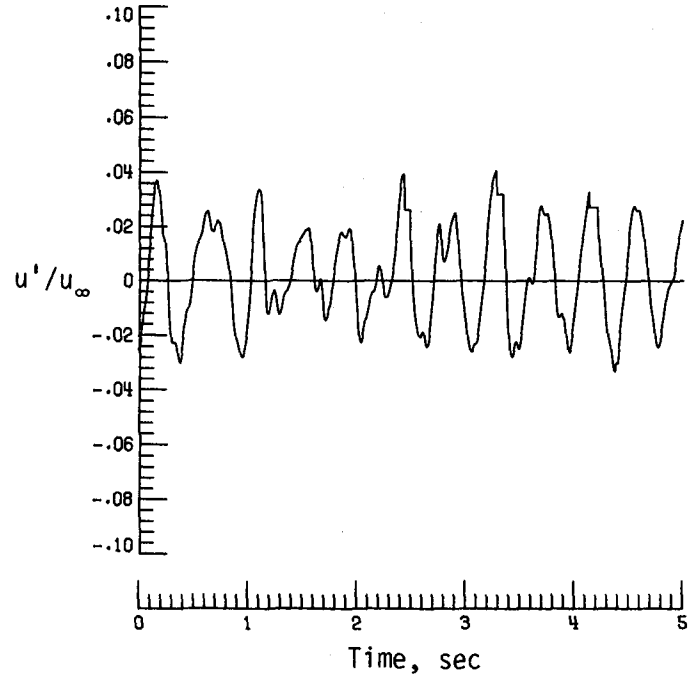

(a) Time history of streamwise velocity fluctuations.

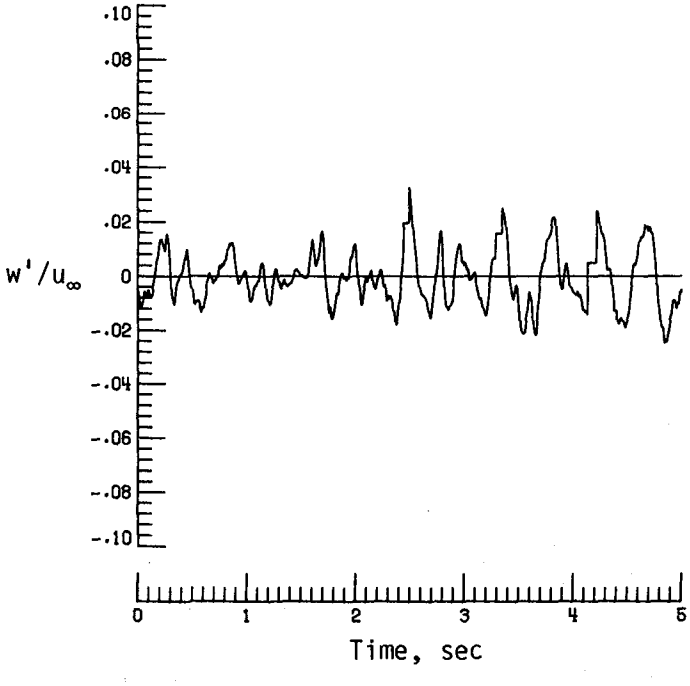

(b) Time history of vertical velocity fluctuations.

Figure B17. Dynamic-flow quality for configuration 6 at $q = 16.05$ lb/ft^2.

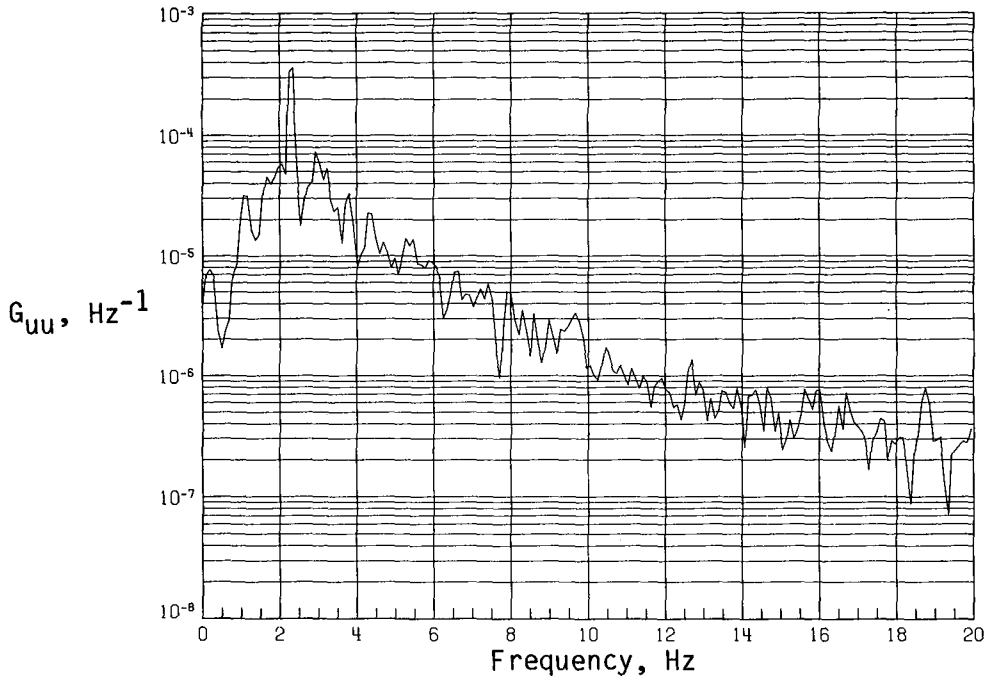

(c) PSD of streamwise velocity fluctuations.

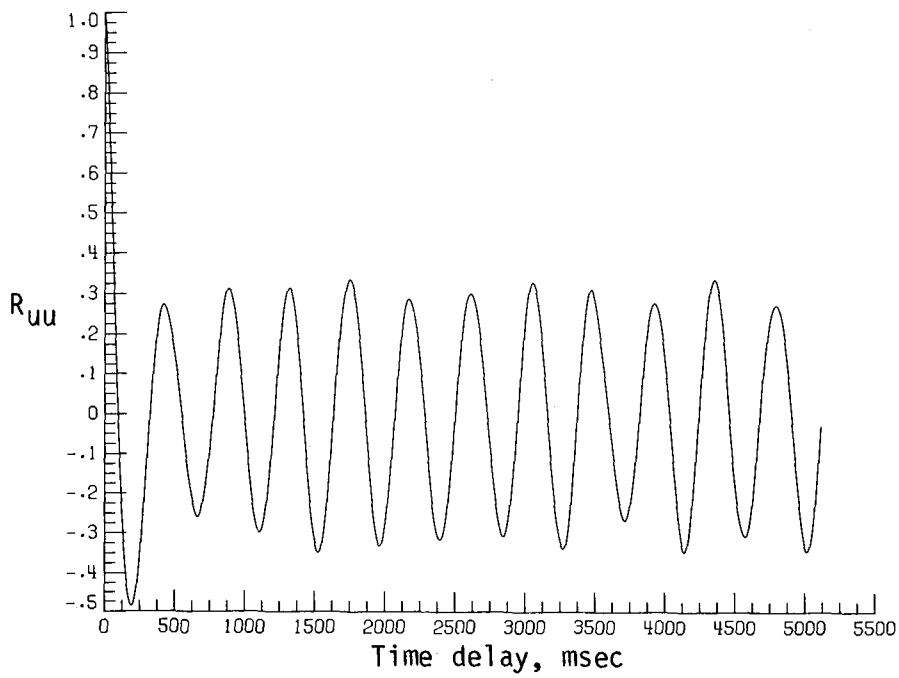

(d) Normalized autocorrelation of streamwise velocity fluctuations. $\sigma = 0.0143$.

Figure B17. Continued.

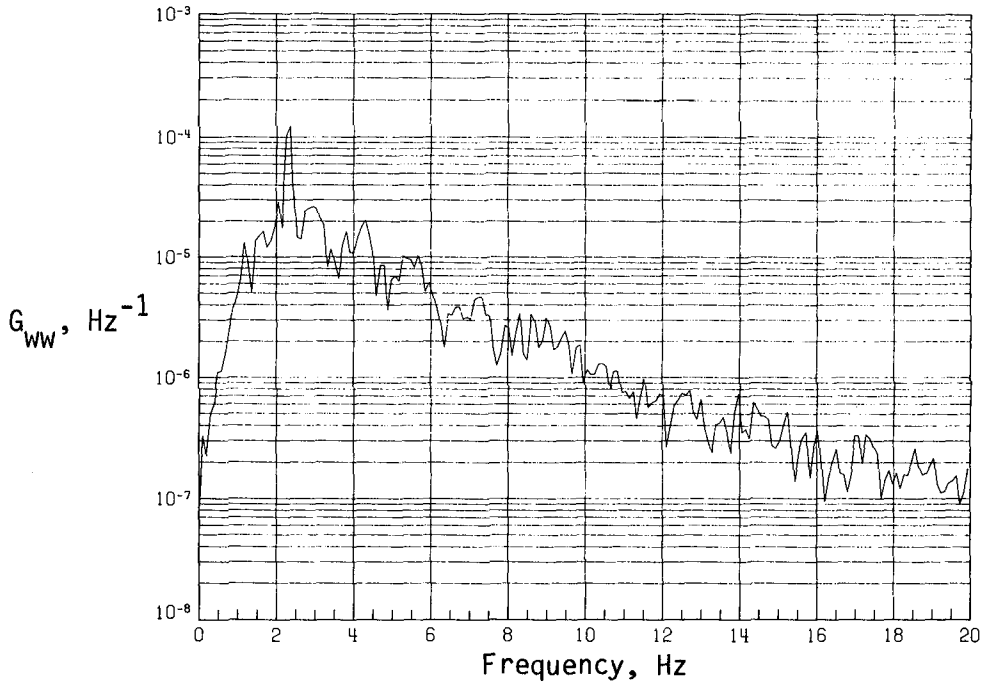

(e) PSD of vertical velocity fluctuations.

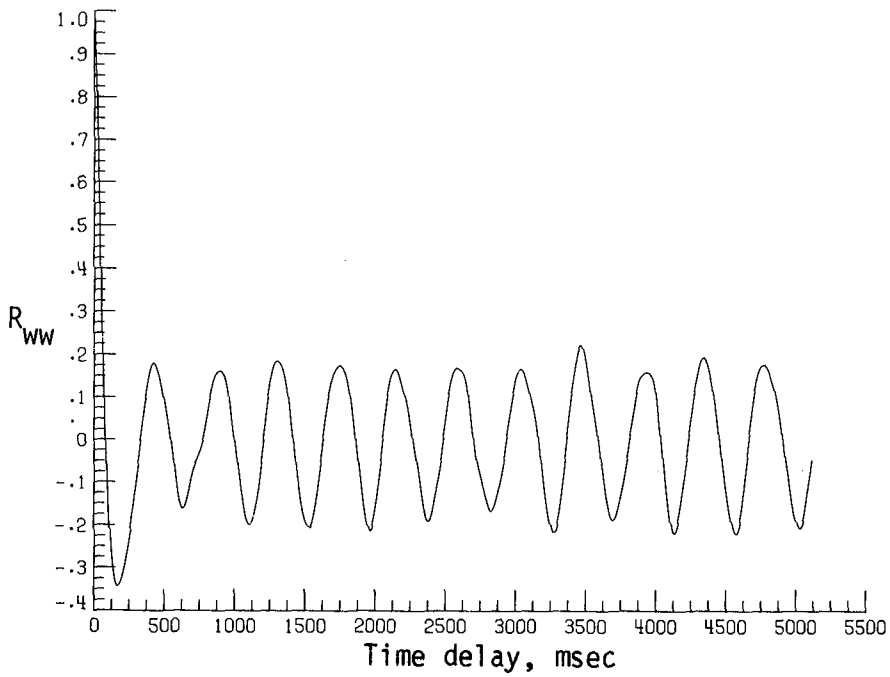

(f) Normalized autocorrelation of vertical velocity fluctuations. $\sigma = 0.0096$.

Figure B17. Concluded.

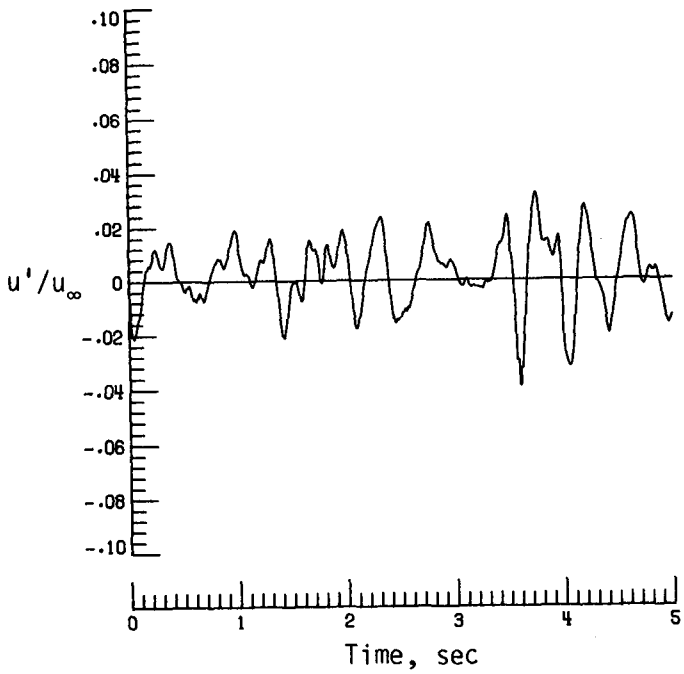

(a) Time history of streamwise velocity fluctuations.

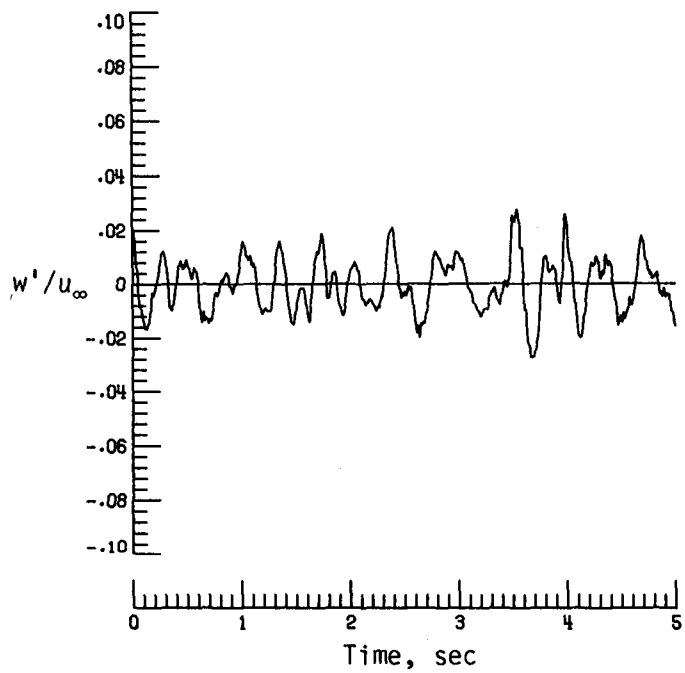

(b) Time history of vertical velocity fluctuations.

Figure B18. Dynamic-flow quality for configuration 6 at $q = 16.98$ lb/ft^2.

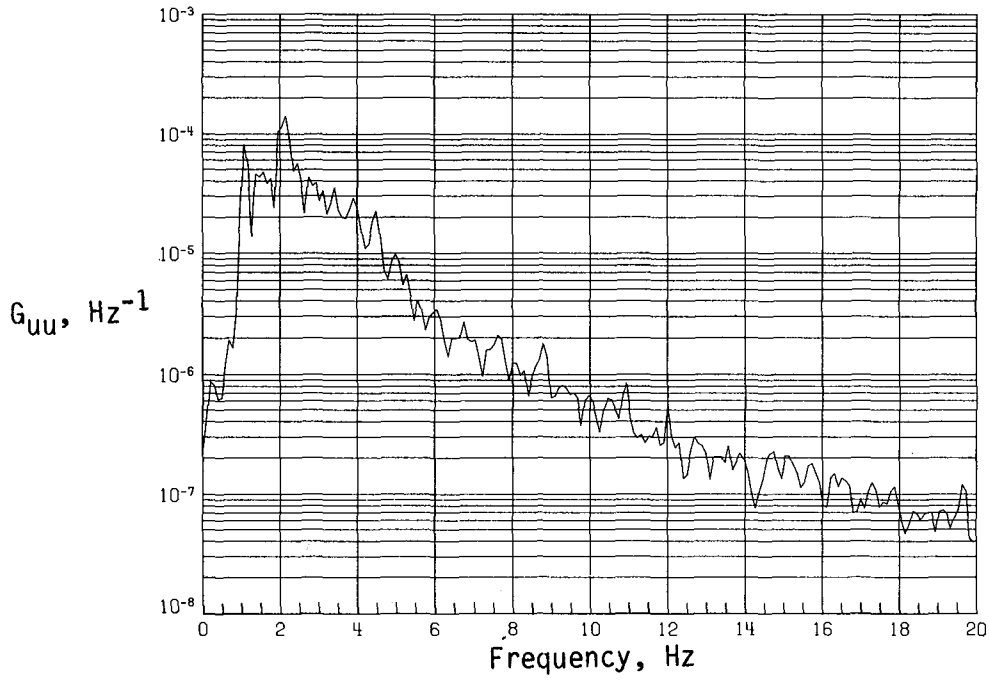

(c) PSD of streamwise velocity fluctuations.

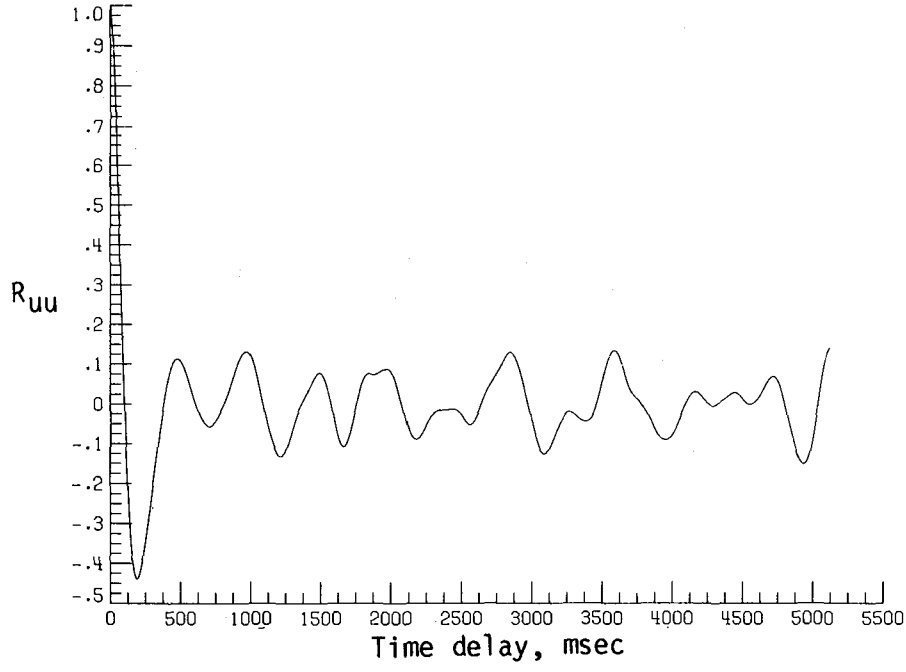

(d) Normalized autocorrelation of streamwise velocity fluctuations. $\sigma = 0.0129$.

Figure B18. Continued.

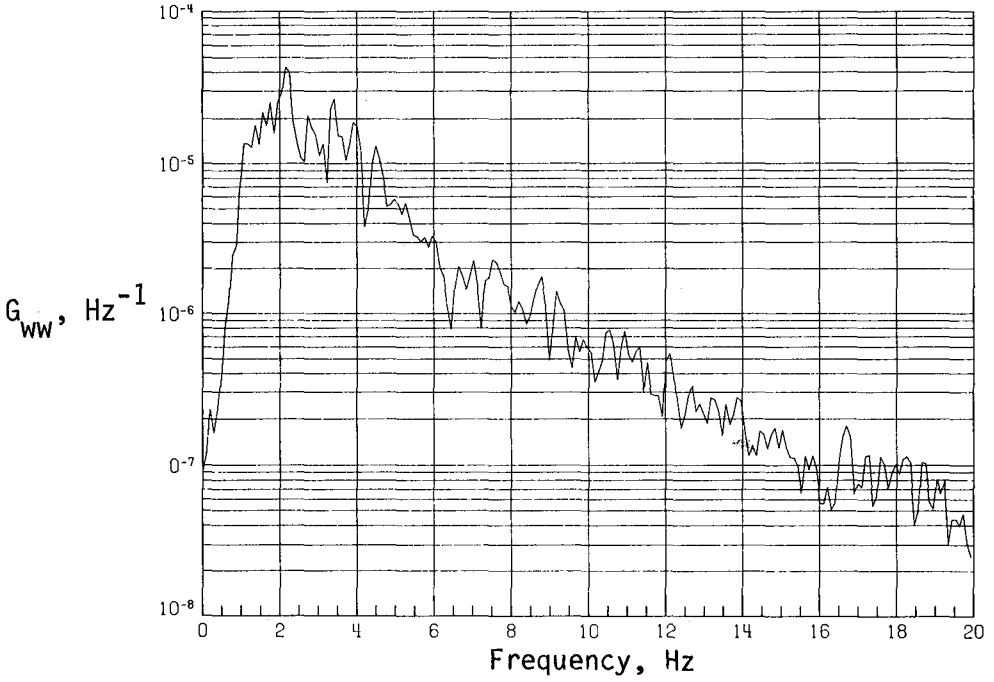

(e) PSD of vertical velocity fluctuations.

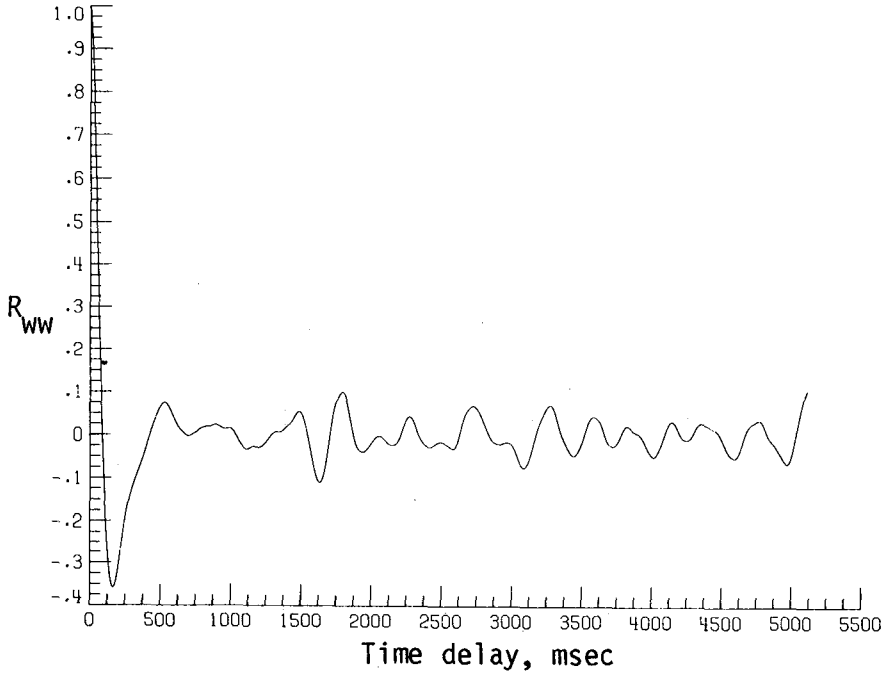

(f) Normalized autocorrelation of vertical velocity fluctuations. $\sigma = 0.0088$.

Figure B18. Concluded.

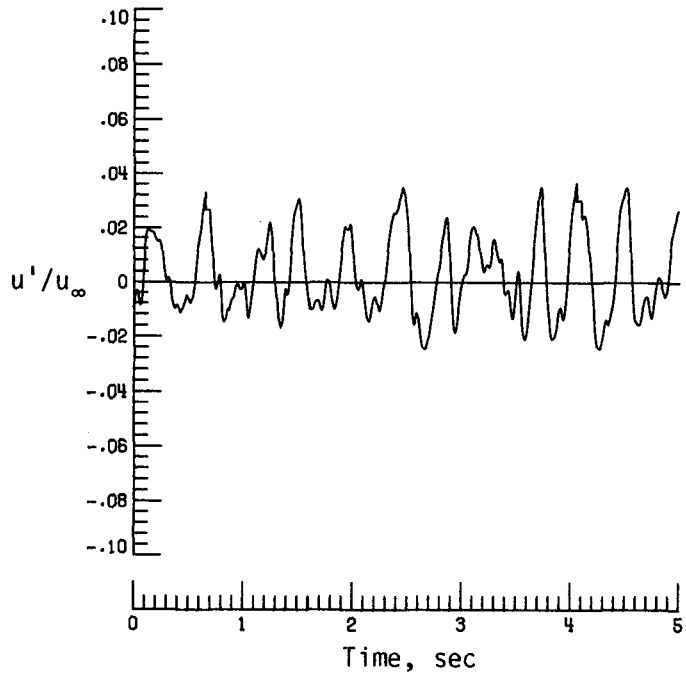

(a) Time history of streamwise velocity fluctuations.

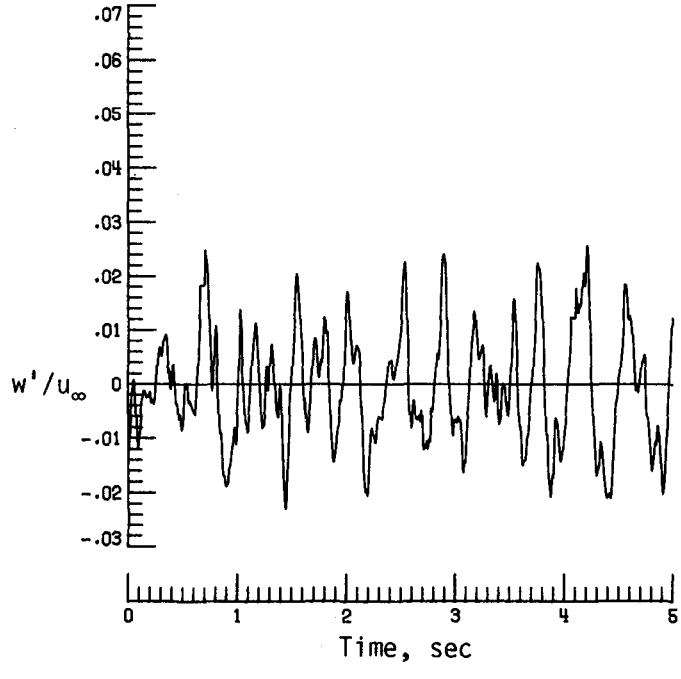

(b) Time history of vertical velocity fluctuations.

Figure B19. Dynamic-flow quality for configuration 6 at $q = 18.08$ lb/ft^2.

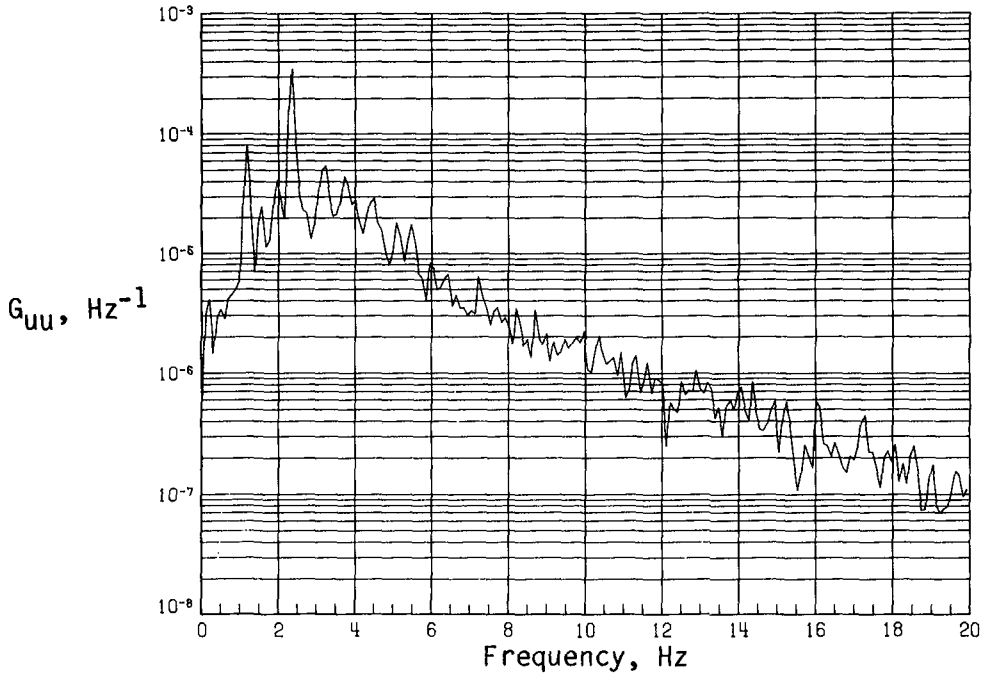

(c) PSD of streamwise velocity fluctuations.

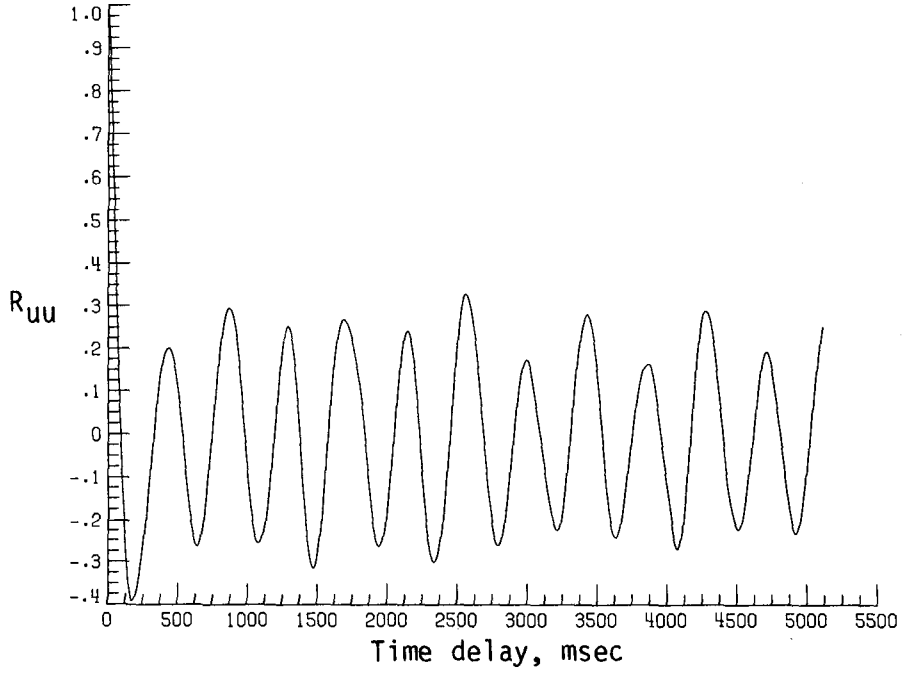

(d) Normalized autocorrelation of streamwise velocity fluctuations. $\sigma = 0.0140$.

Figure B19. Continued.

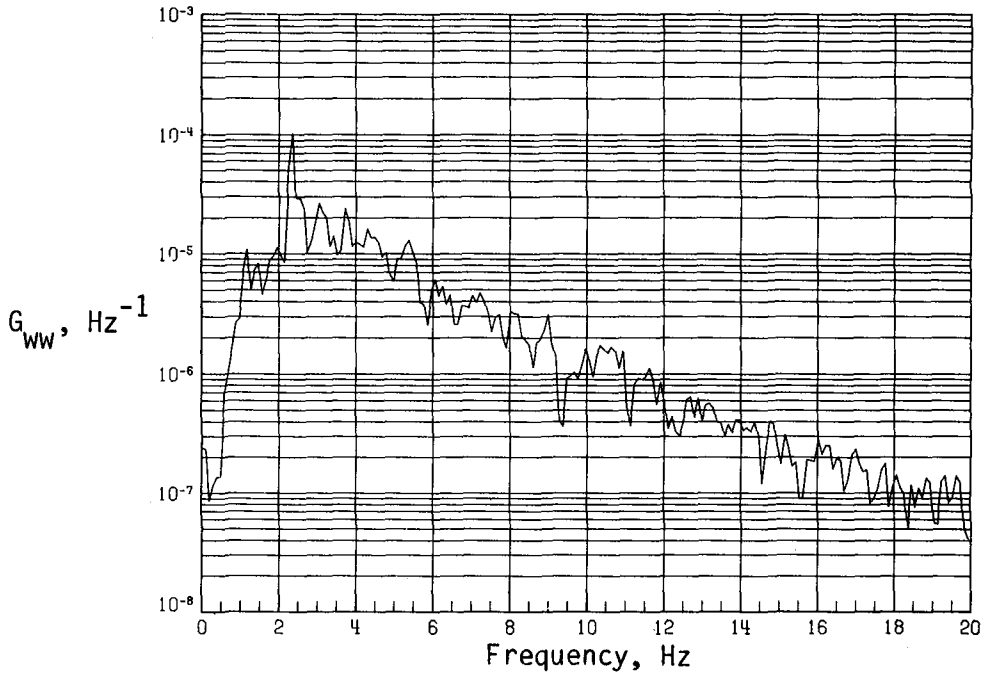

(e) PSD of vertical velocity fluctuations.

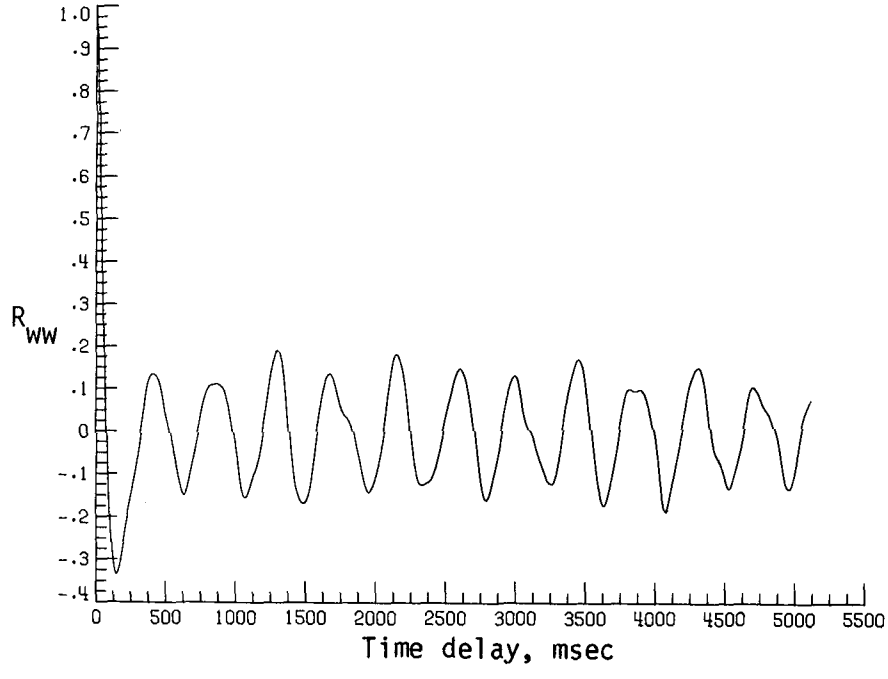

(f) Normalized autocorrelation of vertical velocity fluctuations. $\sigma = 0.0095$.

Figure B19. Concluded.

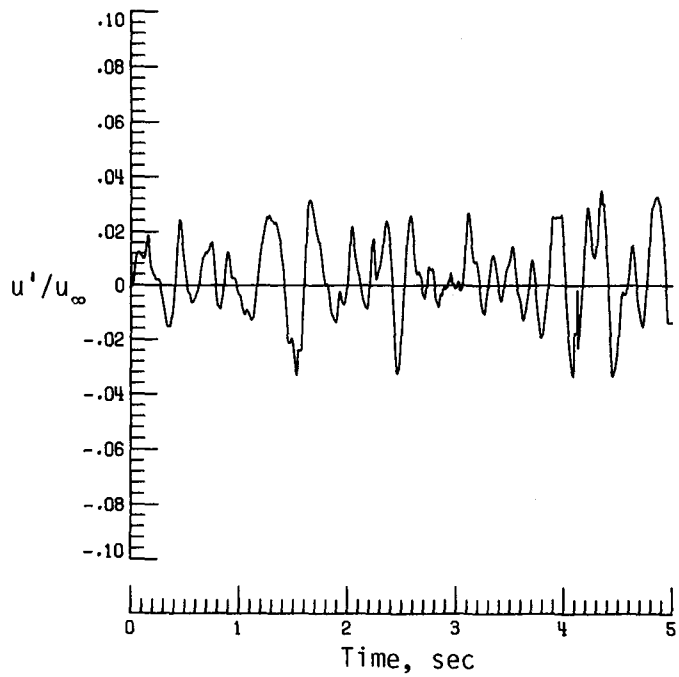

(a) Time history of streamwise velocity fluctuations.

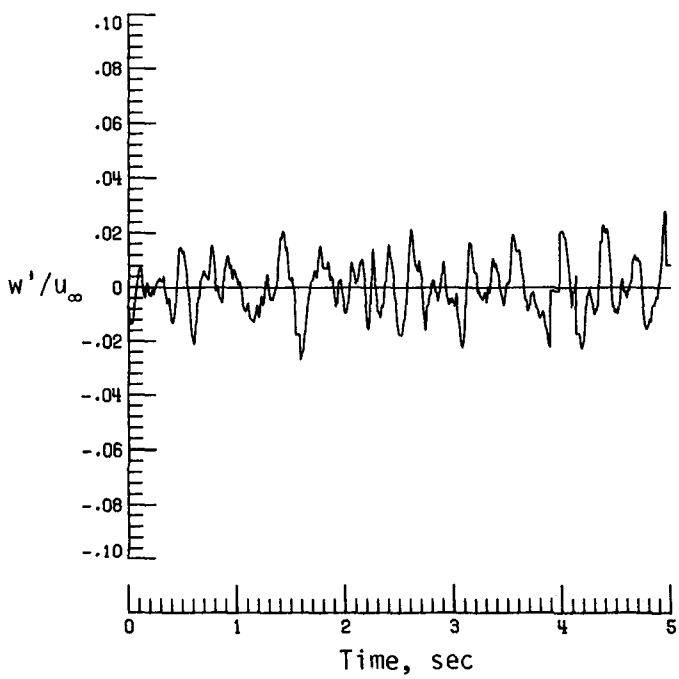

(b) Time history of vertical velocity fluctuations.

Figure B20. Dynamic-flow quality for configuration 6 at $q = 20.00$ lb/ft^2.

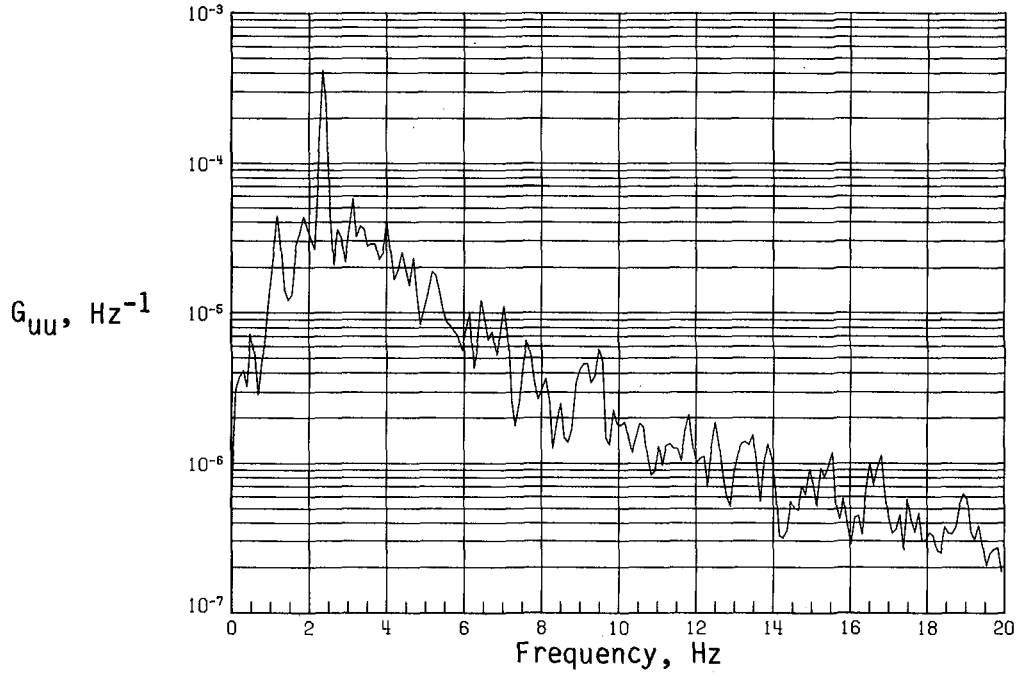

(c) PSD of streamwise velocity fluctuations.

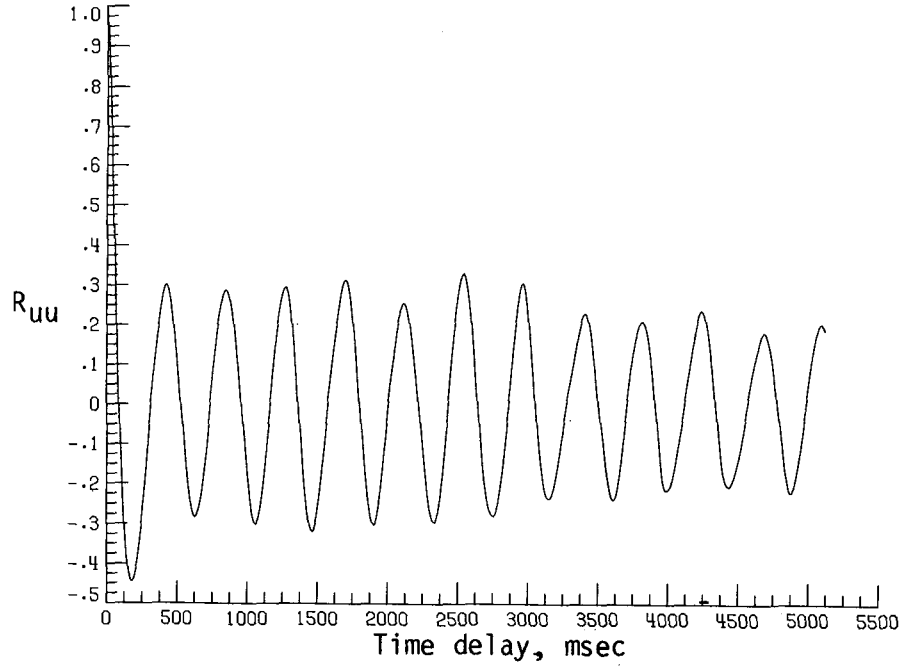

(d) Normalized autocorrelation of streamwise velocity fluctuations. $\sigma = 0.0146$.

Figure B20. Continued.

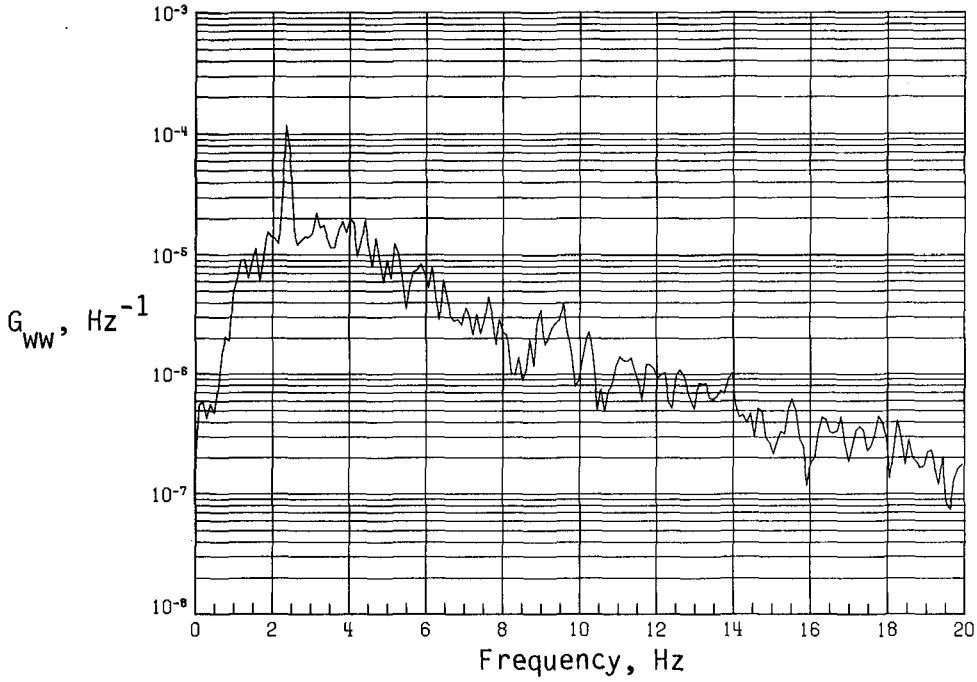

(e) PSD of vertical velocity fluctuations.

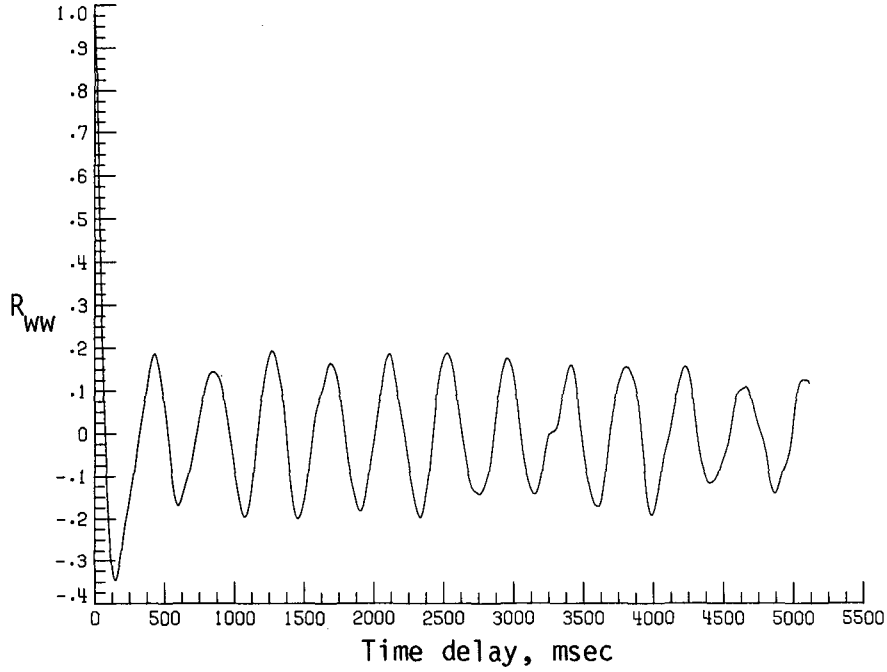

(f) Normalized autocorrelation of vertical velocity fluctuations. $\sigma = 0.0096$.

Figure B20. Concluded.

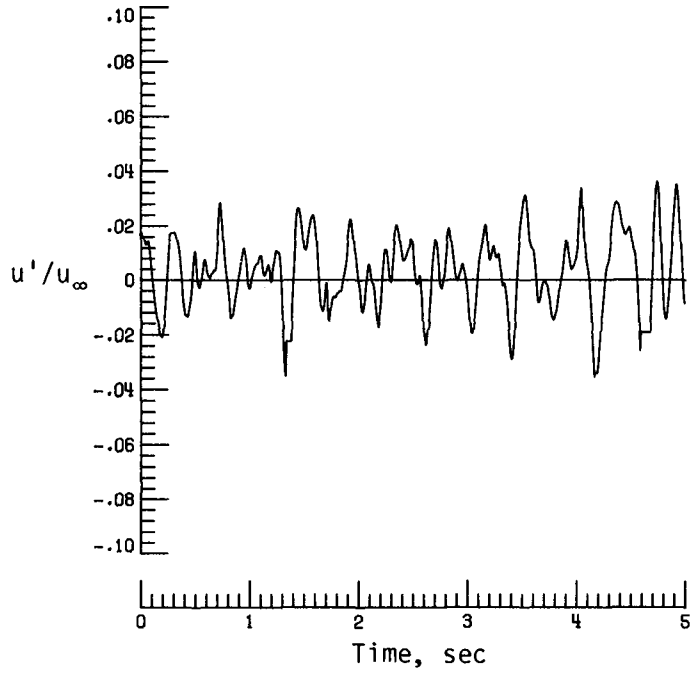

(a) Time history of streamwise velocity fluctuations.

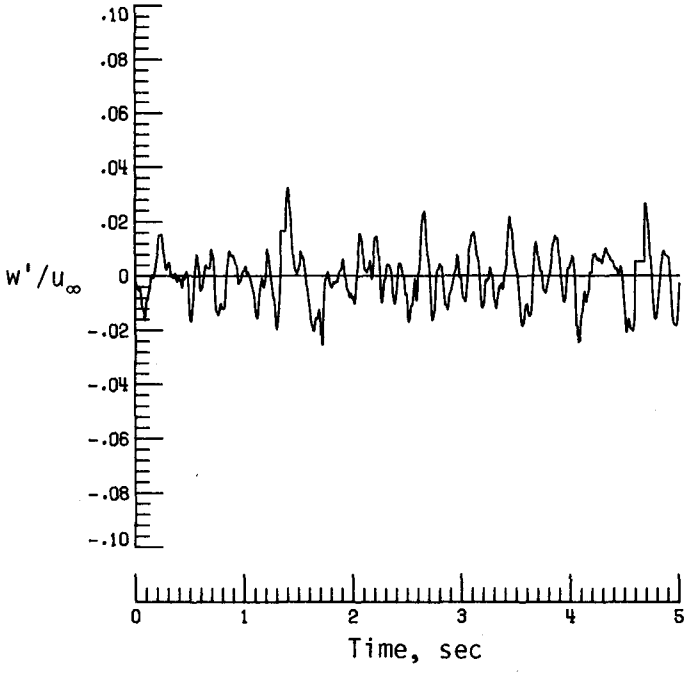

(b) Time history of vertical velocity fluctuations.

Figure B21. Dynamic-flow quality for configuration 6 at $q = 22.49$ lb/ft^2.

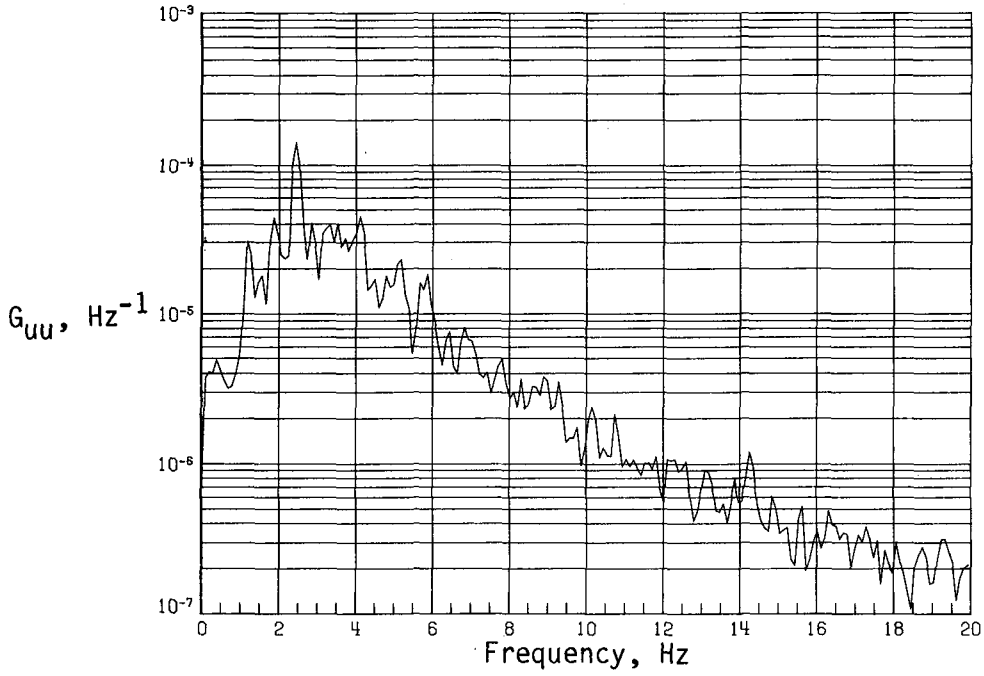

(c) PSD of streamwise velocity fluctuations.

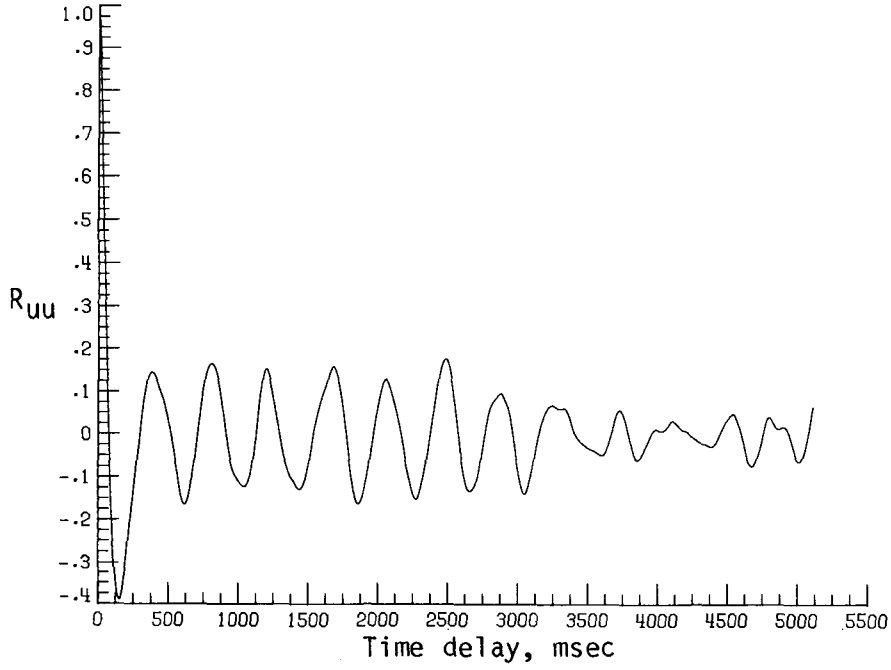

(d) Normalized autocorrelation of streamwise velocity fluctuations. $\sigma = 0.0128$.

Figure B21. Continued.

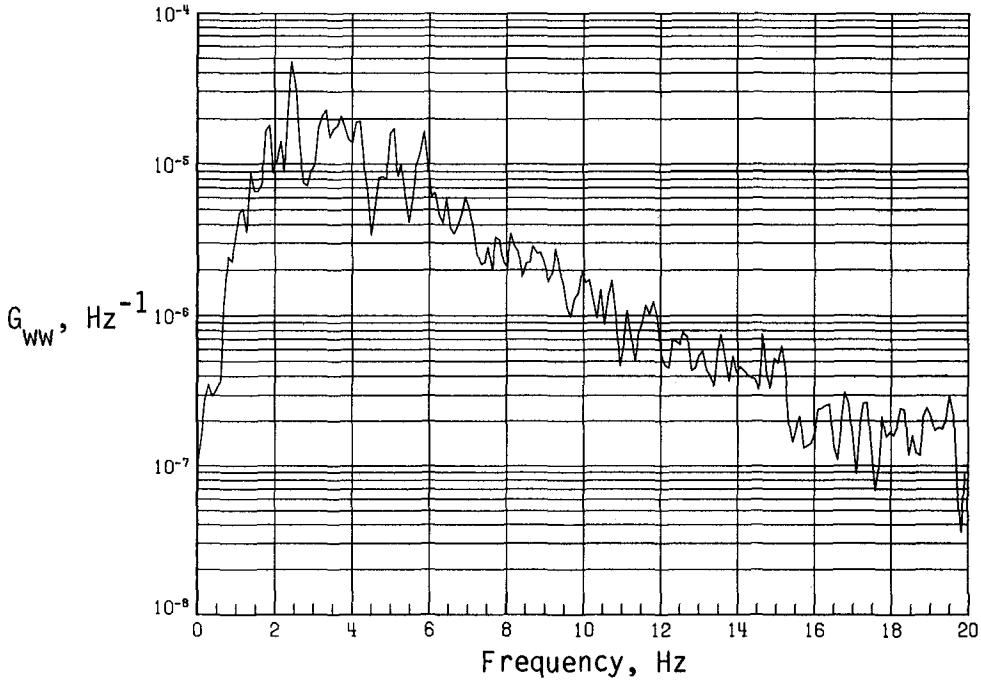

(e) PSD of vertical velocity fluctuations.

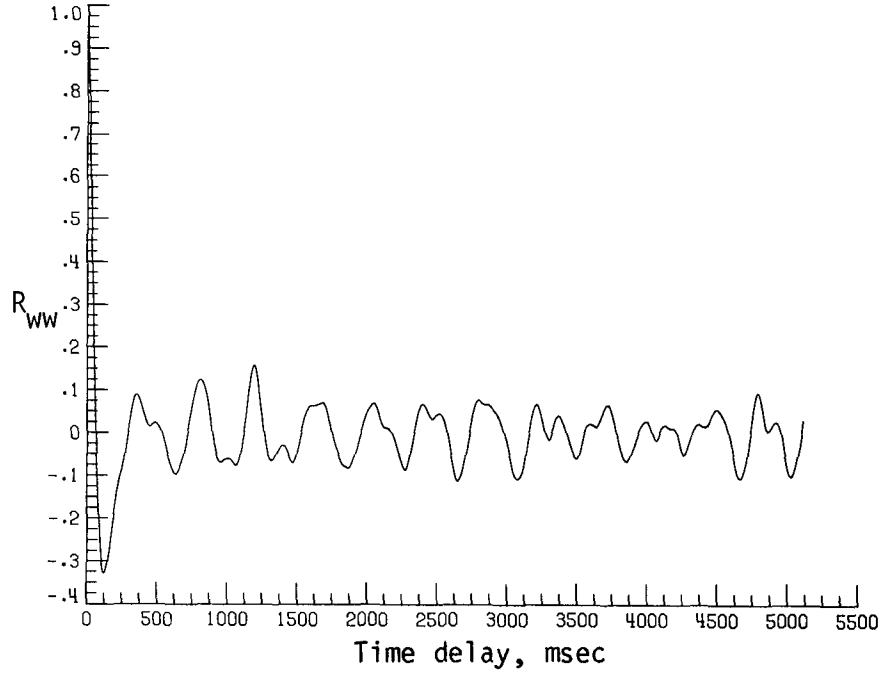

(f) Normalized autocorrelation of vertical velocity fluctuations. $\sigma = 0.0093$.

Figure B21. Concluded.

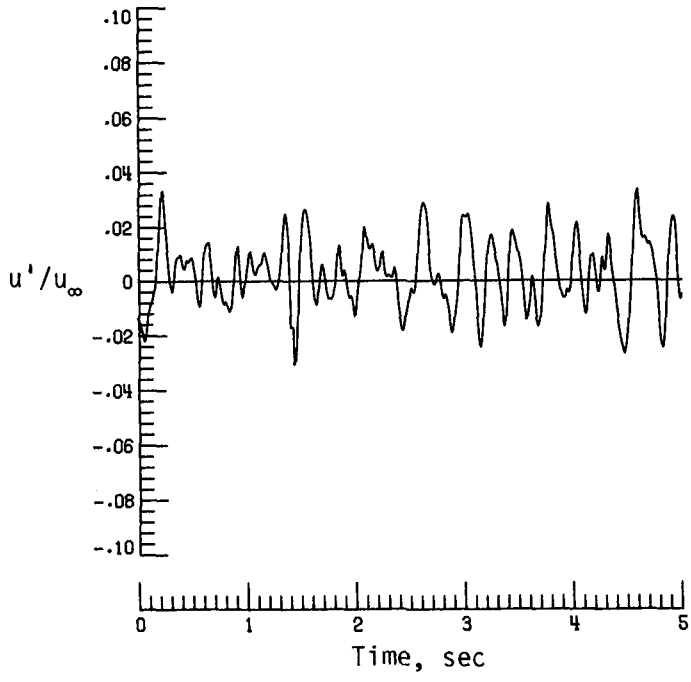

(a) Time history of streamwise velocity fluctuations.

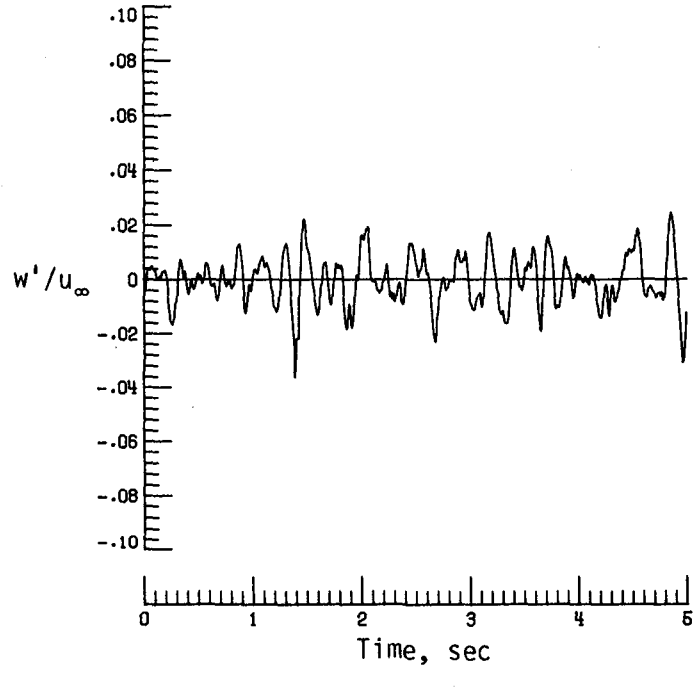

(b) Time history of vertical velocity fluctuations.

Figure B22. Dynamic-flow quality for configuration 6 at $q = 25.09$ lb/ft^2.

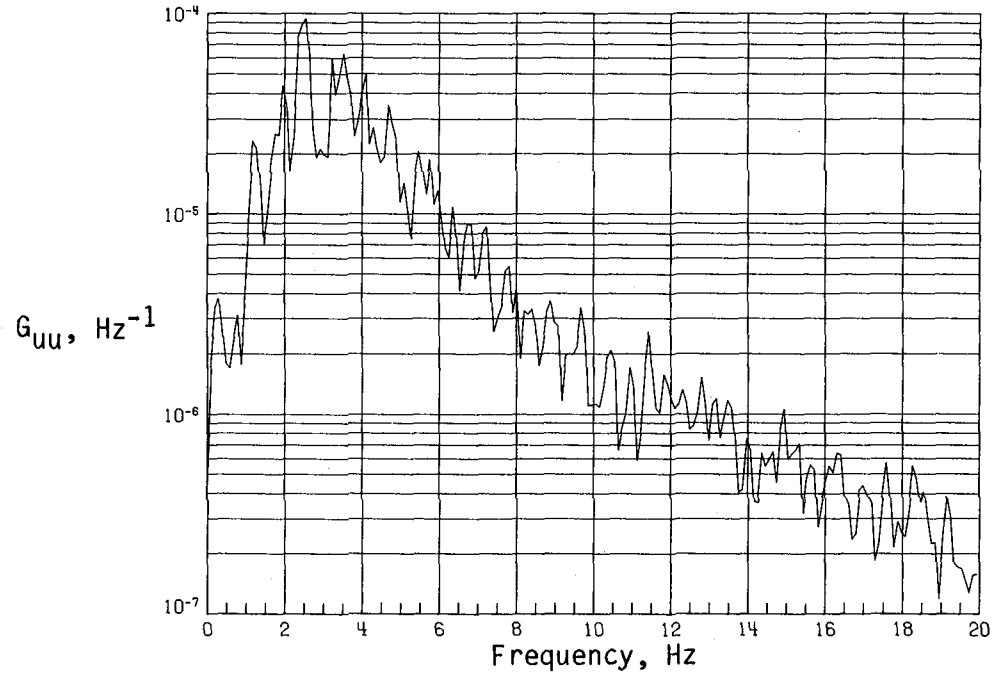

(c) PSD of streamwise velocity fluctuations.

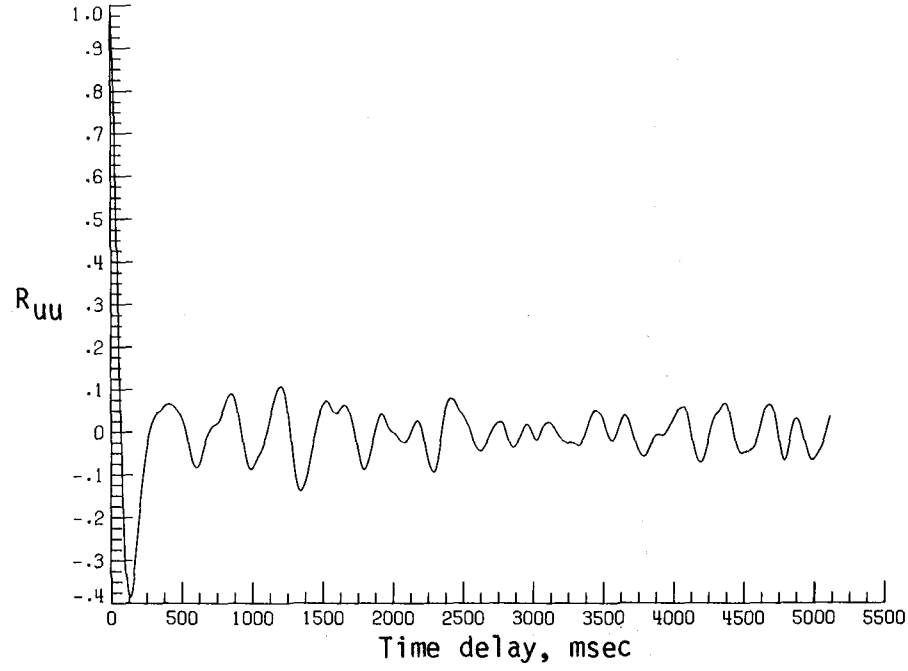

(d) Normalized autocorrelation of streamwise velocity fluctuations. $\sigma = 0.0129$.

Figure B22. Continued.

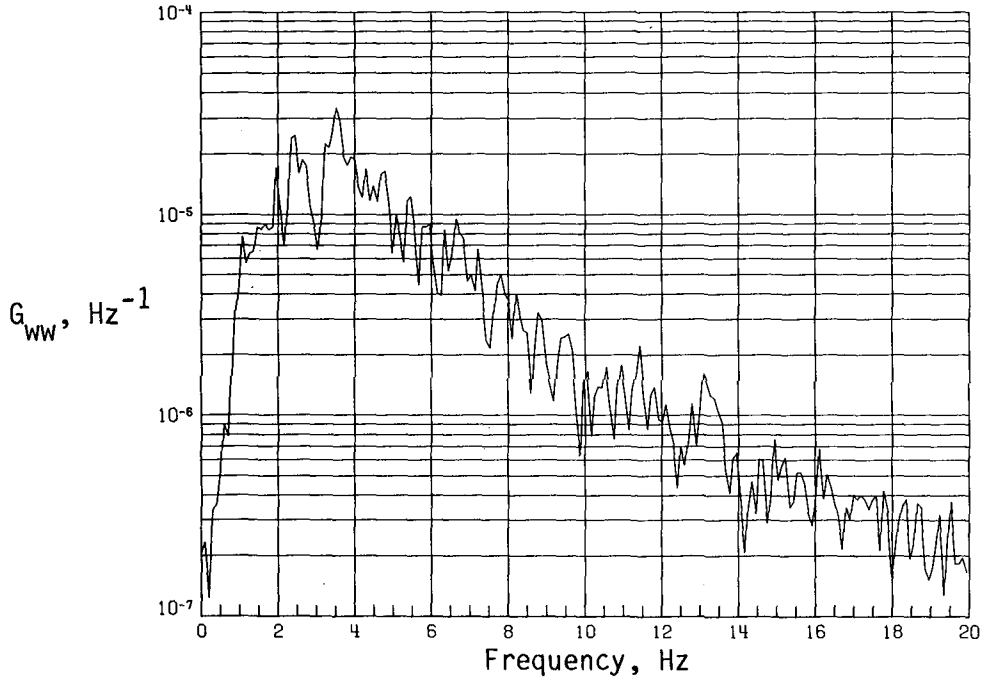

(e) PSD of vertical velocity fluctuations.

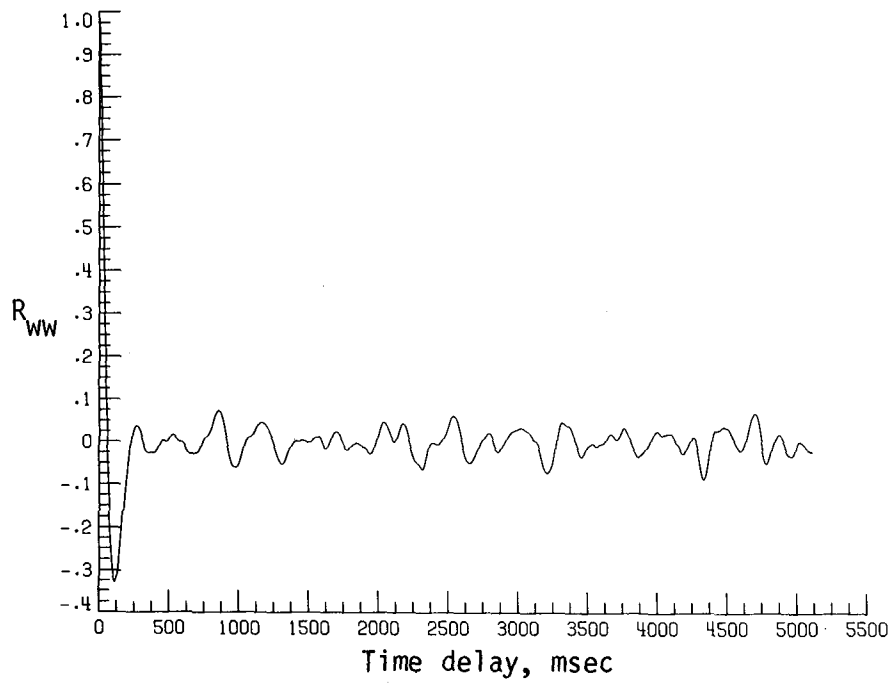

(f) Normalized autocorrelation of vertical velocity fluctuations. $\sigma = 0.0093$.

Figure B22. Concluded.

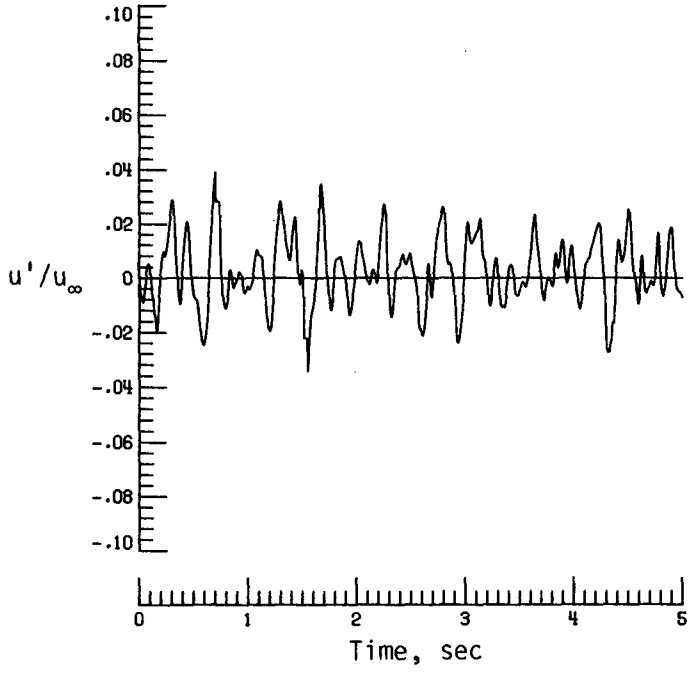

(a) Time history of streamwise velocity fluctuations.

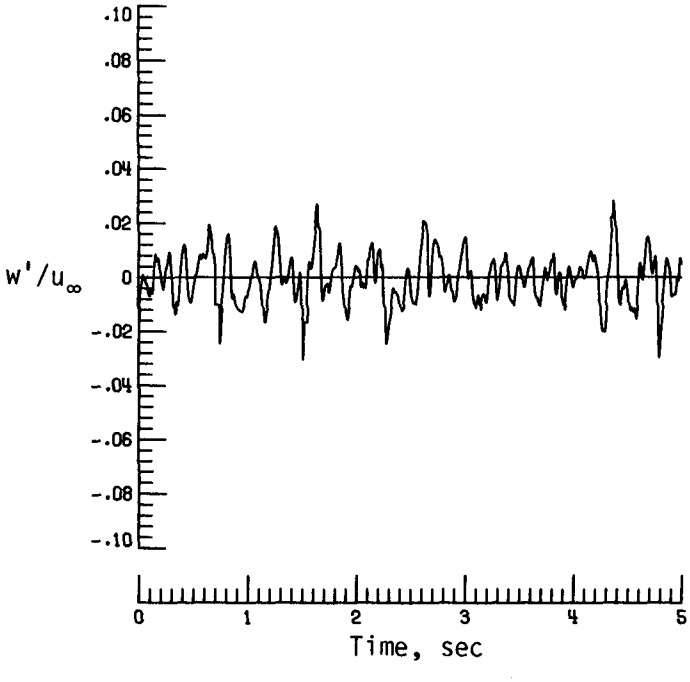

(b) Time history of vertical velocity fluctuations.

Figure B23. Dynamic-flow quality for configuration 6 at $q = 32.10$ lb/ft^2.

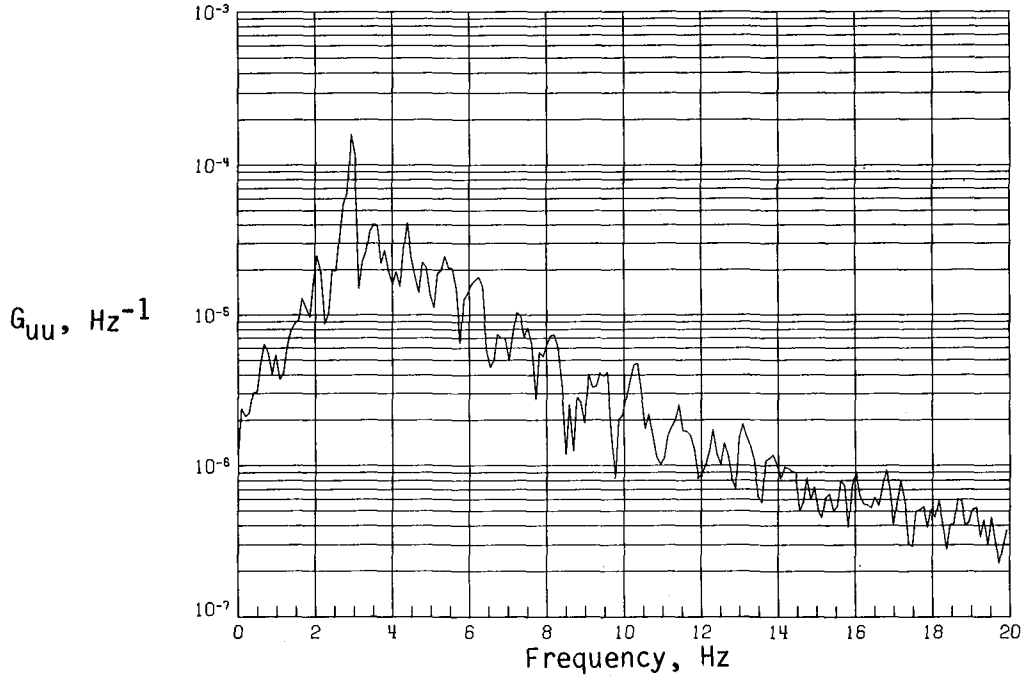

(c) PSD of streamwise velocity fluctuations.

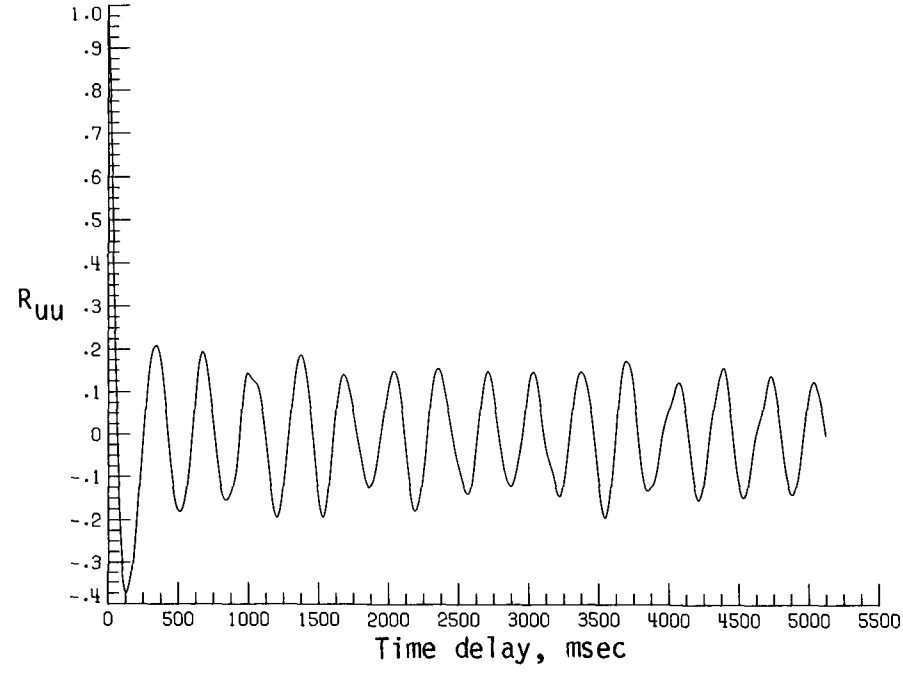

(d) Normalized autocorrelation of streamwise velocity fluctuations. $\sigma = 0.0130$.

Figure B23. Continued.

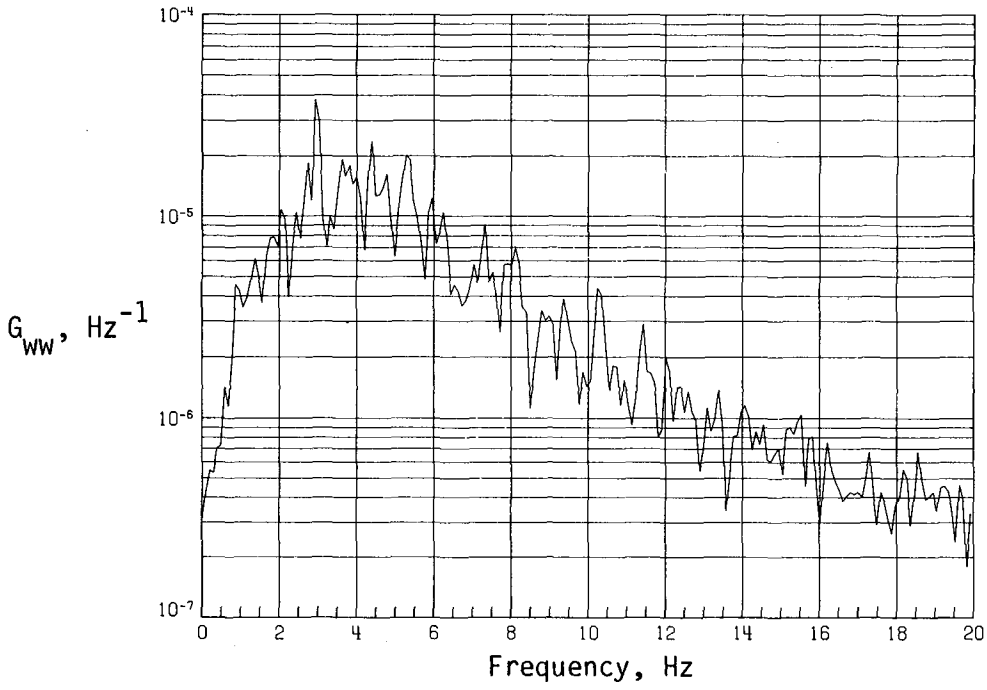

(e) PSD of vertical velocity fluctuations.

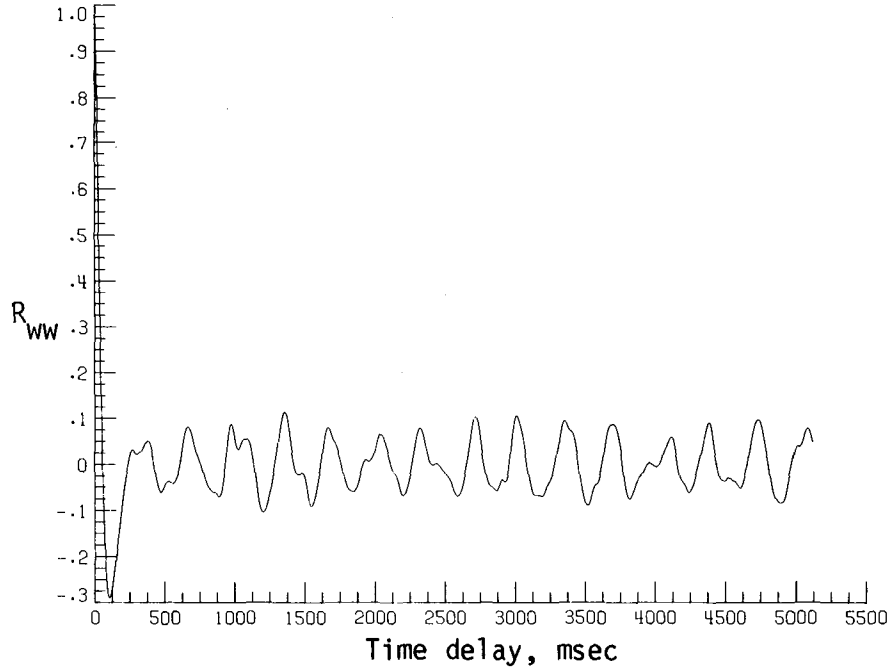

(f) Normalized autocorrelation of vertical velocity fluctuations. $\sigma = 0.0095$.

Figure B23. Concluded.

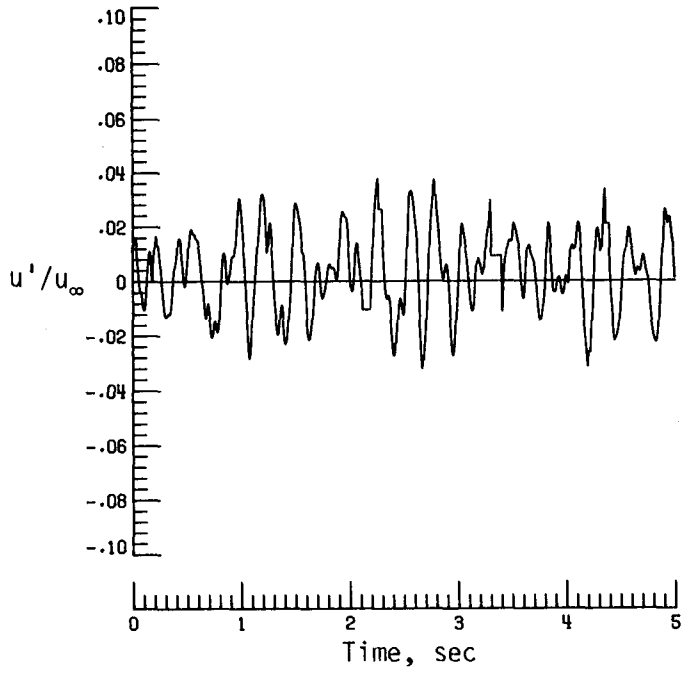

(a) Time history of streamwise velocity fluctuations.

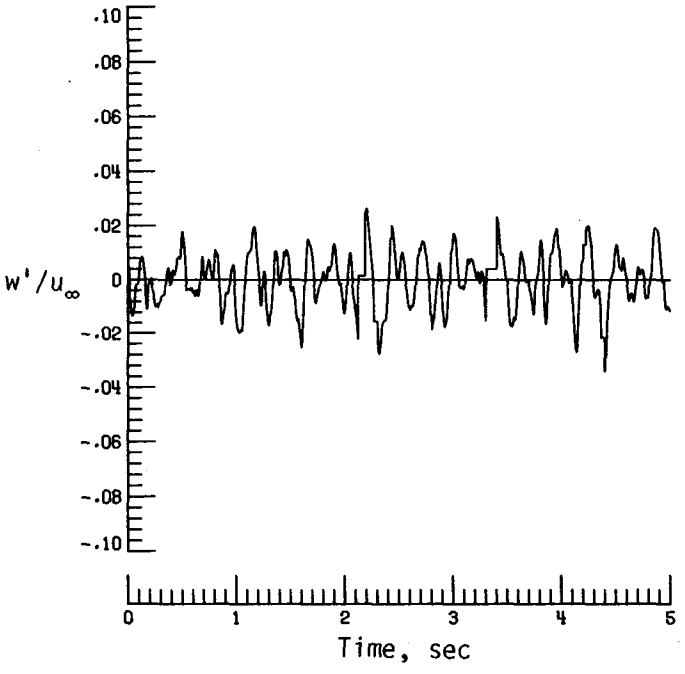

(b) Time history of vertical velocity fluctuations.

Figure B24. Dynamic-flow quality for configuration 6 at $q = 40.01$ lb/ft^2.

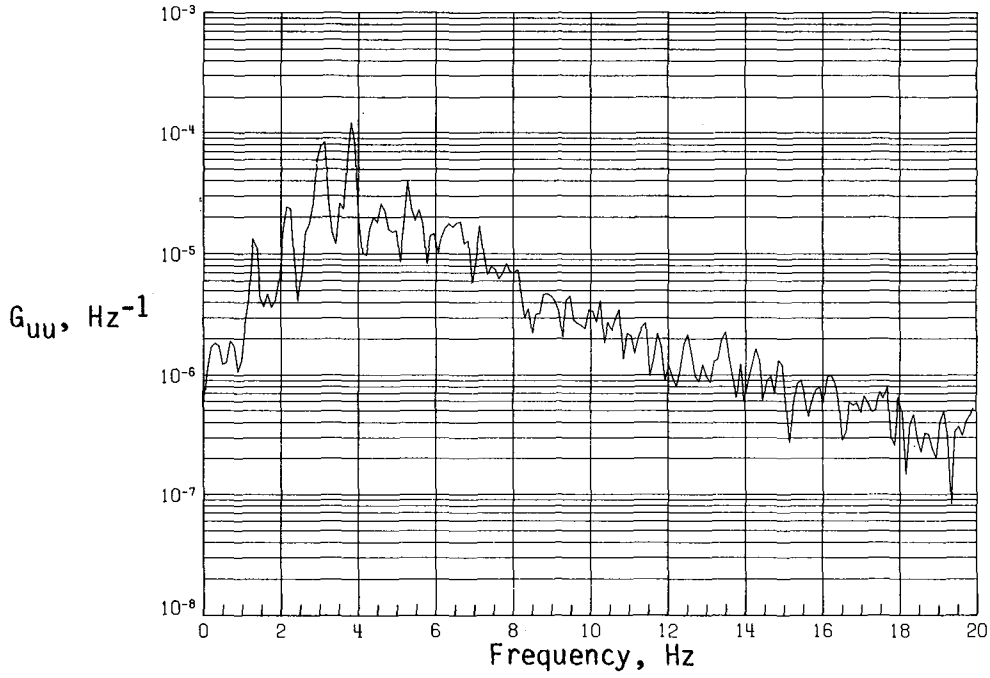

(c) PSD of streamwise velocity fluctuations.

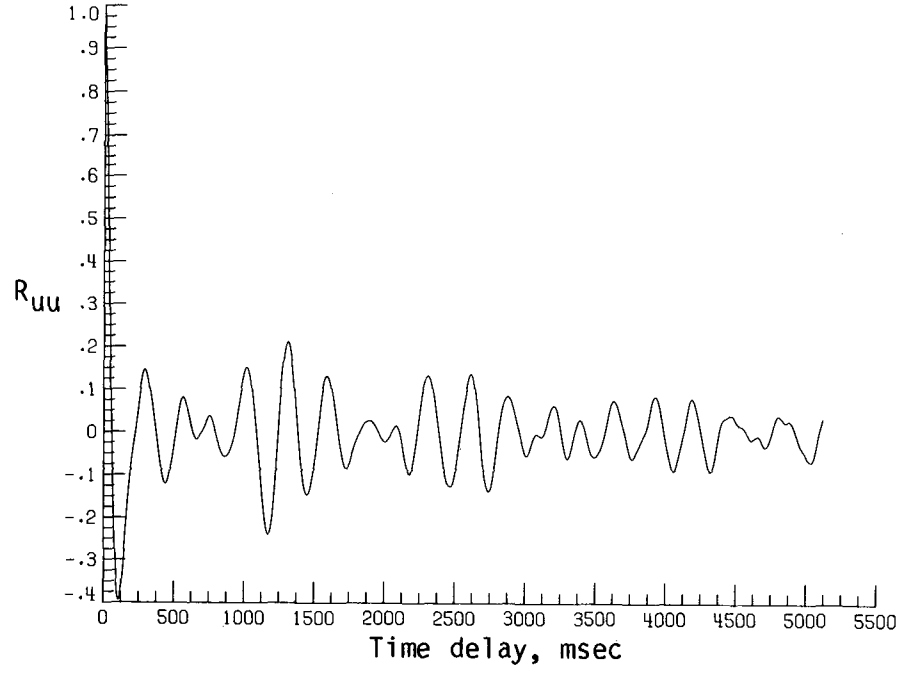

(d) Normalized autocorrelation of streamwise velocity fluctuations. $\sigma = 0.0126$.

Figure B24. Continued.

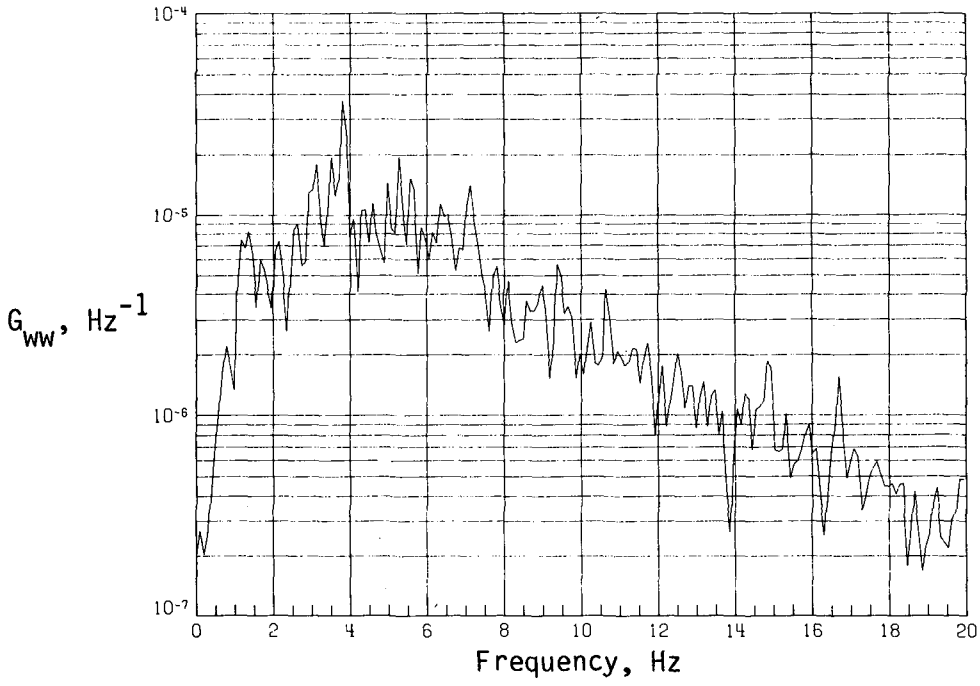

(e) PSD of vertical velocity fluctuations.

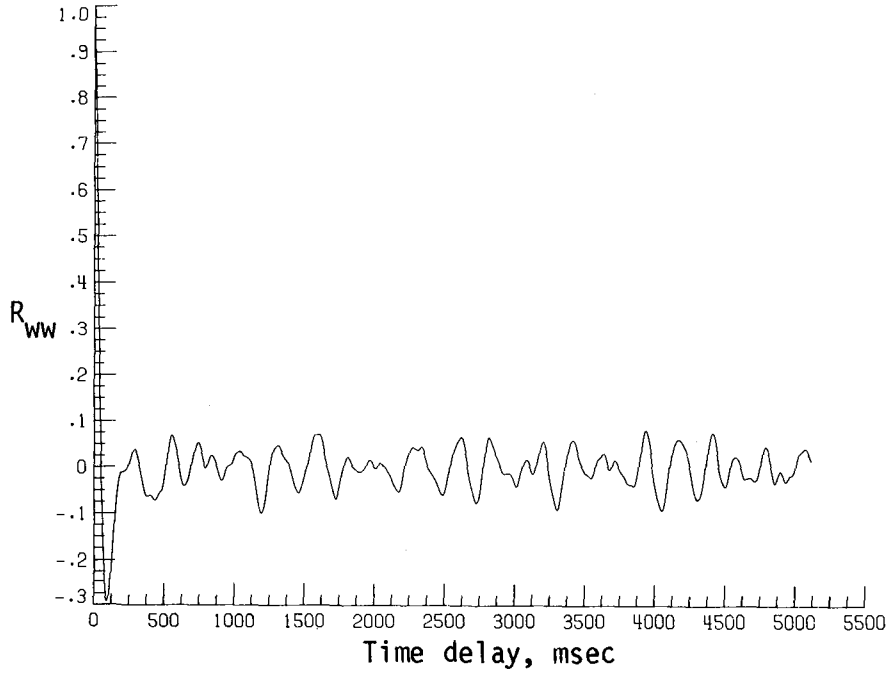

(f) Normalized autocorrelation of vertical velocity fluctuations. $\sigma = 0.0092$.

Figure B24. Concluded.

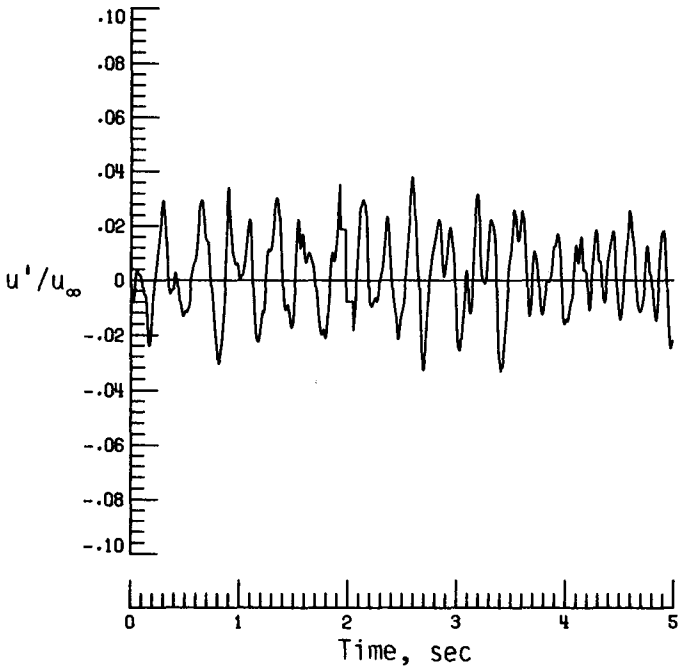

(a) Time history of streamwise velocity fluctuations.

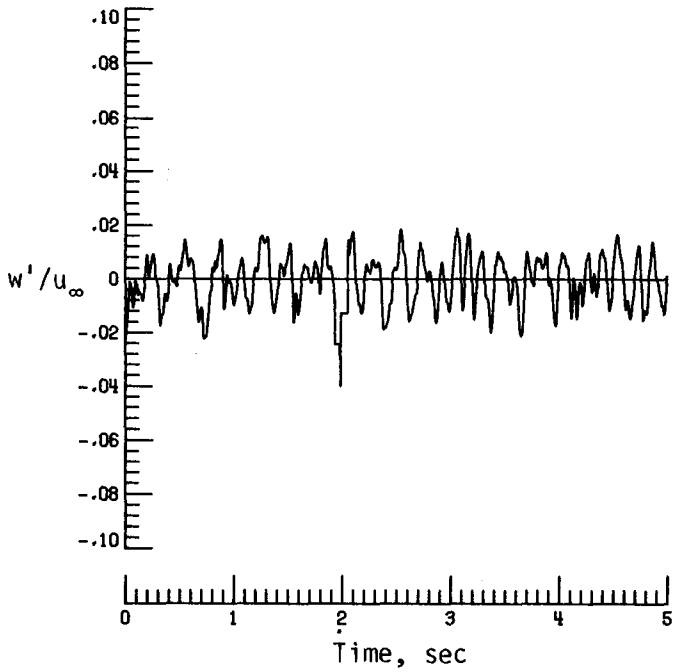

(b) Time history of vertical velocity fluctuations.

Figure B25. Dynamic-flow quality for configuration 6 at $q = 42.60$ lb/ft^2.

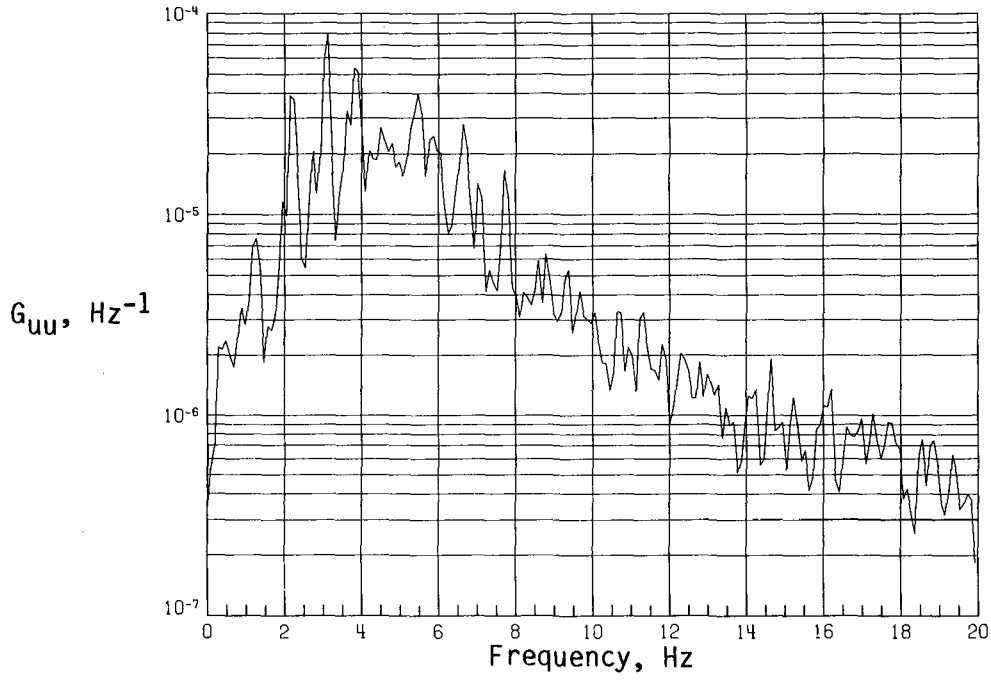

(c) PSD of streamwise velocity fluctuations.

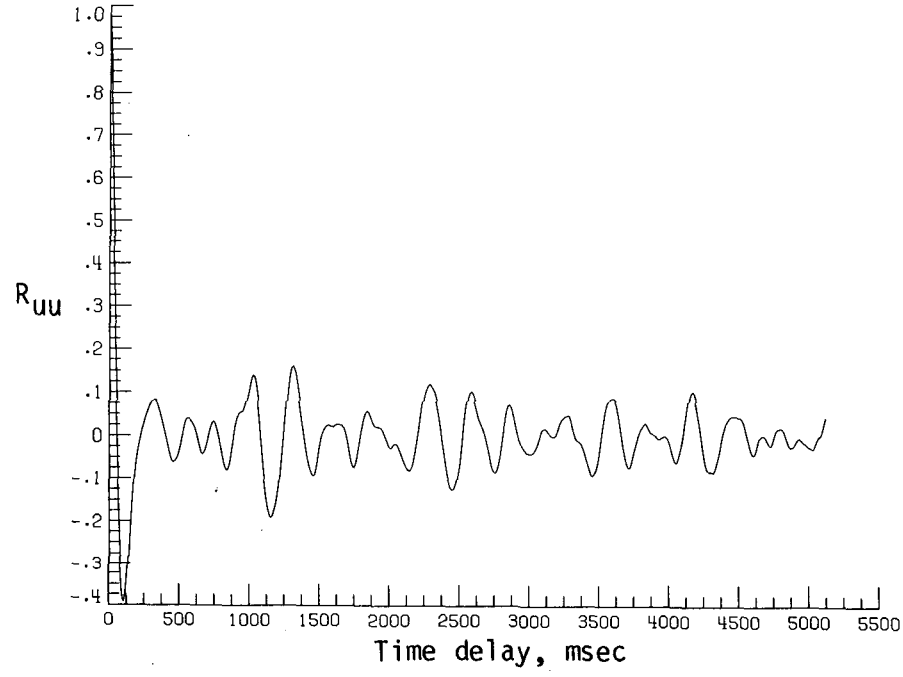

(d) Normalized autocorrelation of streamwise velocity fluctuations. $\sigma = 0.0123$.

Figure B25. Continued.

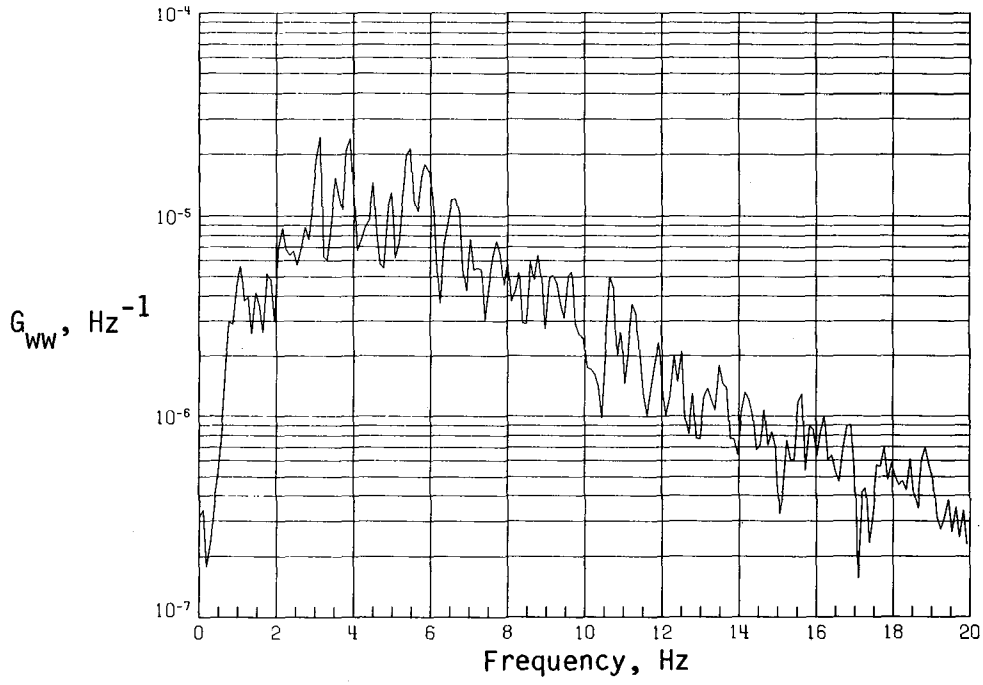

(e) PSD of vertical velocity fluctuations.

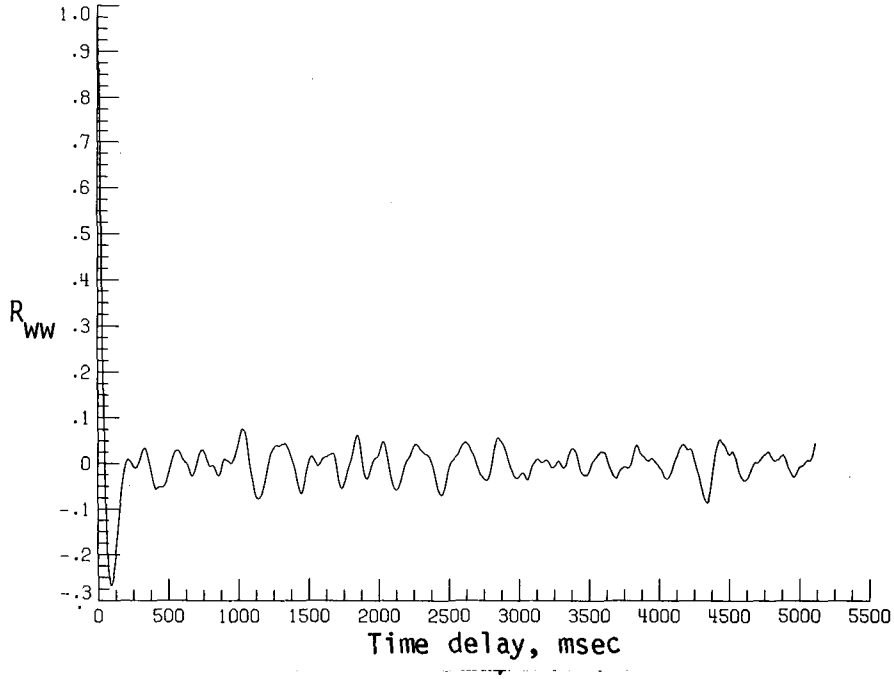

(f) Normalized autocorrelation of vertical velocity fluctuations. $\sigma = 0.0092$.

Figure B25. Concluded.

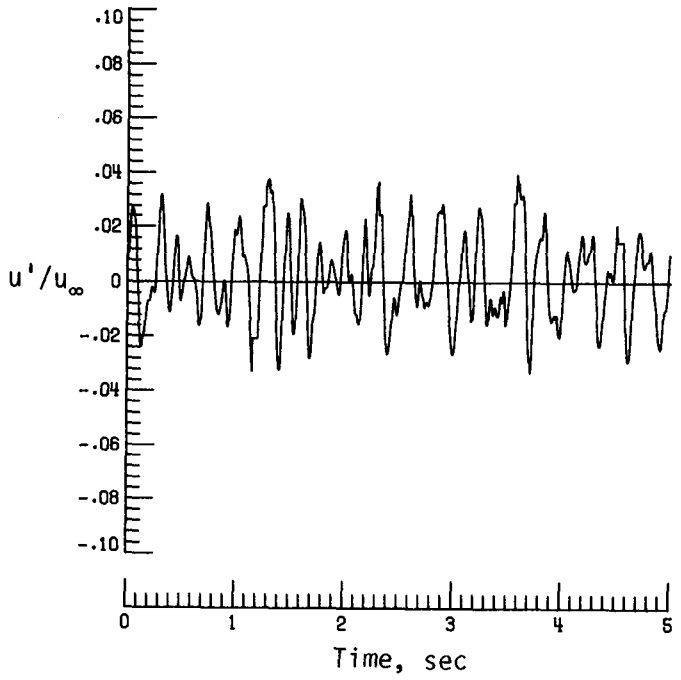

(a) Time history of streamwise velocity fluctuations.

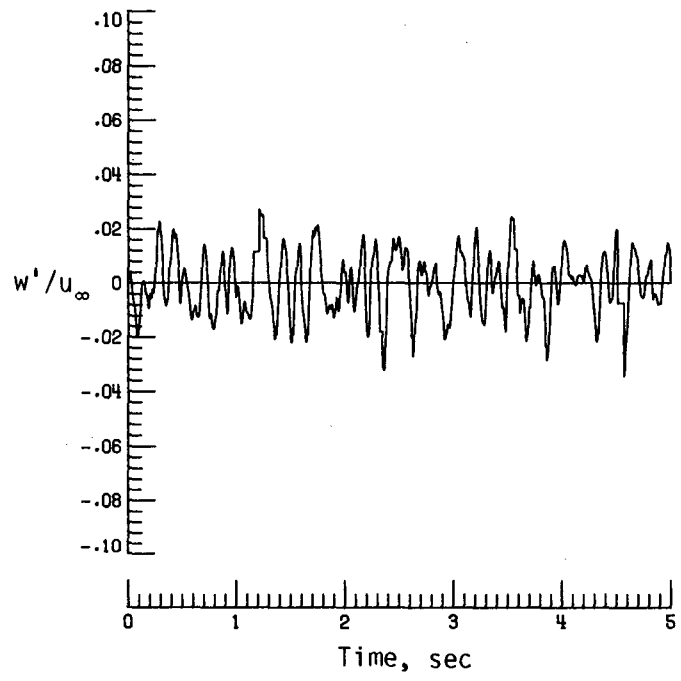

(b) Time history of vertical velocity fluctuations.

Figure B26. Dynamic-flow quality for configuration 6 at $q = 44.98$ lb/ft^2.

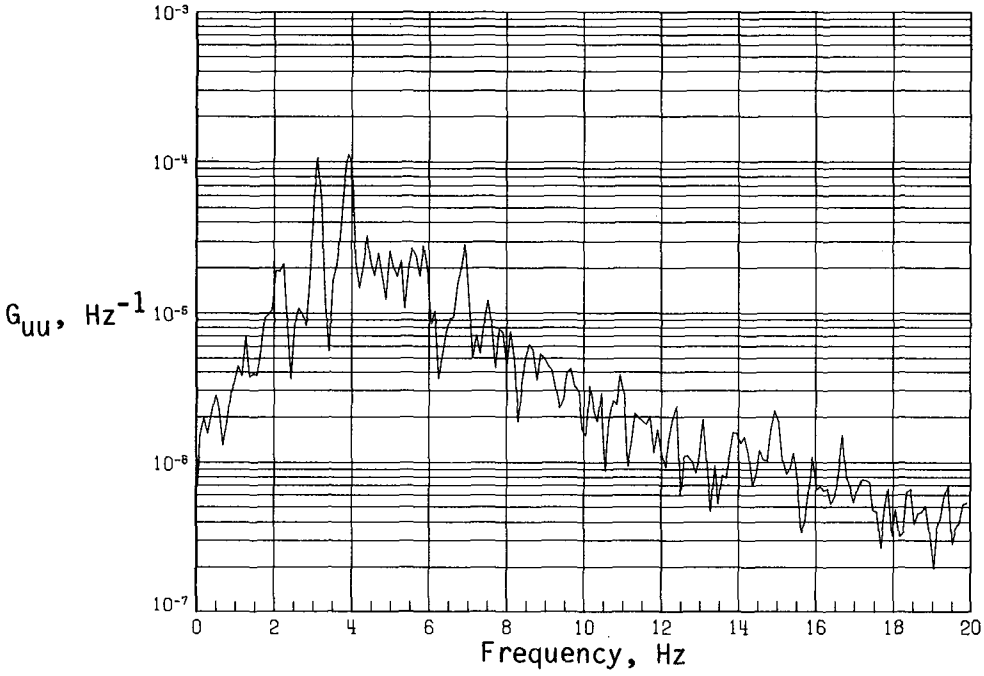

(c) PSD of streamwise velocity fluctuations.

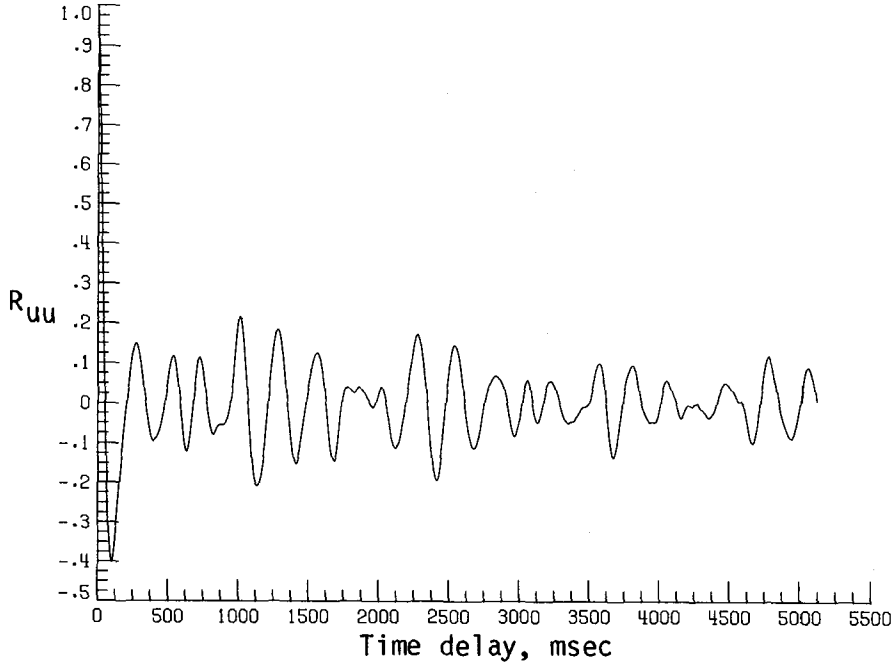

(d) Normalized autocorrelation of streamwise velocity fluctuations. $\sigma = 0.0127$.

Figure B26. Continued.

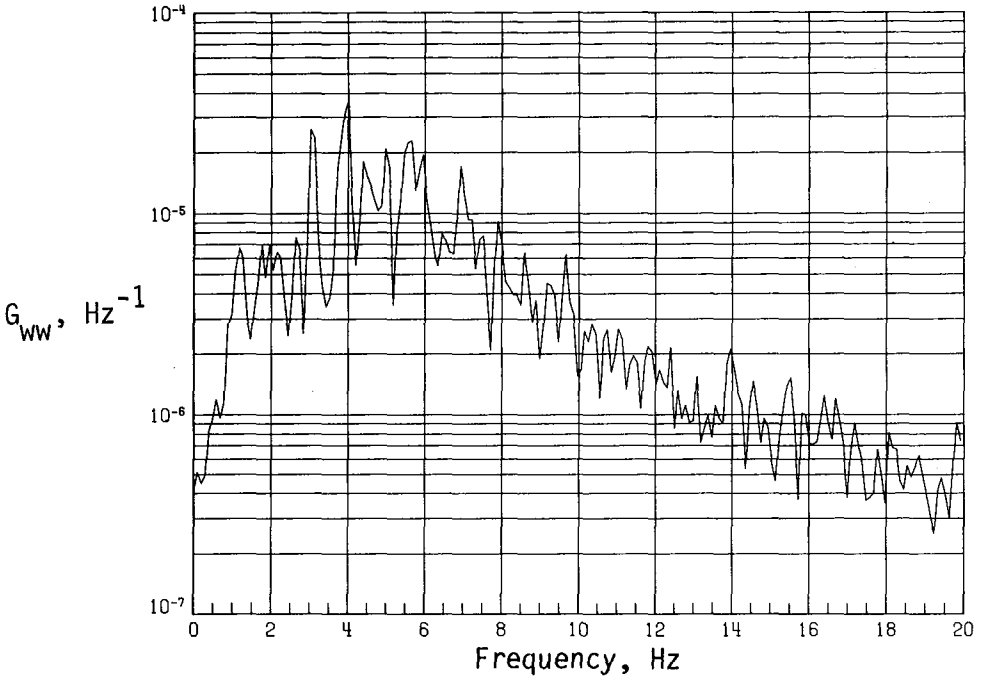

(e) PSD of vertical velocity fluctuations.

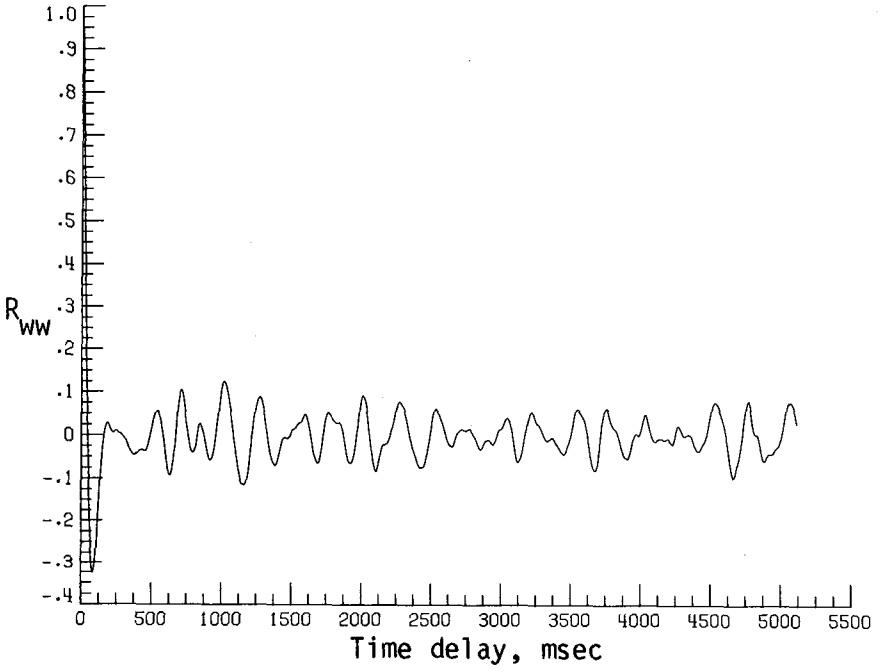

(f) Normalized autocorrelation of vertical velocity fluctuations. $\sigma = 0.0097$.

Figure B26. Concluded.

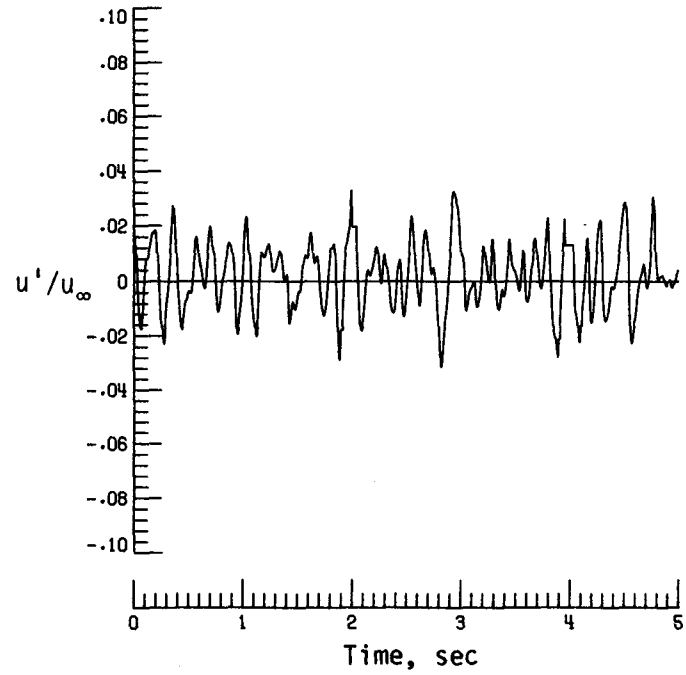

(a) Time history of streamwise velocity fluctuations.

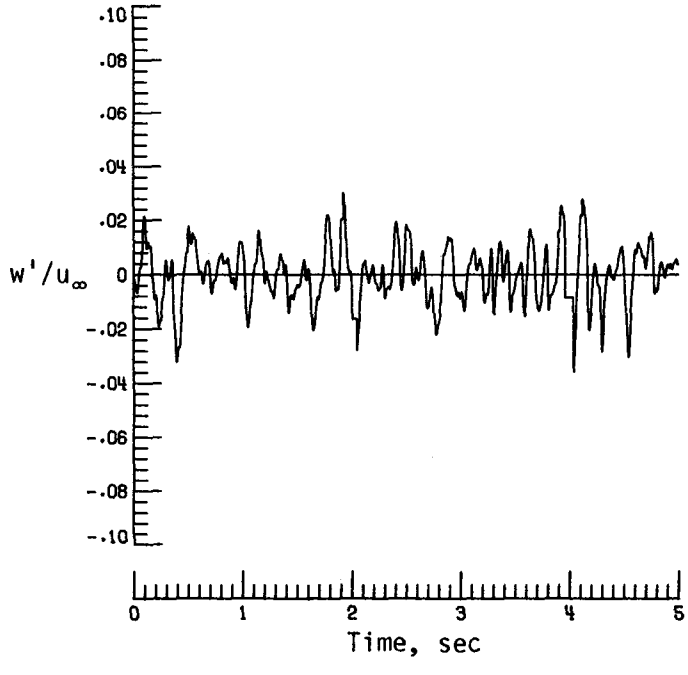

(b) Time history of vertical velocity fluctuations.

Figure B27. Dynamic-flow quality for configuration 6 at $q = 47.46$ lb/ft^2.

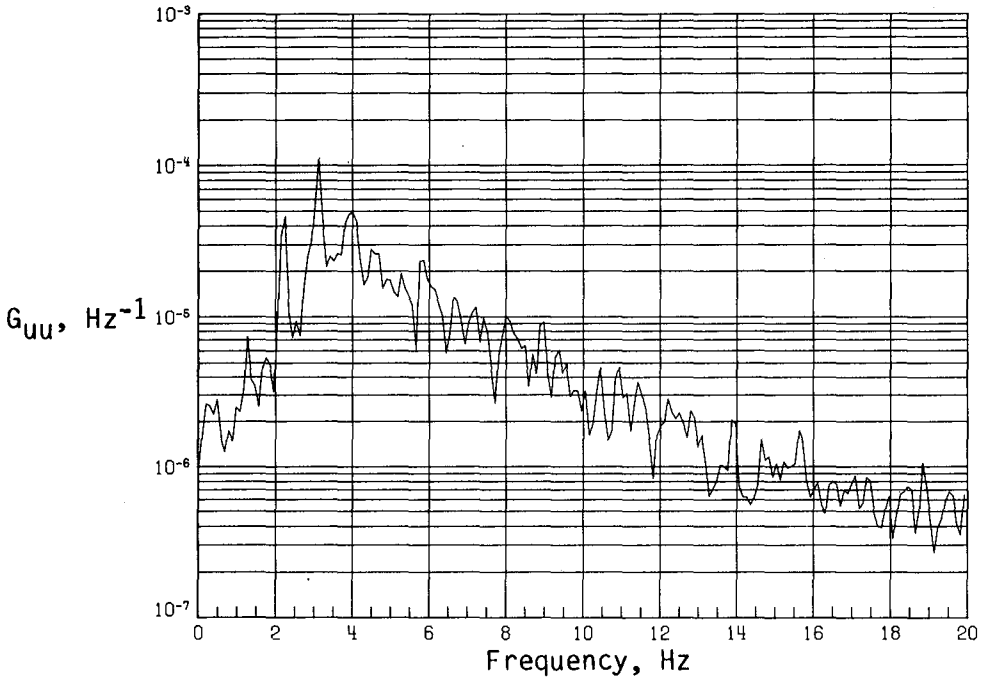

(c) PSD of streamwise velocity fluctuations.

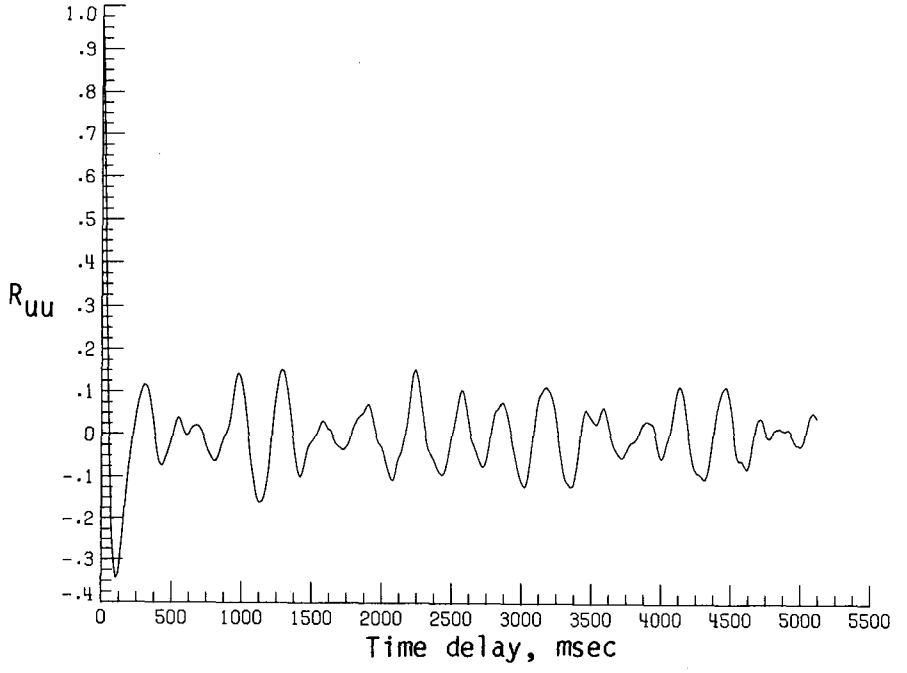

(d) Normalized autocorrelation of streamwise velocity fluctuations. $\sigma = 0.0125$.

Figure B27. Continued.

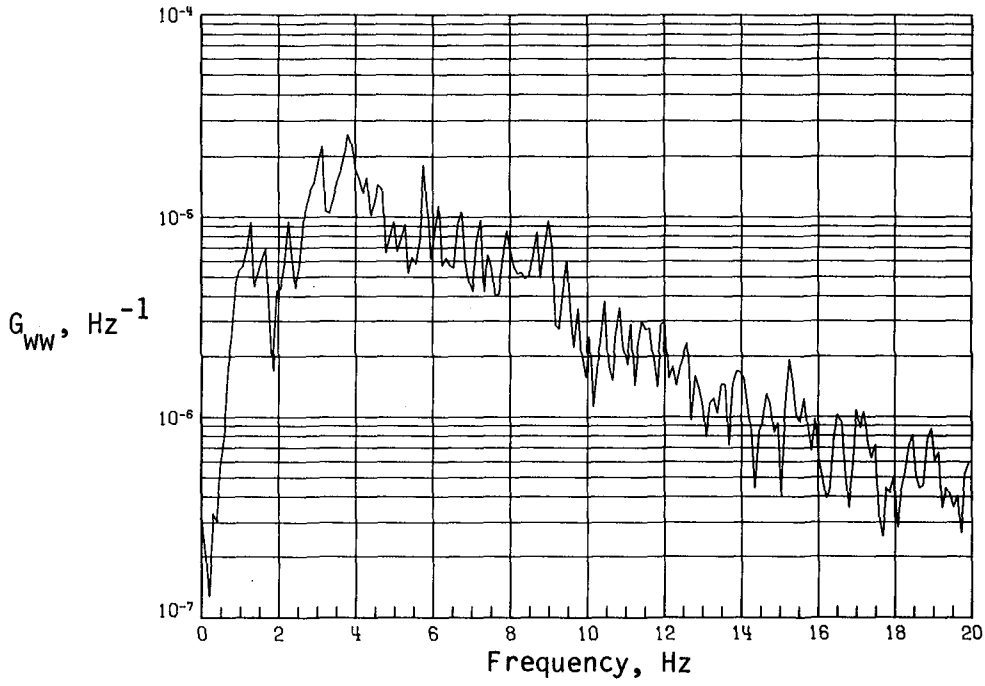

(e) PSD of vertical velocity fluctuations.

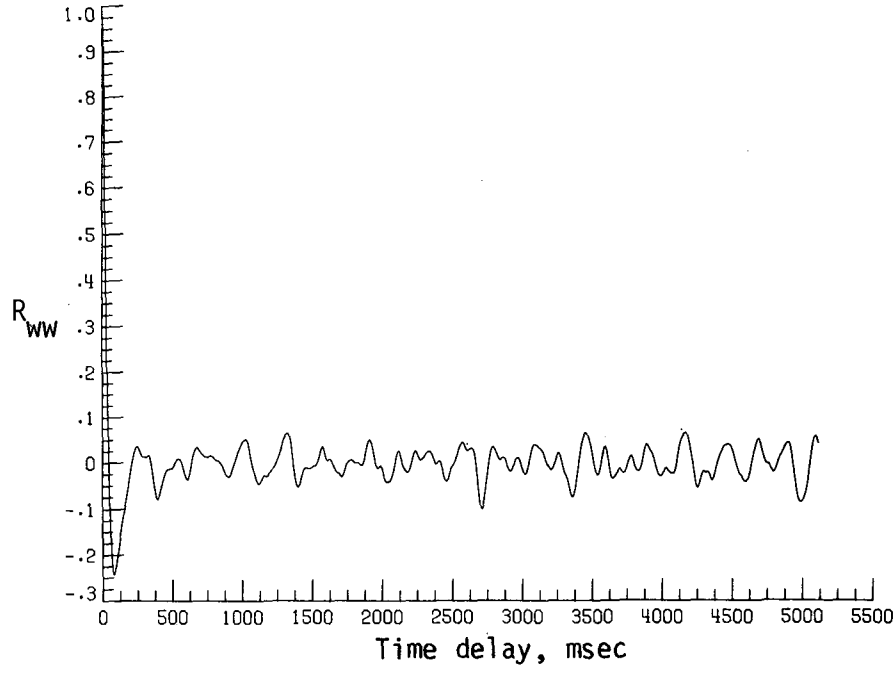

(f) Normalized autocorrelation of vertical velocity fluctuations. $\sigma = 0.0096$.

Figure B27. Concluded.

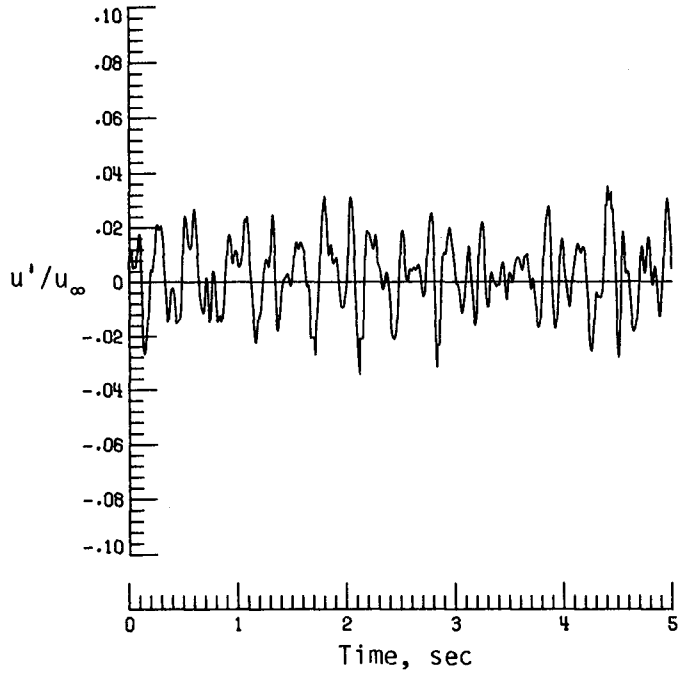

(a) Time history of streamwise velocity fluctuations.

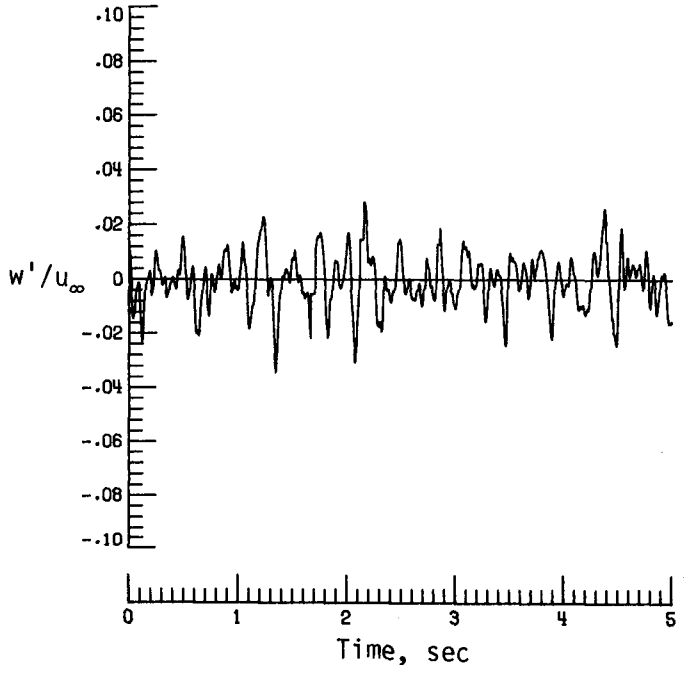

(b) Time history of vertical velocity fluctuations.

Figure B28. Dynamic-flow quality for configuration 6 at $q = 50.17$ lb/ft^2.

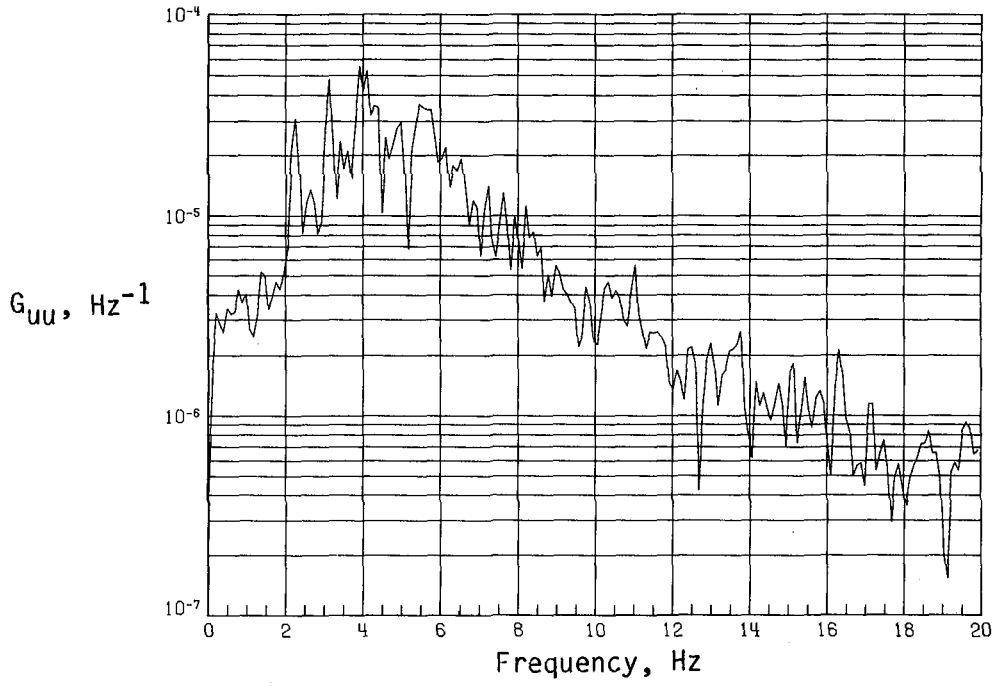

(c) PSD of streamwise velocity fluctuations.

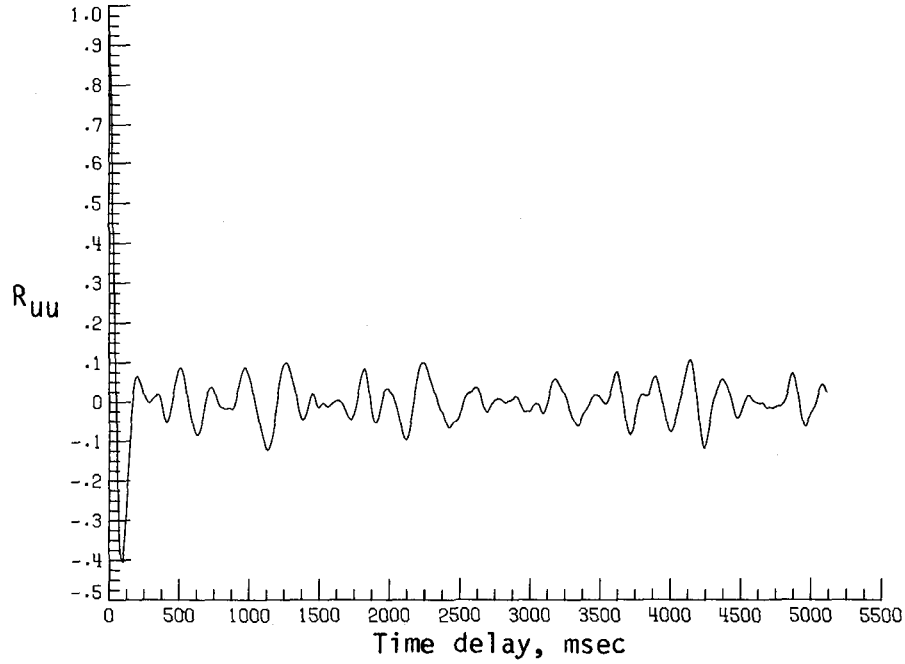

(d) Normalized autocorrelation of streamwise velocity fluctuations. $\sigma = 0.0127$.

Figure B28. Continued.

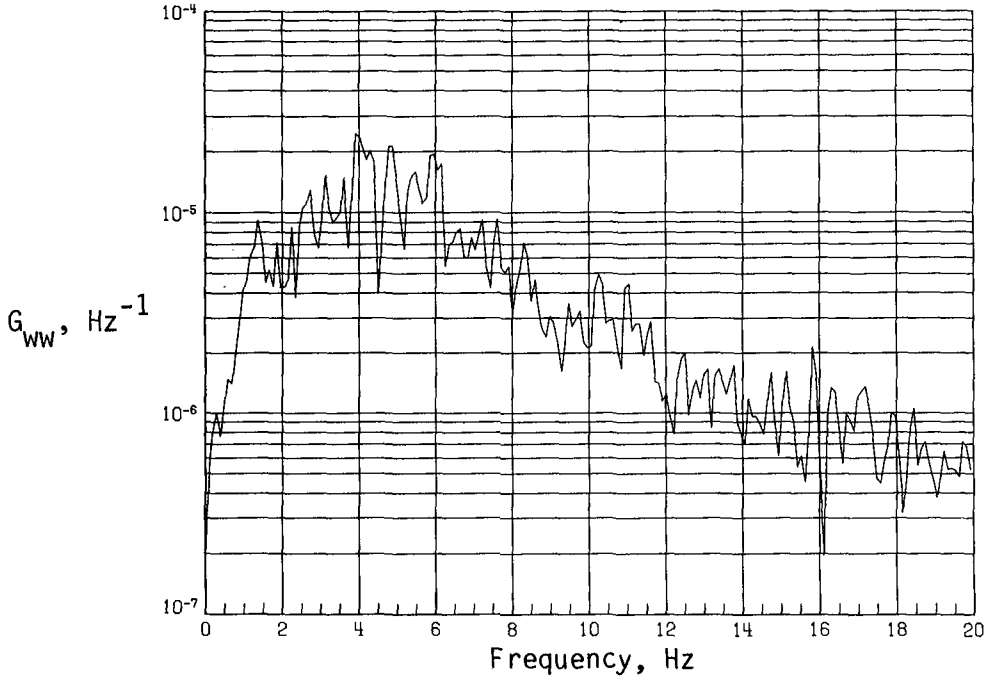

(e) PSD of vertical velocity fluctuations.

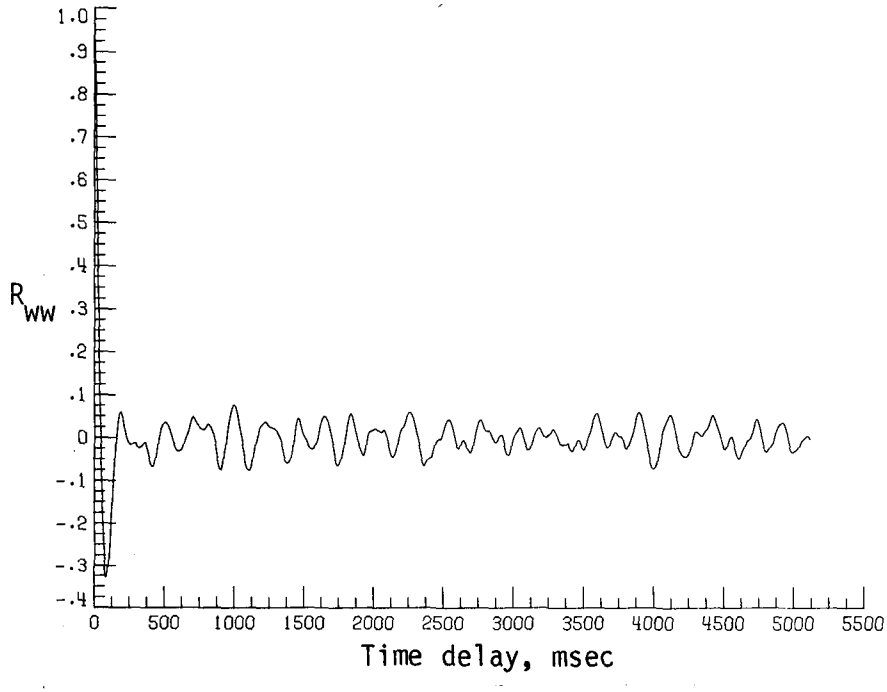

(f) Normalized autocorrelation of vertical velocity fluctuations. $\sigma = 0.0097$.

Figure B28. Concluded.

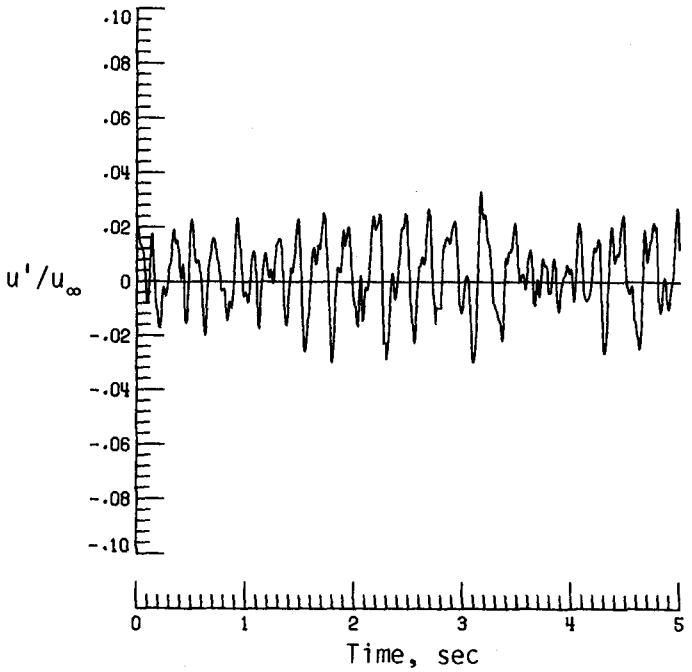

(a) Time history of streamwise velocity fluctuations.

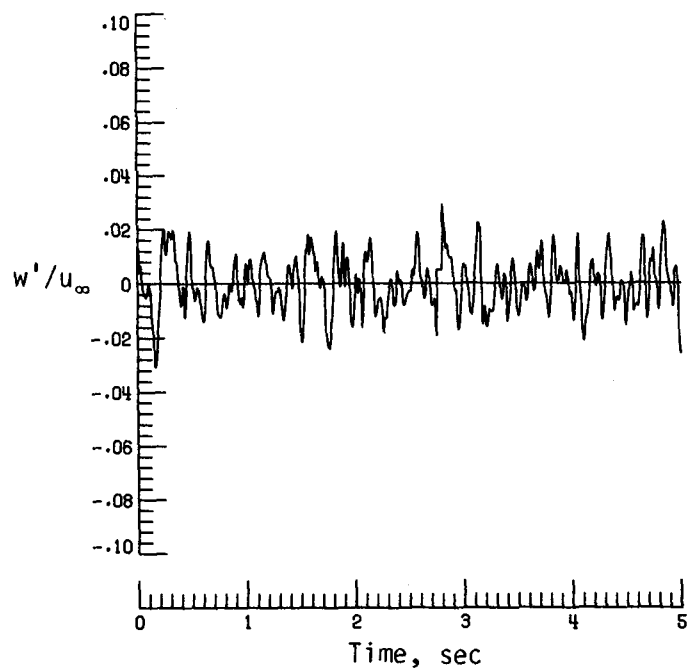

(b) Time history of vertical velocity fluctuations.

Figure B29. Dynamic-flow quality for configuration 6 at $q = 54.81$ lb/ft^2.

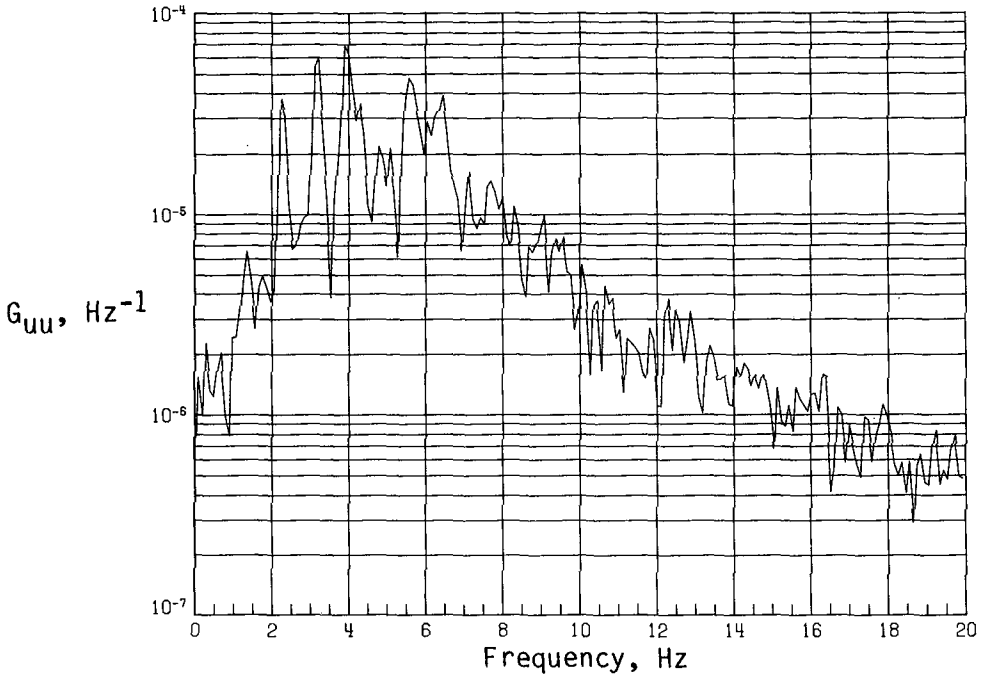

(c) PSD of streamwise velocity fluctuations.

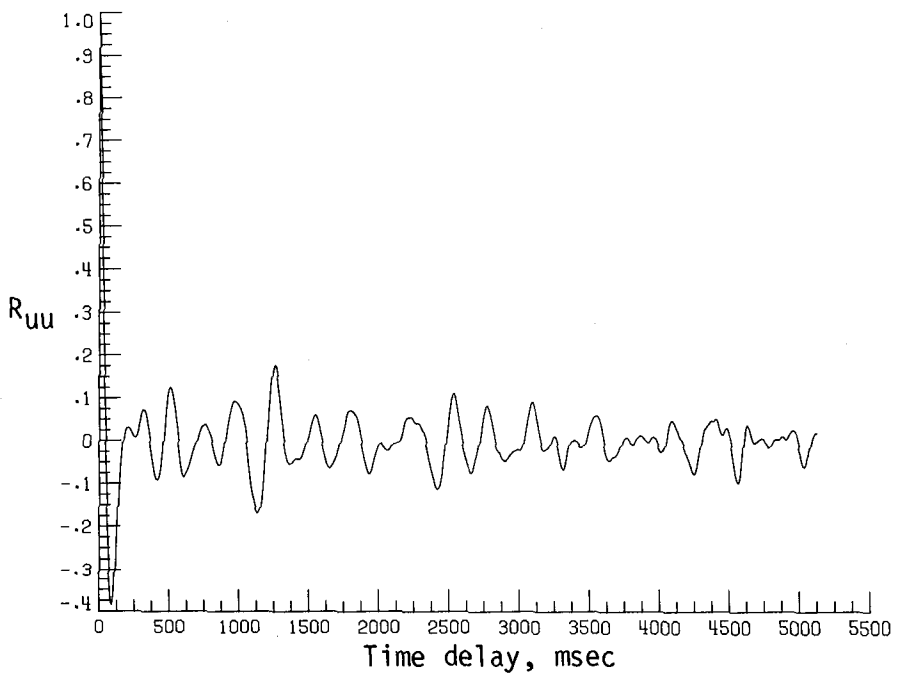

(d) Normalized autocorrelation of streamwise velocity fluctuations. $\sigma = 0.0125$.

Figure B29. Continued.

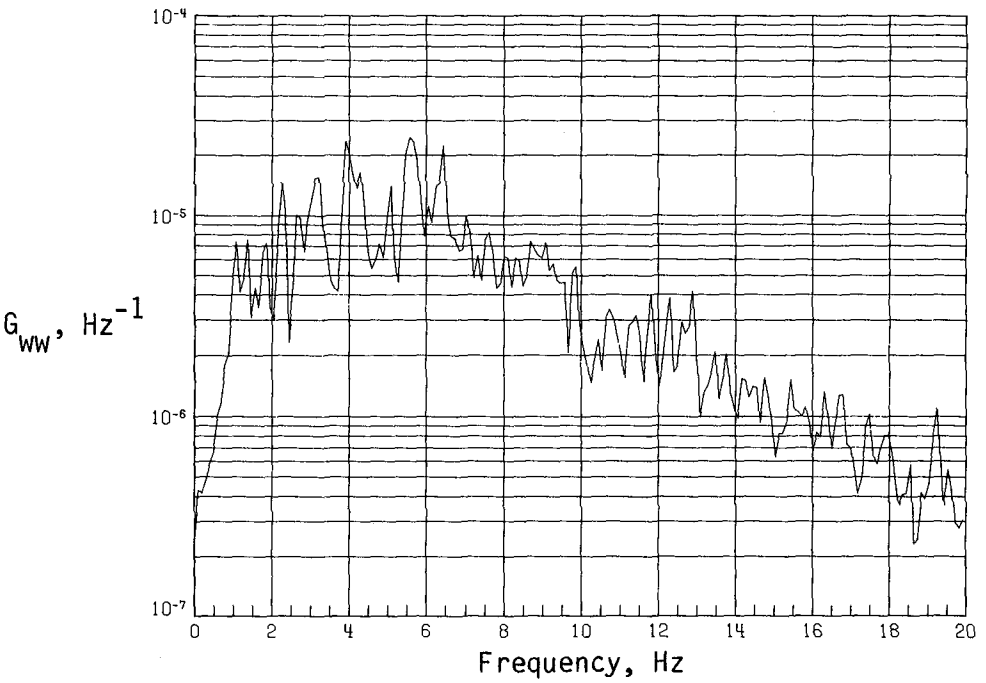

(e) PSD of vertical velocity fluctuations.

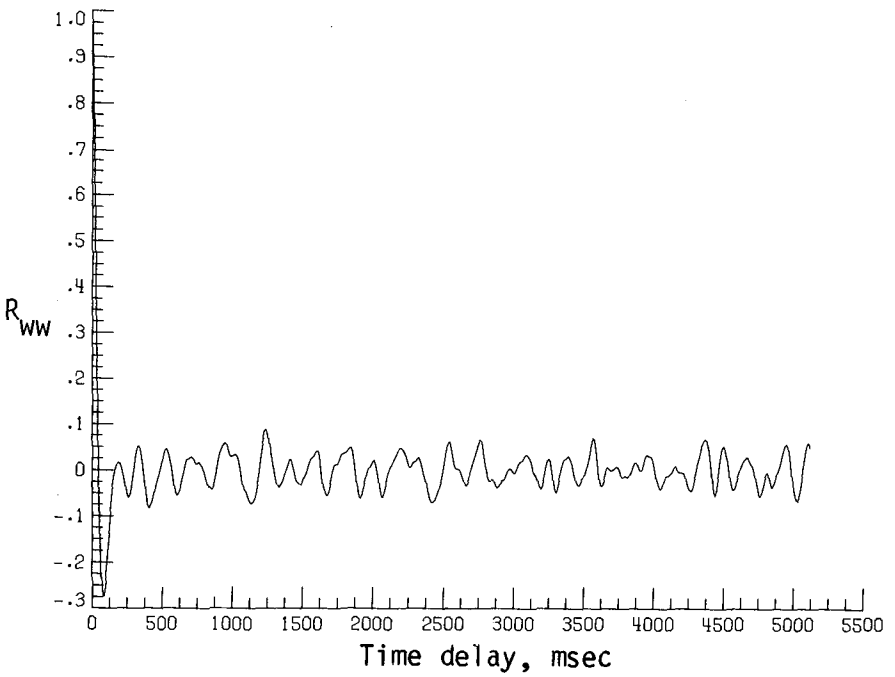

(f) Normalized autocorrelation of vertical velocity fluctuations. $\sigma = 0.0096$.

Figure B29. Concluded.

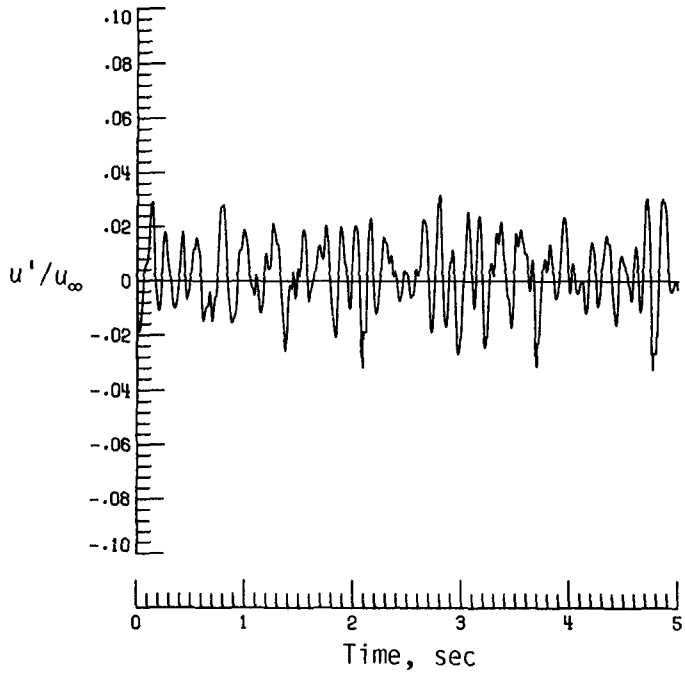

(a) Time history of streamwise velocity fluctuations.

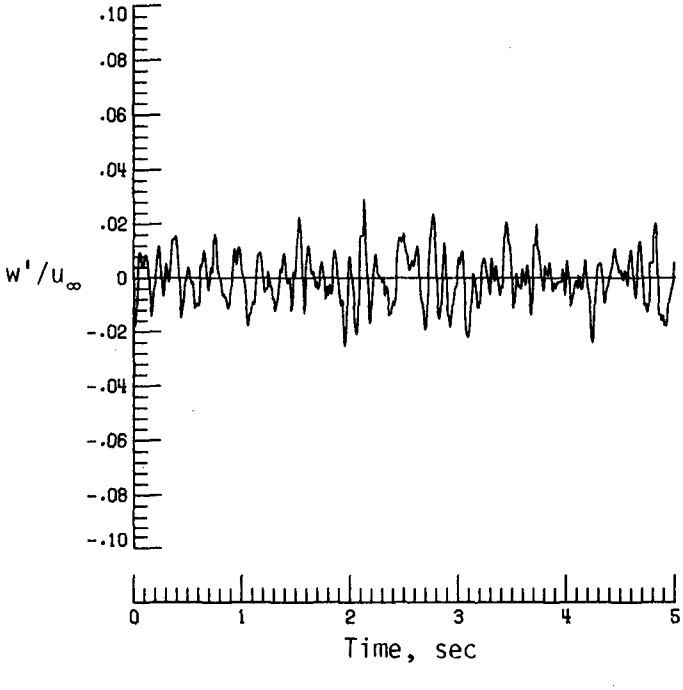

(b) Time history of vertical velocity fluctuations.

Figure B30. Dynamic-flow quality for configuration 6 at $q = 59.55$ lb/ft^2.

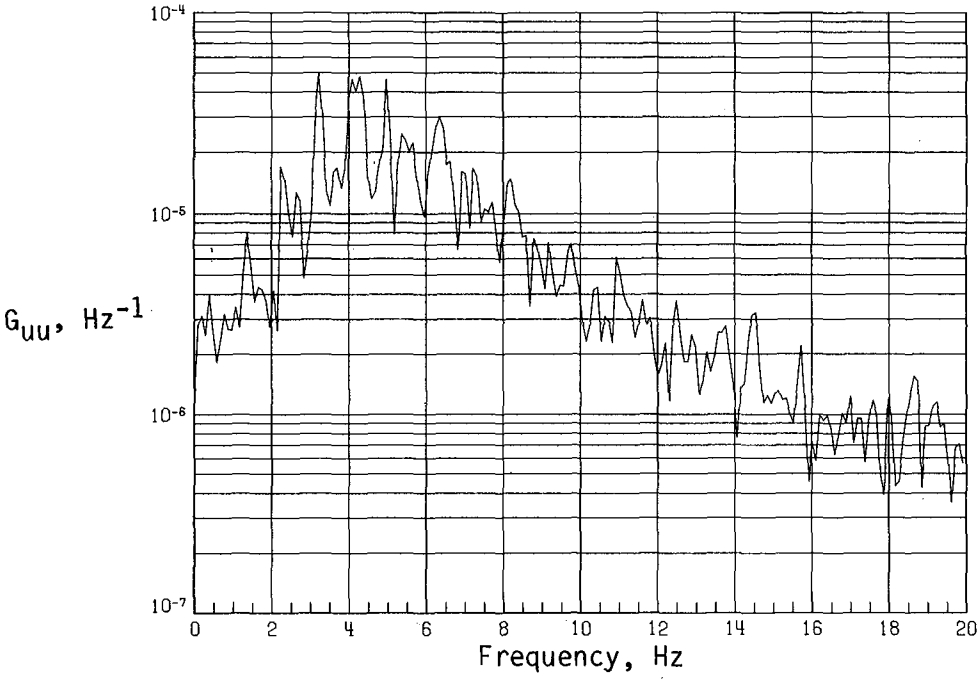

(c) PSD of streamwise velocity fluctuations.

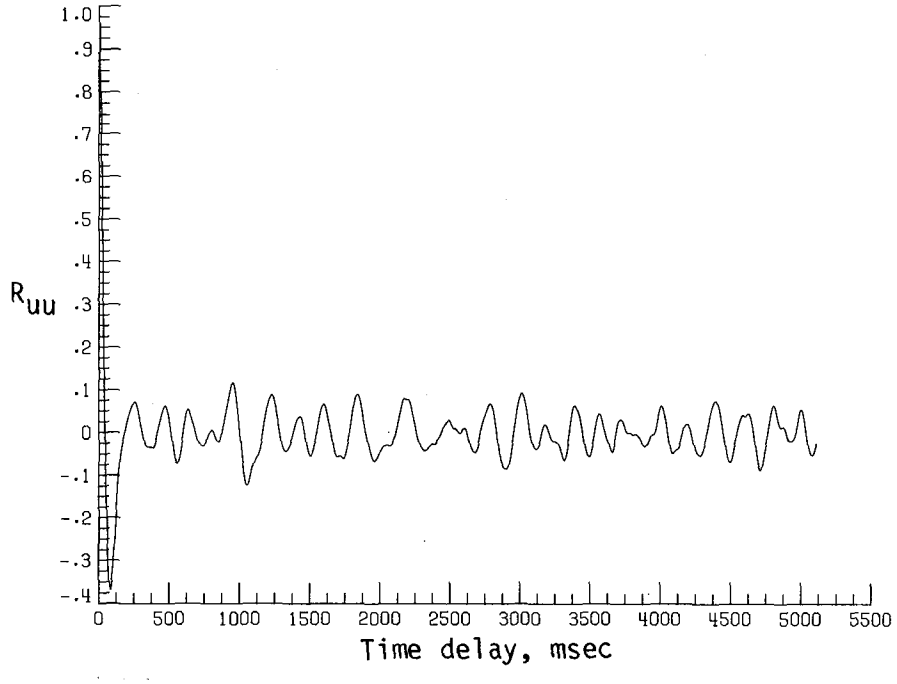

(d) Normalized autocorrelation of streamwise velocity fluctuations. $\sigma = 0.0123$.

Figure B30. Continued.

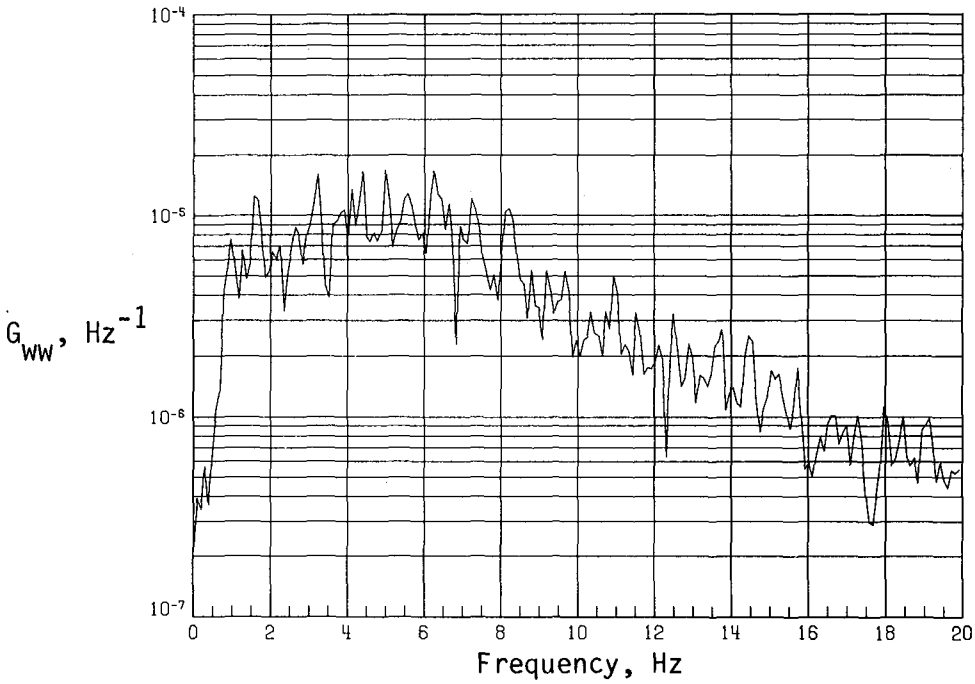

(e) PSD of vertical velocity fluctuations.

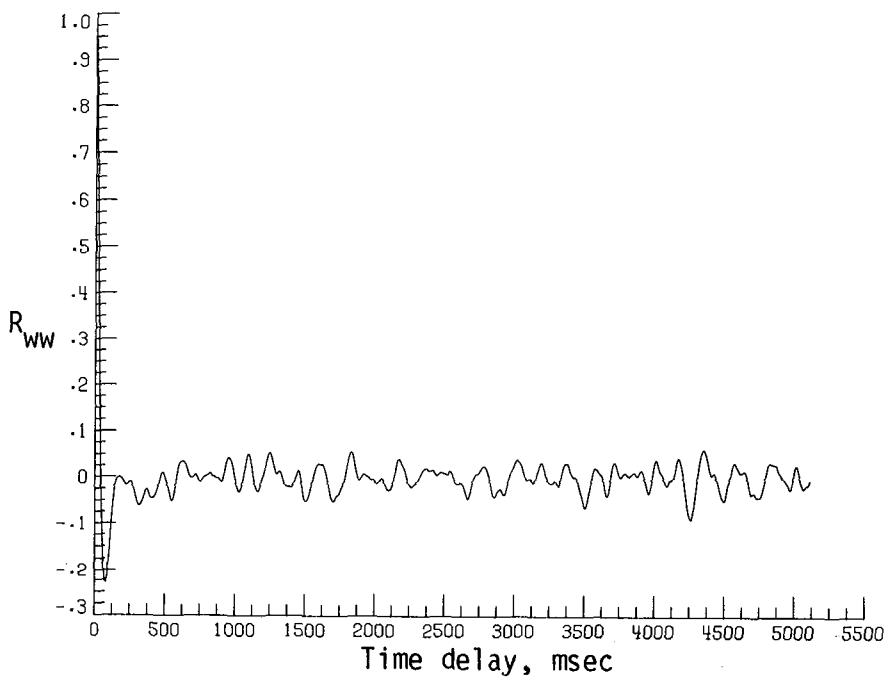

(f) Normalized autocorrelation of vertical velocity fluctuations. $\sigma = 0.0096$.

Figure B30. Concluded.

References

1. Jacobs, Eastman N.: *Investigation of Air Flow in Open-Throat Wind Tunnels.* NACA Rep. 322, 1929.
2. Seiferth, R.: Pre-Calculation and Removal of Oscillations in Free-Jet Wind Tunnels. *D_1 Model Test Technique—I. Test Installations*, R. Seiferth, ed., Reps. and Translations No. 947, British M.A.P. Volkenrode, Aug. 1, 1947, pp. 65–86.
3. Rogers, O. R.: *Wind Tunnel Pulsations.* AAF Tech. Rep. No. 5513, Army Air Forces, Air Materiel Command, War Dep., July 18, 1946.
4. Brodzki, Zdzislaw: *Stream Control for Low Speed Range in Wind Tunnel.* FTD-TT-62-1476/1+2, U.S. Air Force, Nov. 30, 1962. (Available from DTIC as AD 295 779.)
5. Gridley, Doreen: *An Introduction to Time Series Analysis and Data Reduction Programming Capabilities.* NASA CR-165782, 1981.
6. Eckelmann, H. (transl. C. R. Haave): *Measurement of Wind-Tunnel Turbulence by the Hot-Wire Method and Suppression of Wind-Tunnel Vibrations.* CLB-3 T-653 (Contract N00017-72-C-4401), Appl. Phys. Lab., Johns Hopkins Univ., June 2, 1972. (Available from DTIC as AD 744 888.)

1. Report No.	2. Government Accession No.	3. Recipient's Catalog No.
NASA TM-86299		

4. Title and Subtitle	5. Report Date
EFFECT OF JET EXIT VANES ON FLOW PULSATIONS IN AN OPEN-JET WIND TUNNEL	March 1985
	6. Performing Organization Code: 505-43-13-03
7. Author(s): William L. Sellers III, Zachary T. Applin, John K. Molloy, and Garl L. Gentry, Jr.	8. Performing Organization Report No.: L-15810
9. Performing Organization Name and Address: NASA Langley Research Center, Hampton, VA 23665	10. Work Unit No.
	11. Contract or Grant No.
12. Sponsoring Agency Name and Address: National Aeronautics and Space Administration, Washington, DC 20546	13. Type of Report and Period Covered: Technical Memorandum
	14. Sponsoring Agency Code

15. Supplementary Notes

16. Abstract

An investigation was conducted of various jet exit vane configurations in the open test section of the Langley 4- by 7-Meter Tunnel to determine their effectiveness in reducing flow pulsations. The data consist of the instantaneous velocity fluctuations measured with hot-wire anemometers located at the tunnel centerline, 39.5 ft (12.0 m) downstream of the jet exit. The data are presented in the form of measured root-mean-square turbulence levels in the test section and a time series analysis for the baseline jet exit configuration (without vanes) and for the most effective vane configuration, which consisted of triangular vanes alternating into and out of the flow around the jet exit.

17. Key Words (Suggested by Authors(s))

Wind tunnels (open-jet), low-speed
Flow pulsations
Flow surging
Jet exit vanes
Turbulence
Wind-tunnel nozzles
Flow pumping

18. Distribution Statement

Unclassified—Unlimited

Subject Category 02

19. Security Classif.(of this report)	20. Security Classif.(of this page)	21. No. of Pages	22. Price
Unclassified	Unclassified	215	A10

For sale by the National Technical Information Service, Springfield, Virginia 22161

NASA-Langley, 1985

National Aeronautics and Space Administration

Washington, D.C.
20546

Official Business
Penalty for Private Use, $300

SPECIAL FOURTH CLASS MAIL
BOOK

Postage and
National Aer
Space Administration
NASA-451

LANGLEY RESEARCH CENTER
3 1176 00520 7783

U.S. MAIL

NASA

deliverable (Section 158
Manual) Do Not Return

DO NOT REMOVE SLIP FROM MATERIAL

Delete your name from this slip when returning material to the library.

NAME	MS
~~H Heyson~~	—
~~M- Heyson~~	149
~~Libraries~~	~~159~~
~~Hemsch 8-97~~	~~280~~
Reis 3-00	286

NASA Langley (Rev. May 1988) RIAD N-75